



UNIVERSITAT POLITÈCNICA  
DE CATALUNYA  
BARCELONATECH

## *Development of mono and multilayer membranes of polypropylene and ethylene-propylene copolymers via cast film extrusion and stretching*

**M<sup>a</sup> Pilar Castejón Galán**

**ADVERTIMENT** La consulta d'aquesta tesi queda condicionada a l'acceptació de les següents condicions d'ús: La difusió d'aquesta tesi per mitjà del repositori institucional UPCommons (<http://upcommons.upc.edu/tesis>) i el repositori cooperatiu TDX (<http://www.tdx.cat/>) ha estat autoritzada pels titulars dels drets de propietat intel·lectual **únicament per a usos privats** emmarcats en activitats d'investigació i docència. No s'autoritza la seva reproducció amb finalitats de lucre ni la seva difusió i posada a disposició des d'un lloc aliè al servei UPCommons o TDX. No s'autoritza la presentació del seu contingut en una finestra o marc aliè a UPCommons (*framing*). Aquesta reserva de drets afecta tant al resum de presentació de la tesi com als seus continguts. En la utilització o cita de parts de la tesi és obligat indicar el nom de la persona autora.

**ADVERTENCIA** La consulta de esta tesis queda condicionada a la aceptación de las siguientes condiciones de uso: La difusión de esta tesis por medio del repositorio institucional UPCommons (<http://upcommons.upc.edu/tesis>) y el repositorio cooperativo TDR (<http://www.tdx.cat/?locale-attribute=es>) ha sido autorizada por los titulares de los derechos de propiedad intelectual **únicamente para usos privados enmarcados** en actividades de investigación y docencia. No se autoriza su reproducción con finalidades de lucro ni su difusión y puesta a disposición desde un sitio ajeno al servicio UPCommons No se autoriza la presentación de su contenido en una ventana o marco ajeno a UPCommons (*framing*). Esta reserva de derechos afecta tanto al resumen de presentación de la tesis como a sus contenidos. En la utilización o cita de partes de la tesis es obligado indicar el nombre de la persona autora.

**WARNING** On having consulted this thesis you're accepting the following use conditions: Spreading this thesis by the institutional repository UPCommons (<http://upcommons.upc.edu/tesis>) and the cooperative repository TDX (<http://www.tdx.cat/?locale-attribute=en>) has been authorized by the titular of the intellectual property rights **only for private uses** placed in investigation and teaching activities. Reproduction with lucrative aims is not authorized neither its spreading nor availability from a site foreign to the UPCommons service. Introducing its content in a window or frame foreign to the UPCommons service is not authorized (*framing*). These rights affect to the presentation summary of the thesis as well as to its contents. In the using or citation of parts of the thesis it's obliged to indicate the name of the author.

# **Development of mono and multilayer membranes of polypropylene and ethylene-propylene copolymers via cast film extrusion and stretching**

A dissertation submitted to partial fulfilment of the requirements for  
the degree of Doctor of Philosophy by

**M<sup>a</sup> Pilar Castejón Galán**

Department of Materials Science and Metallurgical Engineering  
Doctorate program in Materials Science and Engineering  
Universitat Politècnica de Catalunya – Barcelona Tech

Advisor: David Arencón Osuna



**UNIVERSITAT POLITÈCNICA  
DE CATALUNYA  
BARCELONATECH**

Terrassa, Spain

October 2020



## Acknowledgments

A continuación me gustaría agradecer a todas aquellas personas que me han brindado su ayuda durante todo el tiempo que he invertido en elaborar esta tesis doctoral. Estos años de crecimiento y desarrollo profesional y personal querría dedicarlos a:

Mi director de tesis el Dr. David Arencón Osuna por darme la oportunidad de ser parte de este proyecto y por darme en todo momento el aliento necesario para seguir adelante.

Al Prof. Dr. José Ignacio Velasco por permitirme ser parte de su grupo de investigación y darme la oportunidad de impartir clases en la universidad, una oportunidad de poder trabajar con materias que me interesan y mejorar mis habilidades sociales de comunicación.

Al Prof. Dr. Antonio Martínez Benasat gracias al cual inicié mi camino como investigadora. Él fue el docente capaz de transmitirme su pasión por la investigación y el trabajo duro.

A la Prof. Dr. Maria Lluïsa MasPOCH por permitirme hacer uso de los equipos e instalaciones para desarrollar mi tesis en el Centre Català del Plàstic (CCP).

Al Dr. Marcelo de Sousa, un grandísimo profesional y una persona siempre dispuesta a echar una mano, en especial a nosotros los doctorandos cuando hemos necesitado apoyo en nuestras tesis o en nuestros primeros pasos en el campo de la docencia. La importancia de esas pequeñas grandes cosas que facilitan el camino del tesista.

A Anna Carreras, por estar siempre ahí con su sonrisa, amabilidad y buenas palabras. No olvidaré esas tertulias que teníamos los tres durante y después de la comidas, gracias por esos momentos de respiro y de desconexión de todo.

También querría agradecer a aquellas personas que han aportado su granito en varios momentos y que siempre recordaré con cariño como Susana Ortiz, Hooman Abbasi, la Dr. Vera Realinho, Javier Gómez, Laia Fontelles, Lucía de la Cruz y las figuras del PAS cómo Irene Pérez, Josep Palou y Francisco José Barahona, quienes siempre con una sonrisa y buena voluntad están dispuestos a echarte un cable cuando lo necesitas.

Y ya por último me gustaría hacer hincapié en el agradecimiento a aquellas personas sin las cuales hubiera sido mucho más complicado acabar con éxito esta etapa tan importante de mi vida:

A mi compañero y amigo el Dr. Noel Albíter, mi compañero de máster y doctorado, no olvidaré todo lo que me has ayudado estos años con la tesis y en especial durante este último periodo. Hemos compartido junto a Anna momentos inolvidables y muy divertidos. Deseo que sigas



superando cada obstáculo que se te ponga por delante y consigas todo lo que te propongas como has ido haciendo hasta la fecha, porque sin duda te mereces todo lo bueno que esté por venirte.

Finalmente, agradecer a mis amigos y familia por estar apoyándome todo este tiempo, sin vosotros a mi lado no hubiera sido posible finalizar esta etapa. A mis padres, a quienes agradezco haberme enseñado a conseguir todos los objetivos que decida fijar en mi vida sin importar lo difícil que sea el camino. A ti seguiré dedicándote todos mis logros, quererte fue fácil, olvidarte es imposible.

## Abstract

This dissertation investigates the three-stage method MEAUS (melt-extrusion, annealing, and uniaxial stretching) for producing porous membranes. This method for membrane preparation is a solvent-free process based on the stretching of semicrystalline polymer films containing a row-nucleated lamellar structure. In this regard, the first section of this thesis is dedicated to establishing an initial set of requirements based on the ability of different polyolefin materials for the formation of porous membranes. The influence of the polymer matrix composition and the architecture structure on the flow-induced crystallization was studied. This was done using two linear polypropylenes having different molecular weights and blending them with branched and very fluid PP resins. Lower porosity and permeability values were observed when low molecular weight polypropylenes were employed. Under the same processing conditions, the more prolonged relaxation time behavior of the high molecular weight resin induced a suitable row nucleated structure with a higher orientation. In the second part of this research work, heterophasic and random copolymers of polypropylene–ethylene were selected to study the influence of ethylene comonomer and its distribution along the polymer backbone. Most of these polymers can form a planar stacked lamellar morphology with a high crystalline orientation by selecting appropriate processing conditions.

From a process engineering standpoint, the influence of the extrusion draw ratio was analysed, and an in-depth study concerning the annealing and uniaxial strain stages was performed. After annealing, the films were subjected to a uniaxial stretching step along the machine direction. First, to generate pores at room temperature and subsequently stretched at a high temperature to enlarge the pore size by increasing lamellar separation. This thesis was also conducted as part of a comprehensive study aimed at evaluating the effect of temperature in the stages of extrusion, annealing, and uniaxial strain, as well as the use in some cases of extreme strain rates and strain extents. High levels of molecular orientation can be obtained with high extrusion draw ratios and fast cooling. Regarding the annealing process, an increment in temperature gave rise to a greater molecular orientation and a rearrangement of polymer chains in both the crystalline and amorphous phases, leading to an increase in crystallinity and molecular orientation. A close relationship was found between the starting crystalline characteristics and annealing and stretching conditions. These factors affected the final porous morphology and the trends registered for permeability.

The last section of this thesis is devoted to ascertaining the effects of mineral fillers ( $\text{CaCO}_3$  and talc) on the crystallization and mechanical behavior of multilayer polypropylene/high-density polyethylene porous membranes. This multilayer system is generally produced by various processes, such as lamination and co-extrusion. Celgard initially developed PP/PE/PP trilayer

separators for battery applications combining the lower melting temperature of PE with the high-temperature strength of PP. In this study, the crystallization and crystalline orientation were affected by both the flow-induced crystallization and the nucleation efficiency of fillers. A synergistic effect was observed in the filled samples due to the generation of pores during the uniaxial stretching stages (MEAUS method) and the debonding mechanisms of mineral fillers from the polymeric matrix, which promoted the formation of larger pores giving rise to a change in membrane permeability. The agglomeration of fillers in the composites affected the mechanical properties, the average membrane pore size, and pore size distribution. Compared to monolayers, the trilayer porous membranes showed lower orientation factors and lower permeability values due to the presence of interfaces between layers of different pore size distributions.

## Resumen

En esta tesis doctoral se investiga el método de extrusión en fundido, recocido y estiramiento uniaxial (MEAUS, por sus siglas en inglés) para el desarrollo de membranas porosas. Este método para la preparación de muestras porosas no parte de ninguna solución líquida de polímero, sino que es un proceso basado en el estiramiento de películas hechas a partir de termoplásticos semicristalinos que contienen una estructura no esferulítica denominada estructura “row-nucleated” (estructura nucleada en fila o de lamelas apiladas). La primera parte de esta tesis está dedicada a establecer un conjunto de requisitos iniciales basados en la capacidad de diferentes poliolefinas para la formación de membranas porosas. Se estudió la influencia de la composición y estructura del polímero en su proceso de cristalización seleccionando distintos grados comerciales de polipropileno homopolímero con diferentes promedios de peso molecular, así como un polipropileno con ramificación de cadena larga. En las membranas hechas a partir de polipropilenos de menor peso molecular se obtuvieron valores más bajos tanto de porosidad como de permeabilidad. Bajo las mismas condiciones de procesamiento, el mayor tiempo de relajación de las resinas con mayor peso molecular constituyó un factor clave a la hora de mantener la orientación molecular deseada. En la segunda parte de este trabajo de investigación se seleccionaron dos tipos de copolímero de propileno-etileno (copolímero heterofásico y copolímero al azar) con el objetivo de estudiar la influencia de esta segunda fase y su distribución a lo largo de la cadena principal del material. La mayoría de los polímeros investigados han tenido la capacidad de desarrollar la estructura de lamelas apiladas “row-nucleated” aplicando las condiciones óptimas de procesado.

Teniendo en cuenta las diferentes etapas de fabricación de las que consta este método se ha realizado un estudio en profundidad sobre la influencia que tiene tanto la relación de estirado aplicada durante el proceso de extrusión, como la de las etapas de recocido y estiramiento uniaxial en el desarrollo de la estructura porosa. Tras el recocido de las muestras los films son sometidos a una etapa de estiramiento a dos temperaturas diferentes. En primer lugar, el film recocido es estirado uniaxialmente a baja temperatura con el fin de nuclear poros en el interior de la estructura cristalina. Posteriormente, la misma muestra es estirada uniaxialmente a mayor temperatura con el objetivo de agrandar el tamaño promedio de poro. En esta tesis también se ha evaluado el efecto que tiene la variable de temperatura en las etapas de extrusión, recocido y estiramiento. Se obtuvieron elevados valores de orientación molecular gracias a la aplicación de elevadas relaciones de estirado y enfriamiento del fundido justo a la salida del cabezal de extrusión. Asimismo, durante el proceso de recocido, un incremento en la temperatura también dio como resultado la obtención de mayores valores de cristalinidad y orientación tras el reordenamiento de las macromoléculas presentes tanto en las fases cristalinas como amorfas. Por último, fue posible establecer una estrecha relación entre

las características cristalinas iniciales de las muestras y las condiciones de recocido y estiramiento uniaxial. Estas variables afectaron por igual a la morfología de poro obtenida y a los valores de permeabilidad registrados.

La última sección de esta tesis está dedicada a determinar el efecto de la incorporación de distintas cargas minerales ( $\text{CaCO}_3$  y talco) en la cristalización y el comportamiento mecánico de membranas multicapa polipropileno / polietileno de alta densidad. Este sistema multicapa actualmente se desarrolla empleando distintos métodos como la laminación y la coextrusión. Celgard fue la primera compañía en desarrollar este tipo de separadores de tres capas de PP / PE / PP para aplicaciones en baterías, combinando la temperatura de fusión más baja del PE con la resistencia a mayores temperaturas del PP. En este estudio se demuestra como el proceso de cristalización y orientación de las muestras se ve afectado tanto por las variables descritas anteriormente, como por los mecanismos de nucleación y cristalización producidos por la presencia de las cargas minerales. En estas muestras compuestas se observó también la presencia de poros de mayor tamaño fruto de la combinación de dos fenómenos distintos. Por un lado, la separación lamelar producida durante las etapas de estiramiento uniaxial y por otro, la separación producida entre las cargas inorgánicas y la matriz de polímero tras ser sometidos ambos a esfuerzos externos. La presencia de aglomerados en estos compuestos influyó tanto en las propiedades mecánicas, como en el tamaño promedio y distribución de poros a lo largo de la membrana. En comparación con las muestras porosas monocapa, las membranas multicapa presentaron menores valores de orientación molecular y permeabilidad.

## Table of contents

<b>ACKNOWLEDGMENTS</b> .....	<b>i</b>
<b>ABSTRACT</b> .....	<b>iii</b>
<b>RESUMEN</b> .....	<b>v</b>
<b>TABLE OF CONTENTS</b> .....	<b>vii</b>
<b>LIST OF FIGURES AND TABLES</b> .....	<b>x</b>
Figures .....	x
Tables .....	xv
<b>GLOSSARY OF SYMBOLS AND ABBREVIATIONS</b> .....	<b>xvii</b>
<b>Chapter 1: Introduction</b> .....	<b>1</b>
1.1. Overview of membrane technology and its applications.....	3
1.2. Aims and scope of the work.....	5
<b>Chapter 2: Theoretical literature review</b> .....	<b>7</b>
2.1. Classification of synthetic membranes .....	9
2.2. Membrane fabrication processes .....	11
2.3. Flow induced crystallization .....	16
2.4. Melt-extrusion/annealed/uniaxial stretching (ME AUS) method.....	26
2.4.1. Polymer composition and melt-extrusion conditions.....	26
2.4.2. Thermal annealing and uniaxial stretching process.....	29
2.5. Multilayer microporous membranes .....	36
2.6. Morphological characteristics of polypropylene and polyethylene .....	38
<b>Chapter 3: Experimental details</b> .....	<b>43</b>
3.1. Materials: nomenclature and microstructural characterization.....	45
3.2. Precursor film processing .....	48
3.2.1. Extrusion .....	48
3.2.2. Annealing and uniaxial stretching .....	49
3.3. Precursor film and membrane characterization.....	50
3.3.1. Orientation Features .....	50

3.3.2. Morphology.....	51
3.3.3. Porosity and permeability.....	51
3.3.4. Thermal characterization .....	52
3.3.5. Mechanical characterization .....	53
<b>Results and discussion</b>	
<b>Chapter 4: Polypropylene based porous membranes.....</b>	<b>57</b>
4.1. Influence of polymer composition.....	59
4.2. Influence of draw ratio .....	66
4.3. Influence of uniaxial strain .....	69
4.3.1. Effect of strain rate.....	70
4.3.2. Effect of strain extent.....	74
4.4. Practical case: Membranes as integral parts of lighters. ....	77
4.5. Discussion and main conclusions .....	78
<b>Chapter 5: Polypropylene-ethylene copolymers based porous membranes .....</b>	<b>81</b>
5.1. Influence of extrusion and annealing temperature on neat resins .....	83
5.2. Influence of annealing temperature on polymer blends.....	91
5.3. Influence of temperature during hot stretching step .....	104
5.4. Effect of annealing temperature and polymer composition on the mechanical properties .....	106
5.5. Discussion and main conclusions .....	110
<b>Chapter 6: Multilayer composite membranes .....</b>	<b>113</b>
6.1. The nucleation effect of fillers on the crystallization behavior of composites films.. .....	117
6.2. Morphology and permeability of composite membranes .....	124
6.3. Thermal stability .....	133
6.4. Mechanical characterization .....	136
6.5. Discussion and main conclusions .....	141
<b>Chapter 7: Conclusions and future research lines.....</b>	<b>143</b>
7.1. Conclusions .....	145
7.2. Future research lines .....	149

<b>References .....</b>	<b>150</b>
<b>List of publications .....</b>	<b>165</b>
<b>Annexes.....</b>	<b>167</b>



## List of figures and tables

### Figures

**Figure 2.1.** Classification of synthetic polymer membranes based on their structure. Modified from [2].

**Figure 2.2.** Separation processes differing in the values of mean pore size. Modified from [2].

**Figure 2.3.** SEM images of the cross section of aromatic polyamide made by the Loeb–Sourirajan technique. Reprinted from [2].

**Figure 2.4.** Different stretching procedures to develop symmetric porous membranes [2,27-29, 41-77].

**Figure 2.5.** Schematic diagrams representing the flow-induced crystallization in semicrystalline polymers.

**Figure 2.6.** Schematic of the types of row-nucleated structure under (a) low stress and (b) high stress proposed by Keller and Machin. Image from [78].

**Figure 2.7.** (a) Initial morphology before shear, (b) upon the imposition of a step shear rate, and (c) final morphology after cessation of shear. Schematics of the shear-induced primary nuclei and subsequent lateral crystal growth proposed by Somani et al. Modified from [82].

**Figure 2.8.** Determination of the critical orientation molecular weight ( $M^*$ ) as a function of the imposed shear conditions for a typical molecular weight distribution curve. Image from [82].

**Figure 2.9.** Schematic representation of the primary nucleation and subsequent growth of stacked crystalline lamellae in shear-induced crystallization. Modified from [85].

**Figure 2.10.** Schematic diagram of representative HDPE, LDPE and LLDPE crystalline forms and structure-tear resistance relationship proposed by Zhang et al. Modified from [90].

**Figure 2.11.** Thickness ( $df$ ) as a function of the lateral coordinate averaged ( $\bar{y}$ ) over different positions along two cast films (L-PP and LCB-PP) stretched at different draw ratios ( $Dr = 5$  and  $15$ ). Image from [96].

**Figure 2.12.** Result graph of film width ( $Bf$ ) along the drawing direction ( $x$ ) for two cast films (L-PP and LCB-PP) stretched at different draw ratios ( $Dr = 5$  and  $15$ ). Image from [96].

**Figure 2.13.** Optical micrographs of samples crystallized non-isothermally by cooling at rate of 10°C/min. (a) linear polypropylene (homopolymer), (b) random copolymer and (c) homopolymer-copolymer blend (98wt% and 20 wt%, respectively). Reproduced from Sadeghi et al [30].

**Figure 2.14.** Relationship between Gurley number and percent extension applied during the cold and hot stretching to produce PMP microporous films. (a) -□- Tca = 40°C, -◻- Tca = 70°C, -△- Tca = 80°C, -▼- Tca = 90°C, and (b) -□- Tca = 120°C, -◻- Tca = 160°C, -▼- Tca = 180°C. Reproduced from Johnson [117].

**Figure 2.15.** Stress-strain curves for the same polypropylene films, one non-annealed and the second one annealed at 145 °C. Image reported by Sadeghi et al. [5].

**Figure 2.16.** (a) Average crystallinity of the annealed samples at (i) 140 °C, (ii) 140 °C under 5% extension, and (iii) 120 °C (annealing time= 30min), and (b) crystalline and amorphous orientation parameters both as a function of high Mw PP content. Images reported by Tabatabaei et al [4].

**Figure 2.17.** Microstructural evolution during isothermal annealing. Modified from [13].

**Figure 2.18.** (i) Stress–strain curves of the annealed precursor films at different strain rates and (ii) SEM micrographs of the surface and cross-section of PP membranes prepared at (a) 5 mm/min and (b) 200 mm/min. Cold stretching= 35% followed by hot stretching= 60% (the white arrow indicates the stretching direction). Reported by Saffar et al. [10].

**Figure 2.19.** SEM imaged displaying the interfacial adhesion between etched PP/HDPE multilayer films. Images from [120].

**Figure 2.20.** Chemical structures of ethylene and propylene [103].

**Figure 2.21.** PE and PP crystal unit cells. Modified from [127].

**Figure 2.22.** Chain backbone developing a (a) planar zigzag conformation in PE and (b) helical conformation in PP. Modified from [127].

**Figure 2.23.** Schematic representations of (a) random and (b) block copolymers. The two different repeating units are designated as A and B. Modified from [108].

**Figure 3.1.** Scheme of precursor films manufacturing process.

**Figure 4.1.** (a) Crystalline and (b) amorphous orientation parameters derived from infrared measurements, and (c) crystallinity obtained from DSC thermograms. Precursor films annealed at 140 ° C for 15 min.

**Figure 4.2.** Thermograms differing in sample composition. (a) precursor films, (b) annealed precursor films, (c) membranes.

**Figure 4.3.** Scanning Electron Microscopy (SEM) micrographs of membranes differing in sample composition.

**Figure 4.4.** (■) Crystalline and (▲) amorphous orientation parameters derived from infrared measurements, and (●) crystallinity obtained from DSC thermograms. Precursor films annealed at 140 ° C for 15 min.

**Figure 4.5.** (a) SEM micrographs and (b) DSC thermograms of PP-2BR differing in their draw ratio. Processing conditions: Gap die, 1.9 mm; cold stage 0.3 mm/min, 20%; hot stage, 0.3 mm/min, 130%.

**Figure 4.6.** Influence of same cold and hot strain rates (upper-left, in mm/min) (a) SEM micrographs and (b) DSC thermograms. Common uniaxial strain conditions: Cold stage, 35%; hot stage, 320%.

**Figure 4.7.** Influence of cold strain rate (upper-left, in mm/min) (a) SEM micrographs and (b) DSC thermograms. Common uniaxial strain conditions: Cold stage, 35%; hot stage, 0.3 mm/min, 320%.

**Figure 4.8.** Influence of hot strain rate (upper-left, in mm/min) (a) SEM micrographs and (b) DSC thermograms. Common uniaxial strain conditions: Cold stage, 0.3 mm/min, 20% ; hot stage, 130%

**Figure 4.9.** Influence of cold strain extent (a) SEM micrographs and (b) DSC thermograms. Common uniaxial strain conditions: Cold stage, 1.0 mm/min; hot stage, 1.0 mm/min, 320%.

**Figure 4.10.** Influence of hot strain extent (a) SEM micrographs and (b) DSC thermograms. Common uniaxial strain conditions: Cold stage 0.3 mm/min, 20%; hot stage, 0.3 mm/min.

**Figure 4.11.** Isobutane permeability of some PP-HMw membranes as a function of (a) porous area and (b) average pore size. Each point refers to the following sequence: crosshead speed (cold), strain extent (cold), crosshead speed (hot), strain extent (hot).

**Figure 5.1.** Differential scanning calorimetry (DSC) thermograms of samples PP-HM<sub>w</sub> and PP-B extruded at different temperatures (250 and 270 °C), (a) precursor films, (b) annealed precursor films at 140 °C, (c) membranes (cold stage, 10 mm/min, 35%; hot stage, 10 mm/min, 230%).

**Figure 5.2.** (a) Crystalline and (b) amorphous orientation parameters derived from infrared measurements, and (c) crystallinity obtained from DSC thermograms of PP-HM<sub>w</sub> precursor films annealed at different temperatures. (Extrusion temperature: < ■ > 250 °C < ■ > 270 °C).

**Figure 5.3.** (a) Crystalline and (b) amorphous orientation parameters derived from infrared measurements, and (c) crystallinity obtained from DSC thermograms of PP-B precursor films annealed at different temperatures. (Extrusion temperature: < ■ > 250 °C < ■ > 270 °C).

**Figure 5.4.** Scanning electron microscopy (SEM) micrographs of samples PP-HM<sub>w</sub> and PP-B extruded at two different temperatures (250 and 270 °C).

**Figure 5.5.** DSC thermograms of polymer blends prepared with the PP random and block copolymers, (a) precursor films, (b) annealed precursor films at 140 °C, and (c) membranes (cold stage, 10 mm/min, 35%; hot stage, 10 mm/min, 230).

**Figure 5.6.** (a) Crystalline and (b) amorphous orientation parameters derived from infrared measurements, and (c) crystallinity obtained from DSC thermograms of random copolymer blends annealed at different temperatures. (< ■ > PP-5R < ■ > PP-10R < ■ > PP-20R).

**Figure 5.7.** SEM micrographs of the surface of the porous membranes prepared with the PP-10R blend at four different annealing temperatures.

**Figure 5.8.** DSC thermograms of samples prepared with the PP-10R blend and annealed at different temperatures. (a) Annealed precursor films and (b) membranes.

**Figure 5.9.** (a) Crystalline and (b) amorphous orientation parameters derived from infrared measurements, and (c) crystallinity obtained from DSC thermograms of heterophasic copolymer blends annealed at different temperatures. (< ■ > PP-5B < ■ > PP-10B < ■ > PP-20B).

**Figure 5.10.** SEM micrographs of the surface of the porous membranes prepared with the PP-20B blend at four different annealing temperatures.

**Figure 5.11.** DSC thermograms of samples prepared with the PP-20B blend and annealed at different temperatures. (a) annealed precursor films and (b) membranes.

**Figure 5.12.** Relationship between air permeability and (a) specific surface area, (b) pore volume, and (c) average pore diameter of polypropylene samples.

**Figure 5.13.** SEM micrographs of sample PP-20B. Precursor films annealed at 160 °C and stretched at three different temperatures during the second uniaxial stretching step.

**Figure 5.14.** Stress-strain curves of (a) PP-20B and (b) PP-10R precursor films annealed at four different temperatures.

**Figure 6.1.** (a) Crystalline and (b) amorphous orientation parameters derived from infrared measurements, and (c) crystallinity obtained from DSC thermograms of multilayer precursor films with different type of fillers (a) PP-C / HDPE and (b) PP-T / HDPE.

**Figure 6.2.** (■) Crystalline orientation parameter derived from infrared measurements and (■) crystallinity obtained from DSC thermograms of HDPE intermediate layer.

**Figure 6.3.** DSC heating thermograms for (a) mono and multi-layered unfilled films and (b) filled multi-layered composite membranes.

**Figure 6.4.** SEM micrographs of the surface of the monolayer porous membranes (a) HDPE and (b) PP-HM<sub>w</sub> (annealing at 130 °C).

**Figure 6.5.** SEM micrographs of the surface of the multi-layer porous membranes (PP/HDPE/PP) with different filler type and content (annealing at 130 °C).

**Figure 6.6.** SEM micrographs of the cross-section of the etched multilayer composite membranes. Thickness: 16 μm.

**Figure 6.7.** Relationship between permeability, porosity, and pore size of the composite multilayer membranes. (a) PP-T / HDPE and (b) PP-C / HDPE at different filler contents.

**Figure 6.8.** Relationship between air permeability and (a) BET specific surface area, (b) pore volume, and (c) average pore diameter of unfilled and filled multilayer membranes.

**Figure 6.9.** (a) TGA and (b) DTG curves of the thermal decomposition of different multi-layer porous membranes (1) PP/HDPE, (2) PP-5C/HDPE, (3) PP-10C/HDPE, (4) PP-5T/HDPE and (5) PP-10T/HDPE.

**Figure 6.10.** Young's modulus and Yield stress of the multilayer precursor films with different type of fillers (a) PP-C / HDPE and (b) PP-T / HDPE.

**Figure 6.11.** Tensile strength and Strain at break of the multilayer precursor films with different type of fillers (a) PP-C / HDPE and (b) PP-T / HDPE.

**Figure 6.12.** Young's modulus, Tensile strength and Strain at break of the multilayer membranes, containing different filler type and content < ■ > PP-C / HDPE < ■ ● > PP-T / HDPE.

**Figure A.1.** BJH (a) Adsorption and (b) Desorption dV/dD Pore Volume of the PP-HM<sub>w</sub>.

**Figure A.2.** BJH (a) Adsorption and (b) Desorption dV/dD Pore Volume of the PP-B.

**Figure A.3.** BJH (a) Adsorption and (b) Desorption dV/dD Pore Volume of the PP-10R.

**Figure A.4.** BJH (a) Adsorption and (b) Desorption dV/dD Pore Volume of the PP-20B.

**Figure A.5.** BJH (a) Adsorption and (b) Desorption dV/dD Pore Volume of the PP/HDPE.

**Figure A.6.** BJH (a) Adsorption and (b) Desorption dV/dD Pore Volume of the PP-5T/HDPE.

**Figure A.7.** BJH (a) Adsorption and (b) Desorption dV/dD Pore Volume of the PP-10T/HDPE.

**Figure A.8.** BJH (a) Adsorption and (b) Desorption dV/dD Pore Volume of the PP-5C/HDPE.

**Figure A.9.** BJH (a) Adsorption and (b) Desorption dV/dD Pore Volume of the PP-10C/HDPE.

## Tables

**Table 2.1.** The most common techniques used to prepare polymeric membranes. Images from [2,26].

**Table 3.1.** MFI values for the PP and HDPE resins studied.

**Table 3.2.** Polymer blends prepared in various weight percentages and nomenclature used in this study.

**Table 3.3.** Summary of the processing conditions used to produce precursor films.

**Table 4.1.** Polymer composition analysis in terms of membrane pore morphology and membrane permeability.

**Table 4.2.** Draw ratio analysis in terms of membrane pore morphology and permeability. Gap die, 1.9 mm; cold stage, 0.3 mm/min, 20% ; hot stage, 0.3 mm/min, 130%.

**Table 4.3.** Uniaxial strain analysis in terms of pore morphology and permeability. Gap die 1.9 mm; draw ratio 90.

**Table 5.1.** Characteristics of neat resins extruded and annealed at different temperatures in terms of pore morphology, and air permeability.

**Table 5.2.** Characteristics of membranes prepared with the PP random copolymer differing on blending ratio and annealing temperature.

**Table 5.3.** Characteristics of membranes prepared with the PP heterophasic copolymer differing on blending ratio and annealing temperature.

**Table 5.4.** BET specific surface area and BJH pore size distribution data report for samples with the highest values of measured air permeability. Precursor films annealed for 15 min at 160 °C.

**Table 5.5.** Characteristics of membranes prepared at different temperatures during the second uniaxial stretching step in terms of pore morphology and air permeability.

**Table 5.6.** Mechanical properties of PP-10R and PP-20B precursor films annealed at different temperatures.

**Table 5.7.** Mechanical properties of neat polypropylene and polypropylene-ethylene copolymers precursor films annealed at 140 °C

**Table 6.1.** Thermal properties of the monolayer neat PP and PP-C and PP-T composite precursor films.

**Table 6.2.** Porous structure characterization results of composite membranes with different filler type and content. Precursor films annealed for 15 min at two different temperatures

**Table 6.3.** BET specific surface area and BJH pore size distribution data report for composite membranes with different filler type and content. Precursor films annealed for 15 min at 130 °C.

**Table 6.4.** Thermogravimetric results of unfilled and filled PP/HDPE multi-layer porous membranes with different filler type and content.

# Glossary of symbols and abbreviations

## Glossary of symbols

$A \parallel$	Absorption parallel with respect to reference axes
$A \perp$	Absorption perpendicular with respect to reference axes
$D$	Dichroism ratio
$E$	Elastic modulus/Young's modulus
$f_c$	Crystalline orientation function
$f_a$	Amorphous orientation function
$f_{avg}$	Average orientation function
$n$	Avrami constant
$M^*$	Critical molecular weight for orientation
$M_n$	Number average molecular weight ( <i>kg/mol</i> )
$M_w$	Weight average molecular weight <i>peso</i> ( <i>kg/mol</i> )
$P$	Pressure (Pa)
$t$	Time (s)
$T$	Temperature (°C)
$T_g$	Glass transition temperature (°C)
$T_m$	Melting temperature (°C)
$T_c$	Crystallization temperature (°C)
$T_o$	Onset crystallization temperature (°C)
$X$	Degree of crystallinity (%)
$X_c$	Degree of crystallinity (%)
$\Delta T$	Supercooling (°C)
$\Delta H_C$	Crystallization enthalpy
$\Delta H_M$	Melting enthalpy
$\alpha$	Alpha crystal form
$\beta$	Beta crystal form
$\lambda$	Relaxation time
$\sigma_{max}$	Maximum stress
$v$	Volume of the absorbate in BET (mL)
$v_m$	Monolayer volume of the absorbate in BET (mL)
$w$	Weight fraction



## **Glossary of abbreviations**

BET	Brunauer–Emmett–Teller (specific surface area)
DR	Draw ratio
DSC	Differential Scanning Calorimetry
DTG	Derivative Thermogravimetry
EPR	Ethylene propylene rubber
FTIR	Fourier-transform infrared spectroscopy
HDPE	High density polyethylene
MFI	Melt flow index
MD	Machine direction
MEAUS	Melt extrusion annealing uniaxial-stretching
PP	Polypropylene
PE	Polyethylene
SEM	Scanning Electron Microscopy
TD	Transversal direction
TEM	Transmission electron microscopy
TGA	Thermal gravimetric analysis

**Chapter 1:**  
**Introduction**



## 1.1. Overview of membrane technology and its applications

In its simplest form, a membrane consists of a thin sheet of material that selectively separates or moderates the transport of chemical species through the pores or channels and is usually intended for separation purposes in some laboratories or industries. Many different types of porous membranes can be used in a wide variety of separation processes. Differences in chemical and physical properties enable applications ranging from industrial separation processes such as wastewater treatment and battery separators to medical applications such as artificial organs and drug delivery devices. Industrial applications for polymeric membranes, also known as organic membranes, include seven main groups depending on separator characteristics: microfiltration, ultrafiltration, nanofiltration, reverse osmosis, gas separation, pervaporation, and electro dialysis. Pharmaceutical and medical applications include artificial kidneys, blood oxygenators, and controlled release of pharmaceutical materials [2].

Membrane separation processes are often classified according to the pore size and the separation driving force. The membrane structures can be divided into symmetric (i.e., uniform pores across the entire thickness) and asymmetric (i.e., variable pore diameters). The two models used to describe the mechanism of permeation of species through these barrier membranes are the pore-flow model, in which a pressure gradient over the membrane is assumed to be the main driving force for a flow transport of permeants within the pores, and the solution-diffusion model, in which molecules are dissolved in the membrane material, transported by a diffusive mechanism, and desorbed on the permeate side [2].

It is evident from the literature that there exist several membrane preparation methods to prepare polymer separators subjected to wet and dry conditions. The first (wet) refers to the phase separation technique, also called phase inversion, which consists of preparing a liquid polymer solution and precipitating it to form a solid, polymer-rich phase that forms the pore network of the membrane. The membrane structure is highly dependent on the type of polymer employed, the solvent used to dissolve the polymer, and techniques involving precipitation of the casting solution. These techniques include precipitation by controlled solvent evaporation, immersion in a non-solvent bath, absorption from vapour phase, and precipitation by cooling (thermally induced phase separation). One of the major methods for preparing asymmetric membranes is the Loeb–Sourirajan process, in which precipitation of a casting polymer solution is produced by immersion in water. Other membrane processes that require the use of solvents encompass track-etching and template leaching techniques.

Recently, dry stretch methods have been developed to reduce solvent consumption and waste generation. Void nucleation and growth can occur by four different mechanisms in the stretched

samples: interface separation between immiscible polymer blends, stress-induced polymorphic transitions in crystalline polymers, debonding of particle/matrix interfaces in mineral particle filled polymers, and the separation of the uniform lamellar structure after uniaxial stretching [2].

Production of microporous membranes using the uniaxial stretching method involves three consecutive stages: (1) film extrusion, where the polymer melt is extruded under appropriate conditions to achieve a stacked lamellar morphology (row-nucleated structure) resulting from stress-induced crystallization, (2) thermal annealing to achieve a near-perfect crystalline phase and lamellar thickening, and (3) uniaxial stretching, where the films are deformed along the machine direction, in a test similar to the tensile test, first at room temperature to generate pores and then stretching of the films at a high temperature to enlarge the pore size by increasing lamellar separation. The significance of the morphological characteristics and the state of orientation of the extruded precursor films upon the final pore structure have been highlighted in many studies [4-21].

Blow and cast film extrusion are the most common methods in film production. The principal advantages of cast films overblown films are: (1) can be produced at higher productions rates, (2) have better gauge uniformity (thickness distribution in the machine direction is more uniform), and (3) the cooling of the film is improved efficiently by air supplied from both sides to the cast films leading to a more uniform lamellar structure [4,12]. The critical process parameters that need to be controlled to generate a highly oriented morphology (row structure of planar lamellae) include the extrusion temperature, incoming line speed, draw ratio and draw distance, and the use of air conditioning systems. The literature suggests that high enough extensional strain rates, cooling of the film at a short distance from the die exit, and the reduced film thickness by going to a higher draw ratio lead to crystalline structures that can form porous membranes [4-12].

Other main factors influencing the flow-induced crystallization behavior are the resin characteristics, including the weight average molecular weight, the molecular weight distribution, branching degree, and the degree of stereoregularity. Common materials in the production of stretched membranes comprise semicrystalline polymers such as polyethylene (PE), isotactic polypropylene (iPP), isotactic poly(4-methyl-1-pentene) (PMP), polyoxymethylene (POM), Poly(tetrafluoroethylene) (PTFE) and poly(vinylidene fluoride) (PVDF) [2]. Nowadays, many companies produce porous membranes by uniaxial and biaxial stretching methods, e.g., Gore-Tex is the registered trademark of W. L. Gore and Associates (1969) for a biaxially stretched porous film of PTFE widely used as a breathable and waterproof membrane [2]. Other examples are the production of hollow fibers for blood oxygenator equipment and membrane contactors (e.g., wastewater treatment) and separators in lithium batteries. In this last application, polyolefin uniaxial stretched membranes played an important role in battery safety.

Celgard is a global leader in the development and production of PP and PE membrane separators. Bilayer and trilayer separators of PP/PE are developed to restrict thermal reactions in batteries when these are accidentally overcharged. Due to the differences in melting temperature between PE and PP, when temperature increases the PE layer can shut down the cell current by closing the pores, physically preventing ion flow between the electrodes. On the other hand, the PP external layers still retain good dimensional integrity because of the high melting point of PP. Porous polyolefin membranes covered by a porous ceramic layer are also currently being used in the industry. These ceramic coatings have excellent dimensional integrity at elevated temperatures due to its lower thermal expansion coefficient [1,2,24,25].

## **1.2. Aims and scope of the work**

The present thesis has been carried out in the doctorate program frame on "Materials Science and Metallurgical Engineering" at the Polytechnic University of Catalonia, Barcelona, Spain. This research work originates from a collaboration project between science and industry, in which the customer needed to obtain the required knowledge for manufacturing polyolefin membranes by a dry-stretch process. In an early stage of this project, it was necessary to adapt and improve the machinery (the extrusion calendering line) to accomplish the optimum characteristics for the precursor films of semicrystalline polymers capable of forming porous membranes via the MEAUS methodology.

This dissertation is divided into five chapters. To help the readers acquire and deeply understand the fundamental notions related to the MEAUS process, Chapter 2 presents a literature review of previous works on the fabrication of membranes and the most critical factors affecting the three major processing variables (extrusion, annealing and uniaxial stretching). Chapter 3 describes the materials and the experimental procedure utilized in this project to accomplish the three main aims of this dissertation. The results are introduced and discussed in Chapters 4, 5, and 6.

One of the aims of the present work was to investigate the influence of the composition of the polymer matrix and the architecture structure on the row-nucleated lamellar crystallization by using two linear polypropylenes, PPs, having different molecular weights, and blending with branched and very fluid PP resins. Some researchers have investigated the fabrication of microporous membranes derived from blends of polypropylenes with different molecular weights and different low molecular weight tail contents [4-8,27]. For this investigation, it has used an extremely fluid polypropylene to achieve a greater strain extent during the extrusion and the uniaxial strain stage. To complete this study, it was also performed a detailed investigation of the impact that

have all the variables on the uniaxial stretching stages (both at room and high temperatures) and can be related to structural changes produced in the porous morphology. In some cases, it was used high values of strain rate (up to 50 mm/min) and strain extents (up to 300% elongation) than what is usually applied.

In Chapter 5, different blends of a suitable linear polypropylene with heterophasic and random copolymers of polypropylene-ethylene were prepared. The influence of polymeric composition on membranes prepared through the MEAUS technique was evaluated, as well. Blends of these copolymers were prepared with the main purpose of producing homogeneous porous membranes, increasing, at the same time, the pore size and pore size distribution. Samples from neat resins and their blends were produced at a constant draw ratio using different extrusion temperatures. Then, during the annealing and stretching steps, various temperatures were used to study the influence of this variable in the development of porous morphology, using, in some cases, high values close to the melting point of the PP resins. A detailed investigation to find a close relationship between crystalline features, porous morphology, permeability, and thermal and mechanical stability was also performed.

Chapter 6 focused on producing thin multilayer membranes composed of three layers, HDPE as the middle layer and blends of PP and inorganic fillers (calcium carbonate and talc) as outside layers. These types of fillers have never been used before to manufacture multilayer membranes using the MEAUS technique. We hypothesized that this well-known filler, employed in the industry to improve base polymer properties, would lead to changes in the crystalline structure, thermal stability, and mechanical and permeability properties of the porous membranes. The generation of pores during the uniaxial stretching stages, with the debonding mechanisms of mineral fillers from the polymeric matrix, could have a synergistic effect in forming bigger pores. Furthermore, the influence of annealing and stretching temperatures in these composite membranes was also investigated. Finally, Chapter 7 summarizes the major contributions of this thesis and suggests some future directions for research.

## **Chapter 2:**

### **Theoretical literature review**





## 2.1. Classification of synthetic membranes

A membrane can be described as a selective barrier that moderates the mass transfer between two phases. The permeation rate across the phase interface depends upon the physical and chemical properties of the separator. Membranes can be classified according to different characteristics such as the material used (organic and inorganic), their structure or morphology, and the pore size.

Polymers are still the most popular materials used to develop membranes that meet the requirements of different applications. However, ceramic and metallic separators are becoming commercially available and have found significant industrial applications due to their thermal stability, mechanical properties, and good resistance to solvents and chemicals. If the following discussion restricts itself to membranes made from synthetic organic polymers, there are two general categories of membrane types depending on their pore structure, as is depicted in Figure 2.1.

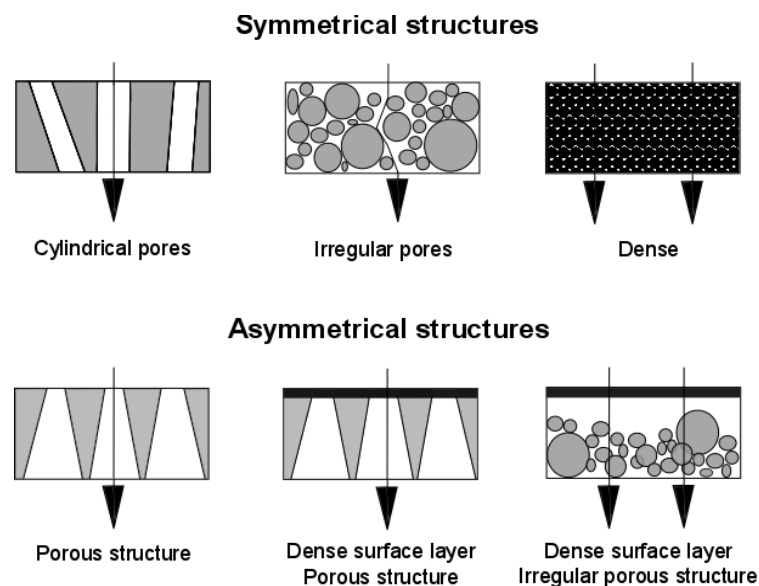


Figure 2.1. Classification of synthetic polymer membranes based on their structure. Modified from [2].

The isotropic membranes (symmetrical structure) possess a uniform structure throughout the entire membrane thickness and can be classified into two groups: porous membranes and non-porous (dense) membranes [2]. Most porous materials of interest consist of regular networks of cylindrical pores or irregular interconnected porous network with pore sizes ranging from 0.01 to 10  $\mu\text{m}$ . Thus, separation of solutes using microporous membranes is mainly a function of pore

interconnectivity, porosity, and pore size distribution. As a general rule, only permeants with a considerably different size may be effectively separated. On the other hand, dense membranes have no open pore structure and their separation performance is associated with diffusion phenomena. The rate of molecular diffusion is intimately connected to the diffusivity and solubility of the components into the membrane material. This symmetrical structure can selectively separate molecules of similar size as long as the permeate solute concentration difference may be large enough to facilitate mass transport within the membrane [2].

Anisotropic membranes (asymmetrical structure) are layered structures made up of one surface layer, which is extremely thin compared with the total film thickness. This surface layer is supported on a porous substructure thick enough to provide mechanical support. In composite membranes, the skin and core materials can be different polymers and may be formed in a single operation or separately. Permeation rates of the membrane will be determined exclusively by the skin layer [2].

Different industrial membrane separation processes have been developed considering the pore size filters. The difference between the solution-diffusion and pore-flow mechanisms lies in the relative size and permanence of the pores [2]. This is schematically depicted in Figure 2.2.

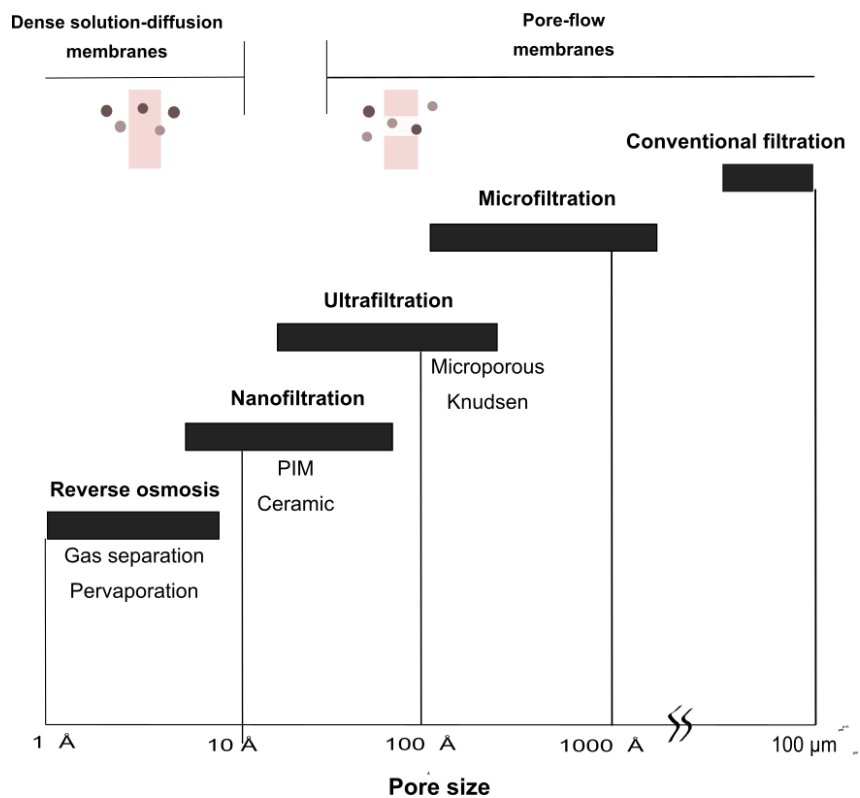


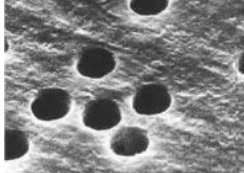
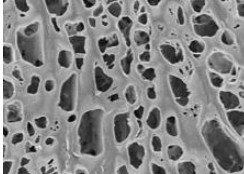
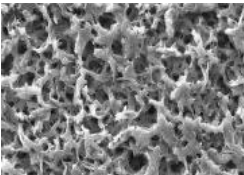
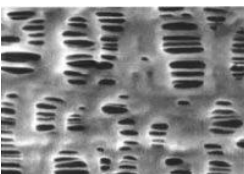
**Figure 2.2. Separation processes differing in the values of mean pore size. Modified from [2].**

Transport across the porous membrane in microfiltration, ultrafiltration, and microporous Knudsen diffusion gas separation membranes processes occur by a pore flow model. Reverse osmosis, pervaporation, and polymeric gas separation membranes generally have pores of very small diameters, between 2–5 Å. These membranes follow the solution-diffusion models for mass transfer, in which the flux of permeant moving through the film is much lower than microporous membranes. A third group of membranes containing pores sizes between 5 and 15 Å exhibit intermediate, including the nanofiltration process, some gas separation membranes such as the polymers with intrinsic microporosity (PIM) ceramic, or carbonized polymer membranes. The International Union of Pure and Applied Chemistry (IUPAC) also provides another classification based on the characteristic pore sizes: macropores with sizes over 50 nm, mesopores with sizes between 2 nm and 50 nm, and micropores with sizes less than 2 nm [2,25].

## 2.2. Membrane fabrication processes

Several processing technologies have been used in the industry to produce polymeric symmetric and asymmetric membranes. Table 2.1 summarizes the most important production techniques for manufacturing membranes. Below, a brief synopsis of each method is given before the in-depth discussion of the specific process studied in this research project.

**Table 2.1. The most common techniques used to prepare polymeric membranes. Images from [2, 26].**

Method	SEM images
Track-etching	
Template leaching	
Phase separation	
Stretching	

In the track-etching method, a polymeric film is irradiated to break some polymer chains and create tracks before immersing the sample in a suitable acid solution. The susceptibility of these tracks is higher, leading to the formation of membranes with cylindrical pores and a tortuosity factor close to one along to the entire thickness [2]. Microporous membranes are also produced via template leaching. This method is based on cast extrusion of mixtures of polymer film and leachable components. The removal of the leachable component using a suitable solvent originates the pore formation. Sintering is a method where a powder of polymeric particles is compressed and sintered just below the polymer melting point. The pore size obtained in this type of membranes depends mainly on the particle size of the powder.

The phase separation membranes include anisotropic membranes in which a liquid polymer solution is precipitated into two phases: a continuous solid polymer-rich phase, and a liquid polymer-poor phase that forms the pores in the solid [2]. There are several procedures to promote precipitation of the cast liquid polymer solution. In one of the most important techniques in membrane technology, the Loeb-Sourirajan method, the precipitation occurs by immersion in a bath of water. The polymer precipitates forming the anisotropic layered structure where the membrane structure changes from the top (dense layer) to the bottom (microporous layer). Polymer solutions based on this method precipitate rapidly forming a dense selective layer. A subsequent slow water diffusion into the solution leads to a more slowly polymer precipitation, and consequently, a more porous substructure is formed just below the dense surface skin. An example of the phase separation membranes developed in terms of research and commercial production industry (the Loeb-Sourirajan water precipitation method) is shown in Figure 2.3.

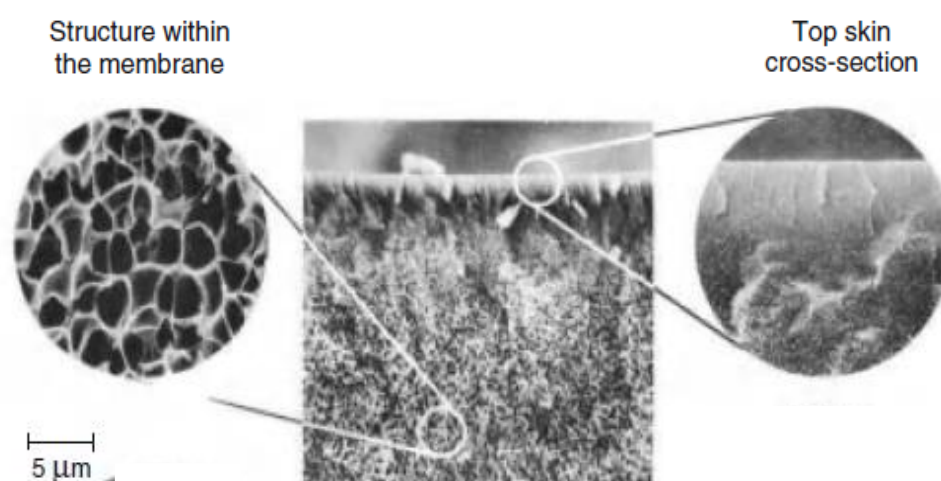


**Figure 2.3. SEM images of the cross section of aromatic polyamide made by the Loeb-Sourirajan technique. Reprinted from [2].**

The precipitation of cast liquid polymer solution to form a solid anisotropic membrane can also be achieved in other ways: (1) by absorption of water from a humid atmosphere, (2) by thermally induced phase separation (TIPS) where a hot solution is precipitated during cooling, and (3) after casting, by evaporating the solvent at room temperature to obtain a thin, uniform polymer film. In the development of anisotropic membranes, many combinations of these processes have been reported [2].

There exist other processes to produce symmetric microporous membranes that do not involve the use of solvents. The savings in safety and cost associated with reducing the use of solvents is possible with methods based on stretching. Figure 2.4 summarizes the most important production techniques for manufacturing membranes through stretching methods.

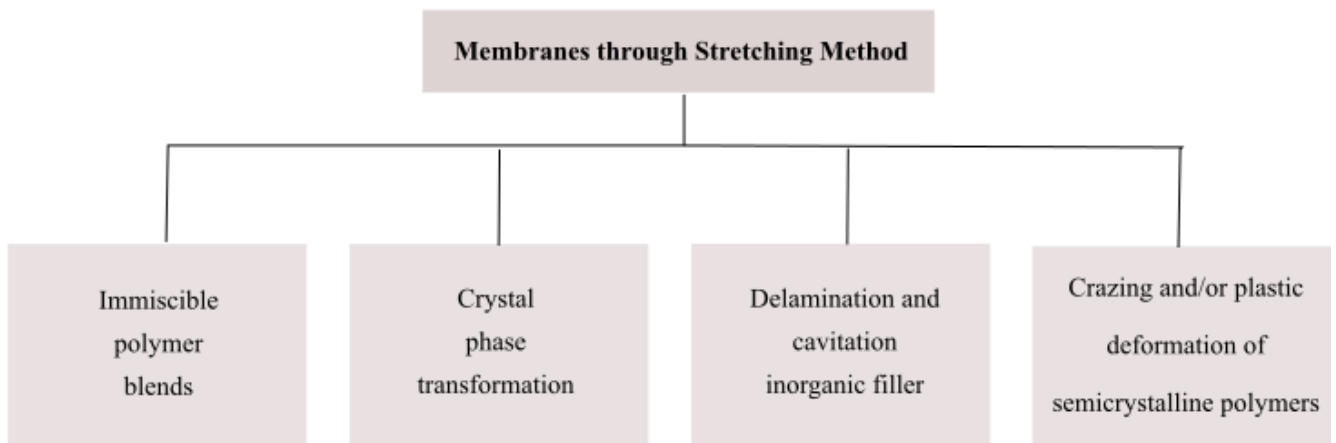


**Figure 2.4. Different stretching procedures to develop symmetric porous membranes [2,27-29, 41-77].**

The stretching of immiscible polymer blends followed by post extrusion treatments allows obtaining porous films that show pore size and degree of porosity similar to those of phase separation membranes. A large variety of thermoplastic polymers with different physical and chemical properties can produce membrane composites with enhanced properties. Chandavasu et al. [27] employed a finite element modeling to study the stretching effect on immiscible binary polypropylene blends. These blends were first compounded in a co-rotating twin-screw extruder and subsequently uniaxially stretched below the glass transition temperature of the minor phase. Microcracks were nucleated and grown at the interface between the two phases, in which the stress concentration was higher. The resulting pore structure depended on the stretching conditions applied, the type, concentration, and degree of dispersion of the minor phase.

Stretching of polymer films with different types of crystal phase is another way to produce a porous membrane. In polypropylene, the  $\beta$  crystalline structure is considered a metastable phase and it has been found to transform into a stable  $\alpha$  crystalline form when it is stretched under a range of specific conditions. The addition of some specific nucleating agents can generate a sufficient amount of  $\beta$ -crystals to form porous structures. The initial pore structure results from the nucleation of voids, owing to a lower density of beta crystals that under applied stress at elevated temperature causes volume contraction between lamellae during phase transformation. Recent studies showed that pore formation upon stretching of  $\beta$ -iPP films is also accompanied by both the crystal slip by pure shearing stress and the cavitation mechanism resulting from the separation between  $\beta$ -lamellae and the surrounded areas amorphous phase. Offord et al. [28,29] produced microporous polymer membranes by extrusion, thermal annealing, and biaxial stretching. They concluded that appropriate post-extrusion annealing was the most important factor in ensuring the growth of stable  $\beta$  crystals. This causes an increase in the porosity of the extruded films.

The stretching of filled polymer films is also a useful technique to prepare porous membranes. Thermoplastic polymers can be blended with a wide range of minerals particles to reduce cost and improve mechanical, thermal stability, and other physicochemical properties such as conductivities or hydrophilic surface characteristics. Therefore, their addition is an effective way of enhancing membrane performance. More recent studies have focused on polymer nanocomposites for the development of improved separators. This is due to the ultra-large interfacial area per unit volume between the nanoparticle and the polymer matrix that can be accomplished [41]. Uniaxial and biaxial stretching of extruded polymer composites causes the formation of pores at the interface between the rigid filler particles and the polymer matrix. As could be expected, the final properties of the membranes depend on the type of polymer, filler nature, filler shape and size, and the filler content and the level of dispersion achieved. To obtain a uniform distribution of filler particles some matrix-filler interactions are required. For this reason, an effective surface treatment with the incorporation of coupling agents on the filler surface prevents agglomeration as well as the reliable control of process parameters during extrusion [41-70].

Nakamura and Nago [45,51] prepared microporous polypropylene sheets with an inorganic filler ( $\text{CaCO}_3$ ) by extrusion and biaxial stretching. They established a relationship between the particle size of the filler and the porous structure. Research shows that using smaller particle size fillers leads to low tortuosity, small pore size, and higher porosity. Other recent studies explored the influence of process parameters such as drawing temperature, stretching ratio, and strain rate on development of composite membranes by stretching. When the drawing temperature is relatively low and the strain rates high, a local cavitation mechanism and debonding of particles from the polymer matrix is the basic pore-forming mechanism. Contrarily, at low strain rates and elevated

temperatures, local shear yielding play a dominating role in determining the theory of pore formation in the extruded composite films.

Alternative methods to develop porous membranes are based on the plastic deformation of semicrystalline polymers (i.e., the deformation of both spherulitic and row nucleated structures). The membrane fabrication involves three main stages: precursor film extrusion, annealing, and uniaxial stretching.

Polymers crystallized from melt in spherulites can create microporous membranes by lamellar separation in the intra- and inter-spherulitic regions. The influence of process conditions in both deformation mechanisms was investigated by Lin K et al. [71]. Their study concluded that a cold-drawn behavior related to the intra-spherulitic deformation was shown in the non-annealed sample due to catastrophic failure, orientation, and close packing of chains. Contrary, an inter-spherulitic deformation was favored by annealing the samples at 140 °C, which strengthened the lamellar structure leading to lamellar separation (initial pore formation). The higher extension ratio decreased the porosity of the annealed samples. It promoted the orientation of spherulites, which implied intra-spherulitic deformation at the late stage of stretching. Regarding the effect of the stretching rate, inter-spherulitic deformation was found with films prepared at lower extension rates, while faster stretch rates result in more significant intra-spherulitic deformation. The effect of stretching temperature was also investigated, and the authors confirmed the presence of a rigid amorphous fraction (RAF) within the spherulitic structure. Concerning the non-annealed samples, the RAF alone was not strong enough to maintain the morphology, and the sample exhibited a cold-drawing behavior, which significantly reduced the pore formation. However, for the annealed samples, the RAF and the strong and more uniform lamellae structure were sufficiently high enough to avoid the possibility of oriented lamellae break; as a result, inter-spherulitic deformation was observed. At higher stretching temperatures, the entire amorphous region was flexible, and the RAF effect was minimized. However, the strengthened annealed lamellae were still able to orient without catastrophic cold-drawn deformation.

Other advances in membrane technology made it possible to develop membrane separators based on the uniaxial stretching of precursor films with appropriate stacked lamellar structure (row-nucleated lamellar morphology). Since the main objective of this thesis is to create polyolefin microporous membranes using this stretching technique, the aim of this chapter is to provide enough information regarding the subject matter covered. This method, commonly called MEAUS (melt extrusion/annealing/uniaxial stretching), was established in the mid-1960s by the Celanese Corporation under the trade name of Celgard® [2,72-77]. The technique can be described as three consecutive stages which are carried out to initiate the pore formation: (1) Melt extrusion of a precursor film with a row-nucleated lamellar structure (molten polymer chains are subjected to



shear or elongation flow fields), (2) Annealing of the film to increase the lamellar thickness and remove irregularities, and (3) Stretching of the annealed film at room and high temperature to create pores and enlarge their size [1-21,27-40].

### **2.3. Flow induced crystallization**

A general discussion of the formation of flow-induced crystallization precursor structures in polymer melts and solutions will first be addressed. The crystallization induced by orientation in polymer solutions produces a so-called “shish-kebabs” structure. First, a central core of the lamellar-fibrous structure (the shish) is formed parallel to the strain direction. Then, from the surface of oriented shish, secondary epitaxial nucleation promotes that many lamellar crystals (the kebabs) grow radially outwards [78-102]. A similar structure is formed during injection molding and extrusion processes when the polymer melt is subjected to high shear and elongational flows and different pressure and cooling conditions. This structure is commonly referred to as the row-nucleated structure. A schematic representation of row-nucleated structure formation via flow-induced crystallization is presented in Figure 2.5.

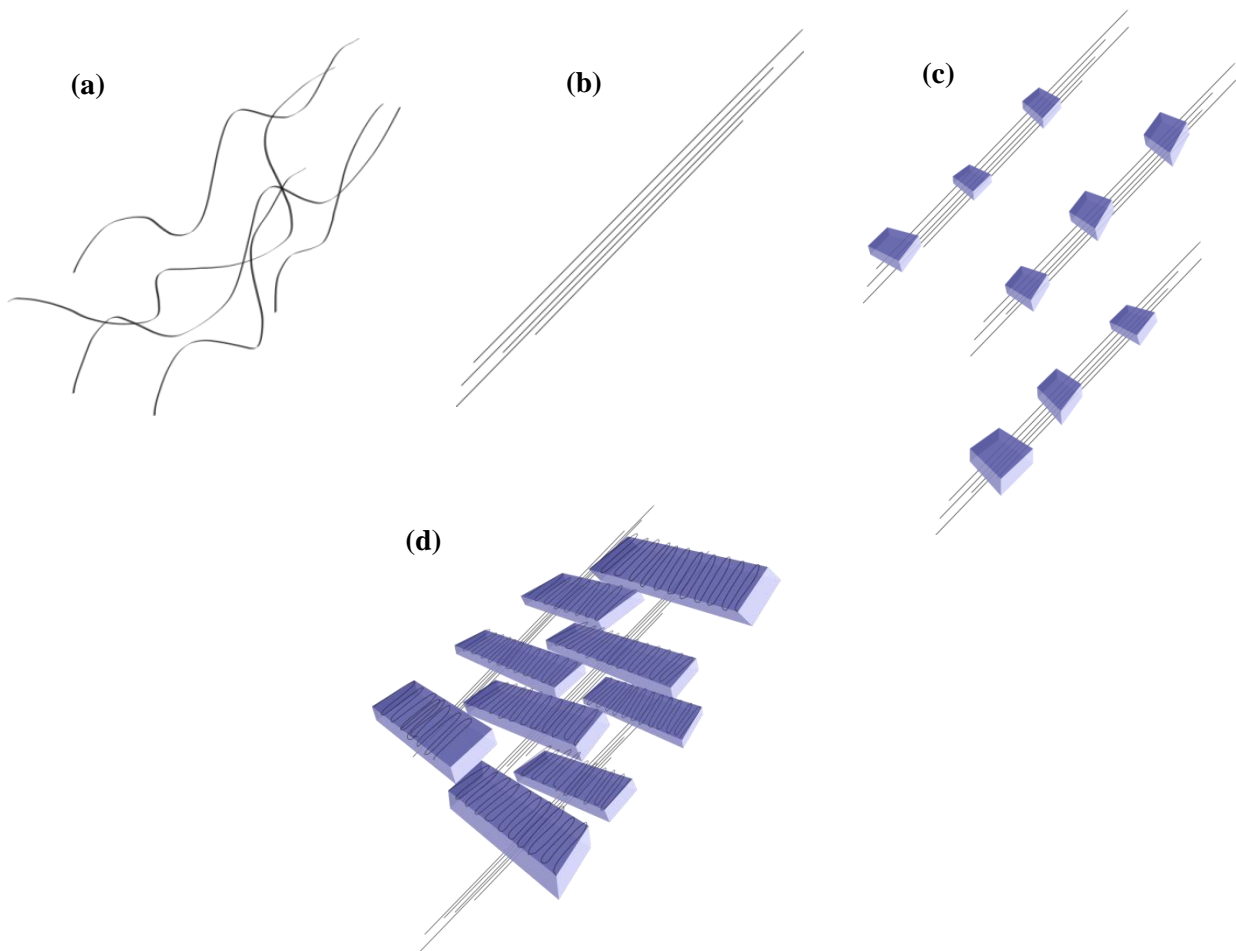


**Figure 2.5. Schematic diagrams representing the flow-induced crystallization in semicrystalline polymers.**

Long fibrous crystals (row nuclei) are formed when polymer melts are subjected to shear and extensional flow. These primary nuclei are oriented parallel to the flow direction and can act as nucleation promoters for later lamellae crystallization (Figure 2.5a-c). This lamellar overgrowth consists of stacks formed by the folding of chains, which are oriented perpendicular to the strain direction (Figure 2.5d). According to Keller et al [78], these structures consist of alternating sequences of crystalline-amorphous regions with interlamellar tie chains connecting adjacent crystal lamellae. These authors also proposed two morphological models related to the level of stress applied (Figure 2.6). Row-nucleated structures with twisted lamellae are produced under low-stress conditions, while planar or flat crystal structures (not twisted lamellae) are often observed to occur when high stresses are applied during processing.

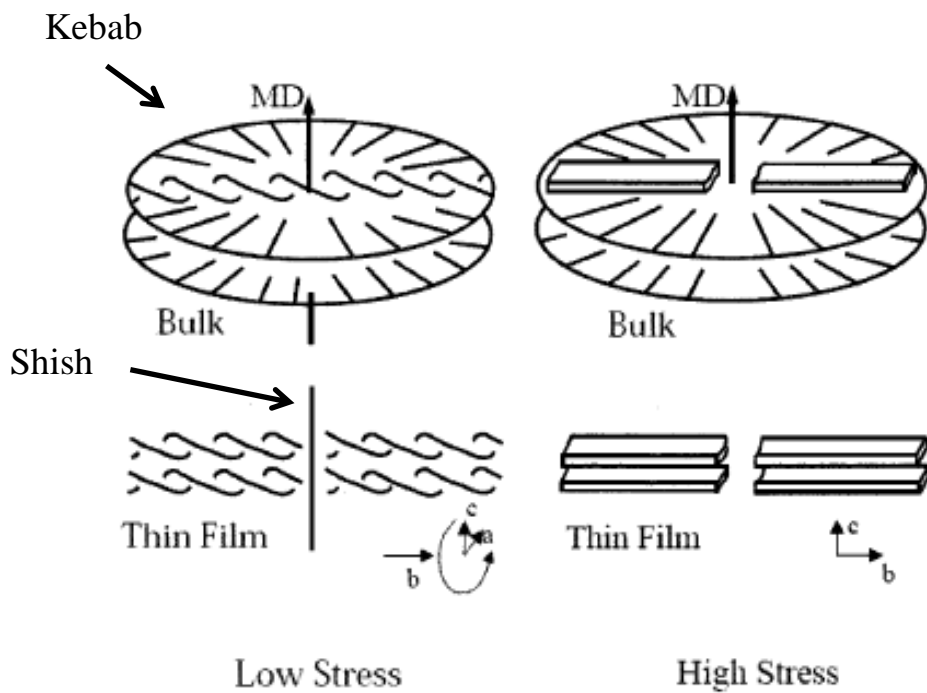
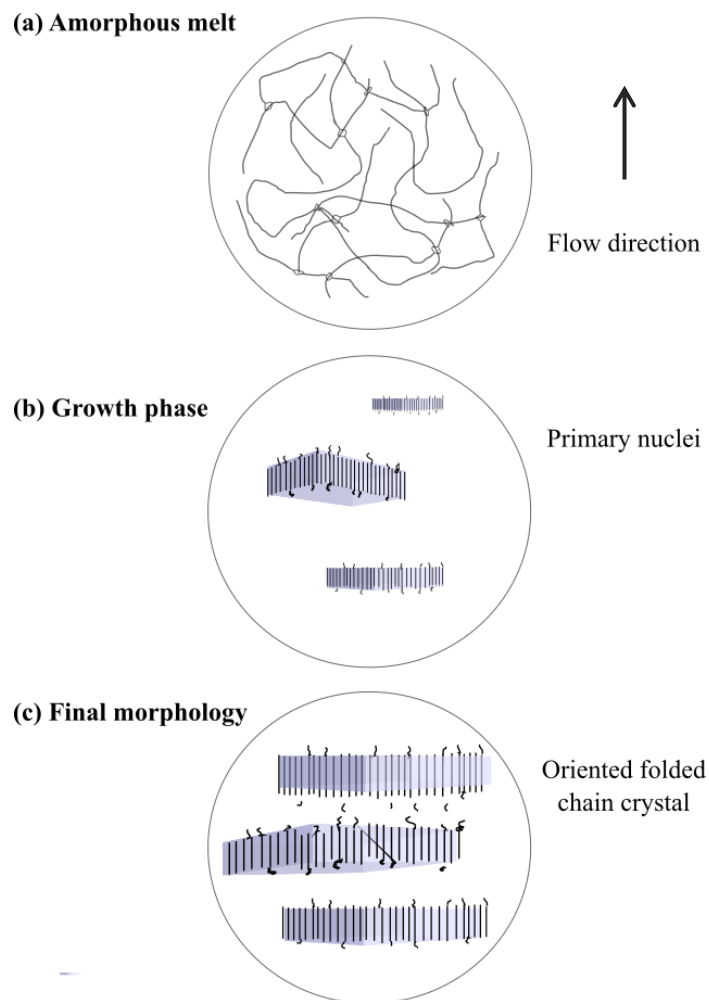


Figure 2.6. Schematic of the types of row-nucleated structure under (a) low stress and (b) high stress proposed by Keller and Machin. Image from [78].

Somani et al. [79-83] studied the shear-induced crystallization of isotactic polypropylene (i-PP). Based on their results of SAXS patterns and TEM micrographs, they proposed a schematic depicting the flow-induced alignment of molecular chains upon the imposition of a step shear rate. This is schematically illustrated in Figure 2.7. The amorphous chains assume a random coil conformation before an external flow field can orient the molecular chains in the flow direction (Figure 2.7a). When a shear rate is imposed on the polymer molecules, primary crystal nuclei are formed as a cluster of aligned chain segments or microfibrillar bundles (Figure 2.7b). These structures promote the radial growth of oriented folded chain lamellae that fill the space perpendicular to the row nuclei (secondary nucleation). The fully crystallized polymer has a stacked lamellar morphology when viewed perpendicular to the flow direction (Figure 2.7c).



**Figure 2.7. (a) Initial morphology before shear, (b) upon the imposition of a step shear rate, and (c) final morphology after cessation of shear. Schematics of the shear-induced primary nuclei and subsequent lateral crystal growth proposed by Somani et al. Modified from [82].**

The authors presented this microstructural model for forming the primary microfibrillar structure and the growth of stacked lamellae. However, based on their TEM and SAXS data, direct evidence of primary crystal nuclei (row nuclei) was not found. The interpretation of these results was that initially extended chain structures can be formed either by a cluster of oriented chains, visible by TEM or SAXS or by some singular extended chain or tiny primary nuclei, challenging to be identified through these characterization techniques [82]. On the other hand, the authors stated that the stability of the induced oriented structures depends on the polymer relaxation rate. In turn, it depends on the molecular weight and molecular weight distribution. Under isothermal conditions, longer chains take a longer time to relax, and after shearing, it is easier than these chains remain more oriented than the shorter ones. In polymer with broad molecular weight distribution, after application of a constant shear rate, longer chains would be potentially crystallizable in a primary nuclei form (bundles of oriented chains). Furthermore, the degree of orientation and stability of these primary structures depends on both shear rate and shear strain. The shear rate must be high enough to increase chain orientation for the subsequent crystallization events.

There exists a relationship between the critical shear rate and the molecular weight in the flow-induced crystallization, as first proposed by Keller et al. [78]:

$$\varepsilon_c = M^{-\beta} \quad (1)$$

where  $\varepsilon_c$  is the critical elongational rate,  $M$  is the critical molecular weight, and  $\beta$  is a factor equal to 1.5 for polyethylene solutions. Somani et al. [82] proposed a similar relationship to explain the results obtained in their samples. They defined a critical orientation molecular weight ( $M^*$ ) above which only some molecules can be oriented and form stable primary nuclei.

$$M^* = K\gamma^{-\alpha} \quad (2)$$

where  $\gamma$  is the shear rate,  $K$  a proportionality constant, and  $\alpha$  is the exponent proportional to  $1/\beta$  (eq. 1).

Figure 2.8 shows a typical molecular weight distribution curve for a polymeric material. It also shows how the critical orientation molecular weight may vary as a function of the shear rate applied. The longer chains with long relaxation times will be oriented (line 1 in Figure 2.8 represented the  $M^*$  value) only at low  $\gamma$  values. Increment of  $\gamma$  does not lead to an increased chain extension but positively influences the polymer chain that can be oriented. This will shift the critical orientation  $M^*$  value to the left in the MWD curve (line 2 in Figure 2.8). However, authors also state that in practice, some restrictions are due to the lower relaxation time of the shortest polymers chains that cannot form an oriented structure after shearing. Thus, there exists limiting value for

the critical orientation molecular weight below which not all molecular chains can be aligned in the flow direction to form stable oriented structures, even if high shear rates are applied.

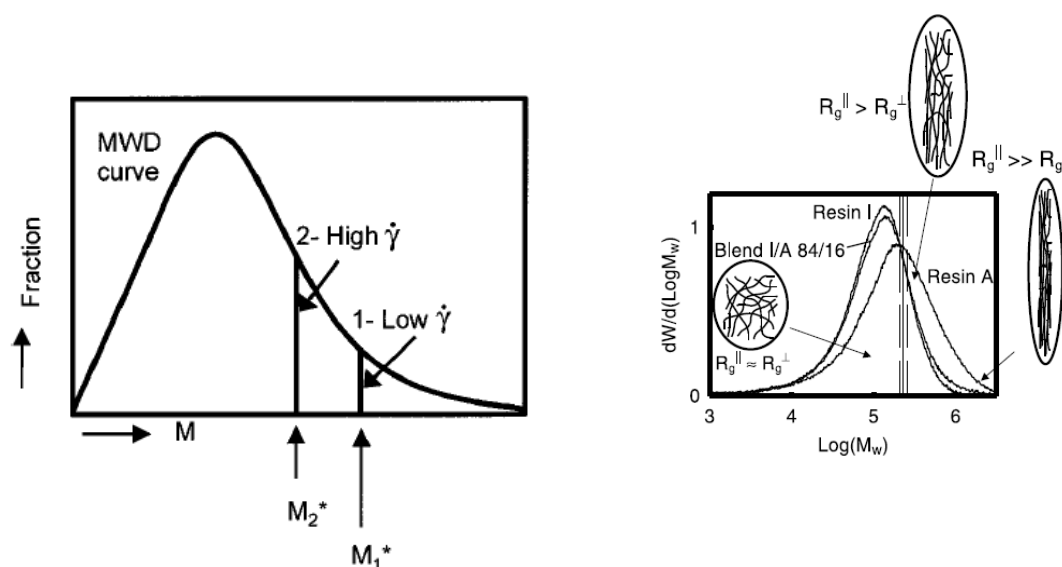


**Figure 2.8. Determination of the critical orientation molecular weight ( $M^*$ ) as a function of the imposed shear conditions for a typical molecular weight distribution curve. Image from [82].**

In another study, Somani and co-authors [80] tried to probe the nature of primary nuclei in sheared isotactic polypropylene (iPP) using the same characterization instruments (SAXS and WAXS techniques). Furthermore, a kinetic study on the crystallization of the blends of i-PP with a high molecular weight atactic polypropylene (aPP) was carried out to evaluate the formation of oriented structures. Their results pointed toward the formation of primary nuclei made up of liquid-crystalline or mesomorphic bundle of oriented stems (oriented chain segments). As a result of self-nucleation phenomena, stable primary crystal nuclei can be formed when a certain number of stems group together, while oriented segments that cannot form stable nuclei and increase in size return to a random coil conformation. Concerning polypropylene blends, authors confirmed that the relaxation time of the low-molecular-weight iPP was influenced mainly by the presence of the aPP polymer, which was significantly more likely to be oriented owing to its high molecular weight. They suggest that the long oriented chains of high-molecular-weight aPP can interact with the oriented chain segments of iPP, preventing the aligned molecules from relaxing after shearing. Thus, due to the presence of aPP in the blend, a larger number of oriented stems of iPP are available to develop stable primary nuclei compared to neat iPP polymer.

Seki and co-authors [85] also proposed a theoretical model to explain the role of long chains in shear-induced crystallization. This was done by blending two polypropylenes with different

molecular weights (Figure 2.9). According to the referenced model, in the initial stage of crystallization under shear flow "pointlike" precursors are formed, which under sustained shearing lead to the formation of oriented row nuclei (threadlike precursor). Long chains (high molecular weight) interact with the surface of pointlike precursors and become elongated due to sustained shear stresses (Figure 2.9a). If an increased number of polymer chains may become tethered to the pointlike precursor, many oriented chain segments on both sides of the primary nuclei surface are formed (Figure 2.9b-c). The strong orientation enhances the longitudinal growth rate of nucleating fibrils (threadlike structure), which promotes the lateral lamellar growth after cessation of shearing (Figure 2.9d). Authors stated that the rate of formation of pointlike precursors was mainly controlled by the local stress (average level of segmental orientation), not so much because of the presence of long chains. The results demonstrated that the addition of high-molecular-weight components greatly enhances the formation of threadlike precursors. The longer the molecular length, the greater the molecular orientation. This is due to the long relaxation times, which might put long chains in a preferred state for being threaded on the precursor surface. Furthermore, orientation can be influenced by the multi-body interaction between long-chain "streamers". The degree of orientation of the resulting "streamers" will be higher if a little chain entanglement is produced with surrounding long chains that are being swept along by the flow.

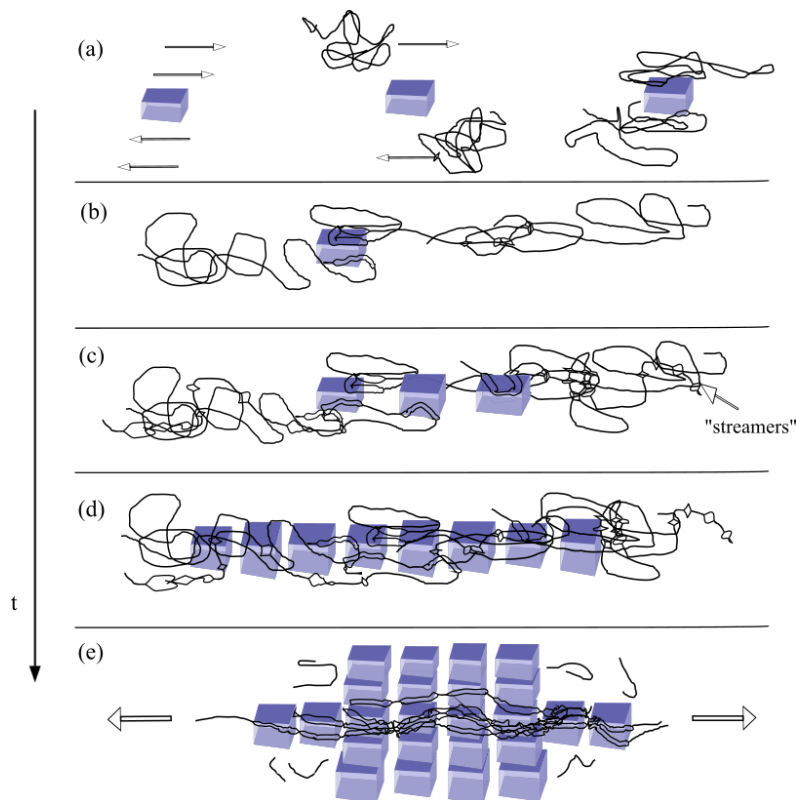


**Figure 2.9. Schematic representation of the primary nucleation and subsequent growth of stacked crystalline lamellae in shear-induced crystallization. Modified from [85].**

Agarwal et al. [84] studied the flow-induced crystallization of long-chain branching polypropylene (LCB-iPP). The WAXD and SAXS results demonstrated that the branched polymers acquire a highly oriented crystal structure during primary crystal nuclei formation. For the LCB-iPP polymers prepared in this study, the highly branched species reside at the high molecular weight part of the distribution. Thus, since the rate of polymer relaxation is a function of its molecular characteristics such as the high molecular weight, for the highly branched molecules, a high degree of orientation was retained because of the long relaxation times. The improved crystallization kinetics in the branched polymers was attributed to an increase in the amount of stable primary crystal nuclei with a high orientation level. Using the Avrami model, the authors obtained qualitative information about crystal growth geometry:

$$1 - X_r = e^{-Kt^n} \quad (3)$$

$$\ln[-\ln(1 - X_r)] = \ln(k) + n \ln(t) \quad (4)$$

where  $X_r$  is the relative crystallinity index,  $t$  is the time, and  $k$  and  $n$  are the Avrami parameters. Since the exponent  $n$  is dependent on the geometry of crystal growth and the nucleation type [84], for the athermal nucleation, growth can occur as rods ( $n= 1$ ), disk ( $n= 2$ ), or sphere crystal growth geometry ( $n= 3$ ). For the linear iPP component an exponent value of  $n= 3$  was obtained, which is representative of the spherulitic crystal growth. Contrarily, lower values of ‘ $n$ ’ were observed in the branched polypropylene,  $n= 2.8$  and  $n= 1.8$ . These results confirm the previous discussion regarding the large number of primary nuclei formed when highly branched molecules are employed that promotes the formation of a rod/disklike crystal growth geometry.

Flow-induced crystallization of thin polyethylene films can also be seen in the literature [86-91]. Zhang and co-authors [90] investigated the crystalline structure and anisotropy of different polyethylene blown films (HDPE, LDPE, LLDPE). According to the findings of their investigation, the molecular orientation obtained for each sample depends on the type of polyethylene used and the processing conditions. The HDPE, at a medium DDR, formed a row-nucleated structure showing non-twisted lamellar orientation. This was due to the long-chain lengths and long relaxation time that affected the crystallization kinetics and increase the degree of crystal orientation. In the LDPE film, at low DDR, randomly oriented secondary nucleation occurs, but at a high draw-down ratio, a row-nucleated structure with twisted lamellae was formed.

As shown in Figure 2.10, the authors proposed an interlocked lamellar assembly model, where the lamellae that meet from different row nuclei are strongly connected or overlapped by the twisted growth. Finally, owing to shorter relaxation time, spherulite-like superstructures were found in LLDPE at all processing conditions. These resins have less chance to form highly oriented row-

nucleated structures due to the relaxation of oriented fibrillar nuclei in the melt or the formation of several short length fibrils. The anisotropy of tensile strength was also an indication of the presence of fibrillar structure in the HDPE and LDPE materials, but not in the isotropic LLDPE component.

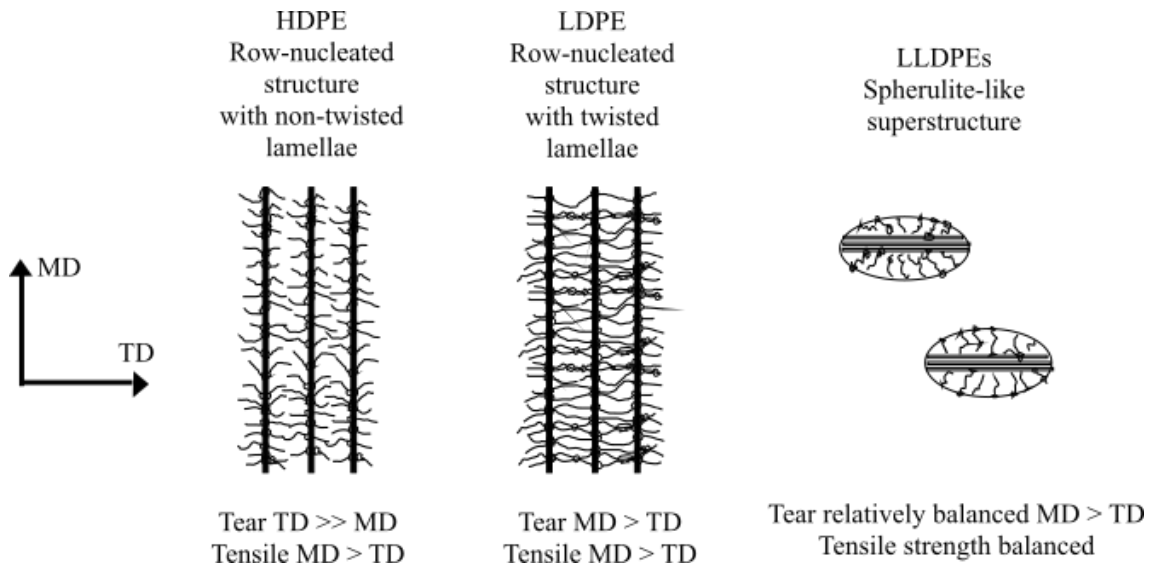


**Figure 2.10.** Schematic diagram of representative HDPE, LDPE and LLDPE crystalline forms and structure-tear resistance relationship proposed by Zhang et al. Modified from [90].

In many processing techniques of polymeric materials, such as extrusion and injection molding, the molten polymer is influenced by both shear and elongational flow. In a sheet extrusion system, molecular orientation is dominated by shear inside extrusion dies and by the extensional flow, which happens when the melt comes into contact with the chill rolls and is stretched in the machine direction. Numerous studies have been conducted to document the effects of shear flow on the crystallization of various resins. Still, only a few studies in the literature have reported the effect of extensional flow on crystallization kinetics for the processing techniques mentioned above.

H. Münstedt [95,96] analyzed different important industrial processes dominated by elongational deformations. His research has shown that in films formed by extrusion and drawing processes with uniaxial or biaxial structures, the film thickness and uniformity are affected by elastic and elongational properties of the melt. The extrusion drawing of films and sheets usually causes the so-called neck-in phenomenon, which is defined as the difference between the film width and die width on one side. Polymer resins that show an increase of the elongational viscosity or tensile stress (strain hardening) provide resistance to neck-in. For a strain-hardening material, the viscosity increases with the extensional strain rate causing higher resistance to flow. For a long time, this



mechanism was considered a self-healing property that counteracted local thinning during stretching and allowed obtaining greater film uniformity [104-108]. The author also stated that for polymer resins that exhibit a strain-hardening tensile response, the polymer becomes stronger when it is deformed at higher strain or draw ratios. The influence of draw ratio in the strain hardening phenomenon and the subsequent thickness uniformity for two cast films prepared using a linear polypropylene resin (L-PP), and a long-chain branched polypropylene (LCB-PP) is presented in Figure 2.11. For the LCB-PP material, the neck-in is smaller, and the film width is larger than for the L-PP, owing to the significant strain hardening at high strains.

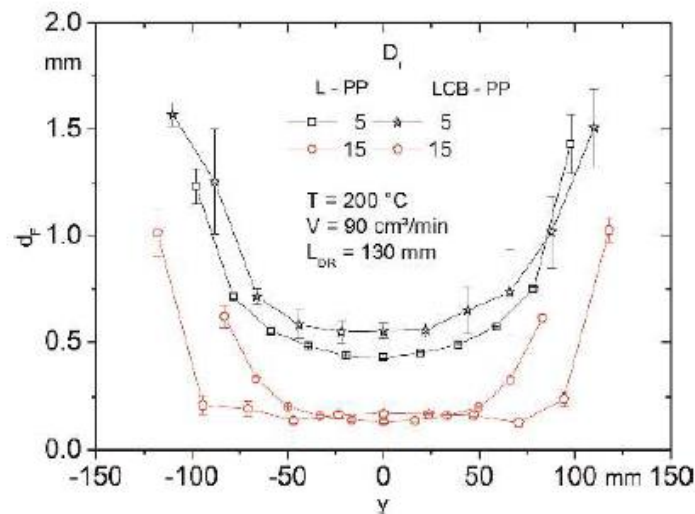


**Figure 2.11.** Thickness ( $d_f$ ) as a function of the lateral coordinate averaged ( $y$ ) over different positions along two cast films (L-PP and LCB-PP) stretched at different draw ratios ( $D_1 = 5$  and 15). Image from [96].

This study also considered the effect of the molecular architecture of both linear PP and branched PP. The extrudate swell is the expansion of molten polymers at the die outlet, which is counteracted to an extent by the drawing [104]. Polymers with long-chain branches usually exhibit marked strain hardening and high extrudate swell. As shown in Figure 2.12, for the L-PP, even at high draw ratios, an increase of neck-in (smaller film widths) was obtained. Contrarily, the long-chain branched material (LCB-PP) showed a neck-in distinctly smaller for larger draw ratio.

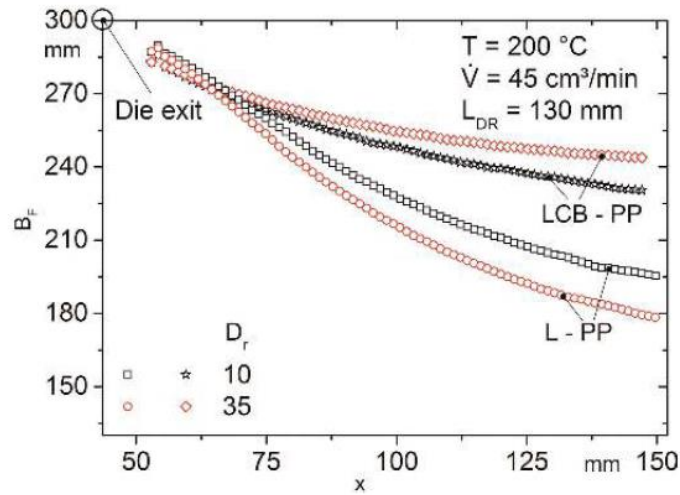


Figure 2.12. Result graph of film width ( $B_f$ ) along the drawing direction ( $x$ ) for two cast films (L-PP and LCB-PP) stretched at different draw ratios ( $D_r = 5$  and 15). Image from [96].

Schrauwen et al. [100] focused on the influence of orientation on the mechanical behavior of injection molding and extrusion of different grades of high-density polyethylene (HDPE) and polypropylene (PP). Chill roll speed, pressure, and draw ratio of the different samples were considered predominant variables in determining the elongational flow effects during sheet extrusion. The analysis of experimental results proves the presence of a row nucleated structure in all extruded samples, in which the orientation appears to be more pronounced for films produced at high draw ratios. Pole figures of the three principal crystallographic directions (a-axis, b-axis, and c-axis) confirmed these results were due to the strongest orientation showed for the c-axis in the direction of flow when samples were subjected a larger draw ratio. Similar results were obtained for both polyethylene and polypropylene resins from tensile tests performed parallel and perpendicular to the flow direction. The yield stress and strain hardening were found to increase in the flow direction due to the molecular orientation –induced crystallization. An increase of extended chains (row nuclei) in the loading direction was proposed as the cause to increase the yield stress, whereas the lamellar structure grown perpendicular to the oriented fibrils increased the strain hardening behavior. Testing the films perpendicularly to machine direction caused multiple crazing and therefore, macroscopic yield failure of the material. This confirmed the effect of anisotropy on mechanical properties.

## **2.4. Melt-extrusion/annealed/uniaxial stretching (MEAUS) method**

The following chapters provide the reader with the essential knowledge of the different stages of the MEAUS technique employed for microporous film production. The crystalline structure development during film extrusion, the effect of annealing and uniaxial stretching steps, and other relevant information will be detailed below. Furthermore, since all porous membranes produced in this research work are based on semi-crystalline polyolefin materials, further information regarding polypropylene and polyethylene properties will also be briefly discussed.

### **2.4.1. Polymer composition and melt-extrusion conditions**

Sadeghi et al. [6] developed microporous membranes based on PP through melt extrusion and stretching processes. The influences of branching, molecular weight, and process conditions on forming a row-nucleated structure were investigated. According to the authors, the long-chain branching modified the shear-induced crystallization mechanism since a more stretched fibrils were created in the first stage of crystallization. If the branched polypropylene resin had lower molecular weight, the fibril length would be much shorter. This was associated by the authors with an increment of lamellae twisting. Contrary, high molecular weight resins formed an extended fibrillar network that acts as a lateral crystal growth site. The understanding of processing parameters was essential to estimate the characteristics of the lamellar structure such as orientation, crystal thickness, and connectivity of the polymer chains. In the same work, Sadeghi and co-authors studied the influence of applying different draw ratios during the precursor film production. They found that higher draw ratios during extrusion processing led to a high molecular orientation and long fibrillar structures forming when high molecular weight resins were employed

Tabatabatei et al. [4] prepared blends of two linear polypropylenes with different molecular weights (adding the high molecular weight polypropylene at four different blending percentages) to develop microporous membranes using the MEAUS process. Their results agreed with the findings of Sadeghi and other authors [5,6,33] since the orientation of the crystalline phase increased with high molecular weight resins and high draw ratios. The effect of blending on the mechanical properties also confirmed a higher degree of orientation of the amorphous and crystalline regions when the higher molecular weight component was added. Due to this higher orientation of tie-chain molecules between adjacent lamellae and the formation of more fibrils, the tensile strength in the machine direction (MD) was much higher than that in the transverse direction (TD). Also, for both, the breaking strain decreased with increasing orientation. Morphological characterization of membranes revealed thicker lamellae and a small number of pores for the neat low molecular weight PP. At a high content of the high molecular weight component, the number of fibrils or nuclei sites increased, as well as the orientation of the crystalline structure, which resulted in the

formation of thinner lamellae, high pore density, uniform pore size, and better pores interconnectivity throughout the membrane.

The effect of the extrusion temperature on the flow-induced crystallization of PP resins was also investigated. The lower temperature during extrusion allows that polymer chains remain extended and preserve the preferred orientation imposed by the extensional flow. Nevertheless, the processability, the polymer melt stretching at the die exit, and the chain mobility for lateral lamellae growth may be adversely affected by low extrusion temperatures. In another study [7], the influence of process conditions (air cooling and drum temperature) on the orientation and conformation of chains in the crystalline and the amorphous regions was evaluated. A highly oriented structure was possible to obtain by an effective quenching protocol of the extruded polymer melt. Cooling at the die exit was needed to prevent the polymer chain relaxation, which enhanced chains' orientation in both crystalline and amorphous phases. Moreover, the air cooling system and the casting roll temperature offered a synergistic effect on promoting crystallization kinetics. Authors realized that with a slow cooling rate, the molecules had enough mobility to form a row-nucleated structure, and no significant structural changes were produced after the extrudate film touched the chill rolls (at any roll temperature). However, for samples produced without air cooling, the use of higher cast roll temperatures (above 110 °C in PP resins) had the same effect of thermal annealing, promoting structural rearrangement and increasing the crystal size and orientation.

Several studies found that using sequential monomer addition of ethylene and propylene, some properties such as transparency, relative softness, and low-temperature impact strength can be improved. However, the presence of random ethylene monomers disturbed the chain regularity and decreased crystallization capability [107,108]. Sadeghi et al. [30] also tried to develop microporous membranes by extrusion and stretching of linear PP (having different molecular weights) and their blends containing 20wt% random copolymer. Here, the authors showed how the introduction of ethylene interfered with both fibril and lamellae crystallization since the random copolymer tends to suppress and flatten the peaks in the melting curves. On the other hand, the addition of a 20wt% random copolymer did not influence the molecular orientation drastically in the machine direction (MD). Still, it decreased the tear resistance significantly for the low molecular weight homopolymer used. These results were related to creating a fragile crystalline network connection between fibrils, which became weaker with the introduction of the ethylene monomer. However, for the high molecular weight resin, the effect was much less pronounced owing to the oriented and thicker densely row nucleated structure, which was hardly influenced by the presence of the random copolymer.

The crystallization behavior and morphological properties of the linear PP in the presence and absence of 20 wt% random copolymer were also investigated using polarized optical microscopy (POM) at a cooling rate of 10°C/min from the molten state. It is evident that for the homopolymer, the spherulites started from a central nucleus and grown uniformly (Figure 2.13a). However, for the random copolymer, a noticeable disruption in the spherulites crystallization is observed since the growth rate is reduced significantly by adding the ethylene monomer to propylene (Figure 2.13b). This and other studies [107,108] have demonstrated that incorporating ethylene in some cases can increase the nuclei length per volume. Still, since the growth rate dominates the overall crystallization kinetics, and it decreases with increasing the ethylene content, only small distorted spherulites can be formed. For the blend containing only 20wt% copolymer, the ethylene content slightly hindered the spherulite growth, and only a few irregularly shaped spherulitic areas were seen during the crystallization (Figure 2.13c).

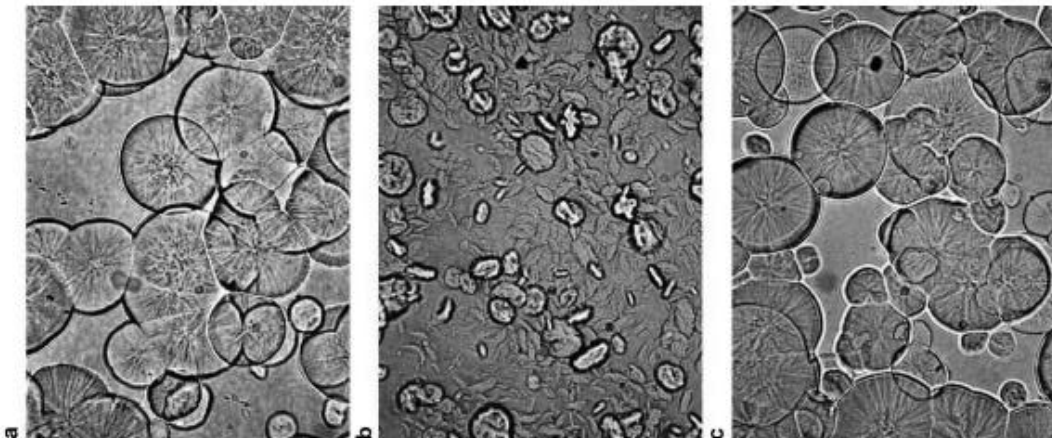


**Figure 2.13. Optical micrographs of samples crystallized non-isothermally by cooling at rate of 10°C/min. (a) linear polypropylene (homopolymer), (b) random copolymer and (c) homopolymer-copolymer blend (98wt% and 20 wt%, respectively). Reproduced from Sadeghi et al [30].**

#### 2.4.2. Thermal annealing and uniaxial stretching process

In a dissertation by Yu [116], two different HDPE resins that had identical molecular weights ( $M_n$ ) but different distributions ( $M_w/M_n$ ) were melt-extruded into uniaxially oriented tubular films. The results confirmed that under the same processing conditions, the more prolonged relaxation time behavior of the high molecular weight resin is essential for controlling the formation of extended chain threads or fibril nuclei in a row nucleated structure. The author also investigated the structural and morphological changes produced after the annealing of HDPE precursor films. Variables considered during annealing studies included the temperature, time, and extension applied during the thermal treatment. Annealing of the samples at a higher temperature (120°C vs. 105°C) induced high orientation when a small amount of extension was applied.

In contrast, the annealing time was observed to have only a tiny effect on the crystalline orientation function. The defect diffusion model was needed to describe the annealing behavior of the HDPE extruded films. Due to the greater chain mobility achieved during this thermal treatment, it was possible to produce an increase of the crystalline phase density, which resulted in the formation of a stable microporous structure by further stretching process.

A study utilizing isotactic poly(4-methyl-1-pentene) and polyoxymethylene (POM) was undertaken by Johnson [117] to produce microporous films by stretching. This work described in detail the proposed annealing treatment in terms of its temperature, time, and extension level. The increase of lamellar thickness and degree of crystallinity were more pronounced in samples with higher annealing temperatures and times. During heat treatment, below the melting point of the polymer, the thermal relaxation occurred. This was accompanied by the redistribution and structural changes within the crystalline domains. About the tension applied to the film during annealing, this parameter did not have a significant influence on morphology. However, if the tension level was too high, the lamellar network experienced an irreversible deformation, and small voids (cracks) were observed.

After thermal annealing, the films were uniaxially stretched at low and high temperatures to produce microporous membranes. Figure 2.14 shows the dependence on the Gurley number on both the cold and hot stretching steps when different temperatures and extension levels are applied to make the PMP microporous membranes. The Gurley number, which is defined as the time required for a specific amount of air to pass through a specific area of a separator, is a measure of the air permeability. The Gurley number decreased with increasing extension levels for the cold and hot stretching stages for the PMP membranes. This happened only until the optimum value of 80 per cent.

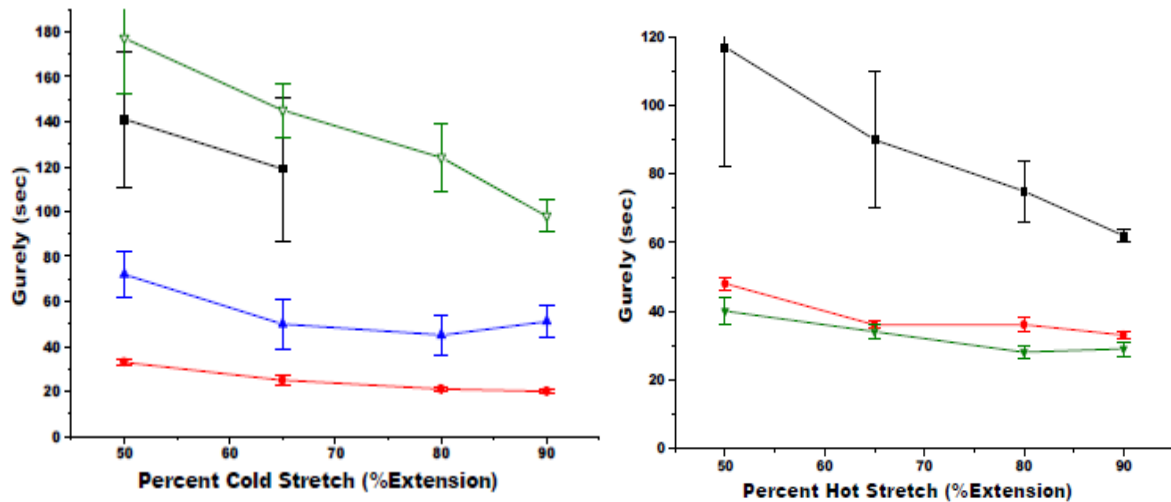


Figure 2.14. Relationship between Gurley number and percent extension applied during the cold and hot stretching to produce PMP microporous films. (a) -□- Tca = 40°C, -■- Tca = 70°C, -△- Tca = 80°C, -▼- Tca = 90°C, and (b) -□- Tca = 120°C, -■- Tca = 160°C, -▼- Tca = 180°C. Reproduced from Johnson [117].

The porosity and pore size distribution were also significantly influenced by the stretching temperature. As shown in Figure 2.14a, the Gurley number decreased when the stretching temperature increased from 40 to 70°C. Still, upon increasing the temperature from 70 to 90 °C, the Gurley value increased, which meant lower porosity and permeability. Johnson proposed that the initial decrease in the Gurley number with increasing the cold stretch temperature resulted from greater mobility within the amorphous phase rather than the crystal one. Suppose the PMP glass transition temperature is considered (35°C). In that case, the more restricted mobility of the amorphous phase at 40°C accounts for the greater frequency of film rupture during stretching (pore formation). Then, stretching at higher temperatures promoted greater activation of the  $\alpha$  relaxation, and the transnational chain mobility within the crystalline phase occurs more readily.

However, further deformation either by chain slip or breakage of the lamellae along the draw direction was observed when the stretch temperature was above 70 °C, which reduced the porosity and increased the Gurley number. Conversely, chain slippage was desirable for the hot stretching step (Figure 2.14b) since promoted greater lamellar separation when high levels of the extension were applied, which resulted in significantly increased pore size and higher permeability (lower Gurley number).

The effect of thermal annealing and cold and hot uniaxial stretching on the development of five different polypropylene microporous membranes was studied by Sadeghi et al. [5]. After annealing, the area under the curves was increased, and a small peak appeared around 140 °C. These results were mainly due to the crystallization of the end chains between the crystals and the thinner lamellae that could melt and recrystallize into more stable and thicker lamellae during the heat treatment. Furthermore, annealing also increased the orientation in both crystalline and amorphous phases since temperatures above the  $\alpha$ -transition allowed the local sliding between the crystalline blocks and the chain sections within the crystal aligned parallel to the MD.

After annealing, in the final stage of the MEAUS process, precursor films with a planar stacked lamellar morphology are uniaxial stretched parallel to the MD. In these studies, Sadeghi investigated changes produced in the crystal structure during both the cold and hot stretching. Tensile tests were conducted on annealed and non-annealed samples (Figure 2.15). The initial elastic region was believed to be due to the extension of the short tie chains. The second part of the curve coincided with the scission of these already stretched chains (brittle fracture), which led to the voids (pores) formation. By increasing the applied stress and due to short tie chains scission, the tension was transferred to the longer tie chains causing them to be pulled out of the crystals.

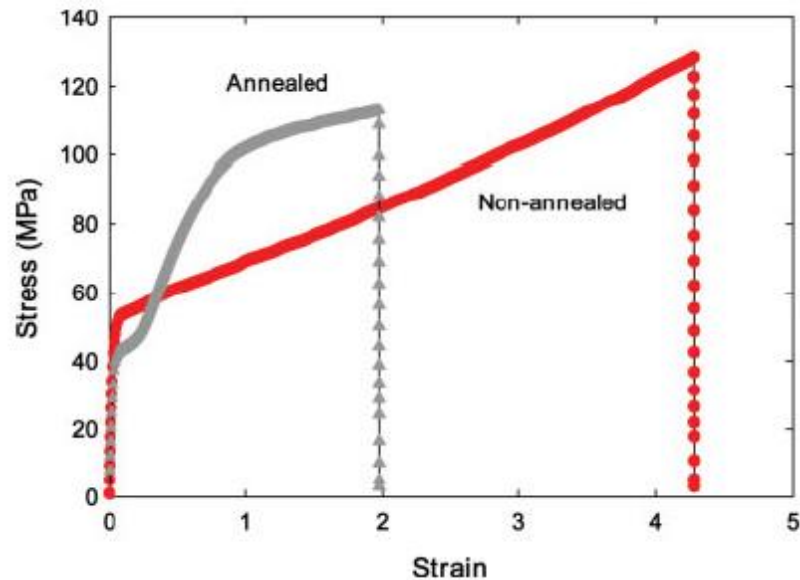


Figure 2.15. Stress-strain curves for the same polypropylene films, one non-annealed and the second one annealed at 145 °C. Image reported by Sadeghi et al. [5].



With additional drawing, the crystallization of the longer tie chains led to the strain-hardening of the samples. This is shown in the stress-strain curve, and it became more pronounced as stretching continued until the stress reached a value large enough to breakdown the interlamellar ligaments. Reorientation of the chains within the crystalline phase occurred for the non-annealed sample. However, the annealed sample possessed a thicker stacked lamellar morphology with the highest orientation along the MD, and the stress was consumed mainly on the crystal blocks separation. For this reason, high tensile strength and a reduction of total strain were also displayed for the annealed film.

In another study carried out by the same authors [6], after the formation of pores (cold stretching), samples were stretched again to 40% at an elevated temperature (140 °C) to enlarge the pore size. They observed that during the stretching at high temperatures, the long tie chains pulled out of the crystals could be melted and recrystallized in the form of the so-called "interconnected bridges", which explained the reduction in the lamellae thickness at high levels of extension.

These tensile tests were performed at the same temperature, applied during the hot stretching (140 °C) to study the stress consumption as a function of the initial draw ratio and the molecular weight of the samples. The authors concluded that most of the stress consumed during this stage was related to the lamellae separation and the crystallization of interconnected bridges. The stress consumption increased for the high molecular weight materials and films produced at higher draw ratios. An increase of both parameters gave a higher degree of orientation and strong interconnection between crystal blocks, which hindered the lamellae separation during the uniaxial stretching.

To determine the optimum annealing conditions that led to the highest degree of crystallinity and orientation of both the crystalline and amorphous phases, Tabatabaei et al. [4] annealed different samples at 120 and 140 °C with and without extension as a function of a high  $M_w$  PP content (added to another linear PP with low  $M_w$ ). The results (Figure 2.16a) suggest that the largest crystallinity degree can be obtained annealing the samples at 140 °C in the absence of strain and increasing the high  $M_w$  PP content in the blends. Contrarily, under a 5% extension concerning the initial length, samples with low crystallinity were observed.

On the other hand, the Herman orientation function of the crystalline phase and the amorphous phase for the non-annealed and annealed precursor films were calculated. As previously mentioned, the annealing performed close to the onset of segmental molecular mobility in the crystalline phase of a polymer ( $T_\alpha$ ) leads to the molecular organization in the crystalline and amorphous regions along the MD. This is displayed in Figure 2.16b. Furthermore, adding up to 10 wt% high Mw PP

enhanced the orientation of both the crystalline and amorphous phases. Although other studies reported that a slight tension during annealing enhances orientation [116], in the experimental work carried out by the writers of this paper, no dramatic improvement was observed.

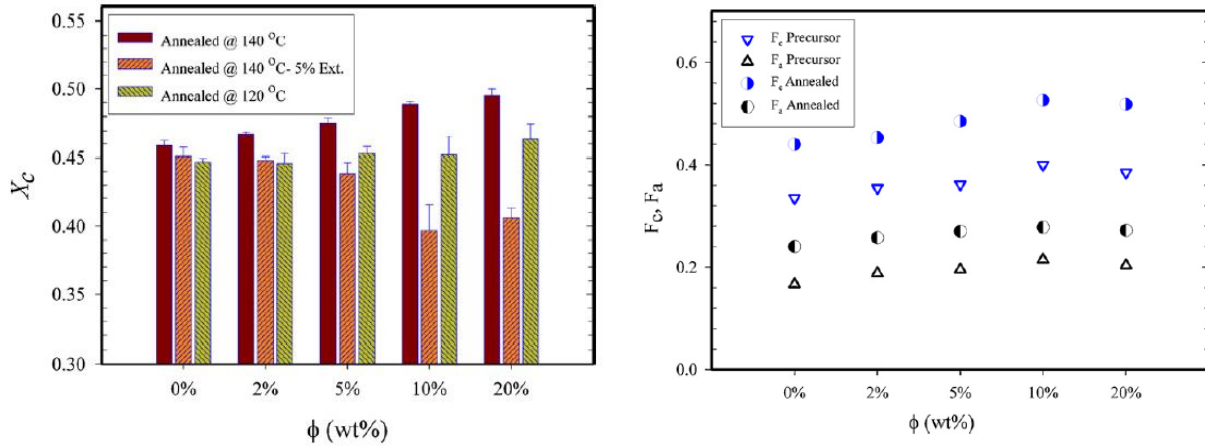


**Figure 2.16. (a) Average crystallinity of the annealed samples at (i) 140 °C, (ii) 140 °C under 5% extension, and (iii) 120 °C (annealing time= 30min), and (b) crystalline and amorphous orientation parameters both as a function of high  $M_w$  PP content. Images reported by Tabatabaei et al [4].**

An in-depth investigation of the effect of the annealing conditions on the properties of PP films and the microporous membranes formed by stretching was also carried out by Saffar et al. [17]. The SAXS, DSC, FTIR techniques, and the measured mechanical properties provided detailed information on the most relevant heat treatment factors: annealing temperature and time. The films were first annealed at different temperatures from 80 to 140 °C (below the melting temperature of the PP resins) for 30 min. From the SAXS patterns, it was observed that the lamellae morphology of the precursor films had a wide distribution of lamellar thicknesses.

A three-phase model (Figure 2.17) in which an interphase region might exist in the structure between the crystalline and amorphous regions of semi-crystalline polymers after annealing has been proposed by some researches [128,129]. In the Saffar's work, a diffuse interface was observed after the heat treatment; however, the thickness of the interphase region was negligible compared to the thickness of the crystal lamellae. Therefore, for annealed films, a simplified two-phase model in which alternating crystalline and amorphous domains having variable dimensions were present. The DSC results for annealed and non-annealed precursor films confirmed these structural changes. The development of a small peak around the annealing temperature for the annealed samples has been observed by others and already mentioned earlier [4-7]. The chain mobility is accelerated at high

annealing temperatures, and the crystalline domain size, the crystalline, and amorphous orientation are increased [4-21,27- 40]. However, the authors noted that the temperature increment should not exceed a particular value to avoid crystalline lamellar structure deterioration.

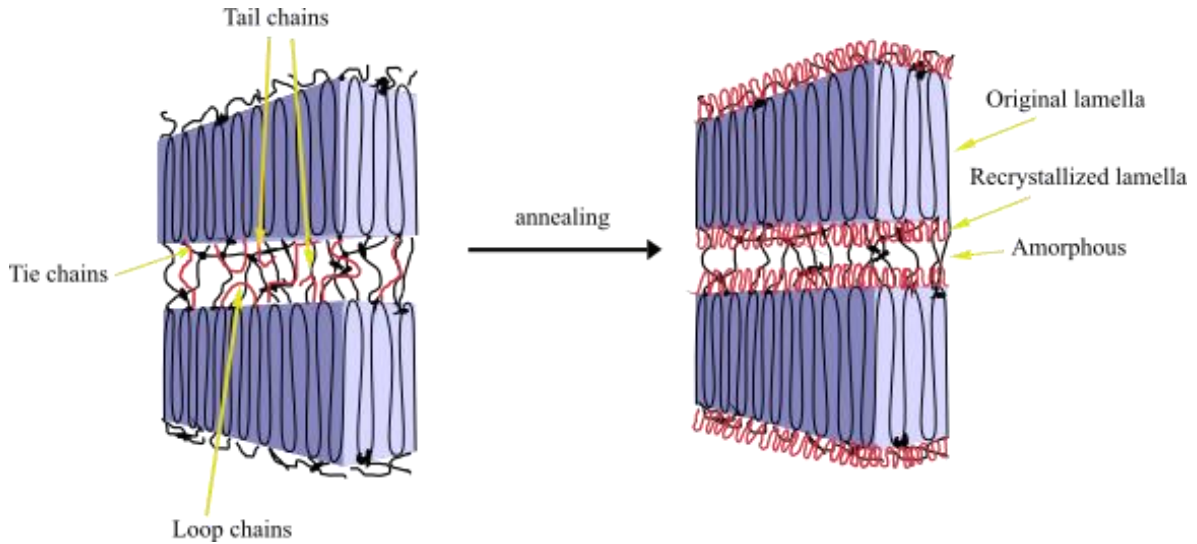


Figure 2.17. Microstructural evolution during isothermal annealing. Modified from [13].

Standard tensile tests for the non-annealed and annealed precursor films at different temperatures were also performed. According to the authors, two yield points for the annealed samples associated with fine and coarse chain slip were observed. At the first yield point, fine chain slip consisted of slight displacements or rearrangements within the lamellae. With increasing stretch ratios, chain tilting and decrease in lamellar thickness occurred until the significant shear displacements of crystals blocks promoted the coarse chain slip, which resulted in lamellar fragmentation upon stretching at the second yield point [4-11]. For the non-annealed films (with low crystalline orientation), most of the stress was spent on the motion and orientation of crystal blocks in the stretching direction, explaining the presence of a yield stress drop before strain hardening. Contrarily, the strength of the double yield point increased with annealing temperature. In this case, due to the presence of thicker lamellae at high annealing temperatures, most of the stress was spent for lamellae separation.

The strain hardening modulus (slope of the stress vs. strain at large strains) was found to decrease during the heat treatment. Some researchers attribute the strain hardening in semi-crystalline polymers to the density of the inter-crystalline links between adjacent lamellae [118-120]. Saffar and co-authors proposed that the crystal structure change during lamellar thickening due to the annealing process led to a decrease in the density of inter-crystalline links and strain

hardening, as well. The other main factor affecting the heat-treatment process is the annealing time. Precursor films annealed at 120 °C using various times were analyzed using the same characterization techniques. The authors observed that 10 minutes was the optimum time for the annealing process since slight changes were seen in the precursor and membrane features at longer annealing times.

In another study from the same research group, the influence of stretching variables on the morphology and permeability of polypropylene microporous membranes was investigated [10]. Figure 2.18 shows that the scanning electron microscope (SEM) micrographs display the surface and cross-section of microporous membranes made at different strain rates. It should be noted that applying a lower strain rate during the stretching steps results in a better lamellae separation and therefore, higher porosity and pore interconnectivity can be obtained. The effect of cold and hot stretch ratios on the membrane morphology was also investigated in this work. To find the optimum cold stretch ratio, annealed films were cold stretched at different draw ratios while hot stretching was kept constant. They found that the low stretch ratio (15%) was not enough to initiate pore formation. In contrast, an increase in the stretch ratio after the second yield point and during the cold stretching caused lamellae fragmentation and the pore structure collapse. Thus, an optimum stretch ratio between 25–50 per cent was found to increase the pore number in the membrane samples.

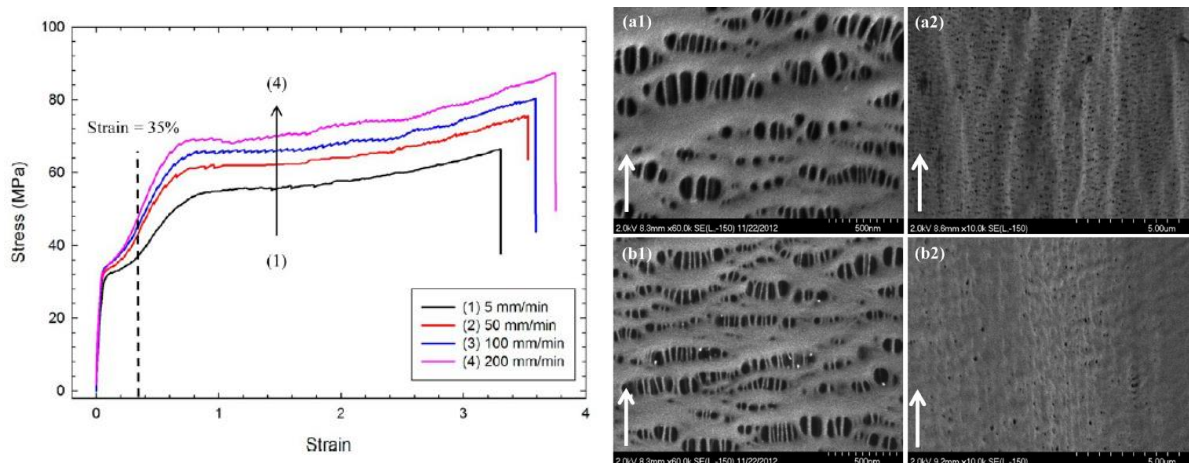


**Figure 2.18. (i) Stress–strain curves of the annealed precursor films at different strain rates and (ii) SEM micrographs of the surface and cross-section of PP membranes prepared at (a) 5 mm/min and (b) 200 mm/min. Cold stretching= 35% followed by hot stretching= 60% (the white arrow indicates the stretching direction).**

Reported by Saffar et al. [10]

The critical role of the cold stretching step in developing microporous membranes was also demonstrated using mercury porosimetry for membranes obtained after hot stretching (only) and stretching at room and high temperatures. A porosity value of 6 per cent was obtained for membranes prepared with hot stretching only, compared to 31.5 percent for the membranes prepared by cold stretching and subsequent hot stretching. Therefore, it was concluded that membranes porosity was significantly increased by stretching first the samples at lower temperatures. The authors also studied the influence of both the hot stretch ratio and the hot stretching temperature. As discussed earlier, stretching at high temperatures leads to the higher flexibility of the amorphous and tie chains between crystal blocks, resulting in an easier lamellae separation. Thus, when the hot stretching temperature and the stretch ratios were increased a much greater increment in the pore size and the permeability values were observed.

## **2.5. Multilayer microporous membranes**

The MEAUS process can fabricate microporous membranes for a wide variety of applications and one of the most significant is the Li-ion batteries [72-77,120-125]. Celgard® is a world leader in battery separator technology and holds a substantial portfolio of patents, including PP/PE bilayer and PP/PE/PP trilayer separators [73-77]. Microporous polyolefin membranes are used as separators placed between the anode and cathode. A commercial PP/PE/PP trilayer separator increases the battery cycle performance and safety since it possesses a shutdown mechanism. These thermal shutdown separators are based on the difference in the melting point of the polyethylene (~120–130 °C) and the polypropylene (~165 °C). When a lithium-ion battery is overcharged, the intermediate PE layer with a low melting temperature melts and closes the pores stopping the ion flow through the cell. In contrast, the external PP layers with a high melting temperature are used to maintain dimensional stability and mechanical integrity to prevent a short circuit between the electrodes [1,24]. The multilayer separators are usually made by laminating different functional layers together through a calendaring process using an adhesive layer or by welding [1,24,121-123]. Alternatively, multilayer separators can be made through a co-extrusion process, in which a simultaneous formation of a dual or tri-layer structure is possible. After co-extrusion, all of the layers must be annealed and stretched together to form a microporous structure.

A (PP/HDPE/PP) multilayer and monolayer microporous membranes were developed by Tabatabaei et al. [120] using the MEAUS technique. The DSC measurements revealed a degree of crystallinity of 44.2 and 74.0 per cent for the PP and HDPE monolayer films, respectively. The degree of crystallinity and the c-axis alignment parallel to the stretch direction measured via WAXD and FTIR were lower for either resin in the multilayer component than the monolayers prepared under the same conditions. From these results, the authors concluded that the higher crystallinity and larger heat of fusion of the HDPE resulted in an excess heat released during crystal

growth, which explained the PP and HDPE values in the trilayer sample. Figure 2.19 depicts SEM micrographs of the cross-section of the multilayer membrane. Despite being considered immiscible polymers, the results showed good adhesion between the HDPE and PP external layers, which was due to the formation of a transcrystalline layer in proximity to each other. The nature of nucleation of the transcrystalline layer can be explained by the difference in the crystallization temperature,  $T_c$ , between HDPE (118 °C) and PP (112 °C). In this case, PE nucleated and overgrew inside the molten PP and normal to the interface as shown in the SEM images.

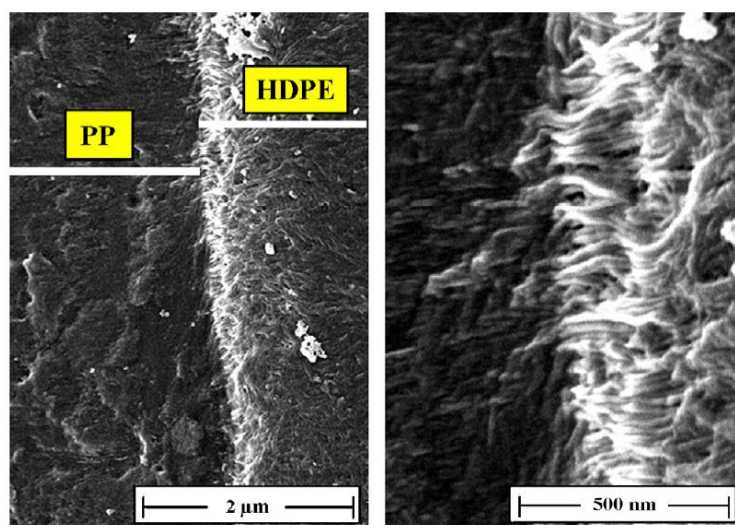


**Figure 2.19.** SEM imaged displaying the interfacial adhesion between etched PP/HDPE multilayer films. Images from [120].

The authors observed a wider plastic deformation region in the tensile curves and a strain-hardening with a lower slope for the HDPE membrane. Due to the presence of longer tie chains (interlamellar linkage) in the polyethylene resins, higher lamellae separation without crystal fragmentation was achieved, thus leading to an increase in the average pore size and mean permeability. On the other hand, despite having smaller pores and lower porosity values, the PP external layers showed a pronounced increase in the tensile strength and the maximum piercing force compared to the HDPE..

From this and other similar studies [121-123], the authors concluded that the main advantage of using a co-extrusion process to develop microporous membranes is to obtain a thin multilayer material in just one operation before the annealing and stretching steps. However, some issues and challenges must be considered to obtain the greatest potential of the membranes, i.e., the

various process conditions that affect each material differently, the lower orientation in the multilayer in comparison to monolayers films, the presence of the interface that can facilitate a decrease in the interconnectivity between pores, etc.

## 2.6. Morphological characteristics of polypropylene and polyethylene

PP and PE are semicrystalline thermoplastic polymers prepared by polymerizing propylene and ethylene, respectively. These resins are commonly produced by Ziegler-Natta or metallocene catalysts under carefully controlled conditions such as heat and pressure [103,107,108]. Propylene and ethylene are unsaturated hydrocarbons with the following chemical formula:



Figure 2.20. Chemical structures of ethylene and propylene [103].

These polymers exhibit varying degrees of crystallinity and different types of crystal structures depending on the molecular conformation, the processing conditions (the mechanism and rate of crystallization), the presence of additives, etc. Their crystalline melting points depend on the amount of crystallinity, but for commercial resins ranges from 160–170 °C for the PP and 120–130 °C for the PE can be found. PP has generally superior mechanical properties and thermal resistance than PE due mainly to the steric interaction of the pendant methyl groups [103,107,108].

PE exhibits three types of unit cells; orthorhombic, monoclinic, and hexagonal, being the most common in commercial resins the orthorhombic cell [103]. In like manner, isotactic polypropylene can crystallize into different morphological forms ( $\alpha$ ,  $\beta$ , and  $\gamma$ ), schematically shown in Figure 2.21 [107,108,127]. The  $\alpha$ -form is obtained under normal processing conditions where the polymer chains crystallize in a helical structure packed in a monoclinic unit cell. The  $\beta$ -form is a more disordered structure with a hexagonal unit cell formed at relatively low isothermal crystallization temperatures or in the presence of nucleating agents. The  $\gamma$ -form exhibits a less densely packed orthorhombic unit cell and with non-parallel, crossed lamellae. The  $\gamma$ -form appears in low molecular weight materials, chains with regular defects (via metallocene catalysts), or when crystallization is performed at high pressures. Different forms can coexist simultaneously, and



changes from one type of polymorphic form to another can occur when some conditions vary [107,108]. Finally, planar zig-zag and helical conformations are usually the backbones of PP and PE chain segments, as is depicted in Figure 2.22.

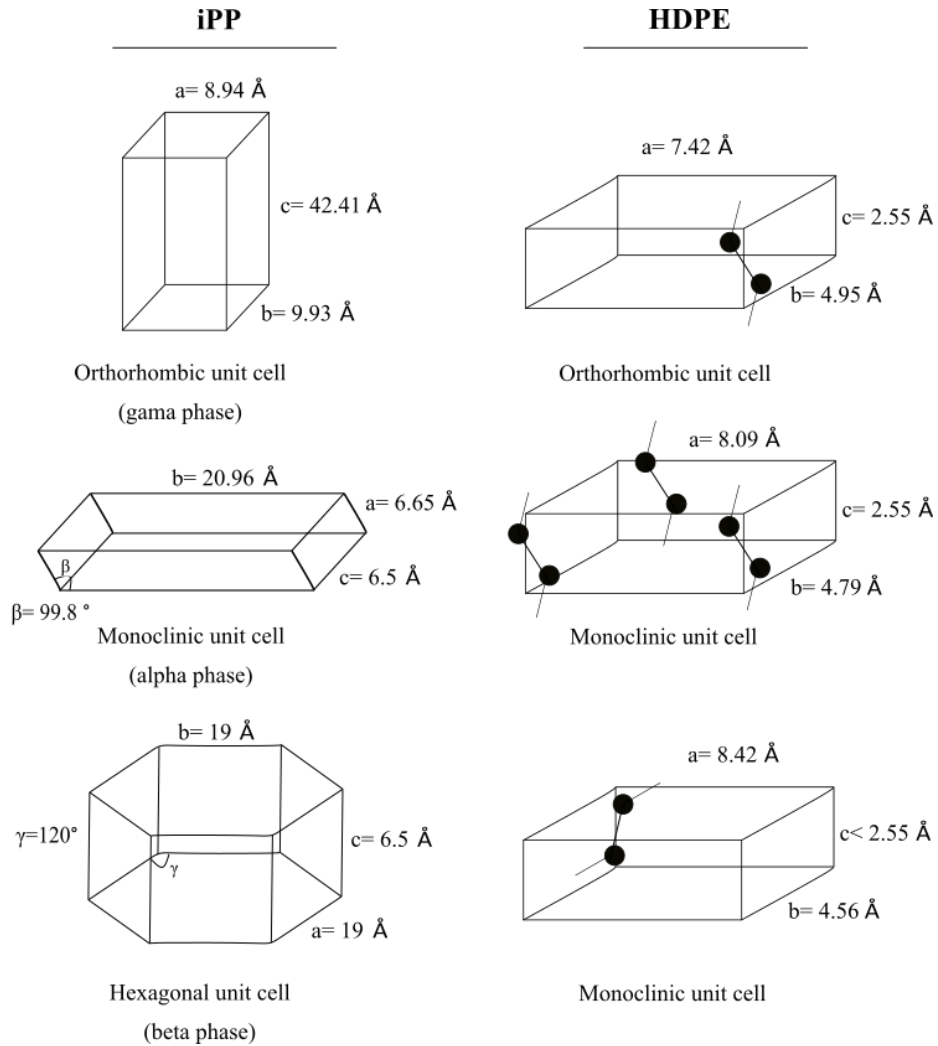
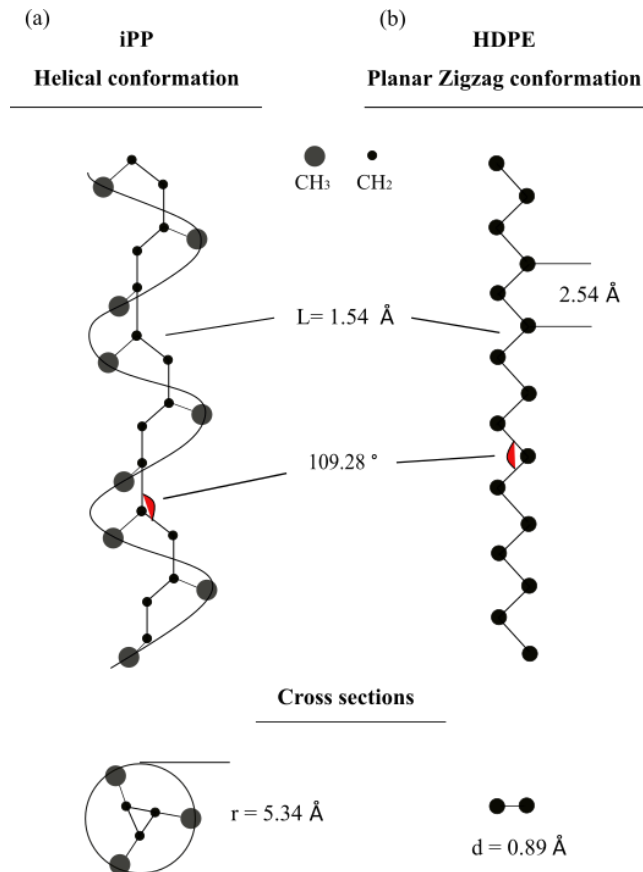


Figure 2.21. PE and PP crystal unit cells. Modified from [127].





**Figure 2.22.** Chain backbone developing a (a) planar zigzag conformation in PE and (b) helical conformation in PP. Modified from [127].

PP and PE are commercially available in many different forms depending upon desired performance properties. In PE, the number, length, and distribution of branches modify the properties of the polymeric material. Generally, the higher the concentration of branches, the lower the degree of crystallinity and the density of the solid [103]. The main types of PE manufactured commercially include: high density polyethylene (HDPE), low density polyethylene (LDPE), linear low density polyethylene (LLDPE), very low density polyethylene (VLDPE), ethylene-vinyl ester copolymers (EVA), and ionomers.

There are three major types of PP with commercial significance: PP homopolymer, PP random copolymer, and PP block, heterophasic or impact copolymer. The homopolymer contains only the propylene monomer, while the copolymers contain one or more different types of monomers in the polymer chain. Random copolymers typically contain 1-7 wt% of ethylene or other comonomers such as 1-butene or 1-hexene. The repeating units are randomly distributed along the polymer chain,

which leads to a reduction of the crystalline content. Due to the lower crystallinity, random copolymers are expected to have a lower melting temperature (i.e. 120 °C for a copolymer containing up to 7% of the ethylene comonomer) and glass transition temperatures similar to those of the homopolymer. The good impact strength at low temperatures, stiffness, moisture barrier properties, and high clarity makes it suitable for different applications [107,108]. The heterophasic or block copolymers can be produced with an addition of ethylene-propylene rubber (EPR), ethylene-propylene-diene monomer (EPDM), PE, or plastomers to homopolymers or random copolymers. These copolymers differ from random copolymers in the molecular arrangement sequence, as illustrated in Figure 2.23. Block copolymers can contain up to 25% of ethylene, forming an elastomeric or rubber phase uniformly distributed throughout the matrix as small domains, which provide impact resistance at low temperatures [107,108].

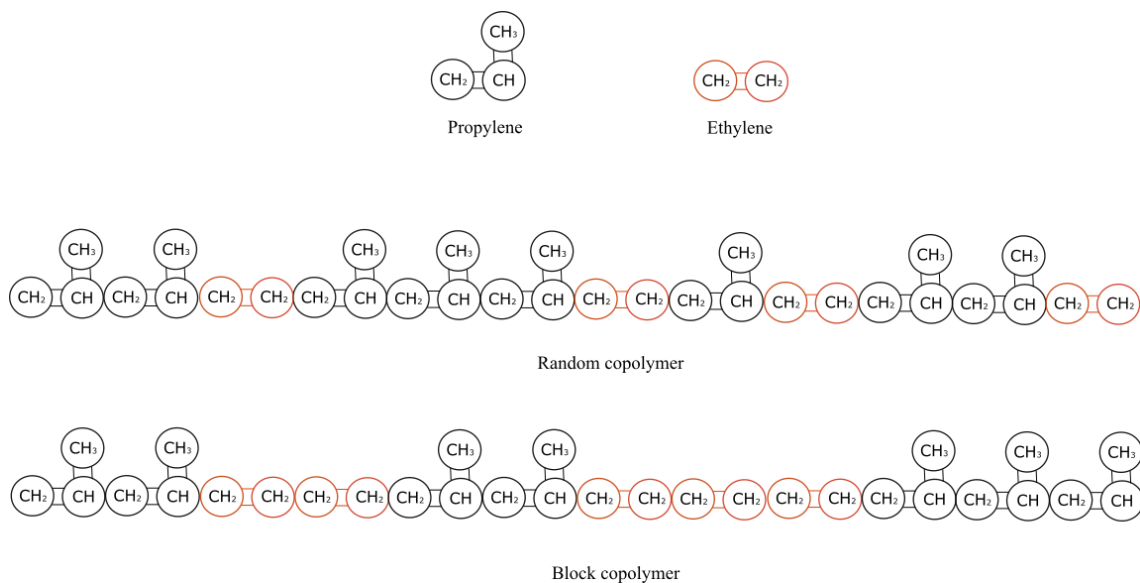


**Figure 2.23. Schematic representations of (a) random and (b) block copolymers. The two different repeating units are designated as A and B. Modified from [108].**



**Chapter 3:**  
**Experimental details**



### 3.1. Materials: nomenclature and microstructural characterization

In this study, four commercial grades of homopolymer polypropylene, a commercial high-density polyethylene, and two copolymer of polypropylene–ethylene (random and block copolymer) were selected. The main characteristics of PP and HDPE neat resins provided by suppliers are presented in Table 3.1.

**Table 3.1. MFI values for the PP and HDPE resins studied.**

<b>Commercial tradename</b>	<b>Company</b>	<b>Nomenclature in this work</b>	<b>MFI<sup>a</sup> (dg/min)</b>
<b>PP- Homopolymers</b>			
ISPLEN PP020 G3E	Repsol S.A	PP-HM <sub>w</sub>	0.9
ISPLEN PP034 W3F	Repsol S.A	PP-LM <sub>w</sub>	2.2
ISPLEN PP099 K2M	Repsol S.A	PP-VF	55.0
DAPLOY WB140HMS	Borealis AG	PP-BR	2.1
<b>PP- Copolymers</b>			
ISPLEN PR230 C1E	Repsol S.A	PP-R	1.6
ISPLEN PB110 H2E	Repsol S.A	PP-B	0.3
<b>HDPE</b>			
HDPE KT 10000 UE	Dow Chemical	HDPE	8.0

<sup>a</sup>MFI (Melt Flow Index) measured according ISO 1133 (230 °C / 2,16 kg)

The viscosity of all these resins has high enough melt strength for the extrusion of precursor films, allowing the high draw ratios necessary to form oriented structures. PP020, PP034, and PP099 were selected to study the effect of molecular weight on the physical properties of porous membranes. PP020 is the homopolymer polypropylene with the lowest MFI value and is assumed to have the highest molecular weight. Daploy WB140 HMS is a long-chain branched polypropylene, which was also selected to study the influence of polymer structure on membranes

production and increase the melt strength during cast film extrusion. As can be seen in Table 3.1, all these materials have been renamed in this thesis as PP-HM<sub>w</sub> (High Molecular Weight), PP-LM<sub>w</sub> (Low Molecular Weight), PP-VF (Very Fluid), PP-BR (Branched), PP-R (Random), PP-B (Block) and HDPE (High-Density Polyethylene).

To produce the thin composite membranes (trilayer system) two different mineral fillers were employed. (1) A commercial micro-sized ultrafine surface-treated precipitated calcium carbonate (M95T) supplied by Reverté Minerals Spain, with an average particle size of 4 µm and surface treatment based on MgCO<sub>3</sub>, Fe<sub>2</sub>O<sub>3</sub> and amino group. (2) A commercial talc grade (Mitrocell M90) provided by Imerys Talc with a micro-lamellar morphology and an average particle size of 3.3 µm and BET surface area of 13.0 m<sup>2</sup>/g.

Composites were prepared by compounding the PP-HM<sub>w</sub> and the CaCO<sub>3</sub> and Talc at different ratios, according to Table 3.2. These blends were made using a twin-screw extruder Collin ZK-35 (Dr Collin GmbH, Ebersberg, Germany). The extrusion temperature profile from the hopper to die ranged from 180 to 240 °C. The melt was extruded through a 3 mm diameter circular die, cooled in a room-temperature water bath, and pelletized. Pure polymers were also extruded at these conditions to provide the same thermomechanical history to all the samples. Table 3.2 is added to help the reader understand blends prepared in this work with their specific terminology.

Table 3.2. Polymer blends prepared in various weight percentages and nomenclature used in this study.

Blends prepared by extrusion	Nomenclature in this work
<b>Homopolymers PP</b>	
PP-HM <sub>w</sub> (98 wt %) + PP-BR (2 wt %)	PP-2BR
PP-HM <sub>w</sub> (98 wt %) + PP-VF (2 wt %)	PP-2VF
PP-HM <sub>w</sub> (90 wt %) + PP-VF (10 wt %)	PP-10VF
<b>Copolymers PP</b>	
PP-HM <sub>w</sub> (95 wt %) + PP-B (5 wt %)	PP-5B
PP-HM <sub>w</sub> (90 wt %) + PP-B (10 wt %)	PP-10B
PP-HM <sub>w</sub> (80 wt %) + PP-B (20 wt %)	PP-20B
PP-HM <sub>w</sub> (95 wt %) + PP-R (5 wt %)	PP-5R
PP-HM <sub>w</sub> (90 wt %) + PP-R (10 wt %)	PP-10R
PP-HM <sub>w</sub> (80 wt %) + PP-R (20 wt %)	PP-20R
<b>Multilayer composite membranes PP/HDPE/PP</b>	
<i>Unfilled outer layers</i>	
PP-HM <sub>w</sub> (100 wt %)	PP / HDPE
<i>Filled outer layers:</i>	
PP-HM <sub>w</sub> (95 wt %) + C (5 wt %)	PP-5C / HDPE
PP-HM <sub>w</sub> (90 wt %) + C (10 wt %)	PP-10C / HDPE
PP-HM <sub>w</sub> (95 wt %) + T (5 wt %)	PP-5T / HDPE
PP-HM <sub>w</sub> (90 wt %) + T (10 wt %)	PP-10T / HDPE



## 3.2. Precursor film processing

### 3.2.1. Extrusion

The first stage of the MEAUS process is the extrusion of mono-oriented films with a high draw ratio and a rapid cooling of the extrudate at the exit of the extrusion die (Figure 3.1). This finished product is typically called a precursor film, as its structure would allow the generation of a row-lamellar structure that could be transformed into a porous membrane. In this Ph.D. Tesis, three cast film extruders were used to produce the precursor films. (1) A single screw extruder (Eurotecno E-3035-D), equipped with a slit die of 200 mm width and variable thickness. (2) A co-rotating twin-screw extruder (Collin Kneuter, 25x36D) equipped with a slit die 25 mm-width and 1.9 mm thickness, and (3) a multilayer co-extrusion system (Teach-Line Collin, E20T and E16T) and a slit die of 100 mm width and 1,9 mm opening.

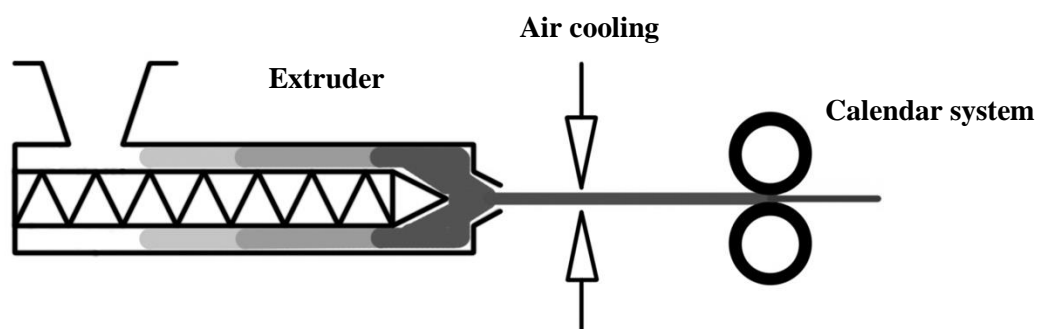


Figure 3.1. Scheme of precursor films manufacturing process.

The precursor film characteristics have been tightly controlled by some experimental variables, such as the amount of airflow and draw ratio (DR) applied. At the exit of the die, slit-open air knives were used to supply air to both sides of the film to achieve fast cooling. Simultaneously, the film underwent uniaxial stretching along the machine direction using a calendar system with variable speed, which allowed the application of different draw ratios to the extruded precursor films (DR defined in each chapter).

### 3.2.2. Annealing and uniaxial stretching

From the precursor films with a ca. 30  $\mu\text{m}$  thickness, rectangular samples were cut out with a width and length of 60 and 100 mm, respectively, to be annealed without an extension at different temperatures in an air-circulating oven during 15 min. For uniaxial strain, a universal testing machine (*SUN2500, Galdabini*) equipped with a climatic chamber was employed. The annealed precursor films were then tightened in two grips in tensile configuration and the direction of the uniaxial strain was parallel to the direction of the drawing of the precursor film during the extrusion. For both the cold and hot stages, different parameters were subjected to study: the crosshead speed and the percentage of strain reached (from now on referred to as strain extent), as well as the temperature at which hot stretching is performed. Finally, once the test was finished and before relieving the films from the imposed strain, all of them were kept at the same hot stretching temperature for 90 s to stabilize the porous structure.

### 3.3. Precursor film and membrane characterization

#### 3.3.1. Orientation Features

##### Fourier transform infrared spectroscopy (FTIR)

For crystalline characterization, a Fourier-Transmission Infrared spectrometer (*Perkin Elmer 1000*) with a spectral resolution of  $1 \text{ cm}^{-1}$  and the polarized beam was used. The data was obtained from the range of  $4000$  to  $600 \text{ cm}^{-1}$ , and the crystalline phase orientation ( $F_c$ ) for samples non-annealed and annealed at different temperatures was determined based on the Herman's orientation function (Eq. 3.1)

$$F_c = (D-1) / (D+2) \quad (3.1)$$

where the dichroic ratio,  $D$ , is the ratio of two absorption values in the two orthogonal directions, parallel ( $A_0$ ) and perpendicular ( $A_{90}$ ) to the reference axis MDO (machine direction orientation) according to Eq. 3.2.

$$D = A_0 / A_{90} \quad (3.2)$$

For polypropylene, the crystalline orientation function ( $F_c$ ) was determined using the absorption at the wavelength of  $998 \text{ cm}^{-1}$ , attributed to the c-axis crystalline phase. On the other hand, at  $972 \text{ cm}^{-1}$  the average orientation function ( $F_{\text{avg}}$ ) can be obtained, which is related to the contribution of both crystalline and amorphous phases. When the degree of crystallinity ( $X_c$ ) is known, then the amorphous phase could readily be calculated using the Eq. 3.3.

$$F_{\text{avg}} = X_c F_c + (1 - X_c) F_{\text{am}} \quad (3.3)$$

For polyethylene, the c-axis orientation function ( $F_c$ ) was determined with the orthogonal equation (Eq. 3.4), where the  $F_a$  and  $F_b$  are the a-axis and b-axis of the unit crystal cell at the absorption wavelength of  $730 \text{ cm}^{-1}$  and  $720 \text{ cm}^{-1}$ , respectively, both calculated according to the Eq. 3.1 [120].

$$F_a + F_b + F_c = 0 \quad (3.4)$$

### 3.3.2. Morphology

#### Scanning electron microscopy (SEM)

A scanning electron microscopy (SEM - *JEOL JSM-5610*) operated at 2kV voltage was employed to examine the membranes surfaces and cross-sections. The samples were first coated with a thin layer of gold alloy in argon atmosphere employing a *BAL-TEC SCD005 Sputter Coater* and the data related to the morphology of membranes surfaces were obtained using an image analysis program (*Buehler Omnimet*). During this analysis and for calculation purposes, a circular-like porous geometry was assumed. The average pore density of the membranes was calculated taking into account the number of pores divided by the analysed membrane area. An etching method was employed to observe the crystal arrangement of the multilayer porous membranes cross-sections. The samples were dissolved in a 0,7 % solution of potassium permanganate in concentrated sulphuric acid. The potassium permanganate was slowly added to the sulphuric acid and the mixture was stirred efficiently with a magnetic stirrer until all the permanganate was dissolved. At the end of the reaction time samples were washed following the process described by Olley and Basset [130].

### 3.3.3. Porosity and permeability

#### Gurley permeability

The permeability to air was measured using a Gurley densimeter (*Lorentzen & Wettre*), according to ISO 5636-5. The Gurley permeability value was calculated according to the Eq. 3.5, where  $t$  was defined as the time for a settled volume (100 ml) of air to pass through the sample with a fixed area ( $0.79 \text{ cm}^2$ ) under the pressure of 0.02 MPa. Longer time values correspond to low air permeability, usually a consequence of a long and tortuous path for air transportation through the pores.

$$\text{Gurley permeability} = 135.5/t \text{ } \mu\text{m}\cdot\text{Pa}^{-1}\cdot\text{s}^{-1} \quad (3.5)$$

#### BET measurement

The Brunauer-Emmet-Teller method was used for evaluating the surface area of porous membranes and comprises two major stages: first, it is necessary to transform a physisorption isotherm into the BET plot and from it derive a value of the monolayer capacity,  $n_m$ . Then, in the

second stage, the calculation of the BET-area from  $n_m$  is made by adopting an appropriate value of the molecular cross-sectional area,  $\sigma$  [131].

The BET equation is conventionally expressed in the linear form:

$$\frac{\frac{p}{p_o}}{n(1 - \frac{p}{p_o})} = \frac{1}{n_m C} + \frac{C - 1}{n_m C} \left(\frac{p}{p_o}\right) \quad (3.6)$$

where  $n$  is the specific amount adsorbed at the relative pressure  $p/p^\circ$ ,  $n_m$  is the specific monolayer capacity and  $C$  is a constant. The procedure for estimating the BET surface area from Eq. (3.6) and the method for mesopore size analysis proposed by Barret, Joyner and Halenda (BJH) can be found elsewhere [132, 133].

### 3.3.4. Thermal characterization

#### Differential Scanning Calorimetry (DSC)

The thermal behavior and amorphous-crystalline phase transformations of samples, before and after the annealing and stretching steps were studied by Differential Scanning Calorimetry using *DSC Q2000 - TA instruments*. Samples with a mass ca. 6-8 mg were heated from 30 to 200 °C at a heating rate of 10 °C/min. The degree of crystallinity was calculated according to Eq. 3.7, where  $\Delta H_m$  is the melting enthalpy measured from the area under the melting endotherm using the standard supplied TA Universal Analysis software,  $w_p$  denotes the mass of PP in each sample, and  $\Delta H_0$  is the theoretical enthalpy for a 100 percent crystalline sample. The value of  $\Delta H_0 = 207.1 \text{ J}\cdot\text{g}^{-1}$  and  $288 \text{ J}\cdot\text{g}^{-1}$  was chosen for the PP and PE, respectively [131]. Furthermore, this thermal analysis allows us to study the nucleating ability of calcium carbonate and talc on polypropylene by considering both melting ( $\Delta H_m$ ) and crystallization enthalpies ( $\Delta H_c$ ). To determine the PP crystallinity in the multilayer composite membranes, the equation 3.7 assumes the fraction of PP contained in each specimen, which is 0.95 and 0.9 for samples with filler contents of 5 and 10 percent, respectively.

$$X_c(\%) = \frac{\Delta H_m}{\Delta H_0 w_p} \times 100 \quad (3.7)$$

### **Thermal gravimetric analysis (TGA)**

Thermal gravimetric analysis (TGA) was carried out to evaluate the membranes' stability with different compositions using a *TGA/DSC 1 Mettler Toledo Star* System. Thermogravimetric analyses were performed heating samples with a weight ca. 8.0 mg from 40 to 700 °C at a heating rate of 10 °C/min and under a nitrogen atmosphere (a constant flow of 30 ml/min). Three different analysis was done for each sample. The rate of change of weight was shown with the first derivative of the TGA curve with respect to temperature, also known as the differential thermogravimetric analysis (DTGA) curve.

### **3.3.5. Mechanical characterization**

#### **Tensile tests**

The mechanical properties of the annealed precursor films and some of the membranes were measured in tensile mode along MDO (machine direction orientation). Tensile tests were performed in a universal tensile machine SUN2500 Galdabini using a 1 kN load-cell and a video extensometer MINSTRON OS-65D. Recommended sample dimensions are set out in ISO 527-3. Tensile tests were performed at room temperature at a strain rate of 50 mm/min and results are the average of tests on five specimens of each sample. The mean and the standard deviation are reported together.



## **Results and discussion**





## **Chapter 4:**

# **Polypropylene based porous membranes**



One of the present work aims was to investigate the influence of the polymer matrix composition and the architecture structure on the row-nucleated lamellar crystallization. This was done using two linear polypropylenes having different molecular weights and blending them with branched and very fluid PP resins.

All the precursor films considered in this chapter were prepared using a single screw extruder equipped with a gap die of 200 mm width and an opening of 1.9 mm. For this investigation, we used an extremely fluid polypropylene (adding up to 10%) to try to achieve a greater strain extent during the extrusion and the uniaxial strain stage. As a complement, we performed a detailed investigation of the impact of all the variables on the uniaxial strain stage (stretching both at room and high temperatures) related to the structural changes produced in the porous morphology. In some cases, we used extreme strain rate values and larger strain extents than what is usually applied (up to 300% elongation).

#### **4.1. Influence of polymer composition**

All the membranes discussed in this section were obtained under the same processing conditions. The extrusion draw ratio was kept to 70 (giving as a result a precursor film of about 27-29  $\mu\text{m}$ ), and the uniaxial strain stage was carried out during the cold stage at 10 mm/min, up to 55% strain extent and during the hot stage at 10 mm/min, up to 300 % strain extent.

The Herman orientation functions of the crystalline and amorphous phases and the crystallinity of the annealed precursor films (of neat resins and all the blends) are presented in Figure 4.1. In the specimens made by extrusion and drawing processes, both the crystalline and amorphous regions were oriented parallel to the machine direction. After extrusion, thermal annealing was used to promote crystallization throughout the entire precursor films, which led to increased crystallinity by crystal growth, as well as to improved crystal orientation [8,13-17,128]. Amorphous regions were also influenced by these structural changes since the mobility of amorphous chain segments near the crystalline lamellae increased at high temperatures, which contributed to enhanced chain alignment. Therefore, in comparison with the non-annealed films (data not presented here), annealed samples showed a significant improvement in both the crystalline and amorphous orientations.

As can be seen in Figure 4.1a-b, the sample PP-LM<sub>w</sub> exhibited the lowest MD orientation due to its lower molecular weight. Chain extension and orientation of high molecular weight polypropylene (PP-HM<sub>w</sub>) are the most important factors affecting membrane characteristics (pore size, pore density, and permeability), as depicted in Table 4.1.

The molecular orientation of the higher molecular weight polymer increased with an increase in the characteristic relaxation time [4-6,33,80-83,97]. The effects of blending 2 and 10 wt % of the very fluid polypropylene with the PP-HM<sub>w</sub> seem to support the previously described results. The addition of the low molecular weight component led to changes in the crystal structure. It promoted row-nucleated structures apparently with a less stable orientation to those formed with the neat resin [4-6]. This results in less uniform lamellar crystals separated by stretching in the final step of the MEAUS methodology, reducing the total porous area and membranes permeability. Besides, a significant reduction in the mean orientation factor was also observed for blends with the PP-2BR. This long-chain branched polypropylene was selected for its high melt strength and extensibility in the melt phase. Even though it improved the melt processability of the films produced under high draw ratios, assuming that high molecular weight is generally considered to be a key attribute to achieve a high degree of orientation, it was speculated that the use of this branched polypropylene with lower molecular weight led to fast melt relaxation of shorter fibrils during film extrusion, increasing the lamellar twisting and reducing the crystalline orientation [4-6].

The crystallinity of the non-annealed and annealed precursor films and the uniaxially stretched membranes were examined using the DSC thermograms shown in Figure 4.2. For the homopolymer resins, the main melting peak in these curves was attributed to the presence of thinner or thicker lamellae distribution of the original crystalline structure obtained in the precursor films [4-6]. In all samples, except for PP-LM<sub>w</sub>, this main peak was quite similar; then, it was assumed that the same average thickness of the lamellar crystals was formed in these specimens. The significant changes among the melting endotherm curves for the neat resins and the blends were shown by the presence of two distinctive shoulders on both sides of the melting peak.

The shoulder at a lower temperature (Figure 4.2b) was due to the annealing process when the polymer chains' mobility in the amorphous region increased due to the higher annealing temperature. During this step, chains located in the amorphous part would have rearranged themselves and recrystallize. Then, the crystalline growth would have occurred around the initial row-nucleated lamellae, creating new secondary crystals, as has been reported previously by other authors [8,13-17]. Thus, for all the samples considered in this study, the crystallinity level increased after applying thermal annealing at high temperatures.

As we stated above, the melting peaks were quite similar except for the sample PP-LM<sub>w</sub>, where the lower molecular weight led to changes in the crystalline structure. The reduction in crystallinity for the low molecular weight component has been related to the appearance of a lower number of active sites for nucleation, which tends to negatively affect (reduce) pore formation, as will be discussed later in this chapter. [4-6]. The reduction in crystallinity was also evident in the DSC as the amount of PP-VF increased, as happens likewise with the orientation. However, the crystallinity

for the samples obtained by blending 2 wt % of the long-chain branching polypropylene was similar to the neat resin. Thus, the greatest difference between these two samples lies mainly in the degree of orientation achieved, as discussed above.

Thermograms of membranes (Figure 4.2c), showed a shoulder at higher temperatures related to the lamellae redistribution after stretching. During the cold and hot stretching steps, pores were created and enlarged due to the stretching of short and long ties chains. This resulted in a local crystallization, which explains the appearance of the so-called “interconnected bridges” that joined main crystal lamellas. The presence of this new and stable recrystallized structure also caused the disappearance of the left plateau related to the annealed precursor films [4-12].

This right shoulder was more pronounced in samples PP-HM<sub>w</sub> and PP-2BR, which was evidence of the generation of a larger number of interconnected bridges and a greater number of pores. Pore morphology micrographs (Figure 4.3) seem to be related to the increase in interconnected bridges, as the pores in PP-HM<sub>w</sub> and PP-2BR were larger in size and density. It is also evident that a more intense lamellar structure was obtained when high molecular weight resin or long chain branched polypropylene was added, due to the longer relaxation time of macromolecules. The size of the pores was similar in both samples, but for the PP-HM<sub>w</sub> a more uniform pore structure was obtained, probably due to the higher degree of molecular orientation. Contrarily, the addition of very low molecular weight polypropylene (PP-VF) caused a gradual reduction in pore density as in the porous area. Thus, the negative influence of low molecular weight on the crystallization process could also be confirmed by SEM. Thicker and less oriented crystals blocks led to a non-uniform lamellar separation that decreased pore formation.

Finally, there was a close correlation between the percentage of the available pore area and the Gurley permeability values for all samples (Table 4.1). This accounts for the primary mechanism of this kind of membranes, acting as a flux restrictor, depending on the pore size and effective porous area.

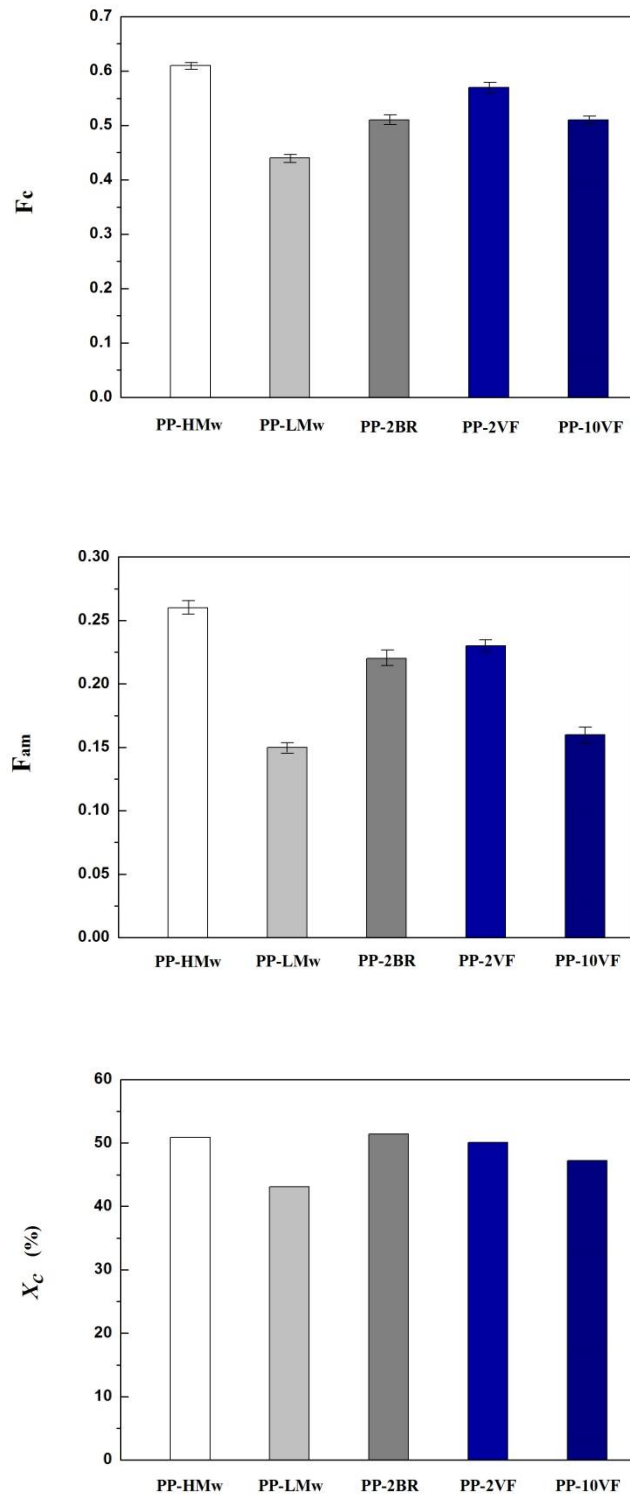


Figure 4.1. (a) Crystalline and (b) amorphous orientation parameters derived from infrared measurements, and (c) crystallinity obtained from DSC thermograms. Precursor films annealed at 140 ° C for 15 min.

Table 4.1. Polymer composition analysis in terms of membrane pore morphology and membrane permeability.

Sample	Pore density (pores/ $\mu\text{m}^2$ )	Porous area (%)	Average pore size ( $\mu\text{m}$ )	Gurley Permeability [ $\mu\text{m}/(\text{Pa}\cdot\text{s})$ ]
PP-HM <sub>w</sub>	8.7	6.3	0.15	0.19
PP-LM <sub>w</sub>	2.1	1.3	0.13	0.01
PP-2BR	10.7	6.2	0.13	0.15
PP-2VF	6.0	4.7	0.17	0.14
PP-10VF	3.7	2.3	0.14	0.02



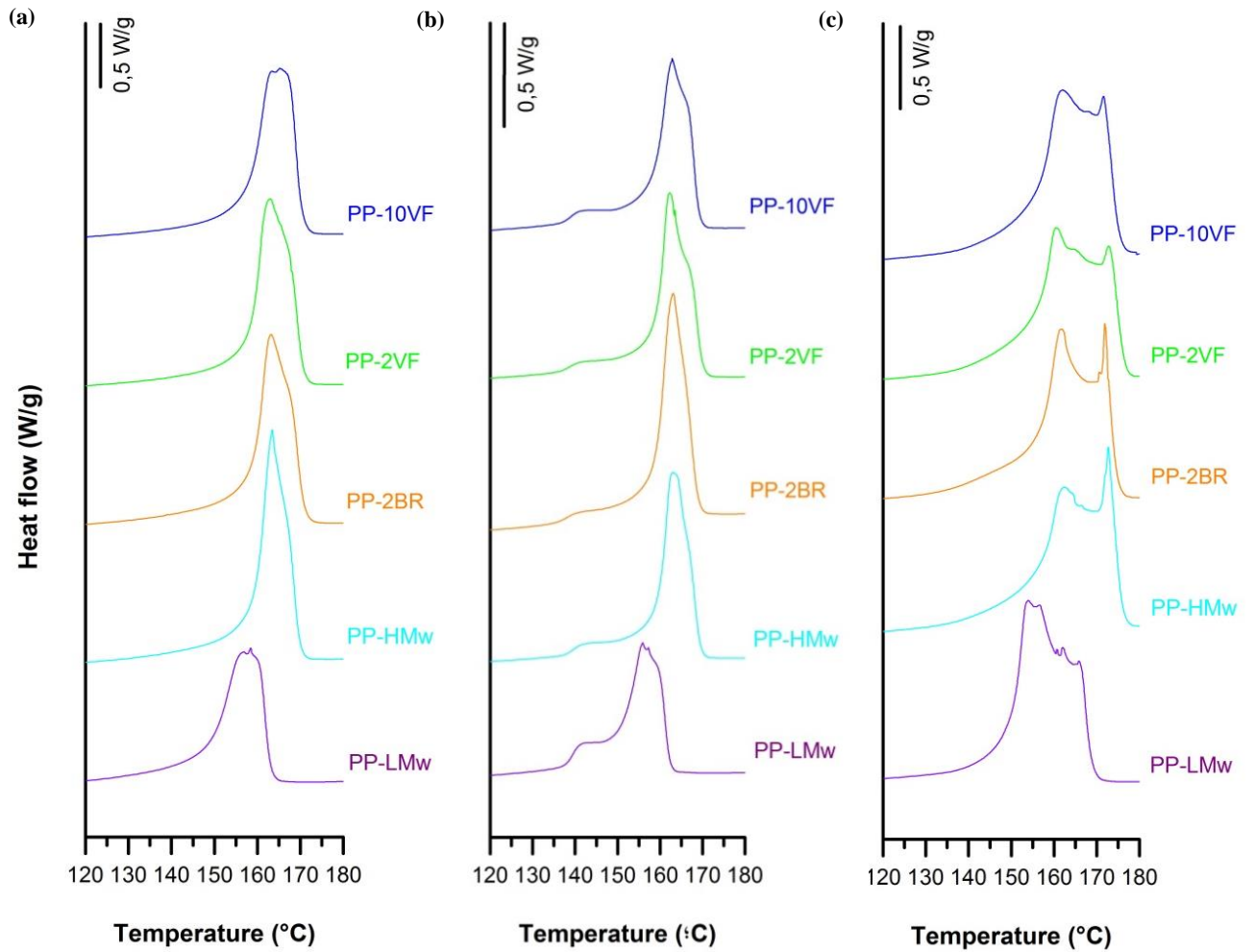


Figure 4.2. Thermograms differing in sample composition. (a) Precursor films, (b) annealed precursor films, (c) membranes.

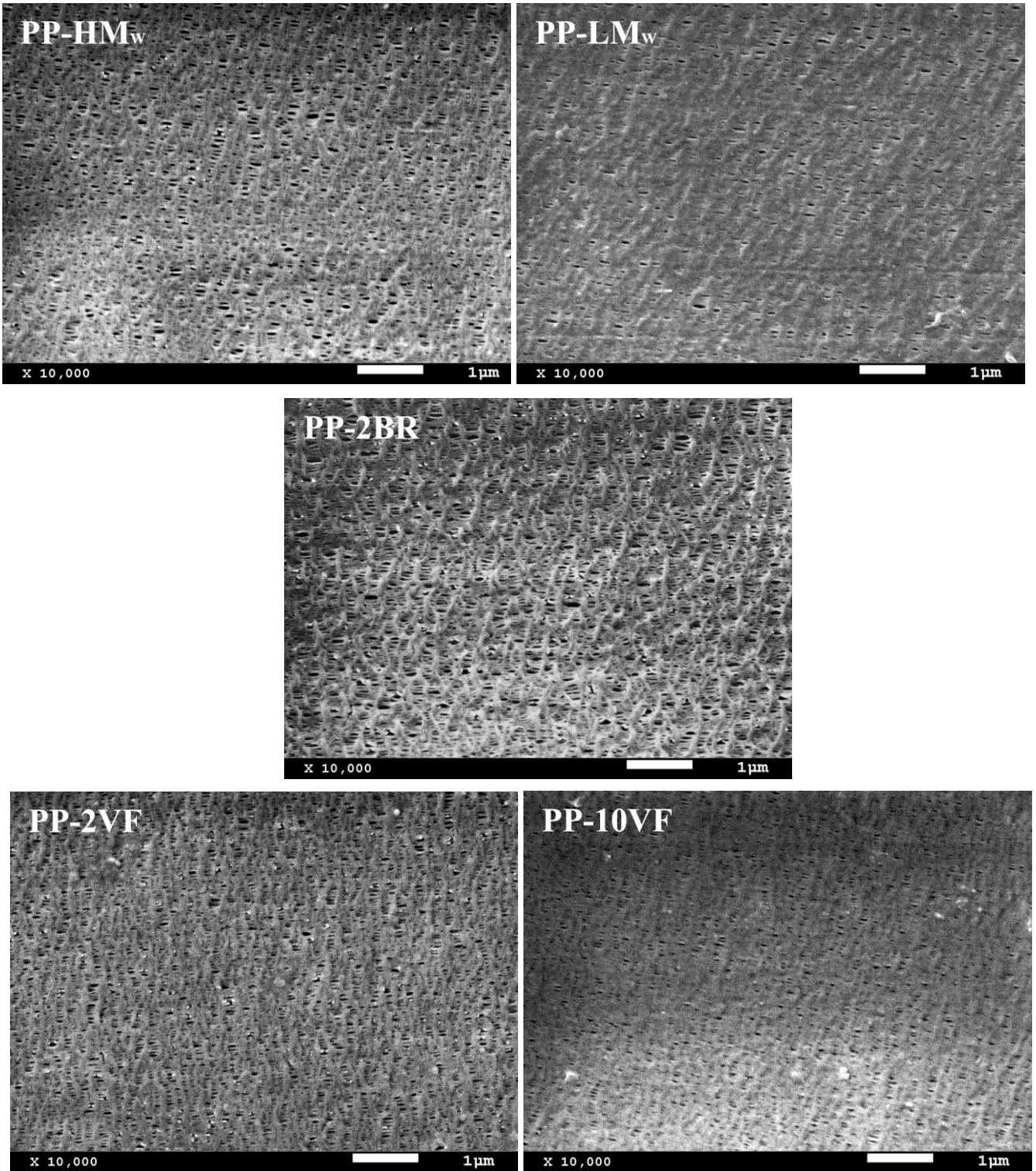


Figure 4.3. Scanning Electron Microscopy (SEM) micrographs of membranes differing in sample composition.

#### 4.2. Influence of draw ratio

For this study, the PP-2BR samples were selected, and the numerical results obtained are presented in Table 4.2. In the cast film extrusion process and before thermal annealing, the molten polymer emerging from a flat die was stretched by applying air cooling and higher draw ratios. Under these conditions, an optimal row-nucleated structure was achieved when the lamellae aligned themselves perpendicular to the machine direction. This enhanced the crystal thickness as well as the orientation of the crystalline and amorphous phases. Thus, samples showed a noticeable increase in the orientation of the crystalline phase when high draw ratios were imposed during the extrusion process, as can be seen in Figure 4.4.

A bimodal distribution of the melting peak was also noticed in the DSC thermograms (Figure 4.5b). As mentioned above, this right shoulder indicated the presence of the so-called “interconnected bridges” formed during lamellae separation. The higher crystalline orientation in the precursor films resulted in the generation of a larger number of pores, and thus a larger number of interconnected bridges formed between them. These results are in agreement with the findings of other authors [4-21]. However, a maximum pore density and a porous area were reflected by the highest Gurley permeability value registered. A higher orientation value drove to the reduction of the amorphous tie chain mobility, leading to the limitations on pore enlargement observed in films produced under high draw ratios. Besides, it was speculated that the highest draw ratio provided finer precursor films that cooled more rapidly, and thus less-than-perfect crystalline entities were formed during the extrusion stage.

**Table 4.2. Draw ratio analysis in terms of membrane pore morphology and permeability. Processing conditions: Gap die, 1.9 mm; cold stage, 0.3 mm/min, 20% ; hot stage, 0.3 mm/min, 130%.**

Sample	Draw ratio	Pore density (pores/ $\mu\text{m}^2$ )	Porous area (%)	Average pore size ( $\mu\text{m}$ )	Gurley Permeability [ $\mu\text{m}/(\text{Pa}\cdot\text{s})$ ]
PP-2BR	80	12.1	9.8	0.17	0.18
	95	12.3	5.9	0.13	0.16
	105	13.4	7.7	0.14	0.16

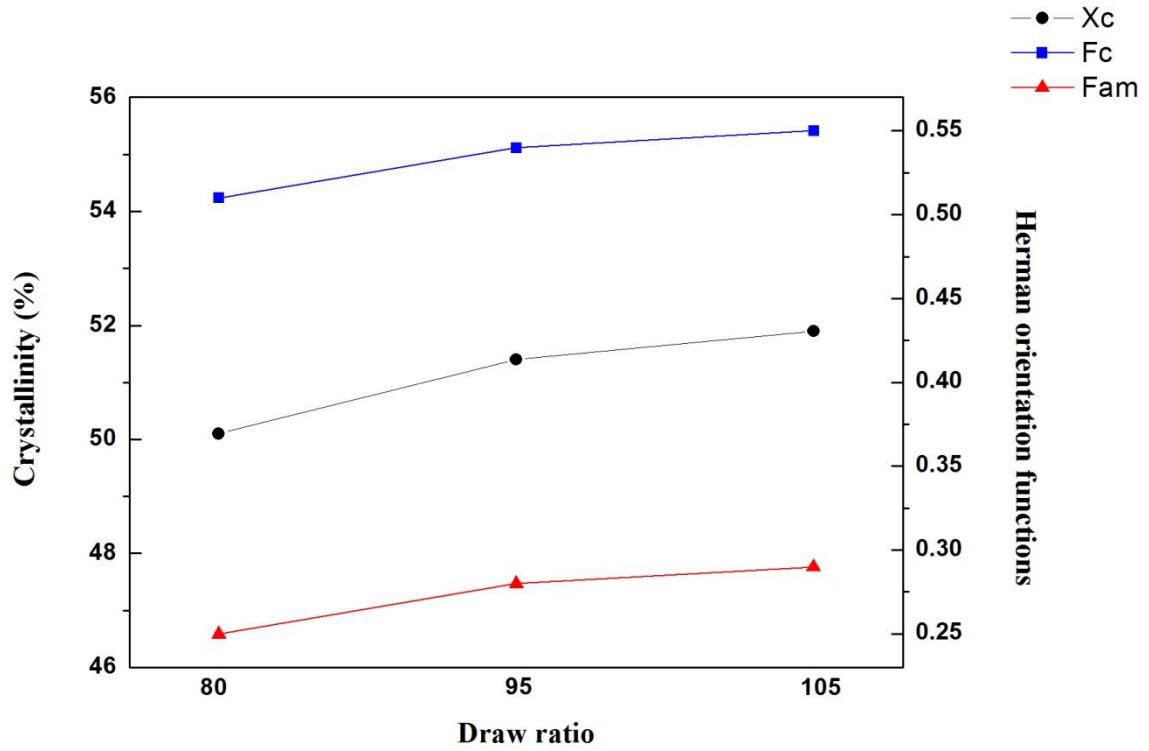
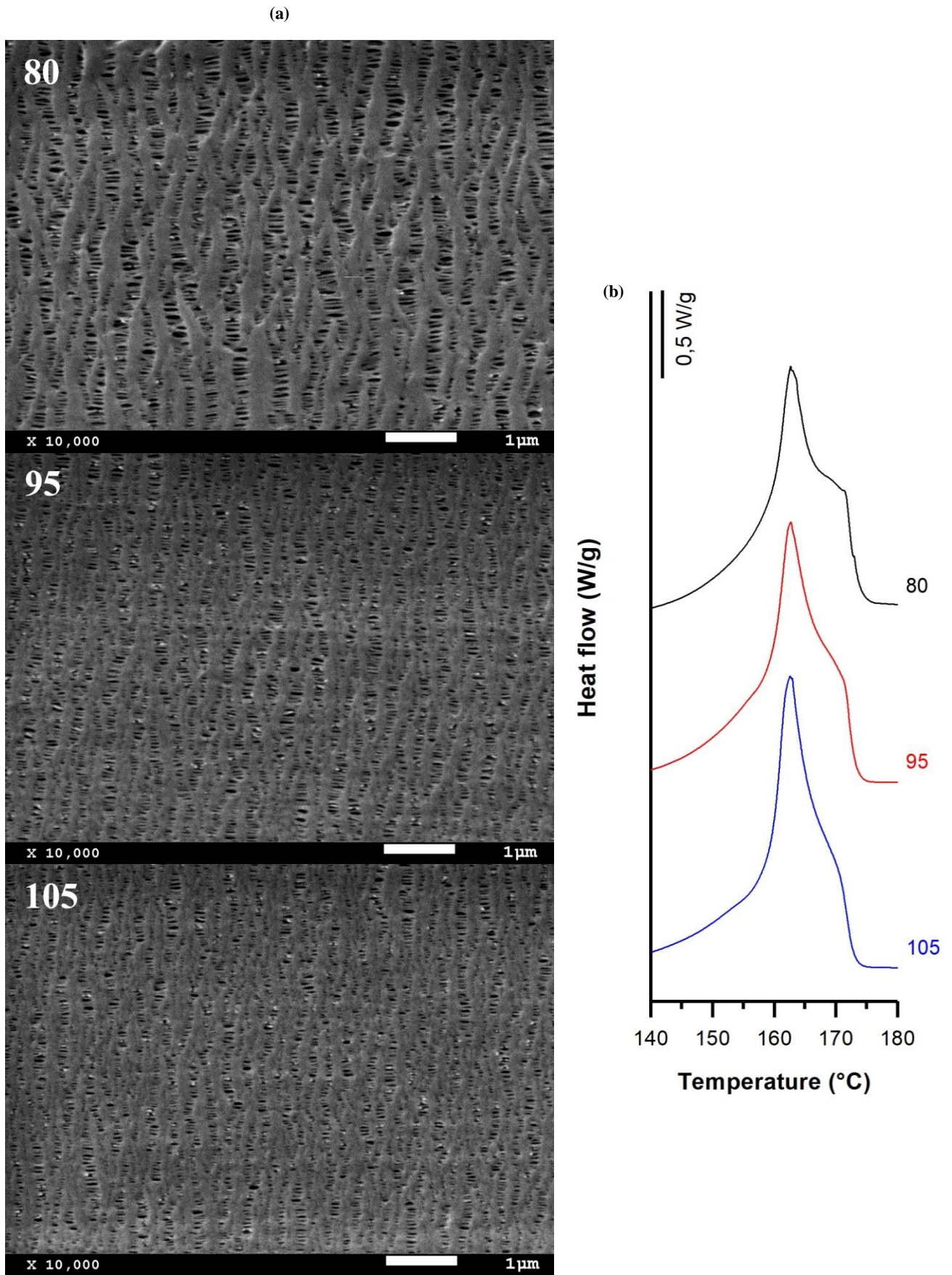


Figure 4.4. (■) Crystalline and (▲) amorphous orientation parameters derived from infrared measurements, and (●) crystallinity obtained from DSC thermograms. Precursor films annealed at 140 ° C for 15 min.



### 4.3. Influence of uniaxial strain

An in-depth analysis of the experimental conditions that affect the uniaxial strain stage is presented in this section. All the samples were obtained using a gap die of 1.9 mm and a draw ratio of 80 in the extrusion stage. The material employed in all cases was PP-HM<sub>w</sub>. Variations of strain rate and extent of deformation were performed in the cold and hot stages. Table 4.3 summarizes the conditions applied and the results in terms of pore morphology and air permeability. All figures in this section show the close relationship between pore morphology (SEM micrographs) and crystalline entities (DSC thermograms).

Table 4.3. Uniaxial strain analysis in terms of pore morphology and permeability.

Cold stage		Hot stage		Pore density (pores/ $\mu\text{m}^2$ )	Porous area (%)	Pore size ( $\mu\text{m}$ )	Gurley Permeability [ $\mu\text{m}/(\text{Pa}\cdot\text{s})$ ]
Strain rate (mm/min)	Extent (%)	Strain rate (mm/min)	Extent (%)				
<b>0.3</b>	35	<b>0.3</b>	320	9.3	20.2	0.36	0.29
<b>1.0</b>		<b>1.0</b>		10.5	17.0	0.25	0.24
<b>0.3</b>	35	0.3	320	9.3	20.2	0.36	0.29
<b>50.0</b>				8.9	18.1	0.33	0.25
0.3	20	<b>0.3</b>	130	9.4	14.6	0.25	0.22
		<b>50.0</b>		12.9	4.9	0.09	0.07
	<b>20</b>			6.8	13.9	0.32	0.22
1.0	<b>35</b>	1.0	320	10.5	17.0	0.25	0.24
	<b>55</b>			8.9	11.3	0.21	0.20
0.3	20	0.3	<b>65</b>	9.3	2.8	0.09	0.02
			<b>100</b>	14.0	5.4	0.11	0.08
			<b>130</b>	9.4	14.6	0.25	0.22
			<b>300</b>	7.8	18.8	0.35	0.26

#### **4.3.1. Effect of strain rate**

As depicted in Table 4.3 and Figure 4.6, at high strain rates the applied stress during lamellae separation was high enough to raise the number of pores. This was attributed to breakage in a greater number of tie chains between the crystals due to less flexibility of the amorphous phase at room temperature. However, this reduction in the molecular motion with increasing strain rate also limited the separation of lamellar blocks, and thus the pore enlargement.

In membranes prepared at higher strain rates during the cold stage, the contribution of shoulder peaks attributed to connecting bridges was lower, as can be observed in Figure 4.7b. In any case, membranes prepared at lower strain rates at room temperature showed slightly larger Gurley permeability values. This made it possible to obtain membranes with similar properties with a significant reduction in testing time.

According to the theory proposed by other authors [4-21,27-39], pores created during the cold extension were enlarged during the hot stretching step as the stress increased linearly. This is due to the larger flexibility of the tie chains located between the crystalline blocks. The SEM micrographs in Figure 4.8 showed a reduction in pore size, reduced lamellar separation, and shorter interconnecting bridges when higher strain rates were employed. Increases in strain rate provided for a more rigid material due to an insufficient time for the chains to move.

Higher porosity and Gurley permeability values were obtained when applying lower strain rates at higher temperatures due to the lower resistance exerted by lamellae separation (the chains slide easily over each other) [10]. Lower pore density and larger pore size for membrane stretched at lower rates could be explained as a possible collapse of pores due to breakage in some connecting bridges. Some chains could be pulled out from the initial lamellae and recrystallized in this stage, forming a thicker and more uniform crystalline structure [16-19].



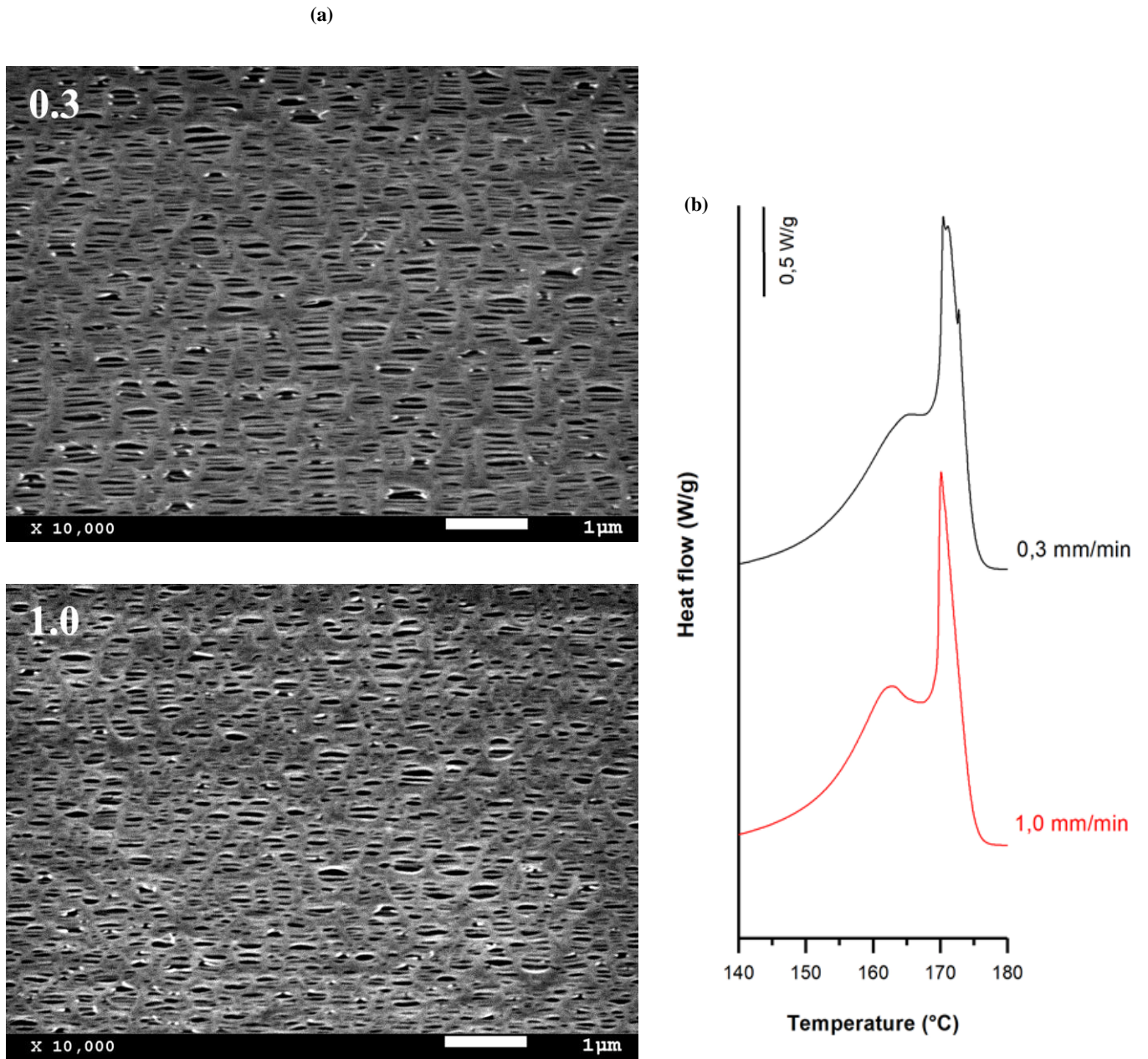


Figure 4.6. Influence of same cold and hot strain rates (upper-left, in mm/min) (a) SEM micrographs and (b) DSC thermograms. Common uniaxial strain conditions: Cold stage, 35%; hot stage, 320%.



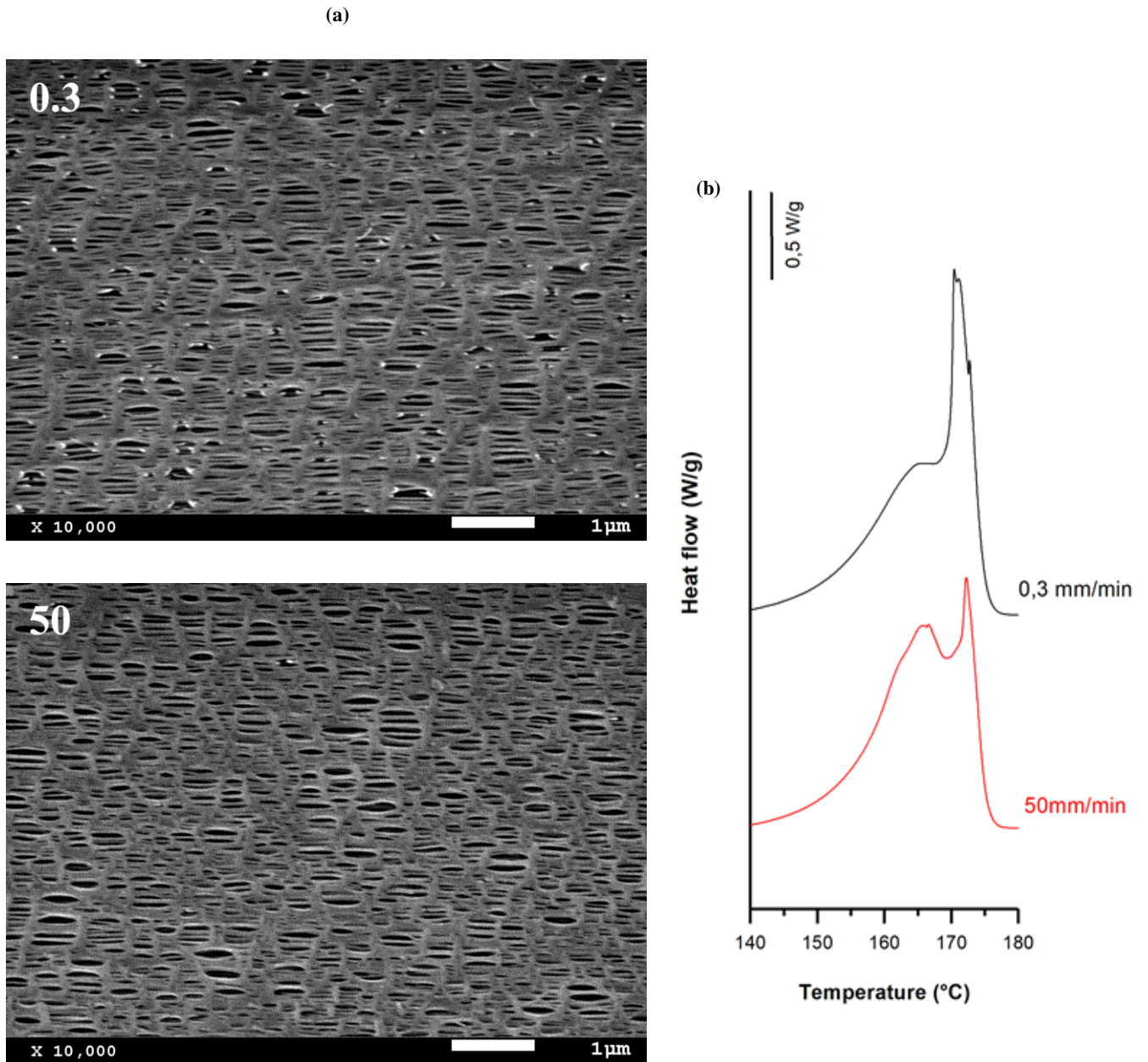


Figure 4.7. Influence of cold strain rate (upper-left, in mm/min) (a) SEM micrographs and (b) DSC thermograms. Common uniaxial strain conditions: Cold stage, 35%; hot stage, 0.3 mm/min, 320%.

(a)

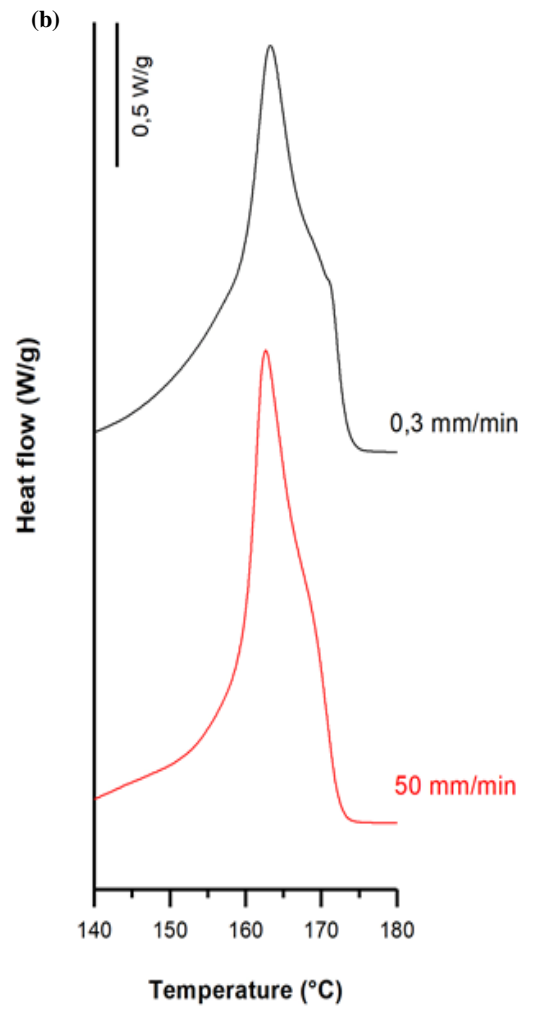
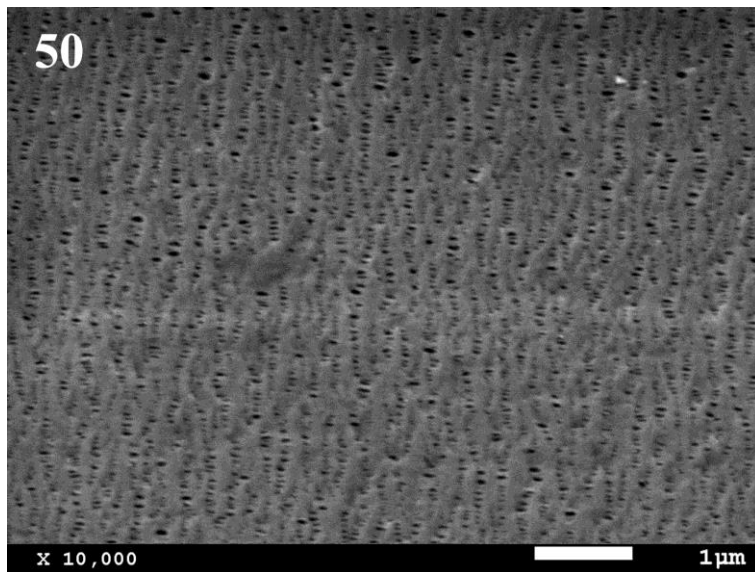
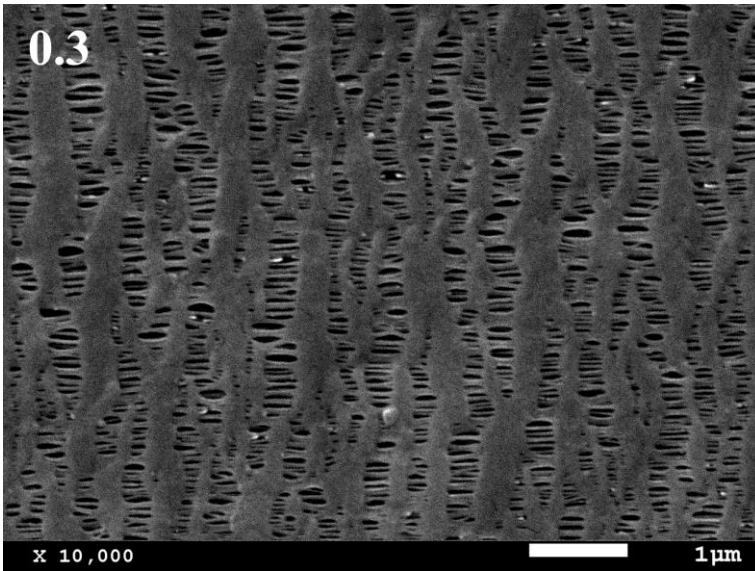


Figure 4.8. Influence of hot strain rate (upper-left, in mm/min) (a) SEM micrographs and (b) DSC thermograms.

Common uniaxial strain conditions: Cold stage, 0.3 mm/min, 20% ; hot stage, 130%.

#### **4.3.2. Effect of strain extent**

During cold and hot stretching, the secondary crystals formed during the annealing process and some chains from the initial lamellae structure created the connecting bridges that separate pores. [4-21]. As stated before, the low mobility of macromolecules and the increase of strain extent during the cold stage led to pores formation due to chain scission during lamellae separation.

Conversely, the effect of applying a higher percentage beyond an optimum value of about 35 % for the cold stretching step caused a reduction in pore density. An explanation could be the lamellae fragmentation produced at higher stretch values, which may have generated a reduction in the crystalline orientation and a collapse of pores when fibrils got closer to each other due to an elastic response [32]. It is of note that this optimal value in cold strain extent was related to a very intense secondary melting point (contribution from connecting bridges) in the main membrane melting peak, as is depicted in Figure 4.9.

The influence of applying a high stretch ratio (up to 300%) during the stretching step at high temperatures was investigated. The larger the hot stage extension, the greater the pore size and uniformity. This phenomenon could be attributed to the higher flexibility and mobility of the macromolecules at elevated temperatures, resulting in a greater lamellae separation and also to the enlargement of some invisible pores after cold extension.

The sample stretched to 300 % had a smaller number of pores but a larger average pore size than previous samples, as shown in Figure 4.10. This could result from the breakage of some connecting bridges that reduced its thickness with a higher stretch ratio. Porosity and thus, Gurley permeability was too dependent on the global strain extent, and their values increased with increases in the global strain. Noticeable growth in the pore size was evident in conjunction with the gradual occurrence of a secondary shoulder in the main DSC peak at greater strain extents. This also related to the presence of longer recrystallized connecting bridges.



(a)

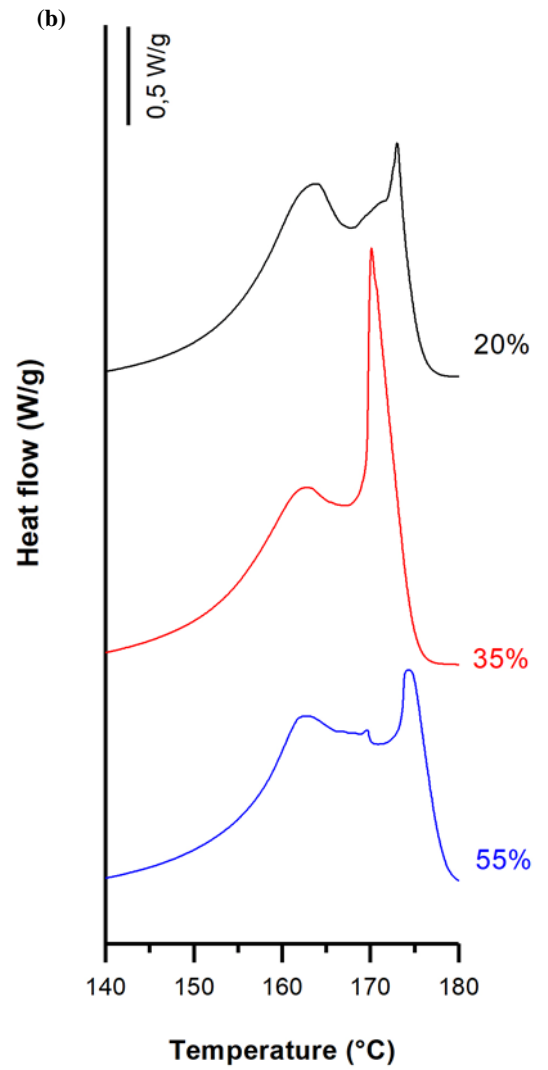
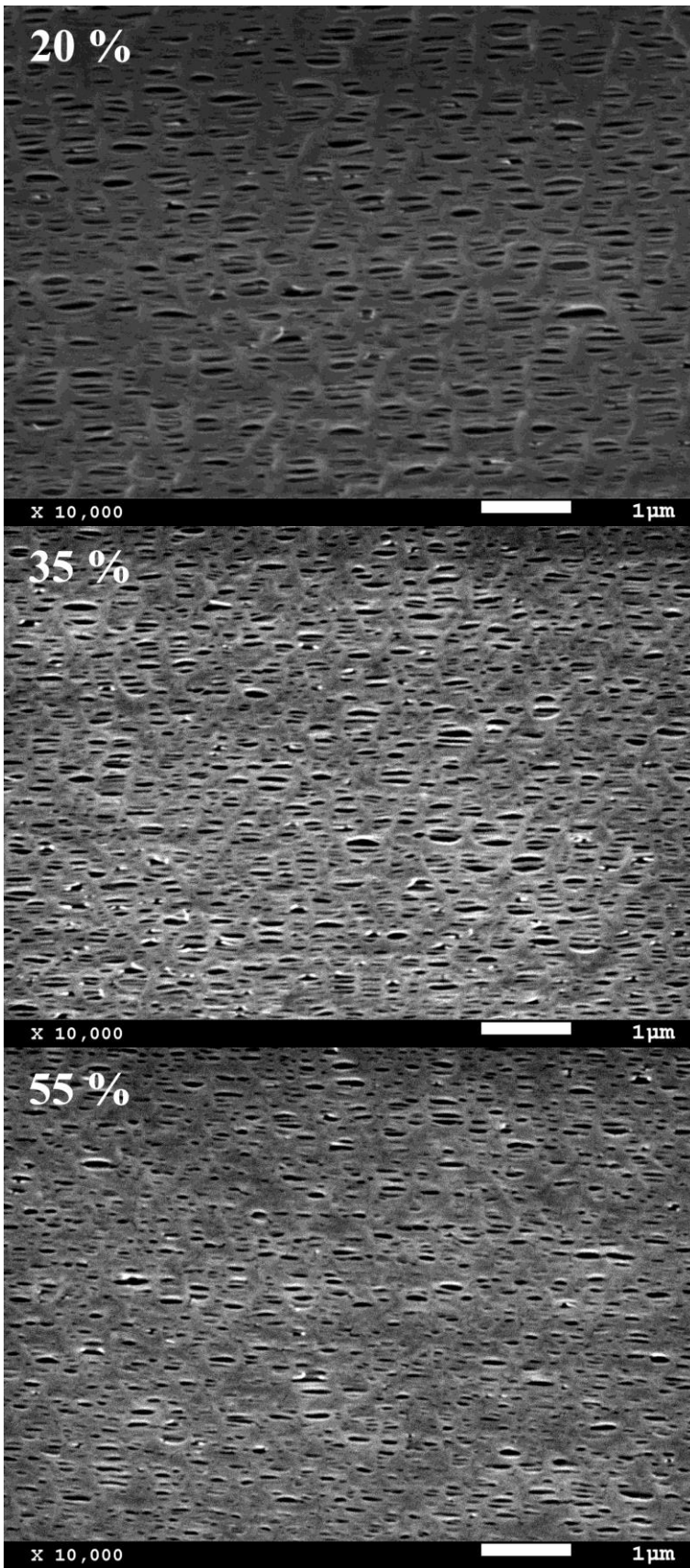


Figure 4.9. Influence of cold strain extent (a) SEM micrographs and (b) DSC thermograms. Common uniaxial strain conditions. Cold stage, 1.0 mm/min; hot stage, 1.0 mm/min, 320%.

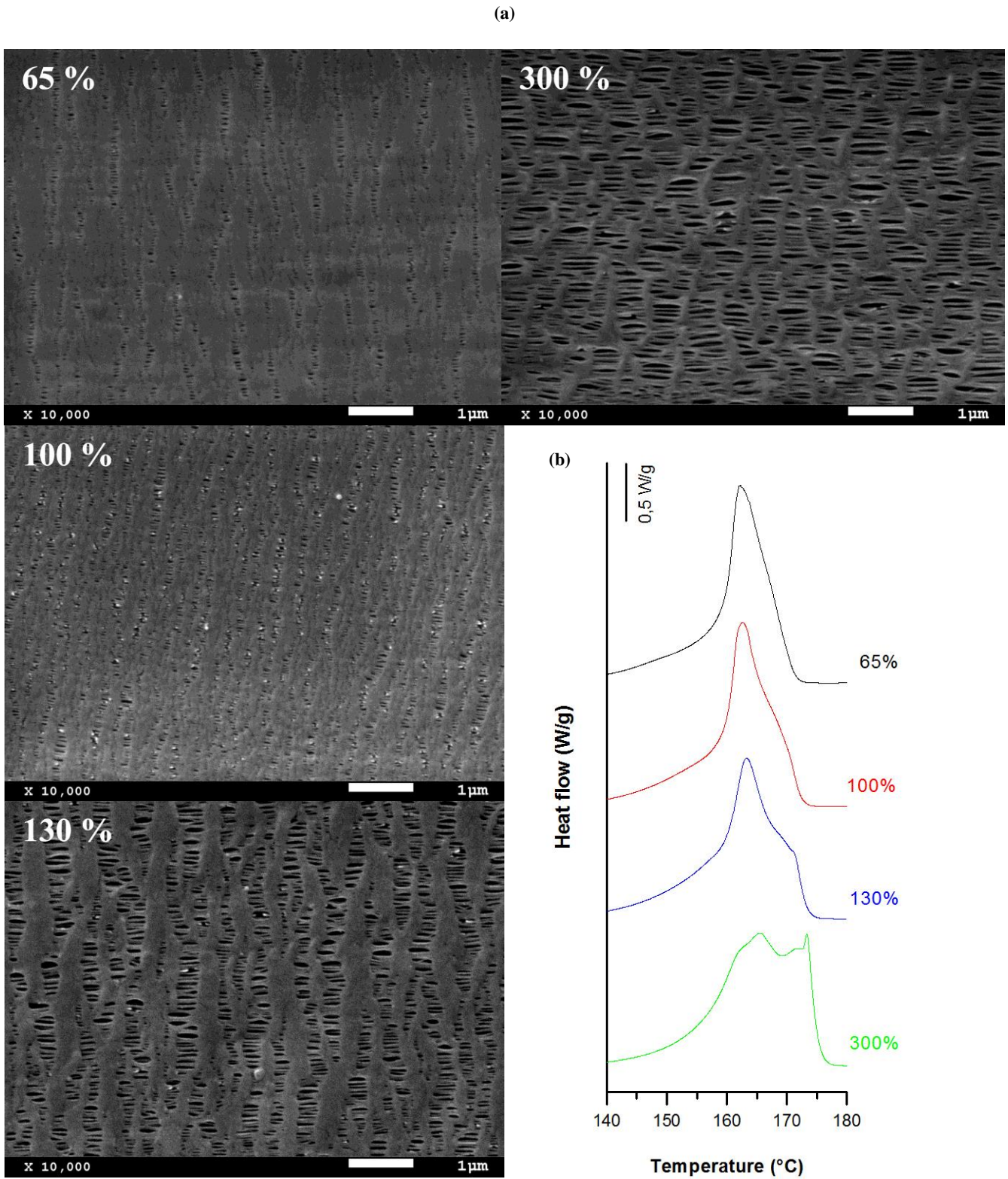


Figure 4.10. Influence of hot strain extent (a) SEM micrographs and (b) DSC thermograms. Common uniaxial strain conditions. Cold stage 0.3 mm/min, 20%; hot stage, 0.3 mm/min.

#### 4.4. Practical case: Membranes as integral parts of lighters.

These membranes can be used as integral parts of lighters, regulating the flux of gas necessary to create a flame. Most lighters use isobutylene as the substance responsible for creating the flame. Figure 4.11 shows a linear trend of the permeability of some of the membranes studied in the uniaxial strain analysis concerning the porous morphology developed. This linear trend is a confirmation of the permeation mechanism of this kind of porous material, acting as a flux restrictor, depending on the pore size and the porous area.

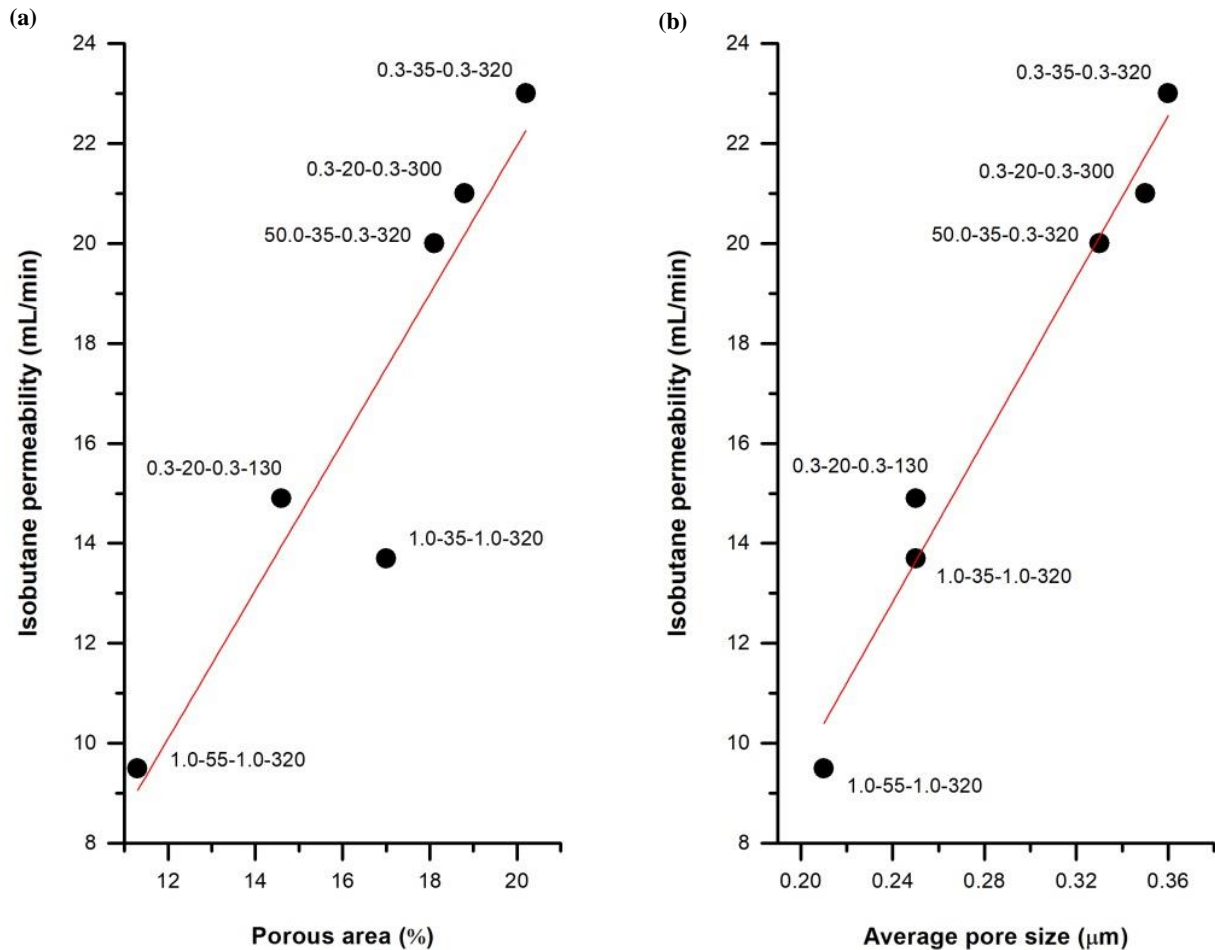


Figure 4.11. Isobutane permeability of some PP-HM<sub>w</sub> membranes as a function of (a) porous area and (b) average pore size. Each point refers to the following sequence: crosshead speed (cold), strain extent (cold), crosshead speed (hot), strain extent (hot).



#### **4.5. Discussion and main conclusions**

In this work, we investigated the influence of polymer composition on the structure of polypropylene membranes. The results support the idea discussed in previous works [4-21] regarding the high importance of the polymeric matrix nature in the generation of precursor films capable of producing a row-lamellar crystalline structure. Based on the SEM micrographs and DSC results of neat polypropylenes with different molecular weights and blends with branched and very fluid PP resins, the discussion of our results can be summarized as follows.

Lower porosity and permeability values were observed when low molecular weight polypropylenes, such as PP-LM<sub>w</sub> and, above all, PP-VF were employed. The use of these polymers is counter-productive with regards to keeping a macromolecular alignment for long enough duration to generate an appropriate row-lamellar crystalline structure. The macromolecular rearranging restricted the hypothesized positive effects with regards to greater deformation during the uniaxial strain stage. Contrary, the pores in PP-HM<sub>w</sub> and PP-2BR were larger in size and density. Pore sizes were similar in both samples, but for the PP-HM<sub>w</sub> a more uniform pore structure was observed due to the higher degree of molecular orientation achieved after extrusion.

Regarding aspects related only to extrusion processing parameters, crystalline phase orientation was found to be highly dependant on the drawing conditions. [6-8]. This imposed macromolecular alignment along the extrusion direction is very relevant with concerning the final morphology of membranes. By increasing the applied draw ratio during the extrusion step, a macromolecular alignment along extrusion direction was imposed, and an optimal row-nucleated structure concerning the final porous membrane morphology was achieved. Nevertheless, values above a certain draw ratio did not show a significant improvement in membrane performance since the higher crystalline orientation limited the pore enlargement and no higher porosity or permeability values were obtained.

Likewise, the uniaxial strain stage was decisive in the porous morphology of membranes. Using extreme strain conditions, that is, very low strain rates or very high strain extent, it was possible to generate a wide range of porous morphologies directly related to the air permeability characteristics of these samples. Main results of this detailed study can be summarized as follows:

Slight porosity and Gurley permeability were obtained by applying very low strain rates for stretching at room temperature. However, related to the strain ratio applied during this cold stretching step, there is an optimum extent percentage close to 35% to produce high performance membranes.

During stretching at high temperatures when the mobility of the macromolecules was increased, a slower strain rate and a higher strain extent had a significant effect on the final porous morphology. Changes in the crystallized structure during this step were produced. Higher permeability values could be obtained due above all to the coalescence of close neighbor pores and the pore enlargement with greater lamellae separation until the total collapse of the crystalline structure occurred. These bigger pores tend to have an elliptical shape and positive consequences regarding the Gurley permeability values registered. However, passing from a total strain extent of 130 % to 300 % did not substantially increase membranes permeability. Nevertheless, it should be taken into account that these extreme conditions would lead to longer production times. Finally, a strong linear relationship between the porous area and the permeability to isobutene has been found.





## **Chapter 5:**

# **Polypropylene-ethylene copolymers based porous membranes**



Porous membranes based on polypropylene-ethylene copolymers were prepared by melt extrusion, followed by annealing and stretching processes. Blends with these copolymers were mainly prepared with the aim of producing homogenous porous membranes, increasing at the same time the pore size and pore size distribution. Samples from neat resins and their blends were produced at a constant draw ratio and using different extrusion, annealing, and stretching temperatures to study the influence of these variables in forming the characteristic pore structure. This chapter presents the results of experiments that examined the effect of polymer composition and processing variables on the crystalline features, porous structure, permeability, and mechanical properties of the porous membranes.

All the samples discussed in this section were obtained under the same processing conditions. A co-rotating twin-screw extruder equipped with a gap die 25 mm-width and an opening of 1.9 mm was used. The extrusion draw ratio was kept to 70 to obtain a precursor film of about 27-29  $\mu\text{m}$ , and the uniaxial strain stage was carried out during the cold stage at 50 mm/min, up to 35% strain extent and during the hot stage at 10 mm/min, up to 230 % strain extent.

### **5.1. Influence of extrusion and annealing temperature on neat resins**

In the first step of the MEAUS technique is possible to control some of the properties of the precursor film and, consequently, the properties of the resulting membranes. For this research investigation, a homopolymer resin of polypropylene (PP-HM<sub>w</sub>) and a heterophasic and random ethylene-polypropylene copolymers (PP-B and PP-R, respectively) were selected to investigate the influence of processing temperature on these materials. To calculate the optimum extrusion temperature for producing precursor films having a row-nucleated lamellar structure, two different processing temperatures were selected: 250 °C and 270 °C.

Some of the parameters derived from DSC analysis included the melting temperature, the heat of fusion, and the degree of crystallinity measured by the heat of fusion. The melting temperature of PP-HM<sub>w</sub> was about 164 °C. In comparison with the PP homopolymer, random copolymers exhibited a low melting point close to 145°C. To determine the total melting point reduction in these copolymers, it was necessary to consider both the amount of ethylene comonomer and its distribution along the polymer backbone [107,108]. On the other hand, the heterophasic polypropylene exhibited the same melting temperature as a homopolymer but had a lower heat of fusion. This was due to the presence of the amorphous, elastomeric phase (ethylene propylene rubber), which reduced the total heat of fusion related to the proportion of the crystalline phase present in the polymer [107,108].

In Figure 5.1, DSC thermograms show the microstructural changes exhibited by the samples produced with the neat PP (homopolymer and heterophasic copolymer) during the annealing and uniaxial stretching steps. The neat PP random copolymer was not a good candidate to form the porous membrane, and for this reason, the data has not been included in this study. From the DSC thermograms shown in Figure 5.1b, it could be observed the presence of a shoulder at lower temperatures from the main melting peak related to the annealing of the precursor films. During this process, a new secondary crystalline structure was formed between the amorphous and the main crystal lamellae, as discussed in the previous chapter. High annealing temperatures promoted an increment in molecular mobility and structural rearrangement, increasing lamellar thickness and reducing irregularities [8,13-17,128].

From the DSC curves shown in Figure 5.1c, corresponding to membranes produced after annealing, this left shoulder disappeared and the total area was wider, which was attributed to the presence of a broad range of crystalline structures with different lamellar thicknesses. Moreover, a more intense right peak was observed due to the molecular orientation induced by stretching. During this uniaxial stretching step pores were formed and pore size increased with greater lamellae separation. This right peak was related to the stable crystalline form achieved in this step, where some tie chains were stretched and promoted the crystallization of the so-called “interconnected bridges” that joined main crystal lamellae and divided the pores [4-12].

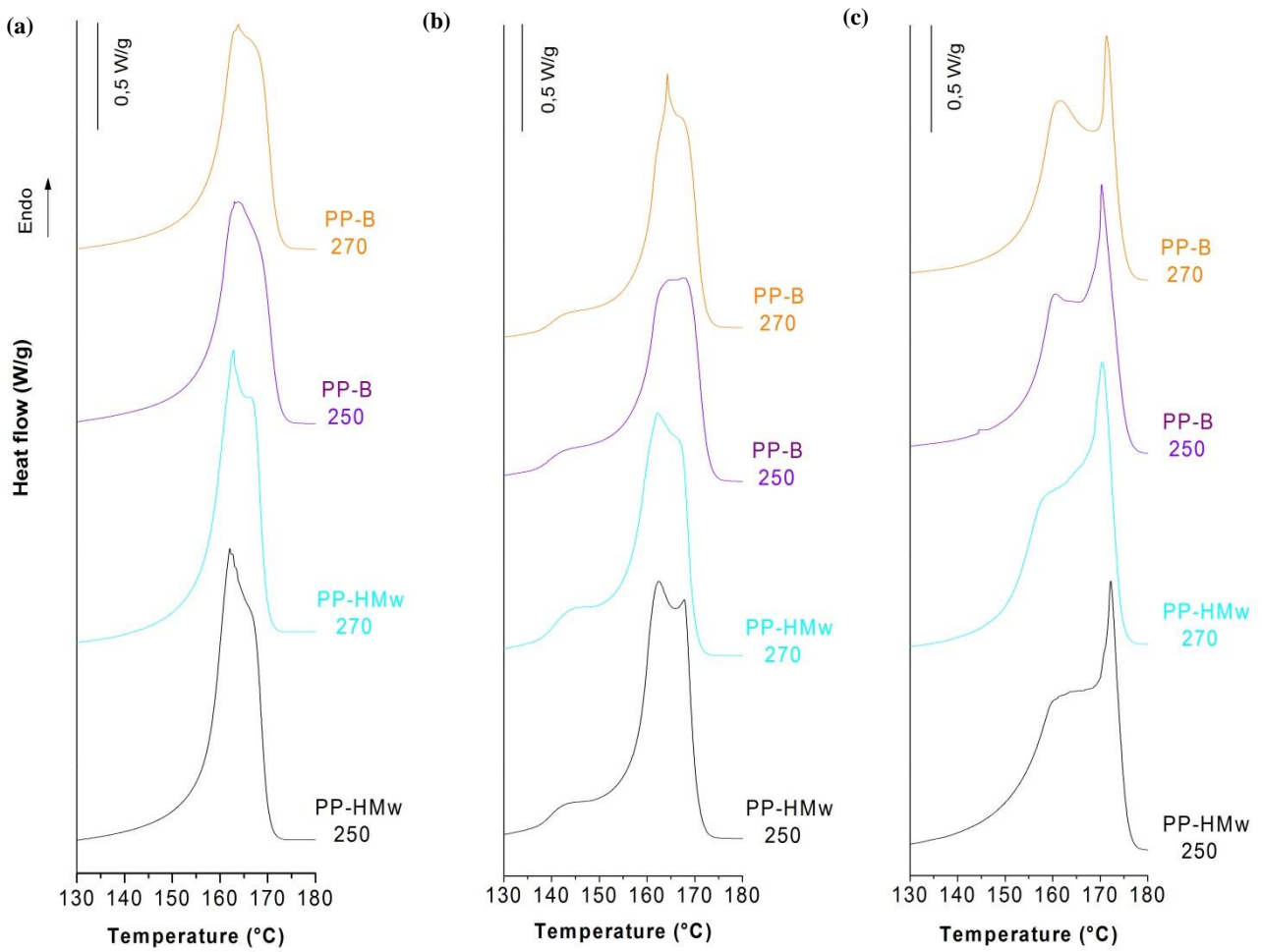


**Figure 5.1. Differential scanning calorimetry (DSC) thermograms of samples PP-HM<sub>w</sub> and PP-B extruded at different temperatures (250 and 270 °C). (a) Precursor films, (b) annealed precursor films at 140 °C, (c) membranes (cold stage, 10 mm/min, 35%; hot stage, 10 mm/min, 230%).**

All membranes' curves showed similar shape and width of the endothermal melting peak, so it was assumed that all samples had similar lamellar thicknesses. Therefore, the main differences between the resins extruded at different temperatures were observed in both the molecular orientation and the pore structure parameters. As displayed in Figures 5.2 and 5.3, there was a progressive increase of the crystallinity and the orientation factor determined by polarized infrared spectroscopy FT-IR when we increased the annealing temperature of precursor films. This phenomenon was due to an increment of the molecular rearrangement kinetics into a more dense and stable secondary form, as discussed above.

Homopolymer and block copolymer extruded at the same draw ratio but at a temperature above 250 °C promoted the formation of a row-nucleated structure with a lower orientation factor, which reduced the porosity and permeability of membranes, as depicted in Table 5.1.

Comparing the SEM micrographs taken from the surface of membranes for the PP-HM<sub>w</sub> and PP-B samples (Figure 5.4), the pore density values were quite similar. Still, it could be noticed that larger pore sizes were obtained when membranes were produced with the heterophasic polypropylene. Some authors have studied the phase-separation structure formed in rubber-modified PP copolymers in which copolymer nodules are distributed throughout the semicrystalline homopolymer matrix [136-139]. It was speculated that the pore size increases due to cavitation effects produced during the uniaxial stretching step, which results in a void space increase between the dispersed heterophasic second phase and the PP matrix. This created larger pores than those obtained using only the homopolymer, giving rise to a higher permeability.

Nevertheless, this second phase seems to interfere with lamellae crystallization in some areas promoting the appearance of non-uniform regions in membranes prepared with this copolymer, as can be seen in the SEM images. For this reason, this study aims to combine both effects by adding different percentages of PP copolymer in the homopolymer resin to achieve homogeneous membranes with greater permeability by increasing the pore size.

Finally, for both neat resins, the optimum annealing temperature seems to be about 160 °C. This temperature value, near the melting point of polypropylene, increased the air permeability by increasing the density, area, and size of pores. This behavior was a consequence of the softening of the crystalline region and the increment of flexibility in the amorphous phase at high temperatures. Furthermore, in heterophasic copolymer, some authors have demonstrated that EPR is prone to thermal degradation at above 150 °C [137,138]. This could also explain the increase in the average pore size seen in SEM micrographs. However, further investigation is needed to confirm these results and elucidate the thermal effects in this sample.

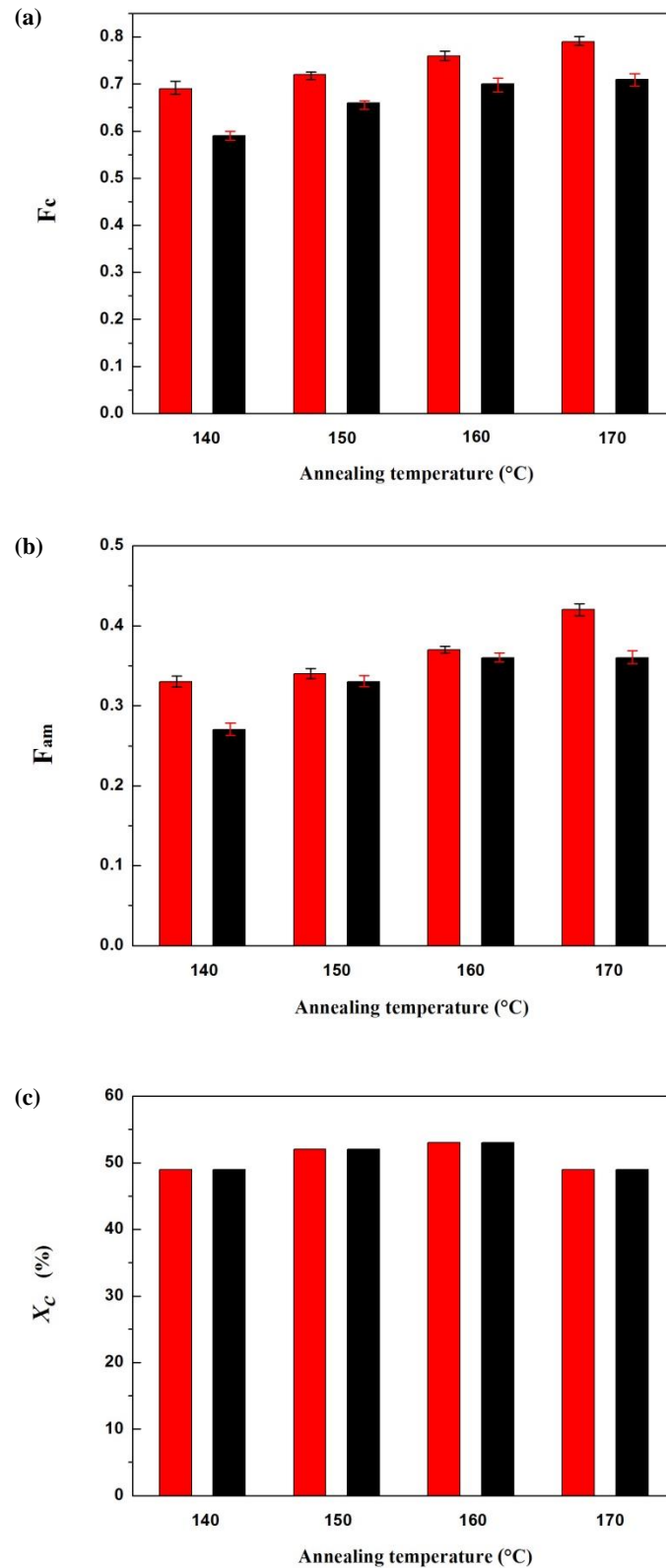


Figure 5.2. (a) Crystalline and (b) amorphous orientation parameters derived from infrared measurements, and (c) crystallinity obtained from DSC thermograms of PP-HM<sub>w</sub> precursor films annealed at different temperatures.

(Extrusion temperature: < ■ > 250 °C < ■ > 270 °C).



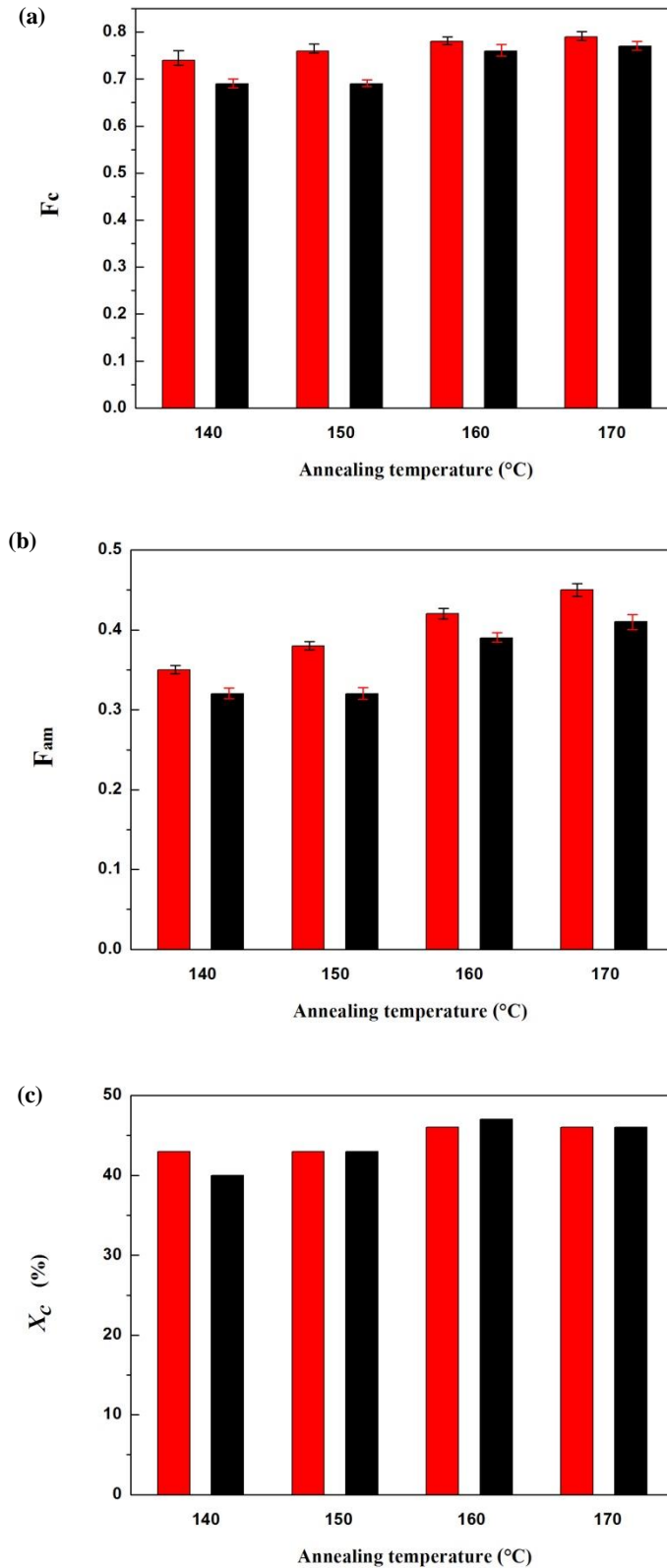


Figure 5.3. (a) Crystalline and (b) amorphous orientation parameters derived from infrared measurements, and (c) crystallinity obtained from DSC thermograms of PP-B precursor films annealed at different temperatures. (Extrusion temperature:  $\blacksquare < 250\text{ }^\circ\text{C}$   $\blacksquare > 270\text{ }^\circ\text{C}$ ).

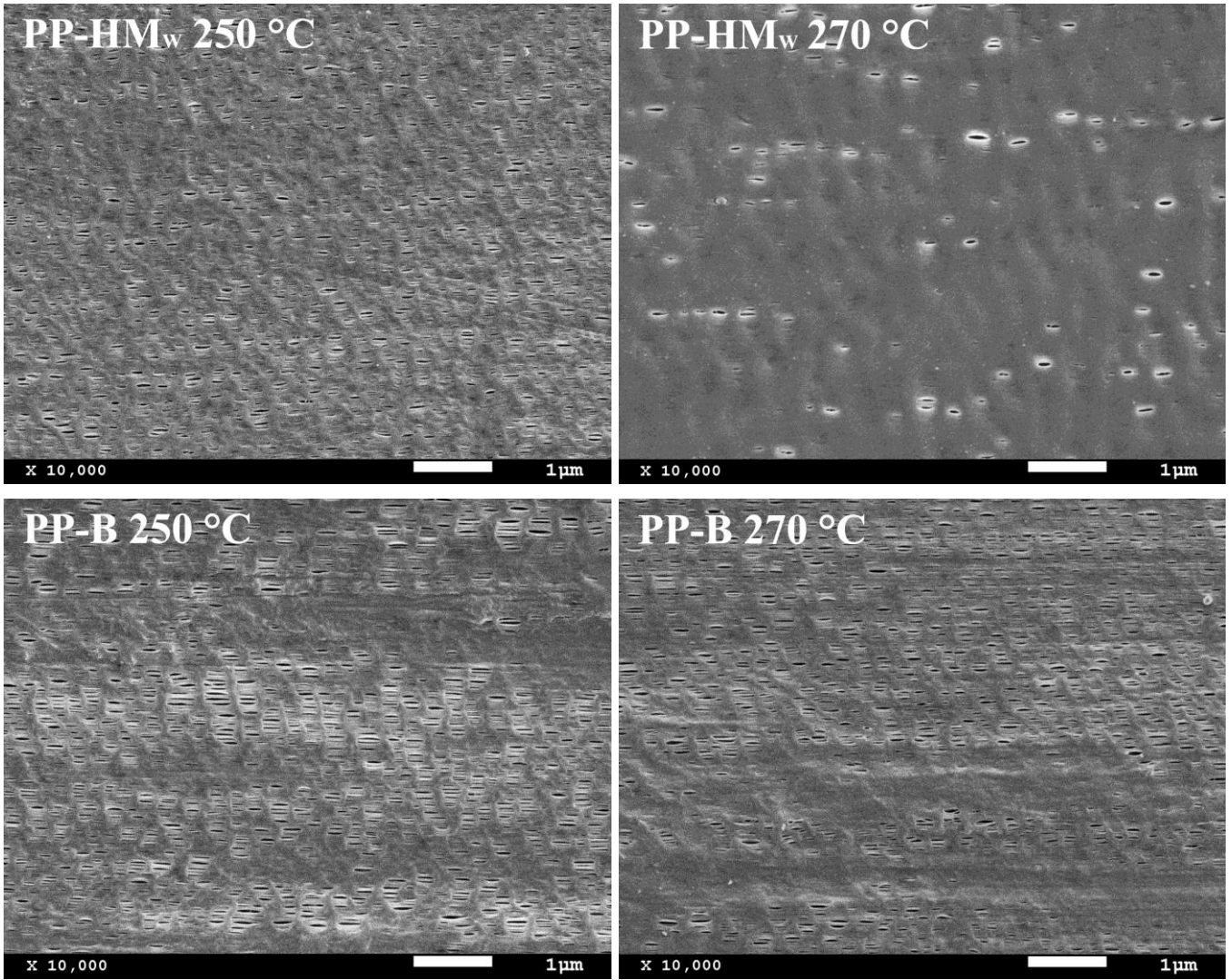


Figure 5.4. Scanning electron microscopy (SEM) micrographs of samples PP-HM<sub>w</sub> and PP-B extruded at two different temperatures (250 and 270 °C).

**Table 5.1. Characteristics of neat resins extruded and annealed at different temperatures in terms of pore morphology and air permeability.**

<b>Sample</b>	<b>Extrusion (°C)</b>	<b>Annealing (°C)</b>	<b>Pore Density (pores/<math>\mu\text{m}^2</math>)</b>	<b>Pores Area (%)</b>	<b>Average Pore Size (<math>\mu\text{m}</math>)</b>	<b>Gurley Permeability [<math>\mu\text{m}/(\text{Pa}\cdot\text{s})</math>]</b>
PP-HM <sub>w</sub>	250	140	9.8	3.9	0.065	0.004
		150	8.3	3.0	0.061	0.018
		160	14.2	5.0	0.062	0.049
		170	13.9	4.9	0.063	0.014
PP-HM <sub>w</sub>	270	140	1.2	0.7	0.072	0.003
		150	6.0	2.9	0.071	0.004
		160	12.5	5.4	0.070	0.005
		170	11.5	3.9	0.062	0.003
PP-B	250	140	9.4	7.7	0.091	0.007
		150	11.9	8.6	0.091	0.018
		160	13.1	11.3	0.098	0.068
		170	10.9	6.4	0.086	0.020
PP-B	270	140	10.0	6.1	0.076	0.005
		150	11.4	8.2	0.088	0.013
		160	12.2	8.3	0.083	0.026
		170	7.5	5.3	0.080	0.011

## 5.2. Influence of annealing temperature on polymer blends

Polymer blends with PP block and random copolymers were prepared at three different percentages to evaluate the effect of blending ratio and annealing temperature. Figure 5.5 illustrates the DSC curves of samples annealed at 140 °C and uniaxial stretched in two different steps, one at room temperature and the other at 140 °C.

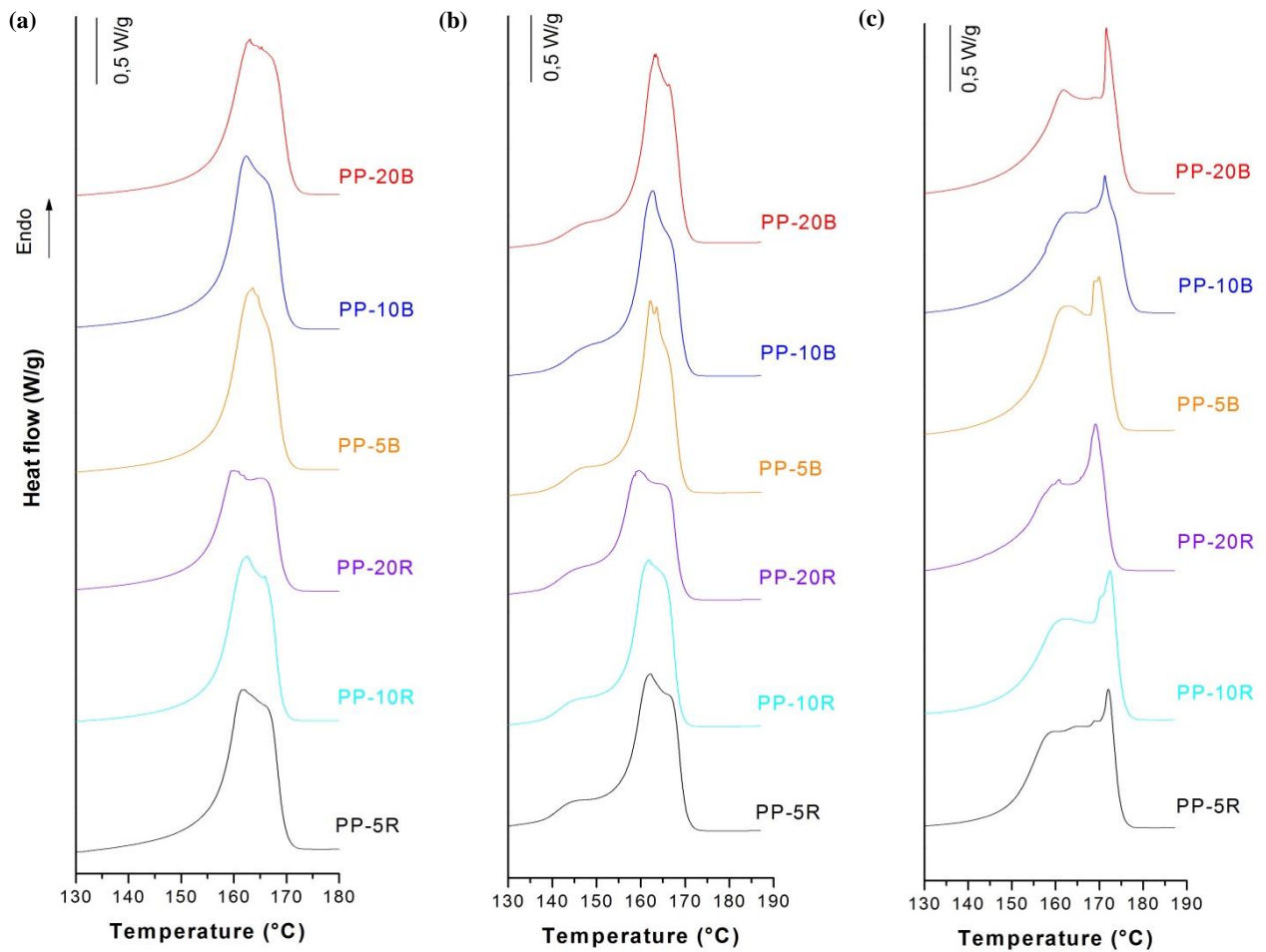


**Figure 5.5.** DSC thermograms of polymer blends prepared with the PP random and block copolymers. (a) Precursor films, (b) annealed precursor films at 140 °C, and (c) membranes (cold stage, 10 mm/min, 35%; hot stage, 10 mm/min, 230).

In the case of the random copolymer blends, endotherm curves were less pronounced as the content of the mixture was increased compared with the heterophasic polypropylene. This was expected due to the presence of the ethylene comonomer and its distribution along the polymer backbone, which reduced both the crystallinity and melting point [107,108,136]. The analysis of experimental data (Tables 5.2 and 5.3) and the SEM micrographs revealed that membranes differing on blending ratio have an optimum value close to 10 per cent for the random copolymer, and 20 per cent for the heterophasic PP, where a higher pore density and a fairly homogeneous pore distribution were achieved. Based on the data obtained, it was also necessary to investigate the effect of annealing temperature on membrane performance for these samples.

With increasing random copolymer content, the crystallinity and the degree of orientation necessary for achieving the desired crystalline structure decreased, as can be seen in Figure 5.6. Thus, with a blend ratio above 10 per cent, a non-optimum row-nucleated structure was formed. Figure 5.7 shows SEM views of the surface morphology of membranes containing 10 per cent random copolymer after being annealed at four different temperatures. Regarding the influence of annealing temperature on membrane performance, a high annealing temperature seems to cause an increment on the orientation factor as determined by FTIR and the number of pores.

Comparing the data collected in Table 5.2, it was observed that membranes produced with up to 10 per cent of blend and having higher porosity and air permeability values were obtained for the precursor films annealed at 160 °C. At this temperature, the degree of crystallinity increased with increasing molecular orientation. This results in a larger pore size and better interconnectivity between the pores after the hot uniaxial stretching step.

Endotherms curves obtained from precursor films and membranes annealed at these temperatures are also shown in Figure 5.8. DSC thermograms above 140 °C displayed significant changes in the shape of melting curves. The shoulder at lower temperatures related to the annealing process and the melting of different crystal populations disappeared progressively as the annealing temperature increased. It seems that the increment in molecular mobility at higher temperatures promoted the formation of a more dense and stable crystalline form [4-13].

Membrane thermograms displayed similar endothermic curves for annealing temperatures above 150 °C. Two types of lamellae distribution after uniaxial stretching appeared. The peaks at high temperatures related to the interconnected bridges formed between main crystal lamellae were more pronounced for samples annealed at 160 °C and 170 °C. Although the annealing temperature of 170 °C increased the precursor film orientation and enhanced the pore density, deterioration of crystalline lamellar structure due to partial melting of some areas promoted a loss in membrane surface homogeneity, and reduced the average pore size and membrane permeability.

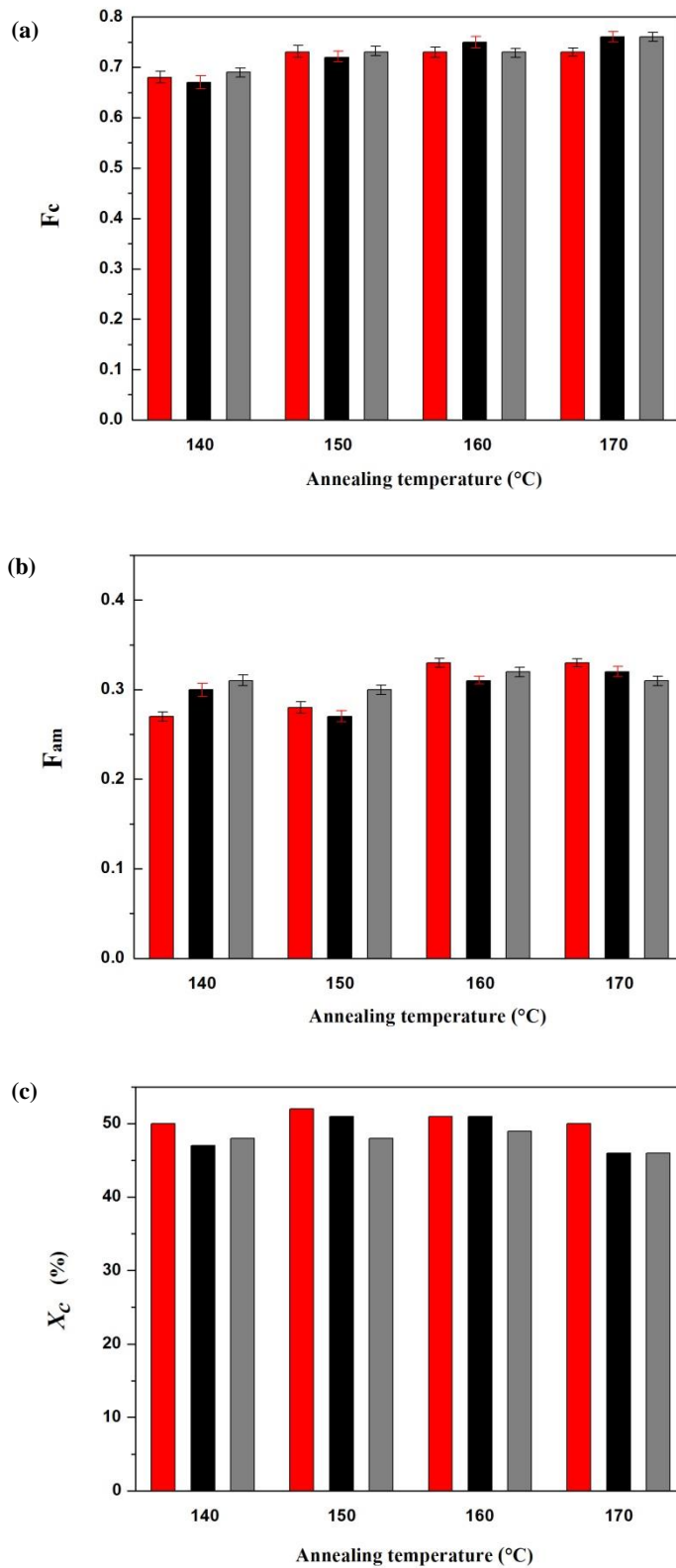


Figure 5.6. (a) Crystalline and (b) amorphous orientation parameters derived from infrared measurements, and (c) crystallinity obtained from DSC thermograms of random copolymer blends annealed at different temperatures.

(■ > PP-5R < ■ > PP-10R < ■ > PP-20R).

**Table 5.2. Characteristics of membranes prepared with the PP random copolymer differing on blending ratio and annealing temperature.**

<b>Sample</b>	<b>Annealing (°C)</b>	<b>Pore Density (pores/<math>\mu\text{m}^2</math>)</b>	<b>Pores Area (%)</b>	<b>Average Pore Size (<math>\mu\text{m}</math>)</b>	<b>Gurley Permeability [<math>\mu\text{m}/(\text{Pa}\cdot\text{s})</math>]</b>
PP-5R	140	1.5	0.9	0.062	0.003
	150	10.4	3.3	0.059	0.011
	160	13.7	5.1	0.065	0.019
	170	13.8	4.5	0.058	0.011
PP-10R	140	6.9	2.4	0.062	0.004
	150	11.2	3.1	0.066	0.008
	160	14.2	5.8	0.070	0.048
	170	13.9	5.1	0.069	0.039
PP-20R	140	7.7	2.6	0.063	0.003
	150	6.0	2.2	0.066	0.006
	160	7.8	3.2	0.069	0.019
	170	7.6	2.7	0.063	0.013



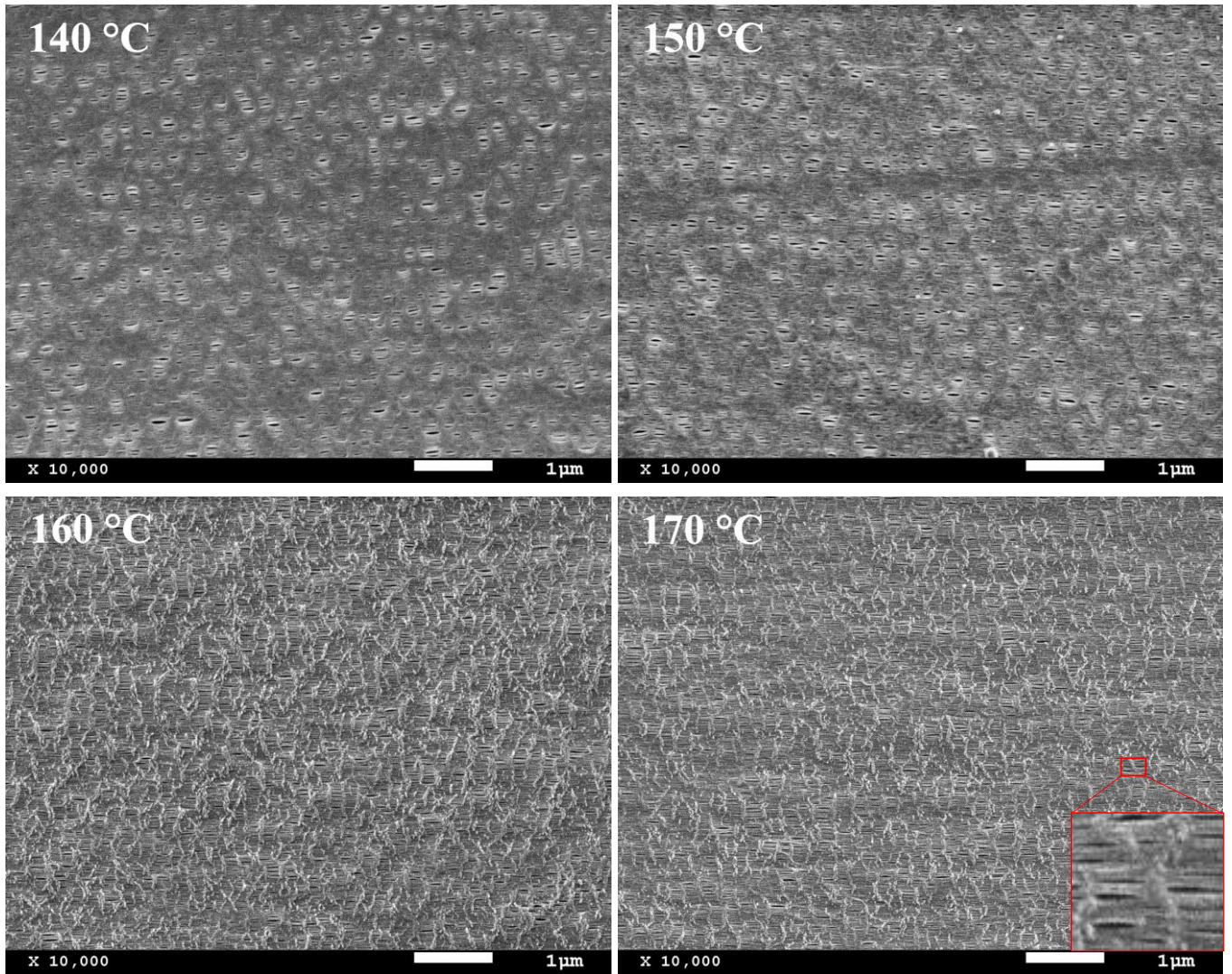


**Figure 5.7. SEM micrographs of the surface of the porous membranes prepared with the PP-10R blend at four different annealing temperatures.**



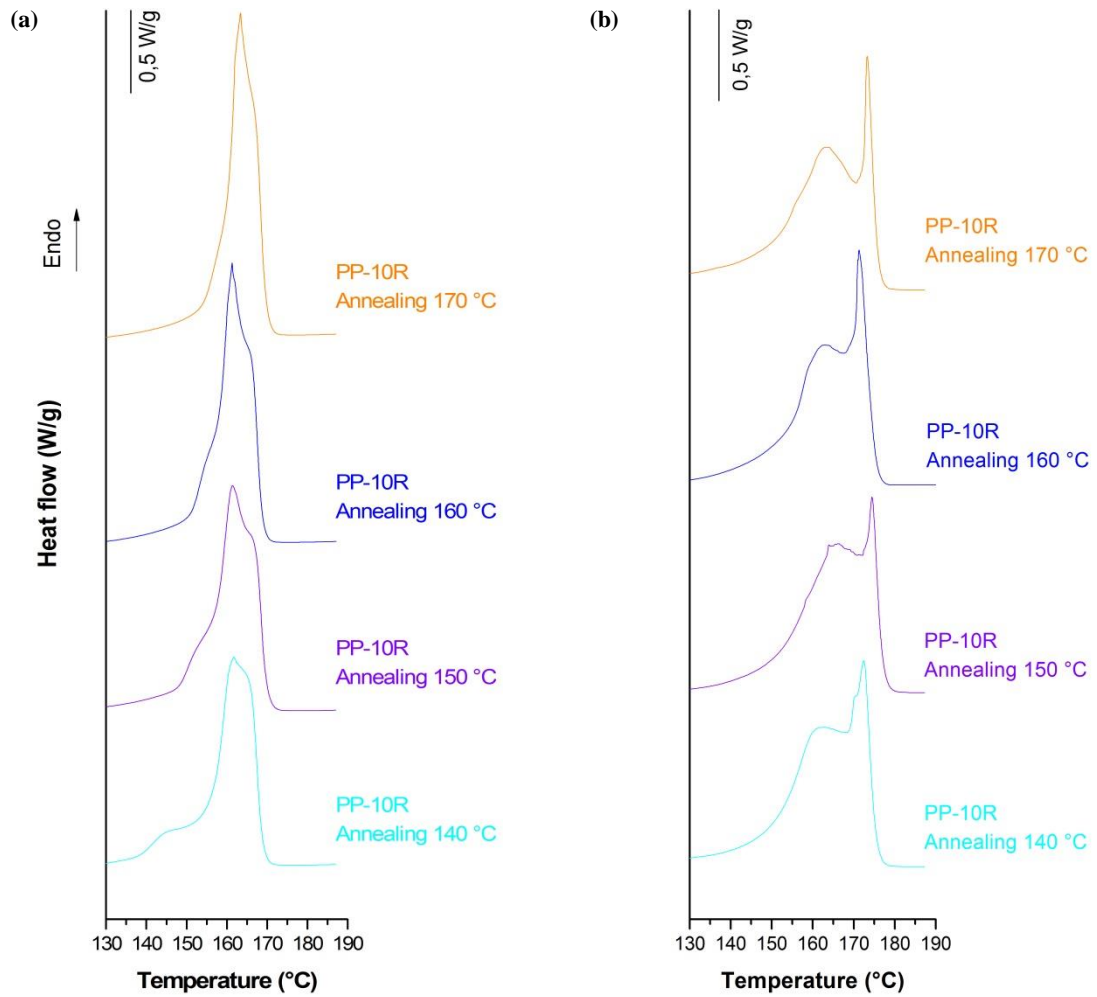


Figure 5.8. DSC thermograms of samples prepared with the PP-10R blend and annealed at different temperatures. (a) Annealed precursor films and (b) membranes.

Blends of the homopolymer and the heterophasic polypropylene copolymer at three different percentages were prepared to obtain larger air permeability values and homogeneous membranes. As stated before, the optimum blending ratio for the preparation of these membranes has a value close to 20 per cent, where higher pore density and fairly homogeneous distribution of the pore diameters have been observed.

The morphological characterization of membranes through SEM and image analysis (Table 5.3) revealed that the addition of a small amount of block copolymer influenced the pore size distribution. As discussed in the previous section, it was speculated that the phase separation between the PP matrix and the EPR dispersed phase increased the average pore size. However, when the content of copolymer was over 20 per cent, both the crystal orientation and the degree of crystallinity were reduced (data not presented here). This resulted in the formation of non-uniform pore distributions within the membrane matrix.

The effect of thermal annealing on the molecular orientation and the degree of crystallinity was also revealed by DSC and FTIR measurements (Figure 5.9). As also previously mentioned, high annealing temperature caused an increment in both parameters due to the increased molecular mobility at high temperatures. The results of the analysis obtained for the sample of 20 per cent of blend content are shown below in Figures 5.10 and 5.11. As depicted in SEM micrographs and DSC thermograms, the precursor films annealed at higher temperatures showed similar results for both random and block copolymers. The DSC curves for precursor films (Figure 5.11a) exhibited a small sub-peaks and relatively narrow melting peaks attributed to crystals with uniform thicknesses. This is further confirmation that the formation of the more dense and stable crystalline structures in precursor films is possible at temperatures above 150°C.

Furthermore, the DSC thermograms for membrane samples (Figure 5.11b) confirmed the difference observed in the peak corresponding to the recrystallized interconnected bridges formed during the hot stretching step. This narrower melting peak becomes more pronounced for membranes in which precursor films were annealed at 160 °C when a more stable crystalline structure improved membrane performance by increasing the size and number of pores (pore density). Finally, when the annealing temperature was further increased to 170 °C, the melting of the crystalline phase induced a heterogeneous pore morphology, resulting in decreased air permeability, pore density and size, and interconnectivity of pores through the membrane.

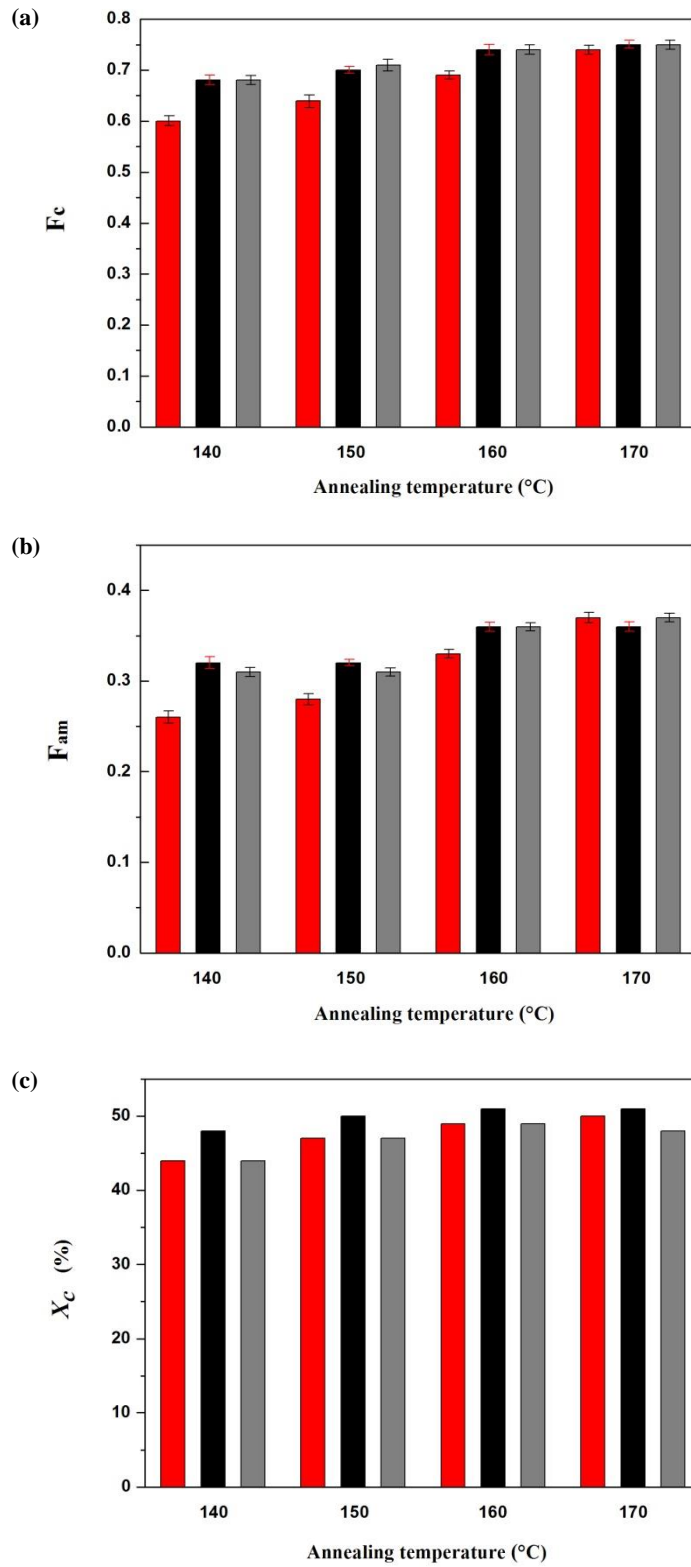


Figure 5.9. (a) Crystalline and (b) amorphous orientation parameters derived from infrared measurements, and (c) crystallinity obtained from DSC thermograms of heterophasic copolymer blends annealed at different temperatures. (< ■ > PP-5B < ■ > PP-10B < ■ > PP-20B).

**Table 5.3. Characteristics of membranes prepared with the PP heterophasic copolymer differing on blending ratio and annealing temperature.**

<b>Sample</b>	<b>Annealing (°C)</b>	<b>Pore Density (pores/<math>\mu\text{m}^2</math>)</b>	<b>Pores Area (%)</b>	<b>Average Pore Size (<math>\mu\text{m}</math>)</b>	<b>Gurley Permeability [<math>\mu\text{m}/(\text{Pa}\cdot\text{s})</math>]</b>
PP-5B	140	16.9	8.7	0.071	0.015
	150	17.8	9.3	0.070	0.019
	160	20.6	9.9	0.073	0.028
	170	20.6	10.1	0.075	0.014
PP-10B	140	24.3	8.4	0.070	0.044
	150	22.6	9.0	0.071	0.032
	160	25.8	9.1	0.068	0.160
	170	25.1	7.8	0.065	0.110
PP-20B	140	26.2	8.8	0.075	0.132
	150	26.5	10.7	0.078	0.120
	160	27.8	11.6	0.079	0.176
	170	25.3	10.9	0.076	0.151

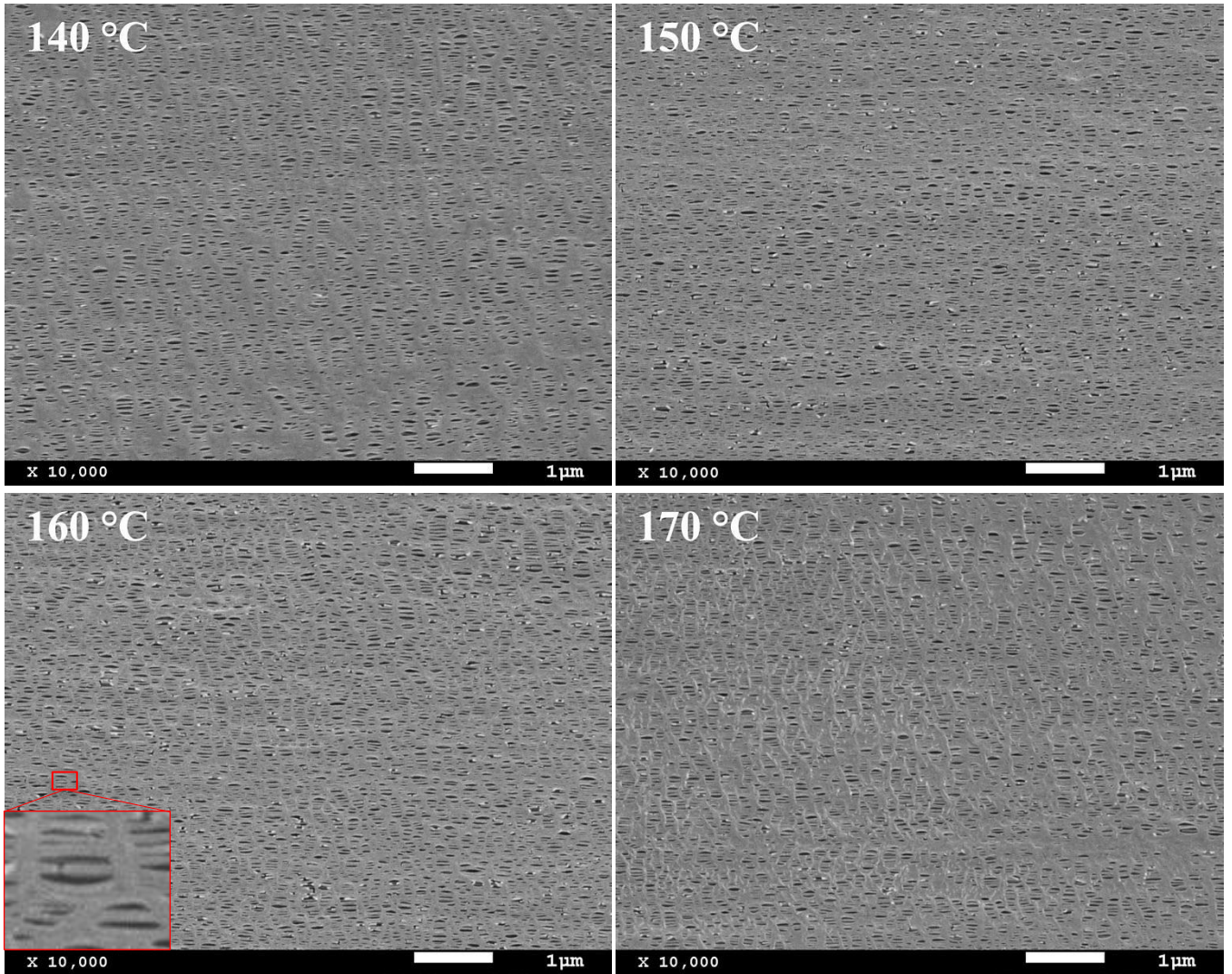


Figure 5.10. SEM micrographs of the surface of the porous membranes prepared with the PP-20B blend at four different annealing temperatures.

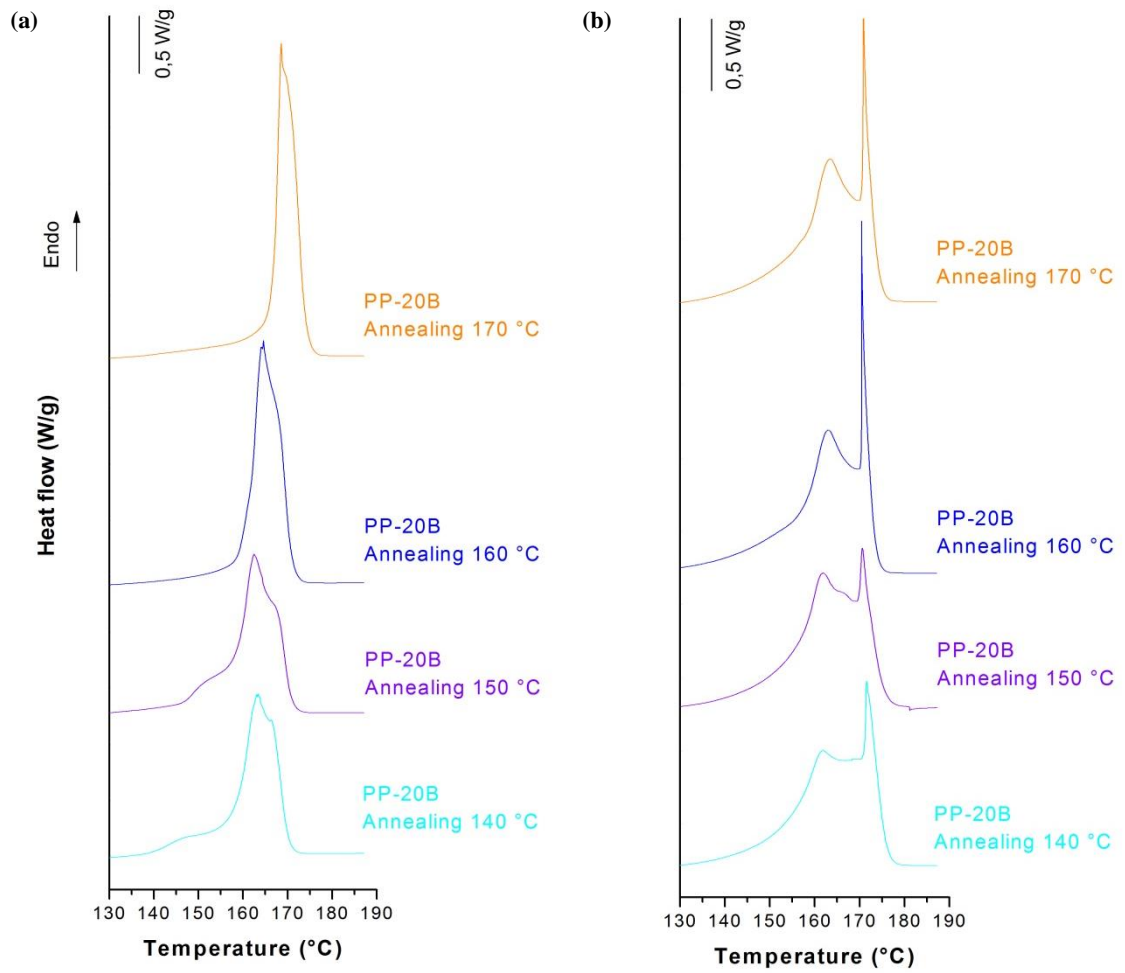


Figure 5.11. DSC thermograms of samples prepared with the PP-20B blend and annealed at different temperatures. (a) annealed precursor films and (b) membranes.

The Brunauer-Emmett-Teller (BET) method and the Barret-Joyner-Halenda (BJH) models [131-133] were used to calculate the surface area, pore volume, and pore size distribution of both neat resins and copolymer blends with the highest values of measured air permeability. The pore size distributions of the four samples obtained from the BJH method are shown in Annex I. These figures show that the pore size distribution of PP samples had only one peak value, which means that the pore distribution was relatively uniform. For all membranes, the average pore diameter was below 60 nm. The calculation results obtained from the nitrogen adsorption-desorption isotherms are shown in Table 5.4. Compared with the PP-HM<sub>w</sub>, the average pore diameter of the membrane made of heterophasic copolymer was larger, contributing to the larger average pore volume. Contrary, the BET specific surface area and BJH surface area of pores were smaller which could be related to the lower porosity of this sample. The experimental data of the PP-10R showed that adding random copolymer to the homopolymer caused a decrease in the specific surface area and pore volume. In contrast, the 20 percent blend of heterophasic copolymer reduced the surface areas only slightly and increased the pore volume and average pore diameter, which confirms the results discussed above.

The relationship between the air permeability and the BET specific surface area, and average pore diameter of these four PP samples is shown in Figure 5.12. It shows that for the PP-20B, the much larger pore size and BET specific surface area, which comprises the outward and the internal (pores) surface area, resulted in increased Gurley permeability. In contrast, the PP-HM<sub>w</sub>, despite having the largest BET surface area, exhibited low permeability due to its smaller average pore diameter, and thus, low pore volume. Likewise, membranes made of heterophasic copolymer, despite having larger pore sizes, showed lower permeability values due to the low BET specific surface area. These results could be attributed to the low porosity of the sample or less well-interconnected pore structure.

**Table 5.4. BET specific surface area and BJH pore size distribution data report for samples with the highest values of measured air permeability. Precursor films annealed for 15 min at 160 °C.**

<b>Sample</b>	<b>BET Surface Area (m<sup>2</sup>/g)</b>	<b>BJH Surface area pores (m<sup>2</sup>/g)</b>	<b>BJH Volume of pores (cm<sup>3</sup>/g)</b>	<b>Average pore diameter (µm)</b>
PP-HM <sub>w</sub>	59.0	71.0	0.39	0.022
PP-B	53.3	62.1	0.85	0.055
PP-20B	59.1	66.9	0.64	0.038
PP-10R	41.2	40.0	0.29	0.030

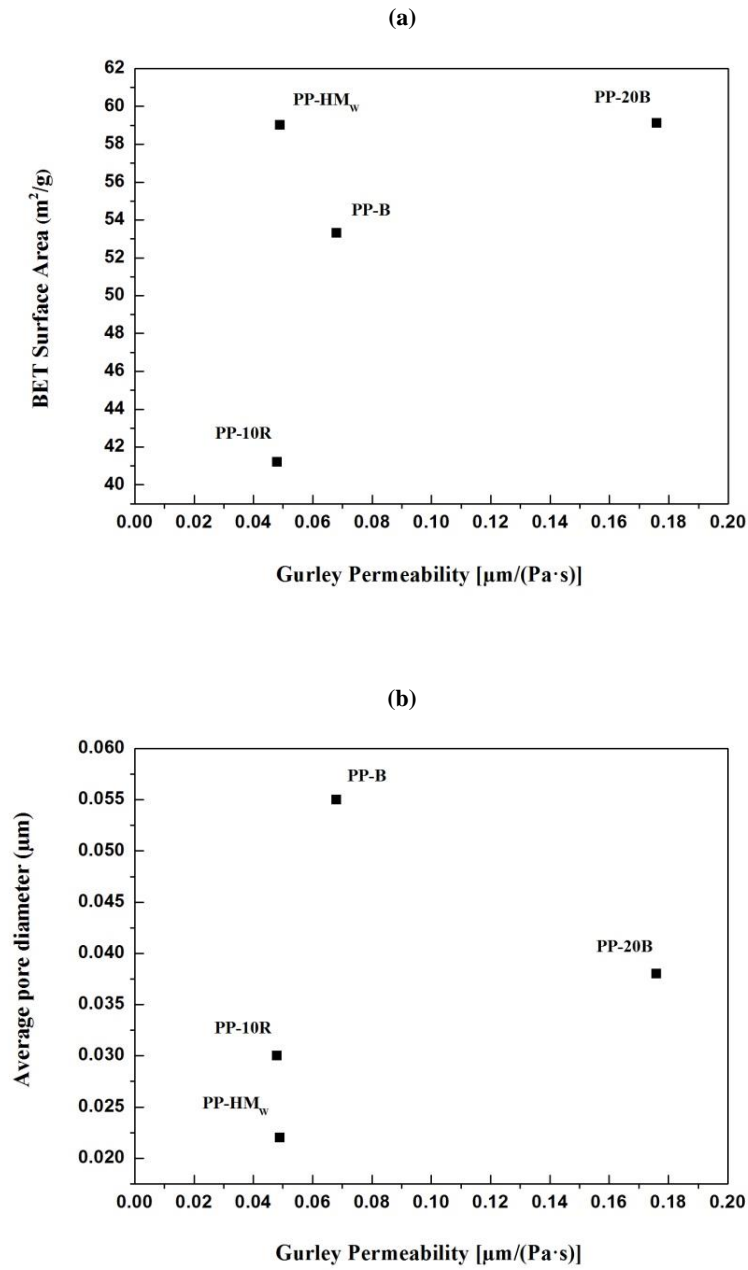


Figure 5.12. Relationship between air permeability and (a) specific surface area, and (b) average pore diameter of polypropylene samples.



### 5.3. Influence of temperature during hot stretching step

The influence of the hot stretching temperature on precursor films obtained from blends with the heterophasic and random PP copolymers was also investigated. Three different temperatures were applied in a further attempt to enhance the pore size and air permeability of membranes. All the samples showed similar behavior; therefore, only the results corresponding to the sample PP-20B are presented in Table 5.5 and Figure 5.13. These results indicated that increasing temperature above 140 °C during the second uniaxial stretching step produced a larger pore size with longer recrystallized connecting bridges between lamellae. At these high temperatures, an increment of the flexibility of tie chains located in the amorphous phase allowed greater separation between lamellar domains and enlarged the existing pores [4-12]. Also, it was speculated that the size increment was also related to collapse between neighboring pores when some interconnected bridges broke at high elongation values, promoting larger average pore size at the expense of reducing pore density [7-10].

An increase of pore size was also expected to increase the air permeability. However, high temperatures too close to the melting point during prolonged stretch could lead to local plastic deformation of porous material. That is the deterioration of the crystalline lamellar structure due to the partial melting of some areas, which led to a reduced pore interconnectivity and crystalline orientation as the lamellar separation occurred. As a result, reduced pore density and membrane permeability values were obtained.

**Table 5.5. Characteristics of membranes prepared at different temperatures during the second uniaxial stretching step in terms of pore morphology and air permeability.**

Sample	Annealing (°C)	Hot Stretching (°C)	Pore Density (pores/ $\mu\text{m}^2$ )	Pores Area (%)	Average Pore Size ( $\mu\text{m}$ )	Gurley Permeability [ $\mu\text{m}/(\text{Pa}\cdot\text{s})$ ]
PP-20B	160	140	27.8	11.6	0.079	0.176
		150	17.9	13.2	0.085	0.093
		160	12.7	10.1	0.089	0.081

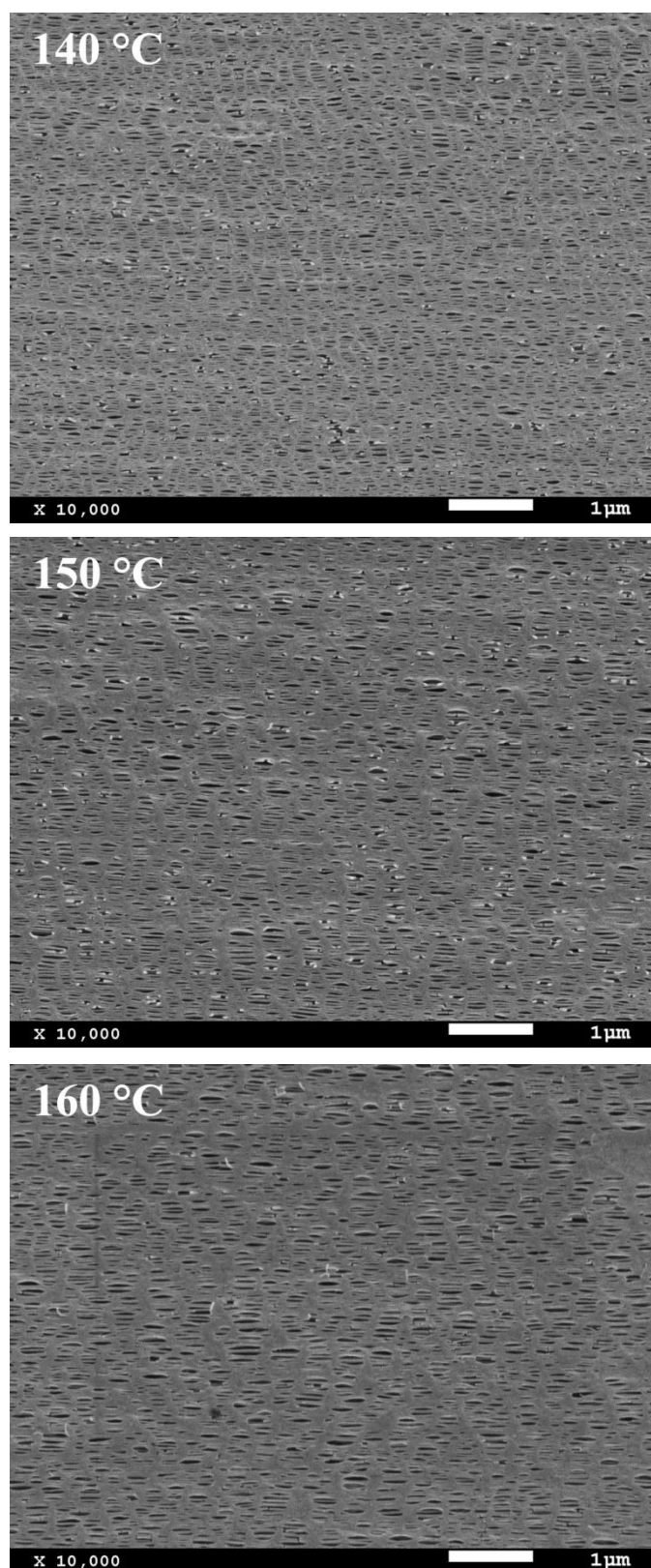


Figure 5.13. SEM micrographs of sample PP-20B. Precursor films annealed at 160 °C and stretched at three different temperatures during the second uniaxial stretching step.

#### **5.4. Effect of annealing temperature and polymer composition on the mechanical properties**

As displayed in Figure 5.14, a similar set of transitions for all tested precursor films were observed in the tensile stress-strain curves. First, the initial elastic response was attributed to the stretching and orientation of the short tie chains without breaking. Then, after the yield point, the stress-strain curves transition to a second plastic zone at which pore formation occurred as a result of chain scissions. This stage continued until the stress was transferred to adjacent longer tie chains and crystals, and strain hardening appeared for all samples at large deformation before fracture. This last phenomenon has been related to the orientational hardening of the amorphous phase and the re-crystallization of longer tie chains that formed the interconnected bridges between crystal blocks [4-12].

Several authors have also studied the influence of sample orientation on the mechanical response [105,109,140-144]. For the non-annealed precursor films, with low orientation functions, part of the stress is generally consumed in rearranging the structure in the stretching direction. However, for the annealed films with a more stable crystalline structure, most of the stress is consumed in lamellar separation and crystalline fragmentation at high deformations. The beginning of the destruction of crystal lamellae is attributed to the low chain mobility upon stretching at room temperature. In fact, in the strain-hardening zone, the fragmentation of neighboring crystal lamellae is determined by the chain entanglement density, which is found to decrease during the annealing treatment [7,10,118,119]. As explained in the preceding chapters, structural changes within the crystalline domains are expected during this heat treatment due to the increased chain mobility at high temperatures. This promotes the increase in crystal thickness in large part due to the crystallization of the end chains between crystals, which leads to a decrease of amorphous entangled network and strain hardening as well [4-17].

The stress-strain curves presented in Figure 5.14 show the response to applied stress of two types of precursor films annealed at four different temperatures. All the samples showed a well-defined yield peak, followed by a strain-hardening regime before the failure occurred. These results can be interpreted in terms of changes in the crystalline structure produced by heat treatment. As shown in Table 5.6, annealing the samples at 150 and 160 °C increased the elastic modulus, yield stress and tensile strength along MD explained by the much better alignment of the lamellae and the increased crystallinity of samples after annealing. As reported by some authors, the crystalline phase greatly affects mechanical properties. Still, it does not contribute to strain hardening behavior since it has been mainly related to the entanglement density of the amorphous phase. As pointed out before, during heat treatment, the chain mobility may be sufficient for the lamellae growth, which decreased the density of chains in the amorphous intercrystalline regions, leading to reduced strain

hardening. On the other hand, some authors related the strain-hardening to the ultimate strength point to the deformation of the new secondary crystalline lamellae formed during the annealing process that cannot remain stable under high stresses [17]. As pointed out in the previous sections, annealing at 160 °C has a significant impact on forming a more dense and stable crystalline structure. Thus, it was speculated that increased strain promoted lamellae separation with a decrease in lamellae fragmentation for these samples. The tensile mechanical data also confirmed the adverse effects of too high annealing temperatures (170°C). As discussed in previous sections, annealing of samples at this temperature could induce a non-uniform pore structure after the partial melting of the crystalline phase.

These stress-strain tests performed at room temperature are also useful in determining the optimum percentage stretch during the cold stretching stage. In chapter 4, it has been demonstrated that a strain value of about 35 % is enough to promote the pore formation as a result of chain scissions. However, applying a higher percentage of deformation during the stretching at room temperature reduced pore density due to the lamellae fragmentation produced at higher stretch values. Beyond this point, during membrane manufacturing processes, samples are stretched at elevated temperatures to avoid this lamellae fragmentation that may also reduce the crystalline orientation. Thus, thermal effects during the second uniaxial stretching step counteract the strain hardening behavior discussed previously. Even at this point, the stresses presented lower values for higher temperatures making lamellar separation easier and more likely to happen [10].

Finally, in Table 5.7, it is presented the tensile properties of precursor films annealed at the same temperature as the blending ratio with both heterophasic and random copolymers increased. It has been already reported in the literature that the presence of ethylene-propylene rubber or ethylene comonomers and its distribution along the PP backbone can affect the mechanical behavior of materials [107,108,136]. The decrease of mechanical stiffness, yield stress, and tensile strength becomes more evident for the random copolymer blends. These findings are in accordance with the results discussed in Section 5.2. The PP-R blends have a lower degree of crystallinity and a lower molecular orientation compared to heterophasic copolymer blends, and both properties are controlled by the copolymer content. The addition of heterophasic copolymer also reduced the stiffness and resistance of precursor films slightly, owing to the presence of the EPR fraction.

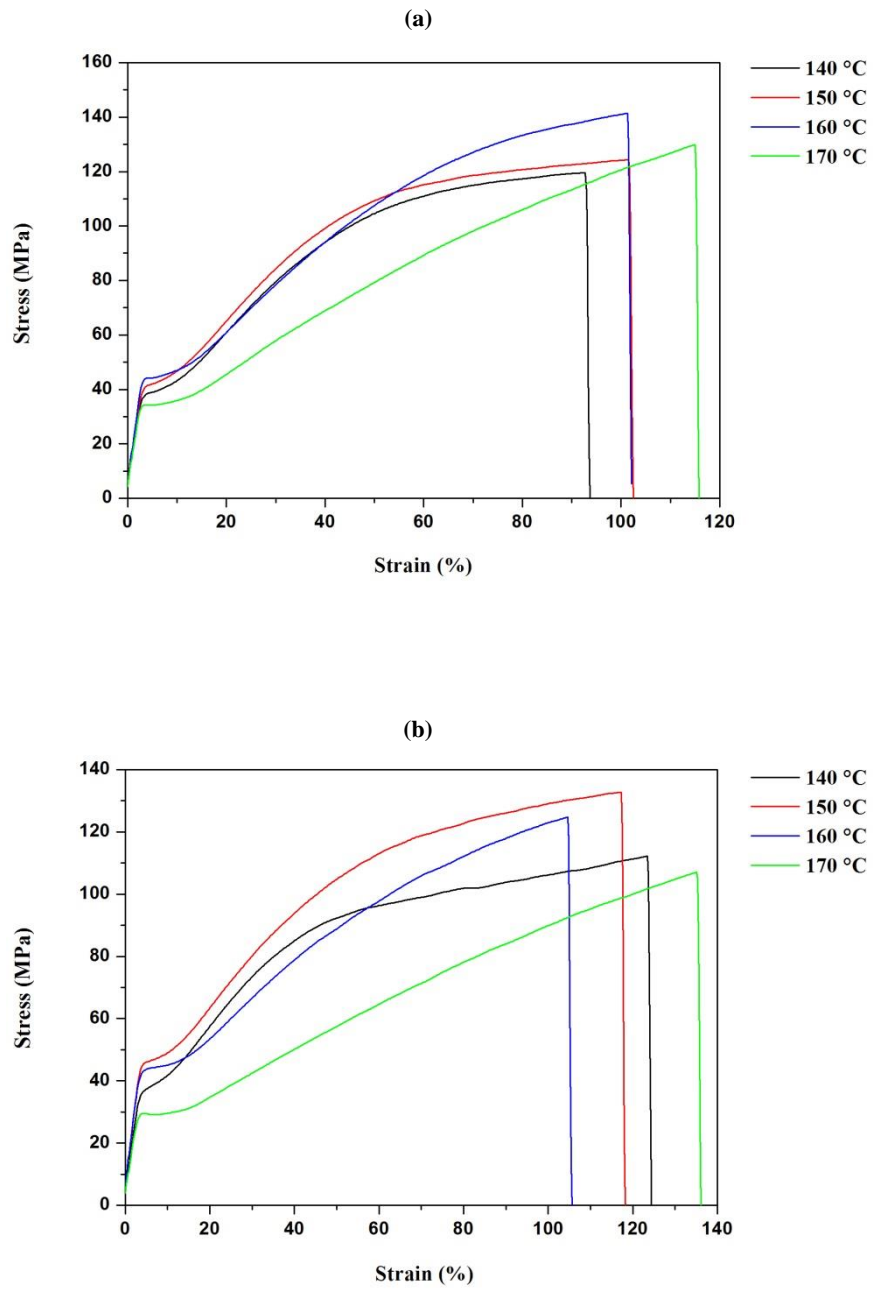


Figure 5.14. Stress-strain curves of (a) PP-20B and (b) PP-10R precursor films annealed at four different temperatures.

Table 5.6. Mechanical properties of PP-10R and PP-20B precursor films annealed at different temperatures.

Sample	Annealing (°C)	Young's Modulus (GPa)	Yield Stress Point (MPa)	Tensile strength (MPa)
PP-20B	140	1.49 ± 0.05	40.1 ± 3.0	119.6 ± 6.0
	150	1.48 ± 0.04	44.0 ± 1.3	124.3 ± 4.3
	160	1.49 ± 0.05	43.8 ± 3.0	141.4 ± 5.7
	170	1.39 ± 0.05	32.5 ± 2.0	129.9 ± 6.1
PP-10R	140	1.20 ± 0.04	37.2 ± 5.0	112.2 ± 4.1
	150	1.31 ± 0.02	45.8 ± 1.0	132.7 ± 5.4
	160	1.31 ± 0.04	44.8 ± 3.2	124.8 ± 5.9
	170	1.01 ± 0.05	29.7 ± 2.9	105.5 ± 4.8

Table 5.7. Mechanical properties of neat polypropylene and polypropylene-ethylene copolymers precursor films annealed at 140 °C.

Sample	Young's Modulus (GPa)	Yield Stress Point (MPa)	Tensile strength (MPa)
PP-HM <sub>w</sub>	1.71 ± 0.05	46.8 ± 3.0	126.3 ± 8.1
PP-B	0.97 ± 0.04	40.2 ± 4.3	119.8 ± 9.2
PP-5B	1.69 ± 0.05	46.6 ± 1.9	125.6 ± 5.1
PP-10B	1.59 ± 0.05	46.1 ± 2.1	126.2 ± 4.5
PP-20B	1.49 ± 0.05	40.1 ± 3.0	119.6 ± 6.0
PP-5R	1.49 ± 0.03	46.1 ± 4.1	121.2 ± 6.3
PP-10R	1.20 ± 0.04	37.2 ± 5.0	112.2 ± 4.1
PP-20R	1.08 ± 0.05	35.3 ± 4.6	110.7 ± 8.1

## **5.5. Discussion and main conclusions**

The polymer composition and the temperature variation in the main stages of the MEAUS technique, such as the melt extrusion, annealing and the second stage of uniaxial stretching have been analysed in this chapter. The main findings in this respect can be summarized as follows.

Specific surface area measurements (BET/BJH) and scanning electron microscopic (SEM) techniques have been used to study membranes' structure. Neat polypropylene random copolymer has resulted in a non-suitable material to produce porous polymeric membranes by the MEAUS technique, mainly due to its low crystallinity degree. However, homogeneous porous membranes with large pore sizes were obtained when the random copolymer percentage in the PP homopolymer blend was up to about 10%. It was speculated that less stiff resins could promote higher lamellar separation increasing the average pore size of membranes. Nevertheless, with a blend ratio above this 10 per cent, a non-optimum row-nucleated structure was formed, and membrane performance was significantly reduced.

The porous membranes with the highest air permeability and the most homogeneous pore structure were obtained from blends up to 20 per cent of the heterophasic copolymer in the PP homopolymer. It was speculated that the phase separation between the PP matrix and the ethylene-rich phase during the uniaxial stretching steps increased the mean pore size of the samples.

The processing temperature during extrusion has a considerable influence on both the crystallinity and the degree of crystal orientation of neat polymer resins. The higher the processing temperature of precursor films, the lower the oriented crystalline structure and performance of membranes. Regarding the annealing process, an increment in temperature gave rise to a greater molecular orientation and a rearrangement of polymer chains in both the crystalline and amorphous phases, which led to an increase in crystallinity and to oriented structure development. The samples annealed just up to 160 °C showed the highest pore structure homogeneity and permeability values. Above this temperature, the melting of some crystals reduced pore density, pore size, and interconnectivity of pores.

During the second uniaxial stretching step, the rise in temperature increased the molecular mobility, obtaining a larger pore size. However, uniaxial stretching above 140 °C produced non-uniform samples, which strongly affects the overall membrane performance.

Thermal annealing on precursor films increased the stiffness and strength due to the increased crystallinity and molecular orientation (until an optimum value of 160 °C). The presence of ethylene or EPR comonomers and its distribution along the PP backbone decreased the mechanical

stiffness, yield stress, and tensile strength of precursor films. This is more evident for the random copolymer blends since the degree of crystallinity and crystal orientation of cast films are generally reduced by random copolymerization. Tensile tests performed at room temperature were useful in determining the optimum percentage stretch during the cold stretching stage. The subsequently stretching at high temperatures counteracted the strain hardening behavior observed in the stress-strain curves and avoided the lamellae fragmentation and reduction in crystalline orientation at high stretch values, improving, therefore, the membrane performance.





## **Chapter 6:**

# **Multilayer composite membranes**



Thin multilayer membranes composed of HDPE as a middle layer and blends of PP and inorganic fillers ( $\text{CaCO}_3$  and talc) as outer layers were also developed in this thesis. This type of filler has never been used before for the manufacture of multilayer membranes using the MEAUS technique. We hypothesized that these well-known fillers, employed in the industry for its effect on the polypropylene matrix, would lead to changes in the crystalline structure, thermal stability, and mechanical and permeability properties of the porous membranes. This effect along with debonding mechanisms during the strain stage could have a synergistic effect in the generation of bigger pores. Furthermore, the influence of annealing and stretching temperature in these composite membranes was also investigated.

The multilayer cast films were prepared using a lab-scale three-layer co-extrusion line equipped with a gap die 25 mm width and 1.9 mm thickness. All the membranes discussed in this section were obtained under the same processing conditions. The extrusion draw ratio was kept to 70 to obtain a precursor film of about 27-29  $\mu\text{m}$  thickness and the uniaxial strain stage was carried out during the cold stage at 50 mm/min, up to 35% strain extent and during the hot stage at 10 mm/min, up to 230 % strain extent.

### **6.1. The nucleation effect of fillers on the crystallization behavior of composites films**

FTIR measurements carried out in uniaxially stretched multilayer cast films allowed to determine the evolution of the polymer chain orientation as a function of the annealing temperature and filler content for both polypropylene and polyethylene layers (Figures 6.1 and 6.2). As reported in the previous chapters, thermal annealing promoted an increment in molecular mobility and structural rearrangement, increasing lamellar thickness and reducing irregularities between the amorphous and the crystalline phase [4-13].

Tabatabaei et al. [120] developed unfilled multilayer PP/HDPE/PP membranes. They observed that the orientation along MD for the PP in the multilayer cast films was lower than in the monolayer made under the same conditions, which was related for these authors to the heat released during the crystallization of the HDPE middle layer. In our study, similar trends were observed for the unfilled multilayer films. However, in the multilayer composite samples, the PP showed similar and even higher orientation values that those reported in the mono-films characterized in the previous chapter. It was speculated that this might be due to the interaction between the inorganic particles and the polymer matrix. Many researchers reported that the nucleation effect of these types of fillers in various composites affects the crystallization kinetics and final orientation of the polymer chains under high stresses. Their observations were confirmed by the results presented in Figure 6.1.

The crystalline phase orientation increased with high filler content for both types of mineral particles. Calcium carbonate is an isotropic particle with a spherical geometry, which has some nucleating effect on PP explained by the heterogeneous nucleation ability of filler. On the other hand, talc is an anisotropic particle with a plate-like morphology and a high aspect ratio that also modifies the crystallization of polypropylene due to its strong nucleation effect [57-66]. When these inorganic particles were oriented parallel to the flow direction, the crystalline polypropylene domain grew highly arranged perpendicular to the talc surface.

Thus, the talc-filled PP composites had higher  $F_c$  values due to the more substantial nucleating effect of talc compared with that of  $\text{CaCO}_3$ . It was also confirmed that applying the annealing treatment to these composite layers facilitated the polymer chain orientation. In the previous chapter, similar trends were observed in which the crystal orientation increased with increasing annealing temperature. This thermal treatment allowed the molecular mobility that promoted further structural rearrangement to obtain a more thermodynamically stable crystal structure with reduced irregularities and increased lamellar orientation and thickness. Although the previous chapter has pointed out that the best results had been obtained for PP films annealed at 160 °C, the maximum annealing temperature applied in the multilayer samples developed in this study was 130 °C, because of the lower melting point of the HDPE resin.

García-López et al [44] tried to explain the influence of possible filler agglomerates on the increase in the orientation of an isotactic PP matrix after thermal annealing. They found that the incorporation of mineral filler into the PP matrix increased the residual stresses that appeared during the extrusion process, which after the thermal annealing at high temperature promoted an increase in polymer chain relaxation and polymer orientation in the residual stress zones near and far away from the matrix-particle interface.

The degree of crystallinity ( $X_c$ ) of membranes prepared using two different filler contents and under different annealing temperatures for the outer and intermediate layers was also shown in Figures 6.1 and 6.2. Mineral fillers such as talc and  $\text{CaCO}_3$  may act as heterogeneous nucleating agents changing the crystallization kinetics of the PP matrix, as stated before. However, the crystallinity practically did not change with a further increase in filler content. It is well known that filler dispersion and orientation affect the nucleation and growth of crystalline units. For this reason, the distribution of mineral particles in the porous film surface of multi-layered membranes was observed by SEM (Figure 6.5). From these images, the presence of spherical agglomerates by the coalescence of smaller particles can be seen. The presence of agglomerates on the polypropylene matrix could be used to confirm the no significant increase in crystallinity, due mainly to the confinement effect of inorganic fillers on the movement of polymer molecular chains [111,112].

Several research investigations [48,54,56,57,61,68] have been carried out to improve the dispersion of fillers, which tend to agglomerate in a polymeric matrix. It is possible to ensure sufficient particle dispersion and high levels of anisotropic mineral particle orientation by increasing the matrix-filler interaction with an active surface treatment [41-70] or controlling some process parameters during the extrusion, such as processing temperature and shear speed and time. In that sense, the uniaxial stretching stages carried out to induce porosity at room and high temperatures can promote significant structural changes in the crystalline structure, and may also lead to a reduction in the level of agglomeration and an increment on the anisotropic orientation of talc particles.

Besides, PP and HDPE resins in the multi-layered components showed a lower degree of crystallinity in comparison with the monolayer developed at similar processing conditions. Repeated observations of the same phenomenon occurred in Tabatabatei's study, as previously discussed [120]. They speculated that the higher crystallinity and heat fusion of the HDPE middle layer directly affects the kinetics of shear-induced crystallization of PP core layers. However, other arguments may also be stated to explain the slightly lower degree of crystallinity for the trilayer structure. Rheological characterization was not considered in this study. In any case, it is well known that the viscosity differences of the neat polymers and other process conditions during the production of multilayer films have a significant influence on both the strain-induced crystallization of polymer matrix and the dispersion and subsequent nucleating effect of mineral fillers.

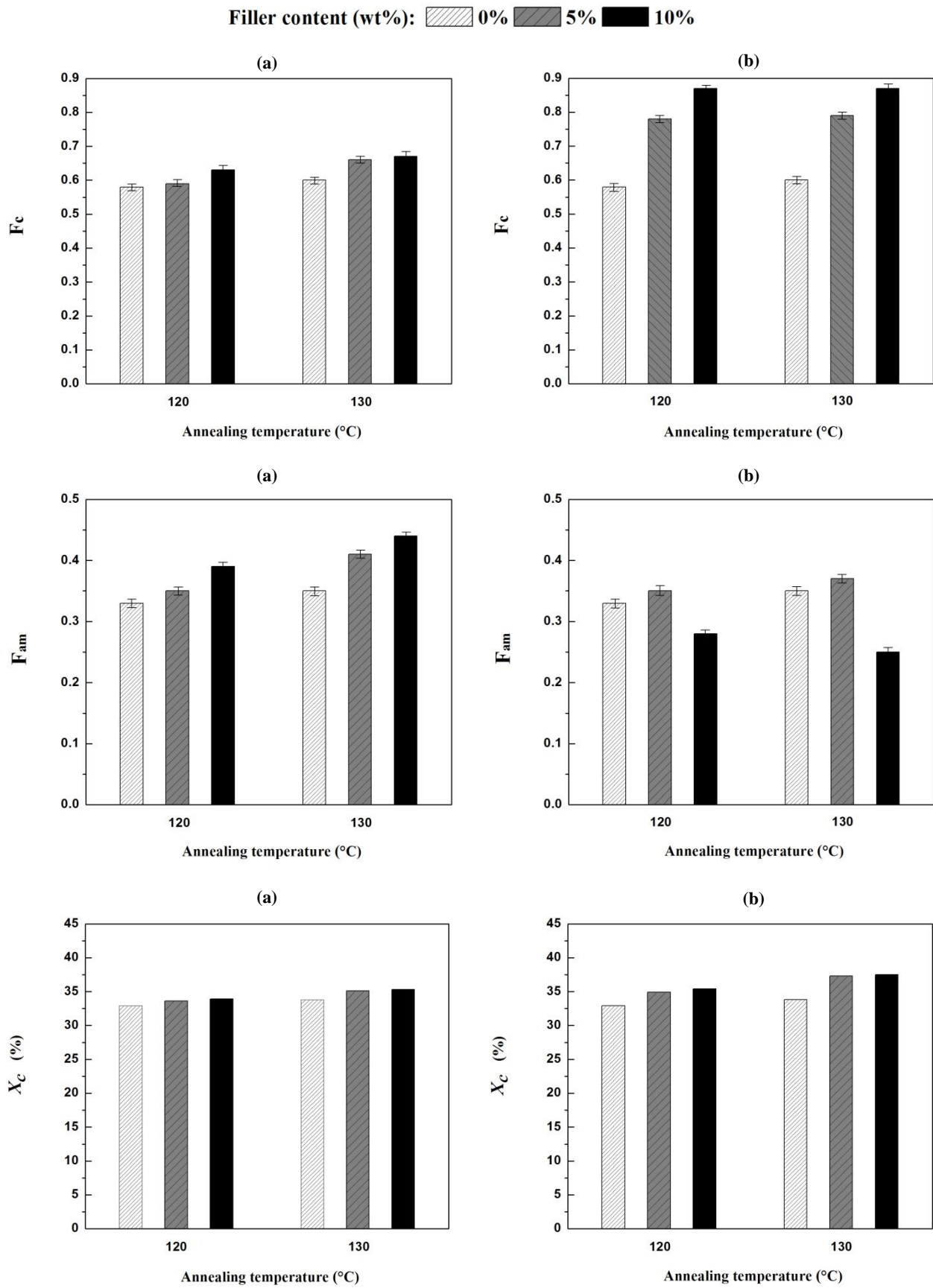


Figure 6.1. (a) Crystalline and (b) amorphous orientation parameters derived from infrared measurements, and (c) crystallinity obtained from DSC thermograms of multilayer precursor films with different type of fillers

(a) PP-C and (b) PP-T.

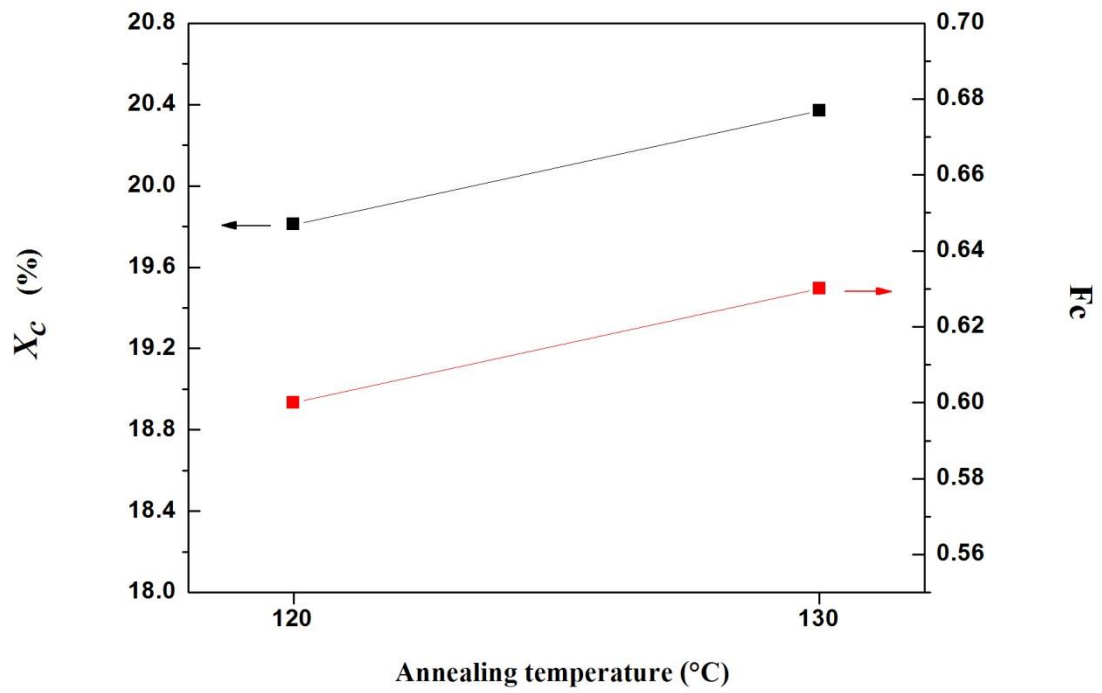


Figure 6.2. (■) Crystalline orientation parameter derived from infrared measurements and (■) crystallinity obtained from DSC thermograms of HDPE intermediate layer.



DSC data for the non-annealed PP and HDPE monolayer precursor films, and their multilayer film is presented in Figure 6.3a. The melting curves for the PP and HDPE multilayer samples exhibited melting peaks for both resins around 164 and 134 °C, respectively. The thermograms of the HDPE resins showed a narrower melting curve without any additional “shoulder” on the melting peak side, indicating the presence of a more uniform crystal size structure. However, for PP curves, a peak and a small shoulder at high temperatures were observed. The presence of a double melting peak in the non-annealed precursor films has been attributed to the presence of lamellae and fibrils (shish crystals) that have a melting temperature much higher (about 5-8 °C) than that of the lamellar crystals [11,131].

For the membranes, a similar but more intense right peak was also observed at high temperatures (Figure 6.3b), which was related for several authors to the molecular orientation induced by uniaxial stretching. As discussed in the previous chapters, during the stretching at high temperatures, some tie chains promoted the crystallization of the so-called "interconnected bridges" that join the main crystal blocks after lamellae separation and divide the pores created during this stage [4-12]. Thus, it was assumed that these interconnected bridges acted like a shish or fibril crystal structures located between crystal lamellas [11].

The DSC thermograms for the membrane composites shown in Figure 6.3b also exhibit the effect of filler type and content on the crystallization behavior of the polymer matrix. Different types of filler or high filler contents did not seem to change the melting peaks; then, it was assumed that the mean lamellar thickness was similar for all these samples. Only for the PP/Talc composites, the right shoulder becomes more pronounced, suggesting the presence of more fibrils or interconnected bridges in the stretched films. These crystalline morphology differences are thought to come from the high molecular orientation achieved with the talc particles.

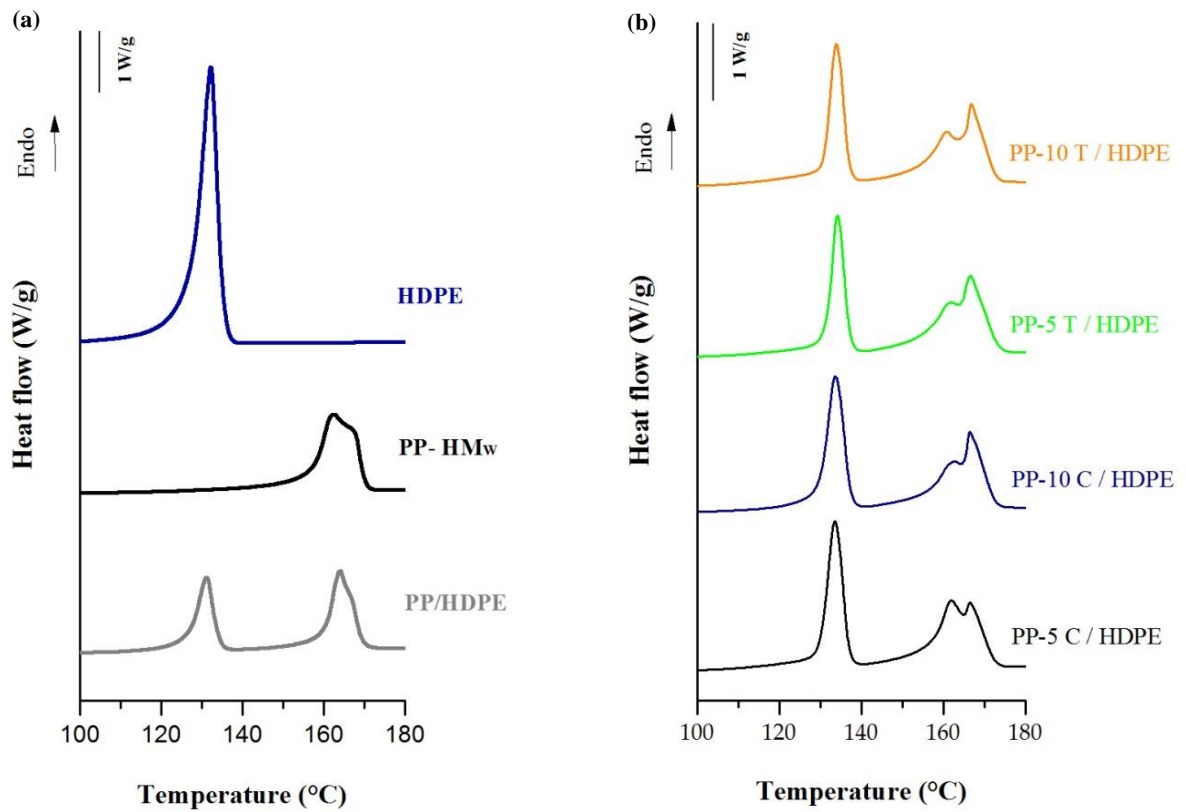


Figure 6.3. DSC heating thermograms for (a) mono and multi-layered unfilled films and (b) filled multi-layered composite membranes.

The nucleation effects of fillers on PP layers could be confirmed from the DSC cooling crystallization curves of both composites. The thermal properties such as melting temperature ( $T_m$ ), crystallization temperature ( $T_c$ ), and the so-called “supercooling” effect ( $\Delta T = T_m - T_c$ ) obtained from the DSC are summarized in Table 6.1. There are two principal mechanisms of nucleation for the polymer crystallites: homogeneous and heterogeneous nucleation. This last one appears mostly at lower undercooling due to the actions of nucleating agents that were intentionally added during processing [52,59,60].

Generally, the presence of mineral fillers may affect the flexibility of chains and lead to an increase in the  $T_m$ . Yet, the DSC test results showed that the melting temperatures of PP/CaCO<sub>3</sub> and talc composites increased only slightly as compared to the neat PP, probably due to the low filler contents. The heterogeneous nucleation effect of mineral fillers in the PP matrix was reflected in the crystallization temperature of composites ( $T_c$ ). This shifts to a higher temperature with the increasing content of both CaCO<sub>3</sub> and talc. The  $T_c$  of PP/Talc composites was higher than that of composites prepared with the calcium carbonate at the same filler content, showing the more substantial nucleation effect of talc on the PP matrix.

Generally, CaCO<sub>3</sub> has a weak nucleation effect on PP crystallization than the talc filler [57,61,62]. The high aspect ratio and plate-like or flake-like shape of talc particles provide more nucleating effect, molecular orientation, and reinforcement than the more spherical-shaped calcium carbonate filler [41,57,61,62,111]. In Table 6.1, the supercooling values of pure PP and PP composites also confirmed these results since the lower the value of  $\Delta T$ , the higher the filler effect on the nucleation and crystallization. This is especially true for the talc fillers.

**Table 6.1. Thermal properties of PP and PP-C and PP-T composites.**

Filler content (wt %)	$T_m$ (°C)		$T_c$ (°C)		$\Delta T$ (°C)	
	CaCO <sub>3</sub>	Talc	CaCO <sub>3</sub>	Talc	CaCO <sub>3</sub>	Talc
0	163.8		114.1		49.7	
5	164.3	164.0	115.0	122.7	49.3	41.3
10	164.2	164.1	116.4	123.8	47.8	40.1

## 6.2. Morphology and permeability of composite membranes

The morphology of the multilayer membranes was evaluated by SEM to observe the pore structure and the distribution of the filler particles in the polymer composite. Many factors influence the development of porous morphology, including the annealing and the stretching conditions, such as the strain rate and strain extent applied at different temperatures [4-12]. Films were first stretched along the extrusion direction at room temperature to create the pores as a result of the lamellar separation. This involves the crazing process of some tie chains, which have less flexibility during this cold stretching. Subsequently, the pore size was enlarged by stretching at high temperatures. A sufficiently high temperature and stretch level are required to increase lamellae flexibility and reach the desired pore size.

The previous chapters and other studies made from the same research group determined these optimum stretching conditions. They also analysed the formation of pores after the interface debonding between the filler and the polymer matrix upon tensile deformation. Figure 6.5, confirmed the debonding mechanism, which promoted void formation surrounding the filler particles. Thus, the synergistic effect of MEAUS process in filled samples was verifiable and led to the generation of pores after the separation of lamellar blocks along with the debonding mechanisms of the mineral fillers from the polymeric matrix. All this promoted the formation of larger pores, giving rise to a change in membrane permeability.

Larger particle size, the presence of large agglomerates at high filler content, the poor filler/matrix adhesion, and the different stretch conditions such as the strain rate, extent, and temperature may lead to an increase in pore size [45,50,51,68]. Structural parameters obtained from SEM micrographs of layer surfaces are listed in Table 6.2. As discussed above, polymer chains can freely move and reorganize into a more ordered crystal structure after annealing. Factors that are directly connected to material and processing conditions, such as thermal treatment at high temperatures, the nucleating effect of mineral fillers, and the debonding phenomenon between filler and matrix have been found to enhance pore formation and improved the permeability of samples.

The presence of large agglomerates of calcium carbonate increased the average pore size. However, the permeability to air was found to be much higher with polypropylene-talc compounds. For reasons mentioned earlier, this type of filler promoted a different crystalline structure with a high orientation degree, leading to high porosity and pore interconnectivity. It also was speculated that the presence of interfaces between layers of different pore size distributions resulted in low vertical pore interconnectivity, thus reducing permeability by increasing the resistance to airflow [120].

Morphological characterization revealed that the HDPE intermediate layer had larger pores than the PP ones. However, due to the melt flow properties of the selected HDPE (low molecular weight resin), the formation of extended chain threads or fibril nuclei in a row nucleated structure was reduced, as well as the orientation of the crystalline structure [89-91]. This promoted the formation of a weaker crystalline network connection between fibrils and resulted in a larger, less uniform pore structure in the membrane, as can be seen in Figure 6.4a.

Porous cross-sections of PP/HDPE multilayer membranes are shown in Figure 6.6. The three layers had similar thicknesses and possessed a uniform porous structure. It is well known that co-extrusion offers a significant degree of adhesion between the intermediate and outer layers since these are joined in a molten state under high pressure and high temperature. Besides, in some noncompatible polymer systems, tie layers or adhesive layers can strongly bind structures together [104]. In this work, no tie layers were employed to join together the polymer substrates. Despite this, an acceptable adhesion was found in the multilayered membranes prepared in this study since there was no evidence of delamination either in the SEM micrographs or in the visual inspections performed during extrusion and film stretching. To explain the adhesion achieved between immiscible polymers, such as PP and HDPE, the effect of transcrystalline morphology has been considered.

Zhang and Ajji [125] prepared five-layer co-extrusion blown films of PP/LLDPE and studied the resulting structure formed at the interfacial region and the adhesion achieved between layers. More specifically, they confirmed the formation of an oriented lamellae crystalline structure at the PE-PP interface. According to their results, transcrystalline layer is formed when a large difference in crystallization temperature between the resins is present. The crystallites are then forced to grow normal to the interface due to the large number of nuclei formed in this region.

These results were confirmed by Tabatabaei et al. [120], who prepared multilayered membranes of PP/HDPE by stretching and also observed this transcrystalline structure between layers. Once again, the differences in the resin crystallization temperatures,  $T_c$ , explained this phenomenon. In this case, the neat HDPE resin showed a lower crystallization temperature than the PP, which promoted molecular diffusion affecting the final interfacial adhesion. In this study, similar trends were observed since the  $T_c$  of the selected HDPE (116.8 °C) was larger than that of PP (114.1 °C) outer layers. However, this condition is not fulfilled for talc composites since, as mentioned before, the presence of these fillers increased the  $T_c$  of the neat PP resin. Thus, further investigations have to be carried out to explain the observed adhesion strength between layers.

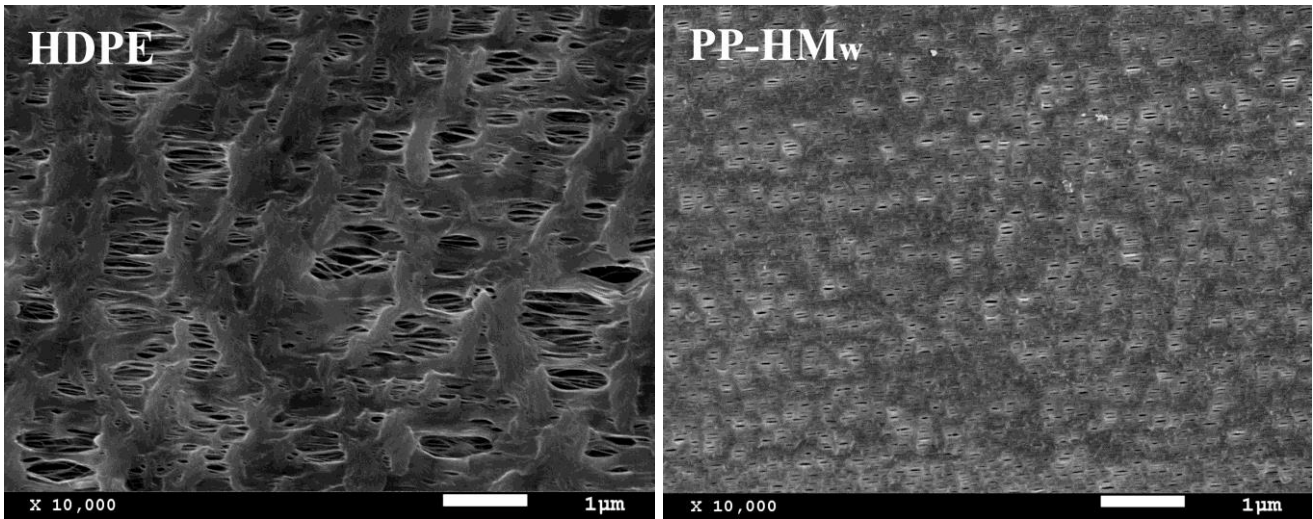


Figure 6.4. SEM micrographs of the surface of the monolayer porous membranes (a) HDPE and (b) PP-HM<sub>w</sub> (annealing at 130 °C).

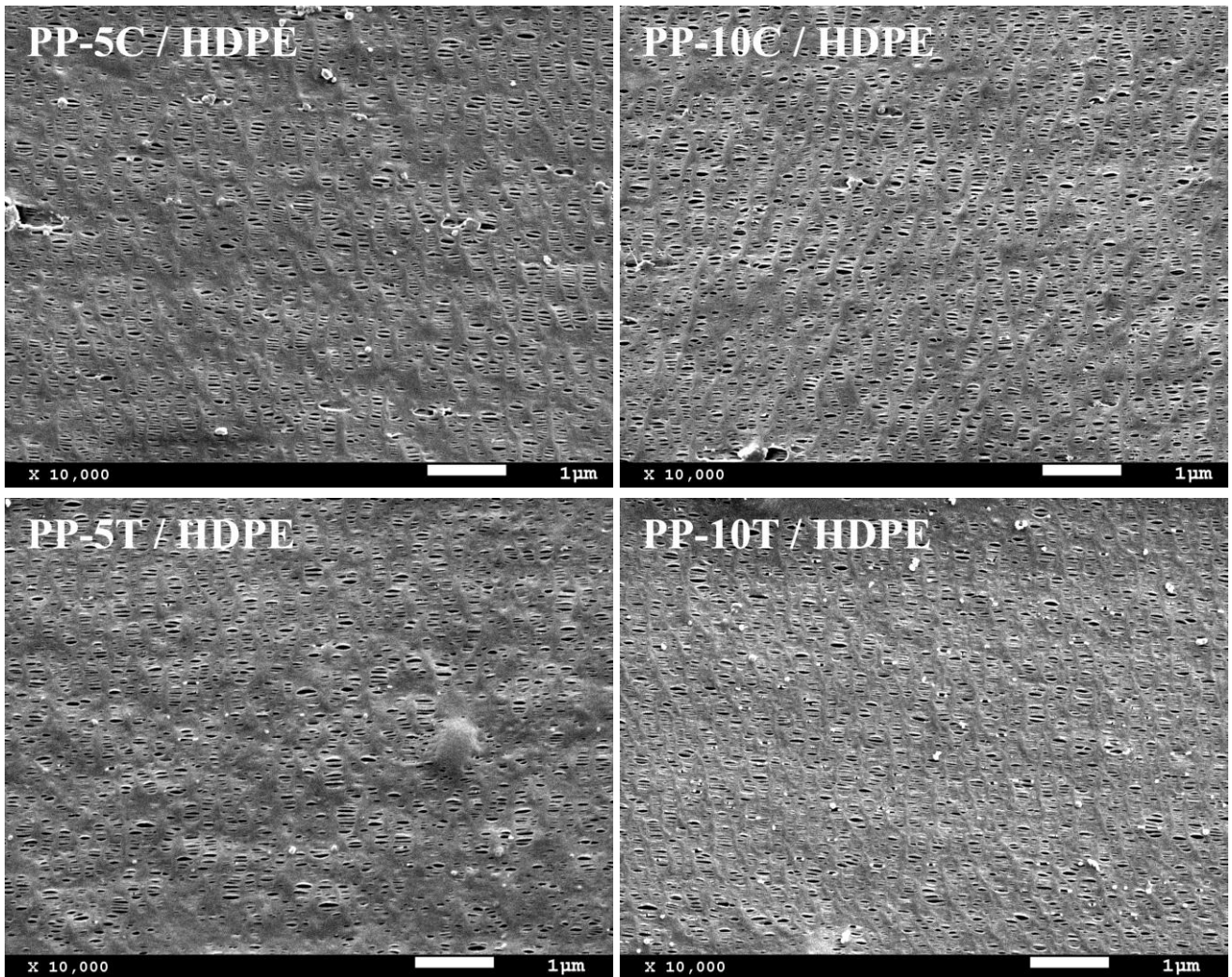
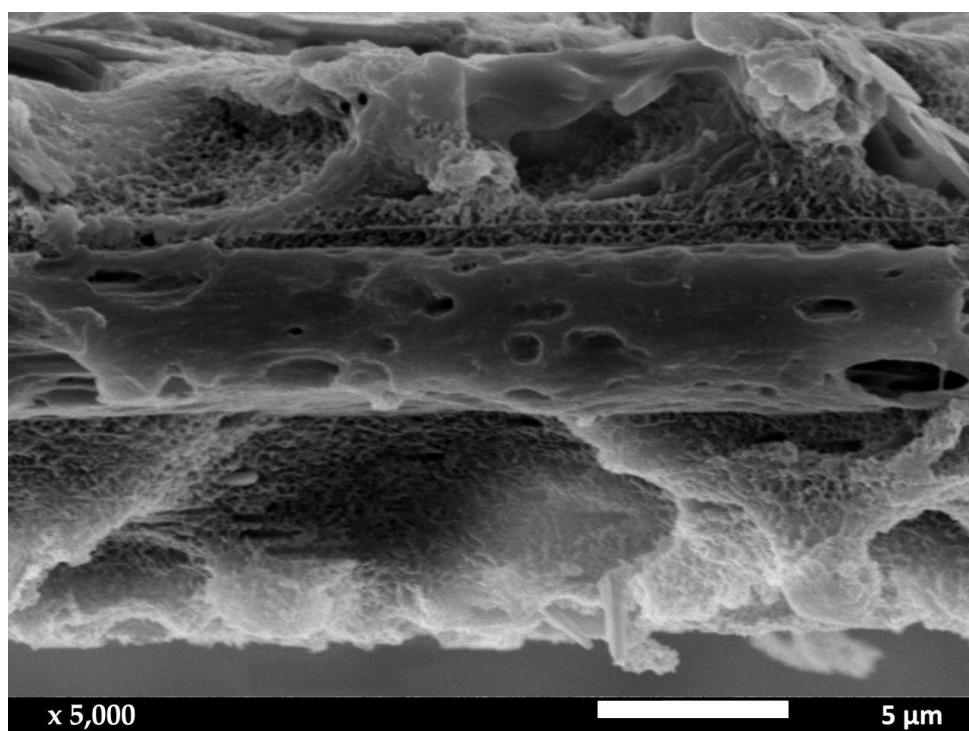
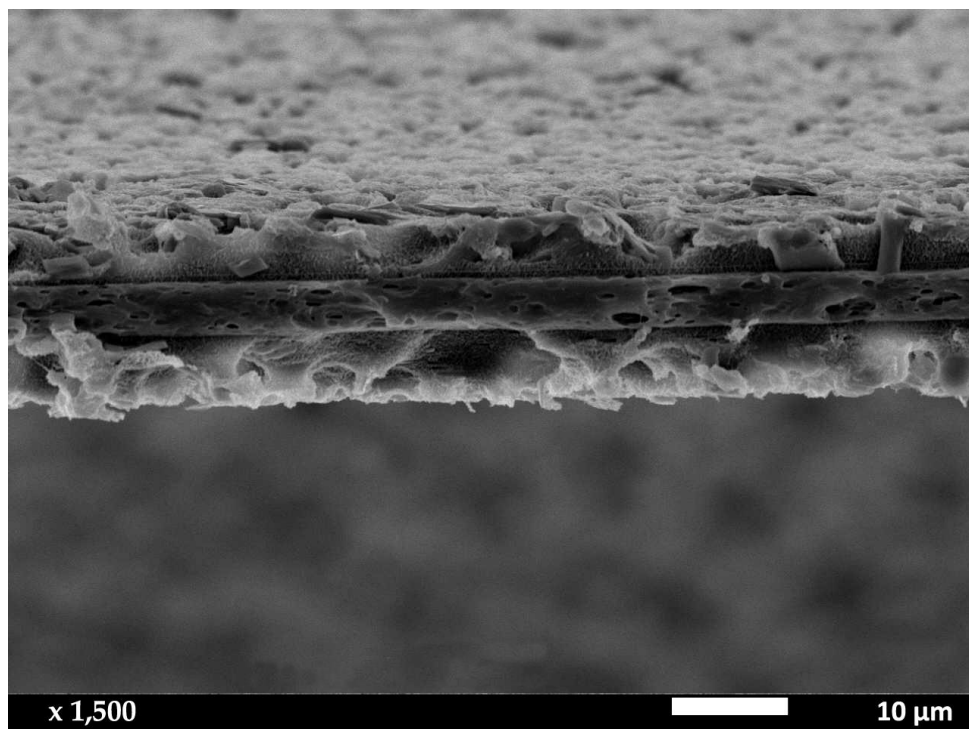


Figure 6.5. SEM micrographs of the surface of the multi-layer porous membranes (PP/HDPE/PP) with different filler type and content (annealing at 130 °C).



**Figure 6.6.** SEM micrographs of the cross-section of the etched multilayer composite membranes. Thickness: 16 μm.

**Table 6.2. Porous structure characterization results from the surface of the multi-layer porous membranes. Precursor films annealed for 15 min at two different temperatures.**

<b>Sample</b>	<b>Filler content (wt %)</b>	<b>Annealing (°C)</b>	<b>Pore density (pores/<math>\mu\text{m}^2</math>)</b>	<b>Pores area (%)</b>	<b>Average pore size (<math>\mu\text{m}</math>)</b>	<b>Gurley permeability [<math>\mu\text{m}/(\text{Pa}\cdot\text{s})</math>]</b>
PP / HDPE	0	120	13.5	4.6	0.059	0.040
		130	14.0	4.8	0.055	0.039
PP-T / HDPE	5	120	18.5	5.5	0.060	0.053
		130	23.9	7.8	0.069	0.115
	10	120	16.1	5.1	0.069	0.052
		130	23.3	5.9	0.071	0.120
PP-C / HDPE	5	120	14.1	5,7	0.071	0.037
		130	18.3	5.9	0.073	0.075
	10	120	17.0	5,4	0.074	0.035
		130	20.9	5,9	0.073	0.086



The Brunauer-Emmett-Teller (BET) method and the Barret-Joyner-Halenda (BJH) models [131-133] were used to calculate the surface area, pore volume, and pore size distribution of composite multilayer membranes. The BJH pore size distributions of the trilayer separators are shown in Annex I. These figures show that the pore size distribution of PP samples had only one peak value, which means that the pore distribution was relatively uniform. For all membranes, the average pore diameter was below 60 nm.

The calculation results obtained from the nitrogen adsorption-desorption isotherms are shown in Table 6.3. Compared with the unfilled multilayer membrane, the BET specific surface area, BHJ surface area of pores and pore volume of the filled samples were much larger. These results confirmed that some filler types, such as minerals, act as suitable nucleating agents and increase membrane porosity, as asserted by previous reports [134] and according to our last discussion.

Compared with the CaCO<sub>3</sub>-filled PP samples, the BET and BHJ surface areas and pore volume of the talc-filled PP were much larger with the average pore diameter slightly smaller. These results confirmed the recent discussion: increasing filler content from 5% to 10% induced larger filler agglomerates of calcium carbonate, which in turn increased the average pore size. In contrast, talc compounds at high talc filler contents showed higher porosity and permeability values (Figure 6.7).

Figure 6.8 shows the relationship between the air permeability and the BET specific surface area, pore volume, and average pore diameter of these five samples. As displayed in Figure 6.8 (a), the air permeability increased with increasing specific surface area. The correlation coefficient was 0.96. Taking also into account the BHJ surface area shown in Table 6.3, it was speculated that the incremental permeability with the specific surface areas arises from the larger porosity of these membranes. Something similar happens if the pore volume and permeability are compared. As shown in Figure 6.8 (b), the pore volume is positively correlated to the air permeability (correlation factor 0.73), which can be attributed to the increase in porosity and average pore size. Finally, Figure 6.8 (c) shows no significant correlation between the average pore diameter and permeability of samples. These results are probably due to the small differences found between obtained pore diameters.

**Table 6.3. BET specific surface area and BJH pore size distribution data report for composite membranes with different filler type and content. Precursor films annealed for 15 min at 130 °C.**

<b>Sample</b>	<b>Filler content (wt %)</b>	<b>BET Surface Area (m<sup>2</sup>/g)</b>	<b>BJH Surface area pores (m<sup>2</sup>/g)</b>	<b>BJH Volume of pores (cm<sup>3</sup>/g)</b>	<b>Average pore diameter (μm)</b>
PP / HDPE	0	39.3	45.8	0.38	0.034
PP-T / HDPE	5	66.6	78.6	0.58	0.029
	10	86.4	98.1	0.81	0.033
PP-C / HDPE	5	45.0	52.1	0.43	0.033
	10	48.8	57.8	0.57	0.039

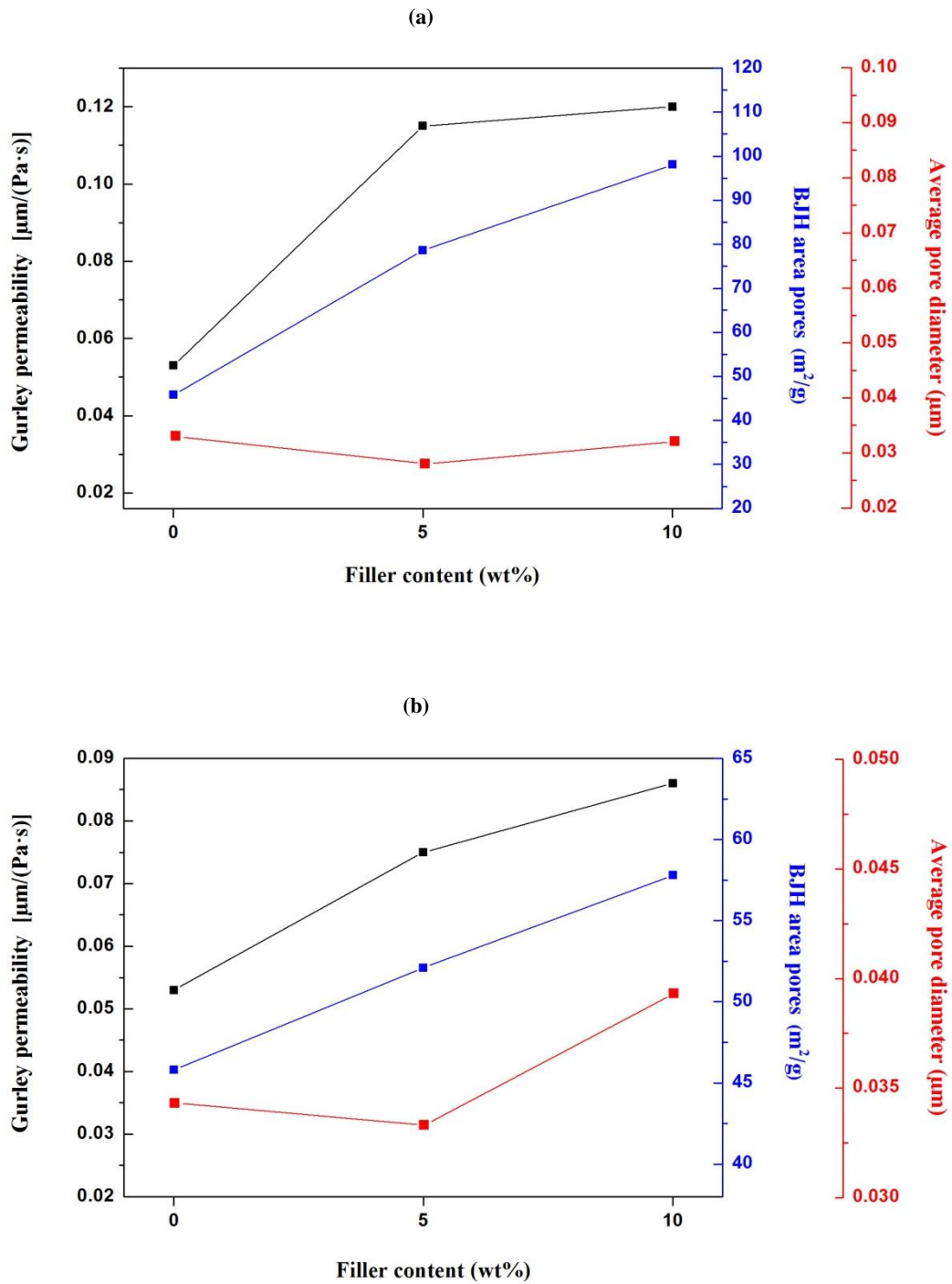


Figure 6.7. Relationship between permeability, porosity, and pore size of the composite multilayer membranes. (a) PP-T / HDPE and (b) PP-C / HDPE at different filler contents.

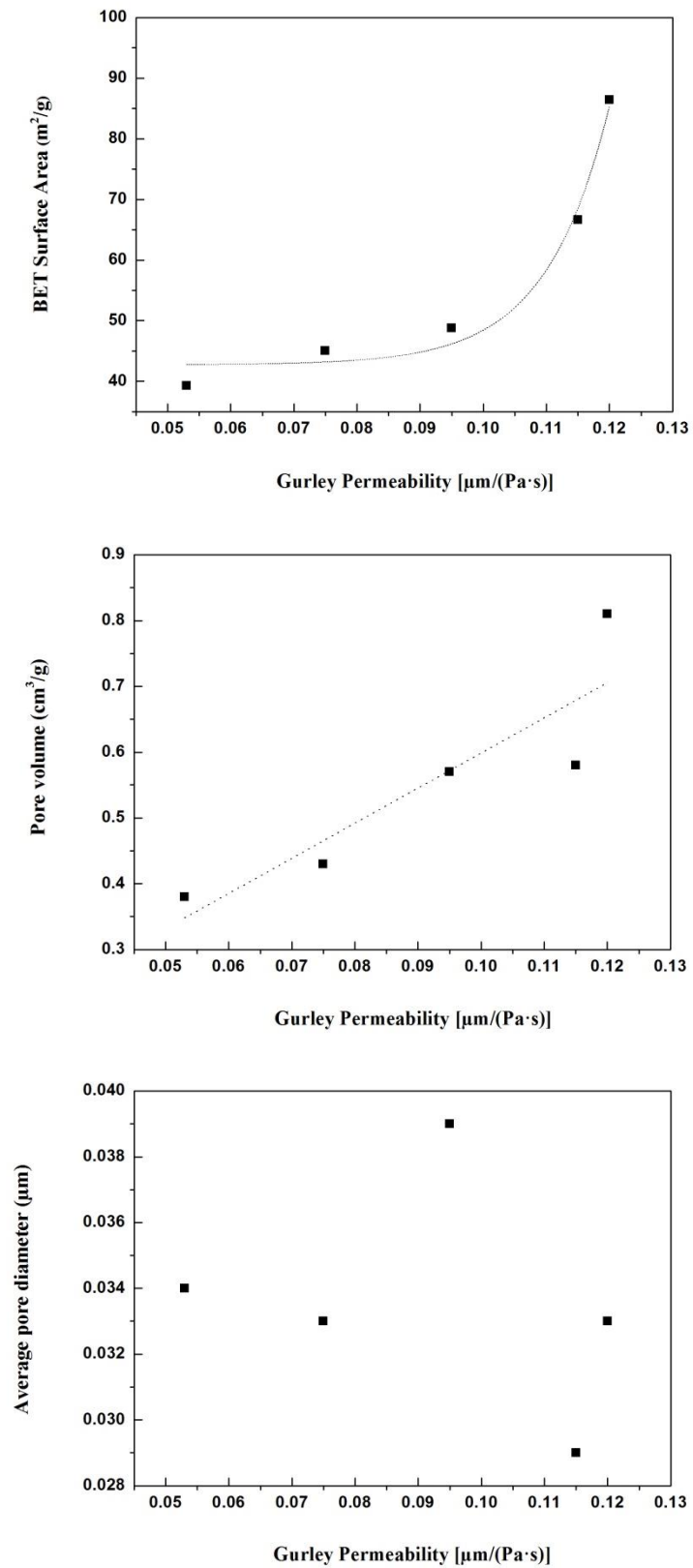


Figure 6.8. Relationship between air permeability and (a) BET specific surface area, (b) pore volume, and (c) average pore diameter of unfilled and filled multilayer membranes.

### **6.3. Thermal stability**

The thermogravimetric analysis (TGA) and its respective first derivative (DTG) have been carried out to estimate the thermal stability of the neat PP/HDPE multilayer membrane and PP-C and PP-T multilayer composites. Figure 6.9 shows the weight loss curves of these samples with different types of fillers and weight contents. From these curves, it was possible to obtain the values collected in Table 6.4. It can be seen the temperatures for a loss of mass of 10 wt % ( $T_{0.1}$ ), 50 wt % ( $T_{0.5}$ ), a relative loss of mass at 400 and 600°C, and the maximum decomposition rate temperature ( $T_{max}$ ).

Several studies have demonstrated that under an inert nitrogen atmosphere, TGA curves for HDPE and PP display a single step degradation process in which the loss in mass is greater between 350 and 450 °C. The thermal degradation mechanism for both HDPE and PP involves a primary degradation pathway that initiates via random scission of the polymer chains, a propagation or free radical transfer process, and a termination step [148-154]. Neat PP/HDPE multilayered membranes started to decompose at about 400 °C, under an inert nitrogen atmosphere. Simultaneously, this temperature was shifted about 7–14 °C to higher values in composites containing both CaCO<sub>3</sub> and talc particles. Concerning values of 10 and 50% weight loss and  $T_{max}$ , they also were increased due to the increase of fillers content.

The observed increase in thermal stability for the PP/HDPE multilayer membranes is thought to be due to several factors. The high barrier properties of mineral particles and the restriction of polymer matrix mobility due to the presence and interaction with fillers, especially in the vicinity of the particle, caused a delay in the volatilization of the decomposition products. It has been reported [41,60,64-70] that this type of fillers has a much higher thermal conductivity than the polymer substrate. This facilitates heat dissipation and, therefore, avoids heat accumulation at a certain point, promoting that the polymer system does start to degrade at a slightly higher temperature.

In addition to particle size, processing factors can also affect the thermal degradation of talc and CaCO<sub>3</sub> polypropylene composites. Some authors found that the thermal conductivity of the PP filled talc composites is higher with increasing filler orientation. Then, this high thermal conductivity seemed to have more influence on delaying sample degradation preventing the heat accumulation and reducing the escape of volatile gases [41,60,64,65]. It is known that the presence of aggregates can also deteriorate overall polymer properties. A higher amount of mineral fillers can be unfavorable because of the tent of fillers to aggregate at higher concentrations. Aggregation reduces the surface area, providing less available contact between the filler particles and the polymer matrix. Thus, the necessary dispersion levels should be achieved during compounding, thereby retarding the thermal degradation of the polymer.

Finally, it was also speculated that the annealing temperature could influence the thermal stability of membranes. Annealing leads to improvements in membrane properties by thickening the lamellae and eliminating internal irregularities. As pointed out in this and the previous sections, one of the changes produced in the crystalline structure during annealing was an increase in crystallinity. Thus, the thermal stability could be slightly enhanced when a reduction in the amorphous phase fraction was achieved at higher annealing temperatures. Some authors related this to a decrease in the air absorbed at the amorphous molecular level, which negatively influences the initial degradation reactions in the presence of oxygen or air [149].

**Table 6.4.** Thermogravimetric results of unfilled and filled PP/HDPE multi-layer porous membranes with different filler type and content.

Sample	Filler content (wt %)	Annealing (°C)	T <sub>0.1</sub> (°C)	T <sub>0.5</sub> (°C)	Lost mass 400 °C (%)	Lost mass 600 °C (%)	T <sub>max</sub> (°C)
PP / HDPE	0	130	425.5	452.5	1.8	99,1	452.7
PP-T / HDPE	5	130	432.1	456.8	1.4	94.7	461.2
	10		437.4	460.9	0.5	91.6	462.9
PP-C / HDPE	5	130	436.1	457.8	2.2	95.3	457.5
	10		438.3	460.4	0.6	91.7	464.2

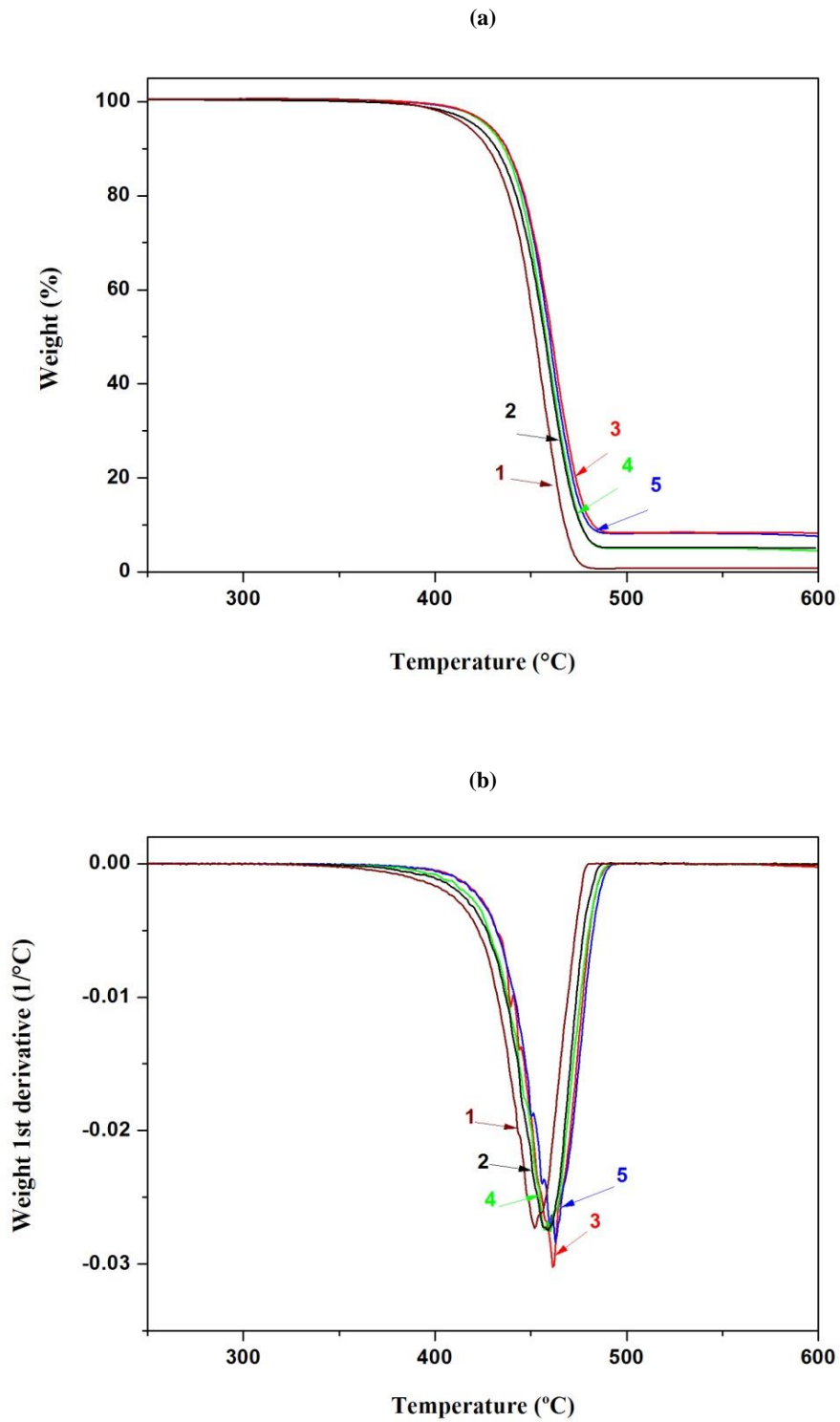


Figure 6.9. (a) TGA and (b) DTG curves of the thermal decomposition of different multi-layer porous membranes (1) PP/HDPE, (2) PP-5C/HDPE, (3) PP-10C/HDPE, (4) PP-5T/HDPE and (5) PP-10T/HDPE.

#### 6.4. Mechanical characterization

Tensile testing has been used to determine and compare the mechanical properties of the unfilled multilayered precursor films and membranes, and its composites with different talc and  $\text{CaCO}_3$  volume fractions. Tensile properties are closely related to the polymer matrix-filler interactions and the flow-induced structural changes in the material as a function of processing. Despite physical differences between fillers, the modulus was increased in both types of polymer composites, as shown in Figure 6.10. In general, an improvement in the stiffness is expected due to the reinforcing effect of fillers. The presence of rigid particles in the polymer matrix caused a reduction in chain mobility by forming the interphase between the inorganic/organic phases.

As stated in previous chapters, a high annealing temperature demonstrated an increment in yield and tensile stress and elastic modulus due to the higher crystallinity of samples. Talc particles have a more pronounced effect on the degree of crystallization due to their strong nucleating ability, as evidenced by the highest  $T_c$  showed previously. Thus, compared with the PP-C composites, the talc-filled samples showed high Young's modulus and tensile strength at the same filler content. Talc with a high aspect ratio can be oriented during processing leading to high crystallinity and crystalline orientation, resulting in improved mechanical properties.

However, a decrease in the tensile yield stresses for the composites at high filler contents can be observed. Yield stress is proportional to the connectivity and crystal thickness [62-64,109]. However, since the polymer composites have similar lamellar thicknesses (as has been estimated experimentally from the melting temperature,  $T_m$ ) the filler-matrix debonding mechanisms can explain the observed yield stress in the composites. Some authors have indeed argued that the debonding between the polymer matrix and the calcium carbonate and talc particles allows that the polymer matrix deforms more easily to achieve shear yielding [49,155].

The debonding stresses can describe the void nucleation and void growth at the particle/matrix interface. This stress level depends strongly on the shape and size particle, and particle-matrix interface adhesion [49,70,155]. Furthermore, other authors also studied the influence of strain rates on the debonding/cavitation stress. They found that the accommodation of stress by the talc particles was low at higher rates of strain, leading to marked debonding/cavitation mechanisms and low yield stress [65].

As shown in Figure 6.11, the strain at break of both types of composites decreased continuously with increasing the filler content, influenced by the polymer-filler interactions and the polymer chain confinement [47,49,60-65]. In general, the tensile properties of composites decrease with an increase in filler content; this may be explained by the formation of larger aggregates (this finding



was verified based on SEM micrographs). These results revealed a competition between self-reinforcement mechanisms and damage mechanisms by debonding in both composites. The presence of large agglomerates in samples leads to stress concentrations in the matrix, which are detrimental to mechanical performance since they could act as stress raisers and promote premature cracking. The reinforcing mechanism of mineral fillers is strongly linked to the good interfacial adhesion between the polymer matrix and the embedded particles. Besides, a good interfacial adhesion gives a more stable and uniform filler dispersion during the compounding process. It is speculated that other surface treatments and the use of nano-size particles could improve the interaction of talc and  $\text{CaCO}_3$  with the PP matrix, leading to composite membranes with enhanced mechanical properties.

The data displayed in Figure 6.12 demonstrated that similar results to those seen in precursor films were obtained in the case of unfilled and composite membranes. However, it is important to consider that after extrusion, precursor films were axially oriented to induce pore formation, which significantly reduced the thickness of the porous membranes. The new structure created during this post-processing can result in increased stiffness and ultimate tensile strength. Still, it also caused a significant reduction in elongation at break for membranes compared to the non-stretched precursor films [4-8].

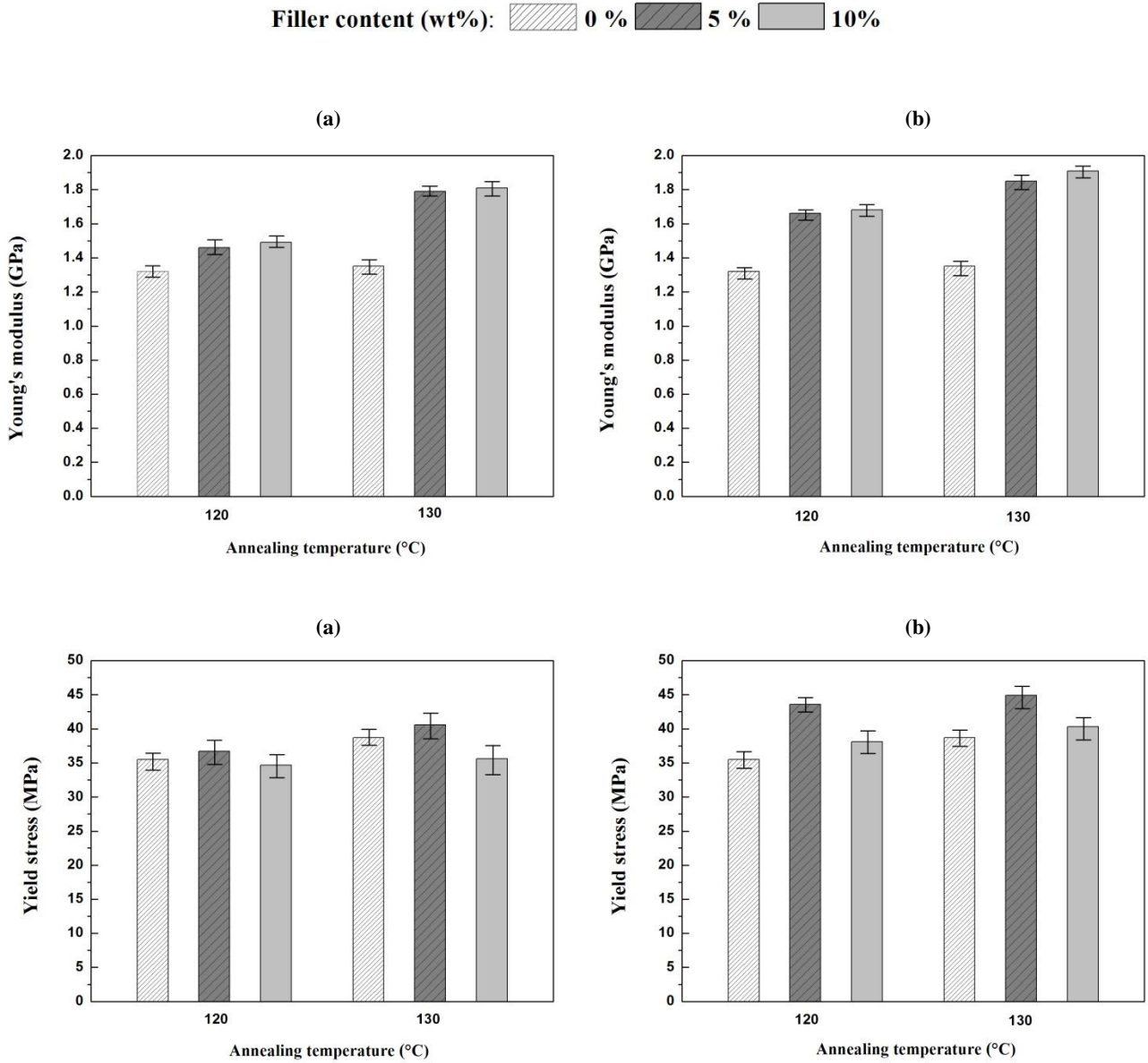


Figure 6.10. Young's modulus and Yield stress of the multilayer precursor films with different type of fillers (a) PP-C / HDPE and (b) PP-T / HDPE.

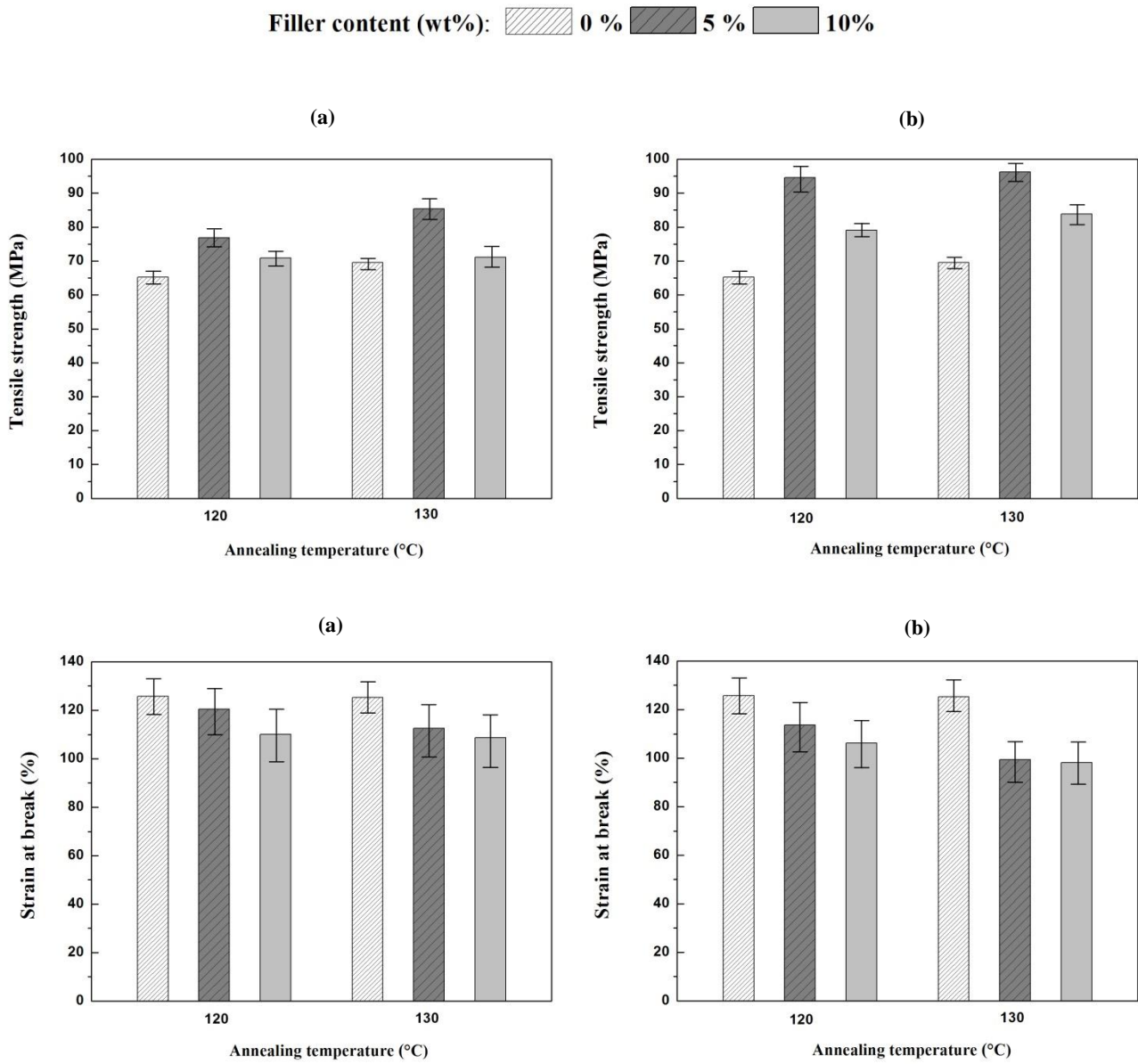


Figure 6.11. Tensile strength and Strain at break of the multilayer precursor films with different type of fillers (a) PP-C / HDPE and (b) PP-T / HDPE.

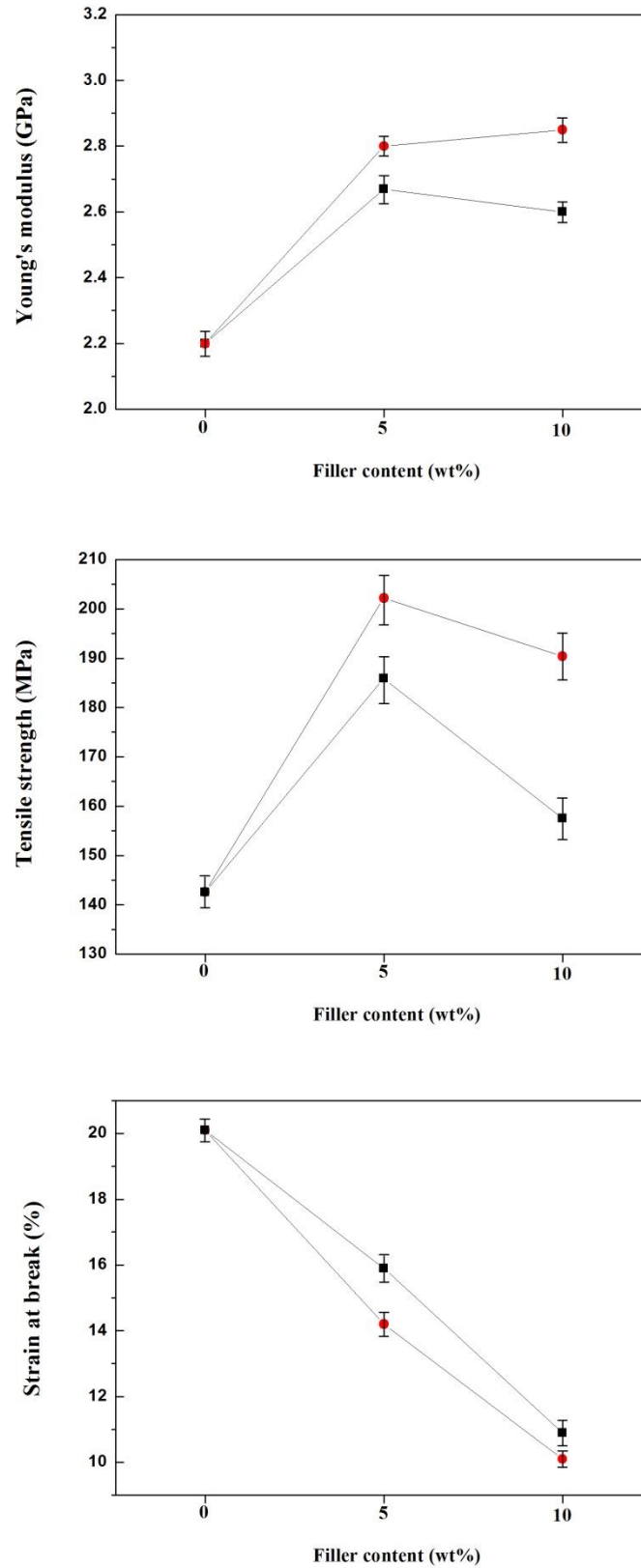


Figure 6.12. Young's modulus, Tensile strength and Strain at break of the multilayer membranes, containing different filler type and content < ■ > PP-C / HDPE < ● > PP-T / HDPE.

## **6.5. Discussion and main conclusions**

This chapter investigated the structure and performance of trilayer porous membranes made from HDPE as an intermediate layer and filled PP with CaCO<sub>3</sub> and talc as outers layers. The discussion of our results can be summarized as follows.

The co-extrusion process is still a major processing method to produce thin multilayer films with a wide range of properties, at low cost, and with a reduced tendency for delamination [104]. The degree of crystallinity and the crystal type and orientation strongly influence the membrane porosity and permeability, as well as its thermal and mechanical properties. The co-extrusion process and post-processing treatments such as annealing and stretching can directly affect crystallinity and orientation of the polymer chains in semicrystalline materials, as in the case of polyethylene and polypropylene. This result aligns well with previous studies demonstrating that annealing before stretching leads to higher permeability by increasing porosity, pore size, and pore interconnection. Nevertheless, low annealing temperature was applied to multilayer films due to the presence of the polyethylene intermediate layer, which compared with PP has a lower melting point.

The analysis also showed that the crystallization of the polymer matrix could occur in the presence of mineral fillers. Therefore, the crystallization and crystalline orientation were affected by both the flow-induced crystallization and the nucleating mechanism of fillers. It is well known that talc is a strong nucleating agent used to achieve a high degree of crystallinity and crystal orientation on polymeric materials. Compared with the CaCO<sub>3</sub>, talc can be oriented along the melt-flow direction. Thus, the addition of talc under extensional flow and the talc orientation promoted the transcrystallization of PP on the filler surface, improving the crystal structure of precursor films.

The results obtained using SEM micrographs and nitrogen adsorption-desorption isotherms (BET method) have revealed that the presence of CaCO<sub>3</sub> and talc particles in polymer blends results in microstructural changes. With sufficiently filler content, the debonding of the fillers from the polymer matrix, plus the pore formation by stretching-induced lamellae separation resulted in more permeable membranes with larger porosity and average pore diameter.

Compared to precursor films, membranes showed a pronounced increase in the tensile strength and a drastic decrease in the strain at break along MD. Something similar happened with reinforcing fillers, which provided a substantial improvement in mechanical properties, exhibiting higher tensile strength but lower elongation at break owing to the confinement effect and reduction in chain mobility. Additionally, these reinforcement fillers have demonstrated to play an important role in improving the membrane's thermal stability due to the interactions between fillers and polymer matrix. However, a homogeneous dispersion of mineral particles in a polymeric matrix is a

challenging task due to the strong tendency of these particles to agglomerate. Agglomerates were observed by SEM, indicating that probably other surface treatments for fillers or high shear forces during the composite processing steps must be applied to disperse  $\text{CaCO}_3$  and talc in the polymer melt and increase membrane performance.

SEM micrographs of the cross-sections of multilayered membranes showed similar layer thicknesses and acceptable adhesion at the interface. Compared to monolayers membranes produced under the same annealing and stretching conditions, the trilayer porous membranes showed lower permeability values, possibly due to the presence of interfaces between layers of different pore size distributions or also due to the lower orientation factors achieved during the processing step. In future works, great efforts might be devoted to the development of coextruded multilayer films by a flat-die chill-roll casting process to produce high-performance filled membranes.



## **Chapter 7:**

### **Conclusions and future research lines**





## 7.1. Conclusions

The wide variety of synthetic polymeric materials for membranes leads to an extensive range of applications in industrial production. Typical polymeric materials to develop membranes by stretching and thermal methods include polypropylene (PP) and polyethylene (PE). This thesis is devoted to developing porous membranes through the three-stage process MEAUS (melt-extrusion, annealing, and uniaxial stretching). It has been organized in three main sections describing the structure and performance of different monolayer and trilayer polyolefin membranes. In this final chapter, the main findings of the research work are reiterated.

We used a lab-scale cast film extrusion to develop and characterize porous membranes made of neat polypropylenes with different molecular weights, and blends with branched and very fluid PP resins. Generally, for precursor films production, the more initially planar and oriented lamellar structure was recognized to enhance membrane performance. In this regard, for films produced from different PP resins, but at the same processing conditions, the crystalline structure and molecular orientation were related to the characteristic melt-relaxation times of polymers. FTIR was employed to measure the orientation of crystalline and amorphous phases. The use of high molecular weight resins influenced the stress-induced crystallization behavior, increasing the melt relaxation time and enhancing the formation of an oriented row-nucleated stacked lamellar structure.

For a given resin, the orientation of precursor films in the machine direction was also strongly dependent on the total draw ratio. This parameter can be used to estimate the degree of molecular orientation during the extrusion step. Increased draw ratio led to a higher macromolecular alignment along machine direction and an optimal row-nucleated structure concerning the final porous membrane morphology. However, drawing up to a very high draw ratio reduced the amorphous tie chain mobility. The main consequence of this reduced mobility was the limitation on lamellar blocks separation and the pore enlargement.

In the third stage, the annealed precursor films were uniaxially stretched along the MD to promote pore formation. The two critical parameters to control membrane properties during the stretching at room and high temperatures were the strain rate and the percent extension. The objective was to determine the effect of these variables on measured air permeability (Gurley number), pore size distribution, and membrane morphology. From the SEM and DSC analyses, the presence of the so-called “interconnected bridges” formed after the stretching stages was observed. These microfibrils oriented along MD were formed after lamellae separation when pores were created and long tie chains pulled out of the crystals melt and recrystallize, which also explained the reduction in the lamellae thickness at high levels of extension. Films subject to slow strain rates at

room temperature showed a slight increase in porosity and Gurley permeability values. During this first stretching stage, the most critical parameter was the strain ratio applied. In this regard, the optimum value of stretch per cent was found to be 35. Higher extension levels produced a reduction in pore density due to the fragmentation of neighboring crystal lamellae, which in turn led to a reduction in the degree of orientation. However, when the stretching takes place at high temperatures macromolecules gained mobility by the thermal energy supplied. The slower strain rates and high strain extents led to a significant enhancement on membrane permeability. That is, under these conditions, the degree of lamellar separation increased, leading to larger pore sizes. A strong linear relationship between the porous area and the permeability to air and isobutene has been found for PP samples prepared at different stretching conditions.

The development of porous membranes from polypropylene-ethylene copolymers and the temperature variation in the main stages of the MEAUS technique (melt extrusion, annealing, and the second stage of uniaxial stretching) were also studied. Neat PP random copolymer resulted in a no suitable material to produce porous polymeric membranes by this stretching method. This was due to the decrease in the crystallization capability of polymer chain segments with the presence of random ethylene comonomer. However, when we added small amounts of PP random copolymer (up to about 10%) in the homopolymer resin, a slight increase in the average pore diameter was observed. Since small amounts of this copolymer led to a reduction of the mechanical properties such as stiffness and tensile strength, it was speculated that these characteristics promoted higher lamellar separation during the uniaxial stretching, increasing the pore size of membranes.

In contrast to the random copolymer films, precursor films from heterophasic PP copolymers could be produced into porous membranes using the same processing conditions. Comparing the SEM micrographs taken from the surface of membranes and the characterization of pore morphology by image analysis, similar pore density values were observed for both the heterophasic copolymer and the homopolymer. However, the largest average pore size and permeability to air were found in membranes made from the copolymer. The difference in crystallinity and phase separation that occurs between the PP matrix and the ethylene-rich phase increased the mean pore size. Nevertheless, some degree of membrane inhomogeneity, in terms of porosity, was observed in these samples. For this reason, different amounts of PP copolymer were added in the homopolymer resin to develop more uniform membranes (pore size distribution) with increased pore size and permeability. All these effects were confirmed by BET method and BJH models. Blends with a PP-B content equal to 20% displayed much larger surface areas, pore volume, and average pore diameter.

In terms of processing temperature during extrusion, the higher the processing temperature of precursor films, the lower the oriented crystalline structure and membrane performance. However,

the structural modifications promoted by annealing became more evident with the rise of temperature since more significant rearrangement of polymer chains in both the crystalline and amorphous phases led to an increase in both the degree of crystallinity and the molecular orientation. The samples annealed just up to 160 °C showed the highest membrane permeability and the largest observable pore size and pore density. Above this annealing temperature, membranes had lower permeability values. When the annealing temperature is too high (170 °C) the melting of the crystalline phase in some areas led to a reduced pore density and interconnectivity of pores. Finally, for the second stretching stage, hot uniaxial stretching temperatures higher than 140 °C provided a larger pore size by increased molecular mobility (increased lamellar separation). However, high temperatures too close to the melting point during a prolonged stretch could lead to local plastic deformation of porous material. That is the deterioration of the crystalline lamellar structure due to the partial melting of some areas, which in turn led to a reduced crystalline orientation as the lamellar separation occurred. As a result, reduced pore density and membrane permeability values were obtained.

Tensile testing was performed to evaluate the mechanical properties of precursor films made from copolymer blends and under different annealing temperatures. Thermal annealing increased the stiffness and tensile strength of precursor films annealed until an optimum value of 160 °C, due to the increased crystallinity and molecular orientation of samples. The presence of ethylene or EPR comonomers decreased mechanical stiffness, yield stress, and tensile strength with the increasing blend content. Tensile tests performed at room temperature were useful in determining the optimum percentage stretch during the cold stretching stage before the stretching at high temperatures counteracted the strain-hardening observed in all specimens.

The development of filled porous membranes from multilayer PP-HDPE resins has been studied in the third section of this thesis. The role that mineral fillers (CaCO<sub>3</sub> and talc) play in the PP outer layers and the process variables that affect the flow-induced crystallization, orientation, and pore morphology was investigated. During the co-extrusion process, three polymer layers (PP/HDPE/PP) were joined together to combine the properties of these different polyolefin materials into a single composite. Even though the optimum annealing temperature for PP resins was found to be around 160°C, low annealing temperature was applied to multilayer films due to the presence of the polyethylene intermediate layer, which compared with PP has a lower melting point.

During melt-extrusion of filled resins, the crystallization and crystalline orientation were affected by both the flow-induced crystallization and the nucleating mechanism of fillers. The nucleating ability of the CaCO<sub>3</sub> and talc fillers on PP has been discussed. Talc is a stronger nucleating agent than CaCO<sub>3</sub>. The addition of talc under extensional flow and its orientation along

the MD promoted the transcrystallization of PP on the filler surface, improving the crystal structure of precursor films by increasing both the crystallinity and the orientation of polymer chains.

These fillers caused changes in membrane characteristics and the separation performance related to the synergistic effects observed during the uniaxial stretching stages. The synergistic effect arising from the combination of filler debonding from the polymer matrix under stress and the pore formation by stretching-induced lamellae separation resulted in larger pores and high membrane permeability. These results were also confirmed by the N<sub>2</sub>-physisorption measurements (BET method). The BET specific surface area, BHJ surface area of pores and pore volume of the filled samples were much larger, confirming the nucleating ability of these materials. Compared to CaCO<sub>3</sub>, talc compounds at high talc filler contents showed higher porosity and permeability values, but reduced average pore diameter.

The tensile test determined the structural modifications promoted by uniaxial stretching. Uniaxial stretching of precursor films induced a more oriented structure in membranes. These samples showed a pronounced increase in the tensile strength and a drastic decrease in the strain at break along MD. Something similar happened with the use of reinforcing fillers. Composite precursor films and membranes exhibited higher tensile strength but lower elongation at break, owing to the confinement effect of inorganic fillers on the movement of polymer molecular chains. The thermal behavior of membrane samples was examined using thermogravimetric analysis (TGA) under nitrogen. Filled multilayer membranes displayed an increasingly higher decomposition retardancy when increasing the amount of CaCO<sub>3</sub> and talc. The effective barrier effect of mineral fillers and the restriction of polymer matrix mobility, especially in the vicinity of the particle, obstructed the escape of volatile products generated during the degradation process.

SEM surface micrographs of the multilayer membrane samples showed the presence of an agglomerated filler portion. The presence of these agglomerates reduced membrane performance by increasing the filler content. A homogeneous dispersion of mineral particles in a polymeric matrix is a challenging task due to the strong tendency of these particles to agglomerate. It is speculated that other surface treatments for fillers or high shear forces during the composite processing steps could improve the properties of the filled monolayer and multilayer membranes.

Compared to monolayers membranes produced under the same annealing and stretching conditions, the trilayer porous films showed lower permeability values. A possible explanation for this behavior is the presence of interfaces between layers of different pore size distributions or the smaller orientation factors achieved during the processing step.

## 7.2. Future research lines

Based on the above final statements concluding this work and in light of the future research direction of this study, concerning the fabrication of porous membranes via the MEAUS method, the following recommendations are provided below:

- The heterophasic polypropylene fulfilled the requisites for the formation of porous films via the MEAUS method. Thus, one possibility is the investigation of heterophasic copolymers with a variation in EPR content or the molecular weight of EPR portion at comparable rubber compositions.
- The co-extrusion process could be extended to other semicrystalline polymers that can form a porous membrane via the stretching method. For example, depending on the type of applications, using other bilayers and trilayers composites made from different hydrophobic or hydrophilic polymers could be possible. Besides, these membranes can be covered by thin coating layers, increasing membrane selectivity and other membrane physical properties.
- During this thesis work, we also produced a three-component system in which the middle layer was made up of polypropylene-ethylene copolymers. We tried to increase the interlayer adhesion and study the role of the ethylene content as a thermal shutdown mechanism in separators for lithium-ion batteries applications. Even though the air permeability was reduced in these samples as the temperature increased, these specimens didn't provide added safety through a thermal shutdown mechanism. Thus, one possibility is the investigation of another semicrystalline neat polymers or blends that satisfies the proposed criteria for thermal shutdown, improving at the same time the interfacial adhesion between layers.
- To improve performance of the multilayer membranes other processing techniques can be used. The purpose would be to select optimum properties for monolayer membranes and to try using alternative processes to manufacture multilayer thin-film structures. For example, a multilayer laminate technology.
- In the case of filled membranes, future studies should focus on the development of polymer nanocomposites. It is speculated that the use of nano-fillers would significantly affect the precursor film characteristics such as degree of crystallinity and orientation, as well as membrane properties such as porosity, permeability, and mechanical and thermal stability. This would be possible, owing to the ultra-large interfacial area per unit volume between the nanoparticle and the polymer matrix [41]. Also, for future investigations, the study and selection of appropriate surface treatments would improve the dispersion of mineral fillers into thermoplastic polymers by increasing the polymer-filler interactions.

## References

- [1] Brodd, R. J. (Ed.). Batteries for sustainability: selected entries from the encyclopedia of sustainability science and technology. Springer Science & Business Media. 2012.
- [2] Baker, R.W. Membrane Technology and Applications, 3rd ed.; JohnWiley & Sons Ltd.: West Sussex, UK, 2012; pp. 1–132.
- [3] Holtbrügge, J.; Kunze, A. K.; Niesbach, A.; Schmidt, P.; Schulz, R.; Sudhoff, D.; Skiborowski, M. Reactive and membrane-assisted separations. Walter de Gruyter GmbH & Co KG. 2016.
- [4] Tabatabaei, S.H.; Carreau, P.J.; Ajji, A. Microporous membranes obtained from polypropylene blend film by stretching. *J. Membr. Sci.* 2008, 325: 772–782.
- [5] Sadeghi, F.; Ajji, A.; Carreau, P.J. Analysis of microporous membranes obtained from polypropylene films by stretching. *J. Membr. Sci.* 2007, 292: 62–71.
- [6] Sadeghi, F.; Ajji, A.; Carreau, P.J. Microporous membranes obtained from polypropylene blends with superior permeability properties. *J. Membr. Sci. Part B Polym. Phys.* 2008, 46: 148–157.
- [7] Tabatabaei, S.H.; Carreau, P.J.; Ajji, A. Effect of processing on the crystalline orientation, morphology, and mechanical properties of polypropylene cast films and microporous membrane formation. *Polymer* 2009, 50: 4228–4240.
- [8] Johnson, M.B.; Wilkes, G.L. Microporous membranes of polyoxymethylene from a melt-extrusion process: (II) Effects of thermal annealing and stretching on porosity. *J. Appl. Polym. Sci.* 2002, 84: 1762–1780.
- [9] Caihong, L.; Shuqiu, W.; Qi, C.; Ruijie, X.; Bing, H.; Wenqiang, S. Influence of heat-setting temperature on the properties of a stretched polypropylene microporous membrane. *Polym. Int.* 2014, 63: 584–588.
- [10] Saffar, A.; Carreau, P.J.; Ajji, A.; Kamal, M.R. Influence of stretching on the performance of polypropylene-based microporous membranes. *Ind. Eng. Chem. Res.* 2014, 53: 14014–14021.
- [11] Tabatabaei, S.H.; Carreau, P.J.; Ajji, A. Structure and properties of MDO stretched polypropylene. *Polymer* 2009, 50: 3981–3989.

- [12] Sadeghi, F.; Aji, A.; Carreau, P. J. Study of polypropylene morphology obtained from blown and cast film processes: Initial morphology requirements for making porous membrane by stretching. *Journal of Plastic Film & Sheeting*, 2005, 21(3): 199-216.
- [13] Ding, Z.; Bao, R.; Zhao, B.; Yan, J.; Liu, Z.; Yang, M. Effects of annealing on structure and deformation mechanism of isotactic polypropylene film with row-nucleated lamellar structure. *J. Appl. Polym. Sci.* 2013, 130: 1659–1666.
- [14] Wang, S.; Saffar, A.; Aji, A.; Wu, H.; Guo, S.Y. Fabrication of microporous membranes from melt extruded polypropylene precursor films via stretching: Effect of annealing. *Chin. J. Polym. Sci.* 2015, 33: 1028–1037.
- [15] Qi, C.; Ruijie, X.; Shuqiu, W.; Changbin, C.; Haibin, M.; Caihong, L.; Li, Z. Influence of annealing temperature on the lamellar and connecting bridge structure of stretched polypropylene microporous membrane. *Polym. Int.* 2015, 64: 446–452.
- [16] Caihong, L.; Weiliang, H.; Ruijie, X.; Yunqi, X. The correlation between the lower temperature melting plateau endotherm and the stretching-induced pore formation in annealed polypropylene films. *J. Plast. Film Sheet* 2012, 28: 151–164.
- [17] Saffar, A.; Carreau, P.J.; Aji, A.; Kamal, M.R. The impact of new crystalline lamellae formation during annealing on the properties of polypropylene based films and membranes. *Polymer* 2014, 55: 3156 - 3167.
- [18] Lin, Y.; Meng, L.; Wu, L.; Li, X.; Chen, X.; Zhang, Q.; Li, L. A semi-quantitative deformation model for pore formation in isotactic polypropylene microporous membrane. *Polymer* 2015, 80: 214–227.
- [19] Caihong, L.; Shuqiu, W.; Ruijie, X.; Qi, C.; Bing, H.; Xinlong, P.; Wenqiang, S. Formation of stable crystalline connecting bridges during the fabrication of polypropylene microporous membrane. *Polym. Bull.* 2013, 70: 1353–1366.
- [20] Xie, J.; Xu, R.; Chen, X.; Cai, Q.; Lei, C. Influence of heat-treatment temperature on the structure and properties of polypropylene microporous membrane. *Polym. Bull.* 2016, 73: 265–277.
- [21] Wu, S.; Lei, C.; Cai, Q.; Xu, R.; Hu, B.; Shi, W.; Peng, X. Study of structure and properties of polypropylene microporous membrane by hot stretching. *Polym. Bull.* 2014, 71: 2205–2217.
- [22] Bettotti, P. (Ed.). *Submicron Porous Materials*. Springer. 2017.



- [23] Breitkopf, C.; Swider-Lyons, K. (Eds.). Springer handbook of electrochemical energy. Springer. 2016.
- [24] Arora, P.; Zhang, Z. Battery separators. Chem. Rev. 2004, 104: 4419–4462.
- [25] Ulbricht, M. Advanced functional polymer membranes. Polymer 2006, 47: 2217–2262.
- [26] Wang, B.; Ji, J.; Li, K. Crystal nuclei templated nanostructured membranes prepared by solvent crystallization and polymer migration. Nature communications, 2016, 7(1): 1-8.
- [27] Chandavasu, C.; Xanthos, M.; Sirkar, K. K.; Gogos, C. G. Polypropylene blends with potential as materials for microporous membranes formed by melt processing. Polymer. 2002, 43(3): 781-795.
- [28] Offord, G. T.; Armstrong, S. R.; Freeman, B. D.; Baer, E., Hiltner, A.; Paul, D. R. Influence of processing strategies on porosity and permeability of  $\beta$  nucleated isotactic polypropylene stretched films. Polymer. 2013, 54(11): 2796-2807.
- [29] Offord, G. T.; Armstrong, S. R.; Freeman, B. D.; Baer, E.; Hiltner, A.; Swinnea, J. S.; Paul, D. R. Porosity enhancement in  $\beta$  nucleated isotactic polypropylene stretched films by thermal annealing. Polymer. 2013, 54(10): 2577-2589.
- [30] Sadeghi, F.; Tabatabaei, S.H.; Ajji, A.; Carreau, P.J. Properties of uniaxially stretched polypropylene films: effect of drawing temperature and random copolymer content. Can. J. Chem. Eng. 2010, 88: 1091–1098.
- [31] Saffar, A.; Carreau, P. J.; Ajji, A.; Kamal, M. R. Development of polypropylene microporous hydrophilic membranes by blending with PP-g-MA and PP-g-AA. Journal of Membrane Science, 2014, 462: 50-61.
- [32] Xiande, C.; Ruijie, X.; Jiayi, X.; Yuanfei, L.; Caihong, L.; Liangbin, L. The study of room-temperature stretching of annealed polypropylene cast film with row-nucleated crystalline structure. Polymer 2016, 94: 31–42.
- [33] Caihong, L.; Shuqiu, W.; Ruijie, X.; Xinlong, P.; Wenqiang, S.; Bing, H. Influence of low molecular weight tail of polypropylene resin on the pore structure by room-temperature stretching. Polym. Eng. Sci. 2013, 53: 2594–2602.
- [34] Kim, J.; Kim, S.S.; Park, M.; Jang, M. Effects of precursor properties on the preparation of polyethylene hollow fiber membranes by stretching. J. Membr. Sci. 2008, 318: 201–209.

- [35] Arranz-Andrés, J.; Peña, B.; Benavente, R.; Pérez, E.; Cerrada, M.L. Influence of tacticity and molecular weight on the properties of metallocenic isotactic polypropylene. *Eur. Polym. J.* 2007, 43: 2357–2370.
- [36] Lei, C.; Wu, S.; Xu, R.; Peng, X.; Shi, W.; Hu, B. Influence of low molecular weight tail of polypropylene resin on the pore structure by room-temperature stretching. *Polym. Eng. Sci.* 2013, 53: 2594–2602.
- [37] Chen, X.; Xu, R.; Xie, J.; Lin, Y.; Lei, C.; Li, L. The study of room-temperature stretching of annealed polypropylene cast film with row-nucleated crystalline structure. *Polymer* 2016, 94: 31–42.
- [38] Lei, C.; Huang, W.; Xu, R.; Xu, Y. The correlation between the lower temperature melting plateau endotherm and the stretching-induced pore formation in annealed polypropylene films. *J. Plast. Film Sheet.* 2012, 28: 151–164.
- [39] Lei, C.; Wu, S.; Xu, R.; Cai, Q.; Hu, B.; Peng, X.; Shi, W. Formation of stable crystalline connecting bridges during the fabrication of polypropylene microporous membrane. *Polym. Bull.* 2013, 70: 1353–1366.
- [40] Castejón, P.; Habibi, K.; Saffar, A.; Ajji, A.; Martínez, A.B.; Arencón, D. Polypropylene-Based Porous Membranes: Influence of Polymer Composition, Extrusion Draw Ratio and Uniaxial Strain. *Polymers* 2017: 10, 33.
- [41] Chrissafis, K.; Bikiaris, D. Can nanoparticles really enhance thermal stability of polymers? Part I: an overview on thermal decomposition of addition polymers. *Thermochimica Acta.* 2011, 523(1-2): 1-24.
- [42] Pukánszky, B.; Móczó, J. Morphology and properties of particulate filled polymers. In *Macromolecular Symposia*. 2004, Vol. 214, No. 1, pp. 115-134.
- [43] Supaphol, P.; Harnsiri, W.; Junkasem, J. Effects of calcium carbonate and Its Purity on crystallization and melting behavior, mechanical properties, and processability of syndiotactic polypropylene. *J. Appl. Polym. Sci.* 2004, 92: 201–212.
- [44] García-López, D.; Merino, J. C.; Pastor, J. M. Influence of the CaCO<sub>3</sub> nanoparticles on the molecular orientation of the polypropylene matrix. *Journal of applied polymer science.* 2003, 88(4): 947-952.

- [45] Nakamura, S.; Kaneko, S.; Mizutani, Y. Microporous polypropylene sheets containing CaCO<sub>3</sub> filler. *J. Appl. Polym. Sci.* 1993, 49: 143–150.
- [46] Kao, N.; Chandra, A.; Bhattacharya, S. Melt strength of calcium carbonate filled polypropylene melts. *Polymer international.* 2002, 51(12): 1385-1389.
- [47] Mehrjerdi, A. K.; Adl-Zarrabi, B.; Cho, S. W.; Skrifvars, M. Mechanical and thermo-physical properties of high-density polyethylene modified with talc. *Journal of applied polymer science.* 2013, 129(4): 2128-2138.
- [48] Lin, Y.; Chen, H.; Chan, C. M.; Wu, J. Effects of coating amount and particle concentration on the impact toughness of polypropylene/CaCO<sub>3</sub> nanocomposites. *European polymer journal.* 2011, 47(3): 294-304.
- [49] Karamipour, S.; Ebadi-Dehaghani, H.; Ashouri, D.; Mousavian, S. Effect of nano-CaCO<sub>3</sub> on rheological and dynamic mechanical properties of polypropylene: Experiments and models. *Polymer Testing.* 2011, 30(1): 110-117.
- [50] Armstrong, S. R.; Offord, G. T.; Paul, D. R.; Freeman, B. D.; Hiltner, A.; Baer, E. Co-extruded polymeric films for gas separation membranes. *Journal of applied polymer science.* 2014, 131(2).
- [51] Nago, S.; Mizutani, Y. Microporous polypropylene sheets containing CaCO<sub>3</sub> filler: Effects of stretching ratio and removing CaCO<sub>3</sub> filler. *J. Appl. Polym. Sci.* 1998, 68: 1543–1553.
- [52] Zhang, J.; Ding, Q. J.; Zhou, N. L.; Li, L.; Ma, Z. M.; Shen, J. Studies on crystal morphology and crystallization kinetics of polypropylene filled with CaCO<sub>3</sub> of different size and size distribution. *Journal of applied polymer science.* 2006, 101(4): 2437-2444.
- [53] Barczewski, M.; Kloziński, A.; Jakubowska, P.; Sterzyński, T. Nonisothermal crystallization of highly-filled polyolefin/calcium carbonate composites. *J. Appl. Polym. Sci.* 2014, 131: 41201.
- [54] Kamal, M.; Sharma, C.S.; Upadhyaya, P.; Verma, V.; Pandey, K.N.; Kumar, V.; Agrawal, D.D. Calcium carbonate (CaCO<sub>3</sub>) nanoparticle filled polypropylene: Effect of particle Surface treatment on mechanical, thermal, and morphological performance of composites. *J. Appl. Polym. Sci.* 2012, 124: 2649–2656.
- [55] Ding, L.; Wu, T.; Ge, Q.; Xu, G.; Yang, F.; Xiang, M. Investigation of deformation and pore formation in isotactic polypropylene containing active nano-CaCO<sub>3</sub>. *Polymer International.* 2017, 66(11): 1498-1509.

- [56] Buasri, A.; Chaiyut, N.; Borvornchettanuwat, K.; Chantanachai, N.; Thonglor, K. Thermal and mechanical properties of modified CaCO<sub>3</sub>/PP nanocomposites. *Int. J. Chem. Mol. Nucl. Mater. Metall. Eng.* 2012, 6(8).
- [57] Leong, Y. W.; Bakar, M. A.; Mohd. Ishak, Z. A.; Ariffin, A. Effects of filler treatments on the mechanical, flow, thermal, and morphological properties of talc and calcium carbonate filled polypropylene hybrid composites. *Journal of Applied Polymer Science.* 2005, 98(1): 413-426.
- [58] Nasrin, R.; Gafur, M.A.; Bhuiyan, A.H. Characterization of isotactic polypropylene talc composites prepared by extrusion cum compression molding technique. *Mater. Sci. Appl.* 2015, 6: 925–934.
- [59] Branciforti, M. C.; Oliveira, C. A.; De Sousa, J. A. Molecular orientation, crystallinity, and flexural modulus correlations in injection molded polypropylene/talc composites. *Polymers for Advanced Technologies.* 2010, 21(5): 322-330.
- [60] Qiu, F.; Wang, M., Hao, Y.; Guo, S. The effect of talc orientation and transcrystallization on mechanical properties and thermal stability of the polypropylene/talc composites. *Composites Part A: Applied Science and Manufacturing.* 2014, 58: 7-15.
- [61] Kim, K. J.; White, J. L.; Eun Shim, S.; Choe, S. Effects of stearic acid coated talc, CaCO<sub>3</sub>, and mixed talc/CaCO<sub>3</sub> particles on the rheological properties of polypropylene compounds. *Journal of applied polymer science.* 2004, 93(5): 2105-2113.
- [62] Wang, B.; Wang, Q.; Li, L. Morphology and properties of highly talc-and CaCO<sub>3</sub>-filled poly (vinyl alcohol) composites prepared by melt processing. *Journal of Applied Polymer Science.* 2013, 130(5): 3050-3057.
- [63] Gorna, K.,; Hund, M.; Vučak, M.; Gröhn, F.; Wegner, G. Amorphous calcium carbonate in form of spherical nanosized particles and its application as fillers for polymers. *Materials Science and Engineering: A.* 2008, 477(1-2): 217-225.
- [64] Wang, K.; Bahlouli, N.; Addiego, F.; Ahzi, S.; Rémond, Y.; Ruch, D.; Muller, R. Effect of talc content on the degradation of re-extruded polypropylene/talc composites. *Polymer degradation and stability.* 2013, 98(7): 1275-1286.
- [65] Chrissafis, K.,; Paraskevopoulos, K. M.; Pavlidou, E.; Bikiaris, D. Thermal degradation mechanism of HDPE nanocomposites containing fumed silica nanoparticles. *Thermochemica Acta.* 2009, 485(1-2): 65-71.

- [66] Fiorentino, B.; Fulchiron, R.; Duchet-Rumeau, J.; Bounor-Legaré, V.; Majesté, J. C. Controlled shear-induced molecular orientation and crystallization in polypropylene/talc microcomposites—Effects of the talc nature. *Polymer*. 2013, 54(11): 2764-2775.
- [67] Fiorentino, B.; Fulchiron, R.; Duchet-Rumeau, J.; Bounor-Legaré, V.; Majesté, J. C. Controlled shear-induced molecular orientation and crystallization in polypropylene/talc microcomposites—Effects of the talc nature. *Polymer*, 2013, 54(11): 2764-2775.
- [68] Wang, K.; Liang, S.; Deng, J.; Yang, H.; Zhang, Q.; Fu, Q.; Han, C. C. The role of clay network on macromolecular chain mobility and relaxation in isotactic polypropylene/organoclay nanocomposites. *Polymer*. 2006, 47(20): 7131-7144.
- [69] Saffar, A.; Carreau, P. J.; Kamal, M. R.; Ajji, A. Hydrophilic modification of polypropylene microporous membranes by grafting TiO<sub>2</sub> nanoparticles with acrylic acid groups on the surface. *Polymer*. 2014, 55(23): 6069-6075.
- [70] Chrissafis, K.; Paraskevopoulos, K.M.; Stavrev, S.Y.; Docoslis, A.; Vassiliou, A.; Bikiaris, D.N. Characterization and thermal degradation mechanism of isotactic polypropylene/carbon black nanocomposites. *Thermochim. Acta* 2007, 465: 6–17.
- [71] Lin, K. Y.; Xanthos, M.; Sirkar, K. K. Novel polypropylene microporous membranes via spherulitic deformation—Processing perspectives. *Polymer*. 2009, 50(19): 4671-4682.
- [72] Chen, R. T.; Saw, C. K.; Jamieson, M. G.; Aversa, T. R.; Callahan, R. W. Structural characterization of Celgard® microporous membrane precursors: Melt-extruded polyethylene films. *Journal of applied polymer science*, 1994, 53(5): 471-483.
- [73] Yu, W. C. U.S. Patent No. 6,878,226. Washington, DC: U.S. Patent and Trademark Office. 2005.
- [74] Higuchi, H.; Matsushita, K.; Ezoe, M.; Shinomura, T. U.S. Patent No. 5,385,777. Washington, DC: U.S. Patent and Trademark Office. 1995.
- [75] Yu, W. C. U.S. Patent No. 5,691,077. Washington, DC: U.S. Patent and Trademark Office.
- [76] Yu, W. C.; Hux, S. E. (1999). U.S. Patent No. 5,952,120. Washington, DC: U.S. Patent and Trademark Office. 1997.
- [77] Zhang, X.; Xiao, K. K.; Nark, R. A.; Smith, R. E. U.S. Patent Application No. 14/950,478. 2016.

- [78] Keller, A., Kolnaar, J. W. H. Chain extension and orientation: Fundamentals and relevance to processing and products. In *Orientational Phenomena in Polymers 1993*, pp. 81-102. Steinkopff.
- [79] Somani, R. H.; Yang, L.; Zhu, L.; Hsiao, B. S. Flow-induced shish-kebab precursor structures in entangled polymer melts. *Polymer*, 2005, 46(20): 8587-8623.
- [80] Somani, R. H.; Yang, L.; Hsiao, B. S. Effects of high molecular weight species on shear-induced orientation and crystallization of isotactic polypropylene. *Polymer*, 2006, 47(15): 5657-5668.
- [81] Somani, R. H.; Yang, L.; Sics, I.; Hsiao, B. S.; Pogodina, N. V.; Winter, H. H.; Tsou, A. Orientation-induced crystallization in isotactic polypropylene melt by shear deformation. *Macromolecular Symposia*. Weinheim: WILEY-VCH Verlag, 2002. p. 105-117.
- [82] Somani, R. H.; Hsiao, B. S.; Nogales, A.; Srinivas, S.; Tsou, A. H.; Sics, I.; Ezquerra, T. A. Structure development during shear flow-induced crystallization of i-PP: in-situ small-angle X-ray scattering study. *Macromolecules*, 2000, 33(25): 9385-9394.
- [83] Somani, R. H.; Yang, L.; Hsiao, B. S.; Fruitwala, H. Nature of shear-induced primary nuclei in iPP melt. *Journal of Macromolecular Science, Part B*, 2003, 42(3-4): 515-531.
- [84] Agarwal, P. K.; Somani, R. H.; Weng, W.; Mehta, A.; Yang, L., Ran, S.; Hsiao, B. S. Shear-induced crystallization in novel long chain branched polypropylenes by in situ rheo-SAXS and WAXD. *Macromolecules*, 2003, 36(14): 5226-5235.
- [85] Seki, M.; Thurman, D. W.; Oberhauser, J. P.; Kornfield, J. A. Shear-mediated crystallization of isotactic polypropylene: The role of long chain- long chain overlap. *Macromolecules*, 2002, 35(7): 2583-2594.
- [86] Derakhshandeh, M.; Hatzikiriakos, S. G. Flow-induced crystallization of high-density polyethylene: the effects of shear and uniaxial extension. *Rheologica acta*, 2012, 51(4): 315-327.
- [87] Yang, L.; Somani, R. H.; Sics, I.; Hsiao, B. S.; Kolb, R.; Fruitwala, H.; Ong, C. Shear-induced crystallization precursor studies in model polyethylene blends by in-situ rheo-SAXS and rheo-WAXD. *Macromolecules*, 2004, 37(13): 4845-4859.
- [88] Hsiao, B. S.; Yang, L.; Somani, R. H.; Avila-Orta, C. A.; Zhu, L. Unexpected shish-kebab structure in a sheared polyethylene melt. *Physical review letters*, 2005, 94(11): 117802.
- [89] Keum, J. K.; Zuo, F.; Hsiao, B. S. Formation and stability of shear-induced shish-kebab structure in highly entangled melts of UHMWPE/HDPE blends. *Macromolecules*, 2008, 41(13): 4766-4776.

- [90] Zhang, X. M.; Elkoun, S.; Ajji, A.; Huneault, M. A. Oriented structure and anisotropy properties of polymer blown films: HDPE, LLDPE and LDPE. *Polymer*, 2004, 45(1): 217-229.
- [91] Wei, X.; Collier, J. R.; Petrovan, S. Shear and elongational rheology of polyethylenes with different molecular characteristics. II. Elongational rheology. *Journal of applied polymer science*, 2007, 104(2); 1184-1194.
- [92] Zoukrami, F.; Haddaoui, N.; Bailly, C.; Sclavons, M.; Legras, R. Elongational and shear flow behavior of calcium carbonate filled low density polyethylene: Effect of filler particle size, content, and surface treatment. *Journal of Applied Polymer Science*, 2012, 123(1): 257-266.
- [93] Kumaraswamy, G.; Issaian, A. M.; Kornfield, J. A. Shear-enhanced crystallization in isotactic polypropylene. 1. Correspondence between in situ rheo-optics and ex situ structure determination. *Macromolecules*, 1999, 32(22): 7537-7547.
- [94] Kumaraswamy, G.; Verma, R. K.; Issaian, A. M.; Wang, P.; Kornfield, J. A.; Yeh, F.; Olley, R. H. Shear-enhanced crystallization in isotactic polypropylene Part 2. Analysis of the formation of the oriented "skin". *Polymer*, 2000, 41(25): 8931-8940.
- [95] Münstedt, H.; Kurzbeck, S.; Stange, J. Importance of elongational properties of polymer melts for film blowing and thermoforming. *Polymer Engineering & Science*, 2006, 46(9): 1190-1195.
- [96] Münstedt, H. Extensional rheology and processing of polymeric materials. *International Polymer Processing*, 2018, 33(5): 594-618.
- [97] Nogales, A.; Hsiao, B. S.; Somani, R. H.; Srinivas, S.; Tsou, A. H.; Balta-Calleja, F. J.; Ezquerro, T. A. Shear-induced crystallization of isotactic polypropylene with different molecular weight distributions: in situ small-and wide-angle X-ray scattering studies. *Polymer*, 2001, 42(12): 5247-5256.
- [98] Housmans, J. W.; Peters, G.; Meijer, H. Flow-induced crystallization of propylene/ethylene random copolymers. *Journal of thermal analysis and calorimetry*, 2009, 98(3): 693-705.
- [99] Ma, Z.; Fernandez-Ballester, L.; Cavallo, D.; Gough, T.; Peters, G. W. High-stress shear-induced crystallization in isotactic polypropylene and propylene/ethylene random copolymers. *Macromolecules*, 2013, 46(7): 2671-2680.
- [100] Schrauwen, B. A. G.; Breemen, L. V.; Spoelstra, A. B.; Govaert, L. E.; Peters, G. W. M.; Meijer, H. E. H. Structure, deformation, and failure of flow-oriented semicrystalline polymers. *Macromolecules*, 2004, 37(23): 8618-8633.

- 
- [101] Janeschitz-Kriegl, H.; Ratajski, E.; Stadlbauer, M. Flow as an effective promotor of nucleation in polymer melts: a quantitative evaluation. *Rheologica acta*, 2003, 42(4): 355-364.
- [102] Kitade, S.; Asuka, K.; Akiba, I.; Sanada, Y.; Sakurai, K.; Masunaga, H. Shear-induced pre-crystallization structures of long chain branched polypropylene under steady shear flow near the melting temperature. *Polymer*, 2013, 54(1): 246-257.
- [103] Peacock, A. *Handbook of polyethylene: structures: properties, and applications*. 2000. CRC press.
- [104] Giles Jr, H. F.; Mount III, E. M.; Wagner Jr, J. R. *Extrusion: the definitive processing guide and handbook*. William Andrew. 2n edition. 2004.
- [105] Ward, I. M. (Ed.). *Structure and properties of oriented polymers*. Springer Science & Business Media. 2012.
- [106] Wiley, J.; Sons. *Processing and Finishing of Polymeric Materials, 2 Volume Set*. John Wiley & Sons. 2011.
- [107] Karger-Kocsis, J. (Ed.). *Polypropylene: an AZ reference (Vol. 2)*. Springer Science & Business Media. 2012.
- [108] Maier, C.; Calafut, T. *Polypropylene: the definitive user's guide and databook*. William Andrew. 1998.
- [109] Swallowe, G. M. (Ed.). *Mechanical Properties and Testing of Polymers: an A–Z reference (Vol. 3)*. Springer Science & Business Media. 2013.
- [110] Höhne, G.; Hemminger, W. F.; Flammersheim, H. J. *Differential scanning calorimetry*. Springer Science & Business Media. 2013.
- [111] Jancar, J.; Fekete, E.; Hornsby, P. R.; Jancar, J.; Pukánszky, B.; Rother, R. N. (Eds.). *Mineral fillers in thermoplastics I: raw materials and processing*. Springer Berlin Heidelberg. 1999.
- [112] Guo, Q. *Polymer morphology: principles, characterization, and processing*. John Wiley & Sons. 2016.
- [113] Olabisi, O.; Adewale, K. *Handbook of thermoplastics*. CRC press. 2016.
- [114] De Rosa, C.; Auriemma, F. *Crystals and crystallinity in polymers: diffraction analysis of ordered and disordered crystals*. John Wiley & Sons. 2013.



- [115] Song, J.; Bringuier, A.; Kobayashi, S.; Baker, A. M.; Macosko, C. W. Adhesion between polyethylenes and different types of polypropylenes. *Polymer journal*. 2012, 44(9): 939-945.
- [116] Yu T. H, Processing and structure-property behaviour of microporous polyethylene-from resin to final film, Ph.D thesis, 1995, Virginia Polytechnic Institute and State University.
- [117] Johnson M. B, Investigations of the processing-structure.property relationship of selected semi crystalline polymers, Ph.D thesis, 2000, Virginia Polytechnic Institute and State University.
- [118] Zuo, F.; Keum, J. K.; Chen, X.; Hsiao, B. S.; Chen, H.; Lai, S. Y.; Li, J. The role of interlamellar chain entanglement in deformation-induced structure changes during uniaxial stretching of isotactic polypropylene. *Polymer*, 2007, 48(23): 6867-6880.
- [119] Samuels, R. J. (1979). High strength elastic polypropylene. *Journal of Polymer Science: Polymer Physics Edition*, 1979, 17(4): 535-568.
- [120] Tabatabaei, S. H.; Carreau, P. J.; Ajji, A. Microporous membranes obtained from PP/HDPE multilayer films by stretching. *Journal of membrane science*, 2009, 345(1-2): 148-159.
- [121] Li, Y.; Pu, H. Facile fabrication of multilayer separators for lithium-ion battery via multilayer coextrusion and thermal induced phase separation. *Journal of Power Sources*, 2018, 384: 408-416.
- [122] Li, Y., Pu, H.; Wei, Y. Polypropylene/polyethylene multilayer separators with enhanced thermal stability for lithium-ion battery via multilayer coextrusion. *Electrochimica Acta*, 2018, 264: 140-149.
- [123] Offord, G. T.; Armstrong, S. R.; Freeman, B. D.; Baer, E.; Hiltner, A.; Paul, D. R. Gas transport in coextruded multilayered membranes with alternating dense and porous polymeric layers. *Polymer*. 2014, 55(5): 1259-1266.
- [124] Zeng, F.; Xu, R.; Ye, L.; Xiong, B.; Kang, J.; Xiang, M.; Hao, Z. Effects of Heat Setting on the Morphology and Performance of Polypropylene Separator for Lithium Ion Batteries. *Industrial & Engineering Chemistry Research*. 2019, 58(6): 2217-2224.
- [125] Zhang, X. M.; Ajji, A. Oriented structure of PP/LLDPE multilayer and blends films. *Polymer*, 2005, 46(10): 3385-3393.
- [126] Stokes, K. K.; Mason, W. J.; Xiao, K. K.; Zhang, X.; Summey, B. J.; Moran, R.; Williams, S. P. U.S. Patent Application No. 15/267,566. 2017.

- [127] Nejabat, G. R. A theoretical reasoning on why coordination catalysts supported on mesoporous supports produce HDPE crystalline nanofibers but not iPP crystalline nanofibers. *Polyolefins Journal*, 2018, 5(2): 153-156.
- [128] Ferrer-Balas, D.; MasPOCH, M.L.; Martinez, A.B.; Santana, O.O. Influence of annealing on the microstructural, tensile and fracture properties of polypropylene films. *Polymer* 2001, 42: 1697–1705.
- [129] Hedesiu, C.; Demco, D. E.; Kleppinger, R.; Poel, G. V.; Gijsbers, W.; Blümich, B.; Litvinov, V. M. Effect of temperature and annealing on the phase composition, molecular mobility, and the thickness of domains in isotactic polypropylene studied by proton solid-state NMR, SAXS, and DSC. *Macromolecules*, 2007, 40(11): 3977-3989.
- [130] Olley, R. H.; Bassett, D. C. An improved permanganic etchant for polyolefines. *Polymer*, 1982, 23(12): 1707-1710.
- [131] Brunauer, S.; Emmett, P. H.; Teller, E. Adsorption of gases in multimolecular layers. *Journal of the American chemical society*, 1938, 60(2): 309-319.
- [132] Thommes, M.; Kaneko, K., Neimark, A. V.; Olivier, J. P.; Rodriguez-Reinoso, F.; Rouquerol, J.; Sing, K. S. Physisorption of gases, with special reference to the evaluation of surface area and pore size distribution (IUPAC Technical Report). *Pure and Applied Chemistry*, 2015, 87(9-10): 1051-1069.
- [133] Rouquerol, J.; Rouquerol, F.; Llewellyn, P.; Maurin, G.; Sing, K. S. Adsorption by powders and porous solids: principles, methodology and applications. 2013. Academic press.
- [134] Drioli, E.; Giorno, L. *Comprehensive membrane science and engineering* (Vol. 1). 2010. Newnes.
- [135] Wunderlich, B. *Thermal analysis of polymeric materials*. 2005. Springer Science & Business Media.
- [136] Karger-Kocsis, J. (Ed.). *Polypropylene structure, blends and composites: Volume 2 Copolymers and blends* (Vol. 2). 1994. Springer Science & Business Media.
- [137] Manabe, N.; Yokota, Y.; Nakatani, H.; Suzuki, S.; Liu, B.; Terano, M. Local thermal degradation behavior of heterophasic polypropylene copolymers. *Journal of applied polymer science*. 2006, 100(3), 1831-1835.

- [138] Shanguan, Y.; Zhang, C.; Xie, Y.; Chen, R.; Jin, L.; Zheng, Q. Study on degradation and crosslinking of impact polypropylene copolymer by dynamic rheological measurement. *Polymer*. 2010, 51(2), 500-506.
- [139] D'Orazio, L.; Mancarella, C.; Martuscelli, E.; Cecchin, G.; Corrieri, R. Isotactic polypropylene/ethylene-co-propylene blends: effects of the copolymer microstructure and content on rheology, morphology and properties of injection moulded samples. 1999, *Polymer*, 40(10), 2745-2757.
- [140] Franco-Urquiza, E.A.; Gámez-pérez, J.; Velázquez-Infante, J.C.; Santana, O.; Benasat, A.M.; Maspoch, M.L. Effect of the strain rate and drawing temperature on the mechanical behavior of EVOH and EVOH composites. *Adv. Polym. Technol.* 2013, 32 (Suppl. 1), E287–E296.
- [141] Mourad, A.H.I. Thermo-mechanical characteristics of thermally aged polyethylene/polypropylene blends. *Mater. Des.* 2010, 31: 918–929.
- [142] Gunel, E.M.; Basaran, C. Stress whitening quantification of thermoformed mineral filled acrylics. *J. Eng. Mater. Technol.* 2010, 132: 031002.
- [143] Pae, K.D.; Chu, H.C.; Lee, J.K.; Kim, J.H. Healing of stress-whitening in polyethylene and polypropylene at or below room temperature. *Polym. Eng. Sci.* 2000, 40: 1783–1795.
- [144] López-Barrón, C. R.; Tsou, A. H. Strain hardening of polyethylene/polypropylene blends via interfacial reinforcement with poly (ethylene-cb-propylene) comb block copolymers. *Macromolecules*. 2017, 50(7): 2986-2995.
- [145] Grestenberger, G.; Potter, G. D.; Grein, C. Polypropylene/ethylene-propylene rubber (PP/EPR) blends for the automotive industry: Basic correlations between EPR-design and shrinkage. *Express Polymer Letters*, 2014, 8(4).
- [146] Ramírez-Vargas, E.; Margarita Huerta-Martínez, B.; Javier Medellín-Rodríguez, F.; Sánchez-Valdes, S. Effect of heterophasic or random PP copolymer on the compatibility mechanism between EVA and PP copolymers. *J. Appl. Polym. Sci.* 2009, 112: 2290–2297.
- [147] Chen, H.B.; Karger-Kocsis, J.; Wu, J.S.; Varga, J. Fracture toughness of  $\alpha$  and  $\beta$  phase polypropylene homopolymers and random-and block-copolymers. *Polymer* 2002, 43: 6505–6514.

- [148] Papageorgiou, D.G.; Bikiaris, D.N.; Chrissafis, K. Effect of crystalline structure of polypropylene random copolymers on mechanical properties and thermal degradation kinetics. *Thermochim. Acta* 2012, 543: 288–294.
- [149] Martínez, M.C.; Benavente, R.; Gómez-Elvira, J.M. Molecular weight dependence and stereoselective chain cleavage during the early stages of the isotactic polypropylene pyrolysis. *Polym. Degrad. Stab.* 2017, 143: 26–34.
- [150] Rychlý, J.; Matisová-Rychlá, L.; Csmorová, K.; Janigová, I. Non-isothermal thermogravimetry, differential scanning calorimetry and chemiluminescence in degradation of polyethylene, polypropylene, polystyrene and poly(methyl methacrylate). *Polym. Degrad. Stab.* 2011, 96: 1573–1581.
- [151] Wallis, M. D.; Bhatia, S. K. Thermal degradation of high density polyethylene in a reactive extruder. *Polymer Degradation and Stability.* 2007, 92(9): 1721-1729.
- [152] Peterson, J. D.; Vyazovkin, S.; Wight, C. A. Kinetics of the thermal and thermo-oxidative degradation of polystyrene, polyethylene and Poly (propylene). *Macromolecular Chemistry and Physics.* 2001, 202(6): 775-784.
- [153] Al-Salem, S. M.; Lettieri, P. Kinetic study of high density polyethylene (HDPE) pyrolysis. *Chemical engineering research and design.* 2010, 88(12): 1599-1606.
- [154] Riga, A.; Collins, R.; Mlachak, G. Oxidative behavior of polymers by thermogravimetric analysis, differential thermal analysis and pressure differential scanning calorimetry. *Thermochimica Acta.* 1998, 324(1-2): 135-149.
- [155] Lin, Y.; Chen, H.; Chan, C. M.; Wu, J. Effects of coating amount and particle concentration on the impact toughness of polypropylene/CaCO<sub>3</sub> nanocomposites. *European polymer journal*, 2011, 47(3): 294-304.
- [156] Johnson, M. B.; Wilkes, G. L. Microporous membranes of isotactic poly (4-methyl-1-pentene) from a melt-extrusion process. I. Effects of resin variables and extrusion conditions. *Journal of applied polymer science.* 2002, 83(10): 2095-2113.



## List of publications

### Publications in journals

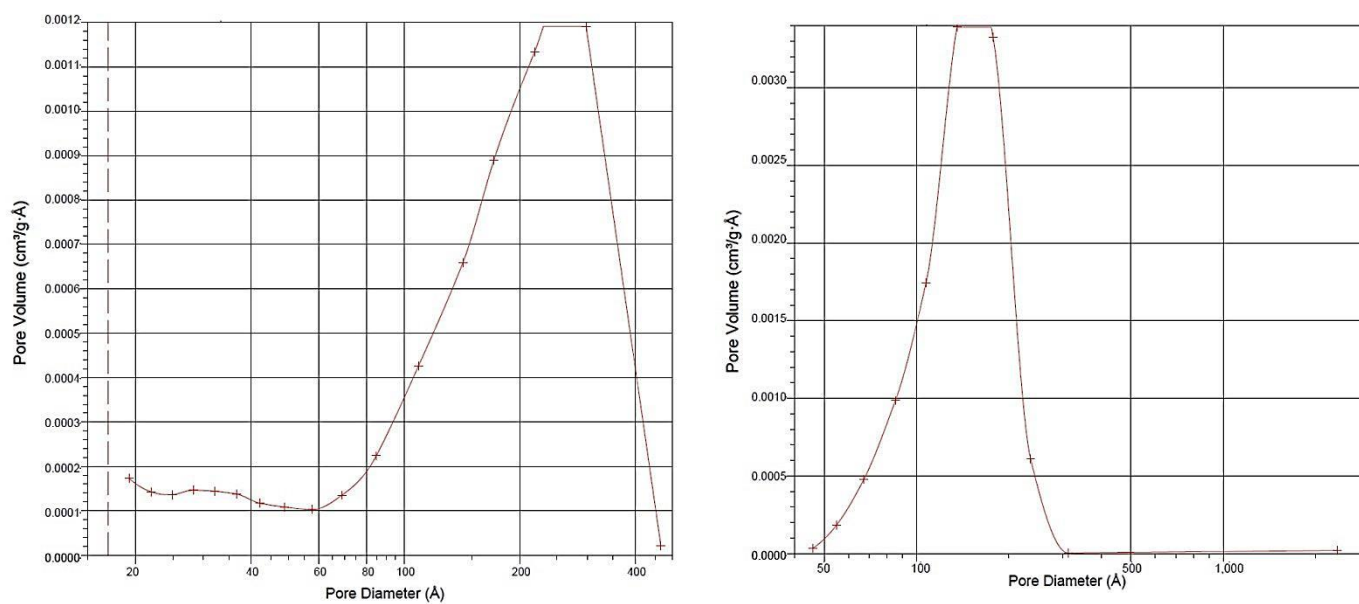
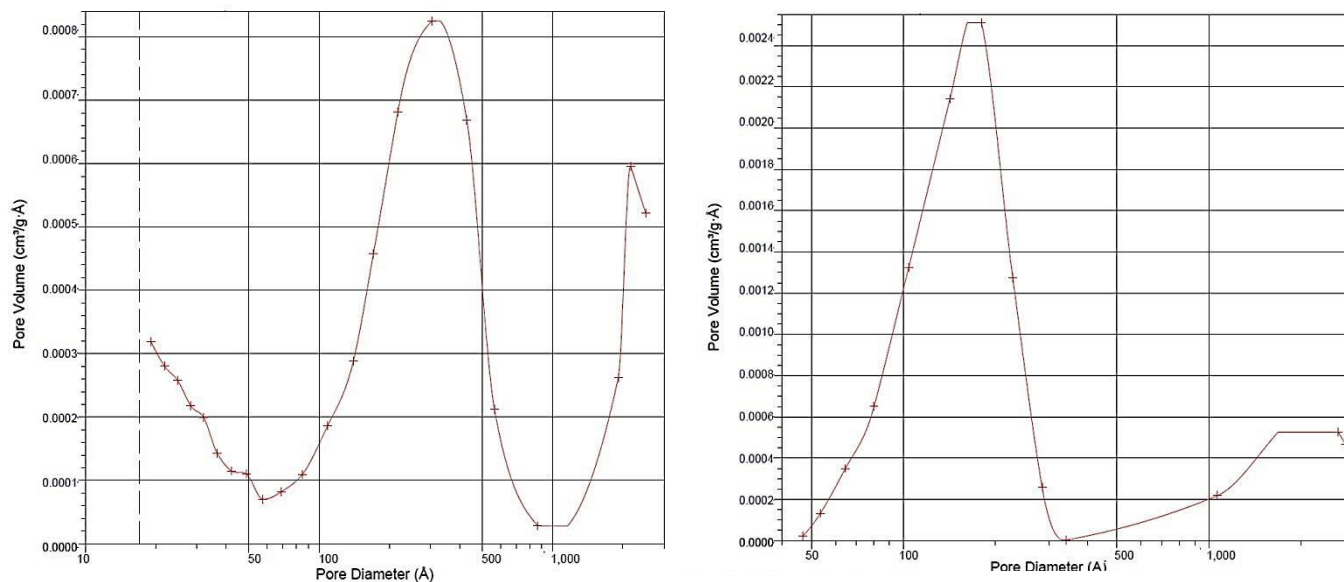
- **Castejón, P**, Habibi, K, Saffar, A, Ajji, A, Martínez, A. B, Arencón, D. Polypropylene-Based Porous Membranes: Influence of Polymer Composition, Extrusion Draw Ratio and Uniaxial Strain. *Polymers*, 2017, 10(1): 33. IF: 3.364, Q1, area: Polymer Science, DOI: 10.3390/polym10010033.
- **Castejón, P**, Arencón, D, Antunes, M, Realinho, V, Velasco, J. I, Martínez, A. B. Porous Membranes Based on Polypropylene-Ethylene Copolymers. Influence of Temperature on Extrusion, Annealing and Uniaxial Strain Stages. *Polymers*, 2018, 10(8): 854. IF: 3.164 Q1, area: Polymer Science, DOI: 10.3390/polym10080854.
- Habibi, K, **Castejón, P**, Martínez, A. B, Arencón, D. (2018). Effect of filler content, size, aspect ratio and morphology on thermal, morphological and permeability properties of porous talc filled—Polypropylene obtained through MEAUS process. *Advances in Polymer Technology*, 2018, 37(8): 3315-3324. IF: 2.137 Q2, area: Polymer Science, DOI: 10.1002/adv.22116.
- León N, Martínez AB, **Castejón. P**, Arencón D, Martínez PP. The fracture testing of ductile polymer films: Effect of the specimen notching. *Polymer Testing* 2017, 63: 180-193. IF: 2.464, Q1 (6/33), area: Materials Science, Characterization & Testing and Q2 (27/86), area: Polymer Science. DOI: 10.1016/j.polymertesting.2017.08.022.
- León N, Martínez AB, **Castejón. P**, Martínez PP, Arencón D. Notch effect on the fracture of a polymeric film, *Theoretical and Applied Fracture Mechanics* 2018, 95: 270-282. IF:2.659, Q1 (24/130), area: Engineering, Mechanical and Q1 (21/133), area: Mechanics. DOI: 10.1016/j.tafmec.2018.03.011

### Conferences

- **Conference:** GEP 2016 XIV Reunión del grupo especializado de polímeros (GEP) de la RSEQ y RSEF. **Title:** Influencia de la etapa de estiramiento en la morfología porosa de membranas de polipropileno obtenidas mediante extrusión. **Authors:** D. Arencón, P. Castejón, K. Habibi, A. Martínez. **Date:** 5th - 8th September 2016. **Place:** Burgos (Spain).
- **Conference:** Polymers: Design, Function and Application **Title:** Porous membranes based on polypropylene-ethylene copolymers. Influence of temperature on extrusion, annealing and uniaxial strain stages. **Authors:** P. Castejón, D. Arencón, M. Antunes, V. Realinho, J. I. Velasco, A. B. Martínez. **Date:** 21 - 23 March 2018. **Place:** Barcelona, España



## Annex I

Figure A.1. BJH (a) Adsorption and (b) Desorption  $dV/dD$  Pore Volume of the PP-HM<sub>w</sub>.Figure A.2. BJH (a) Adsorption and (b) Desorption  $dV/dD$  Pore Volume of the PP-B.



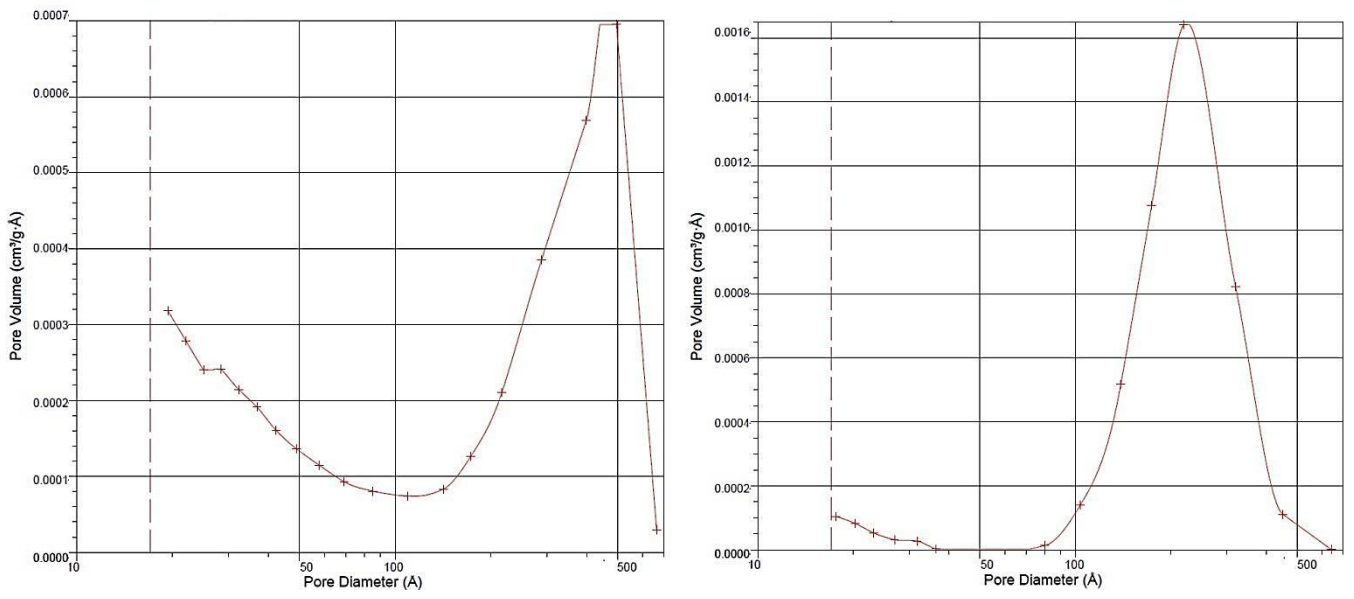


Figure A.3. BJH (a) Adsorption and (b) Desorption dV/dD Pore Volume of the PP-10R.

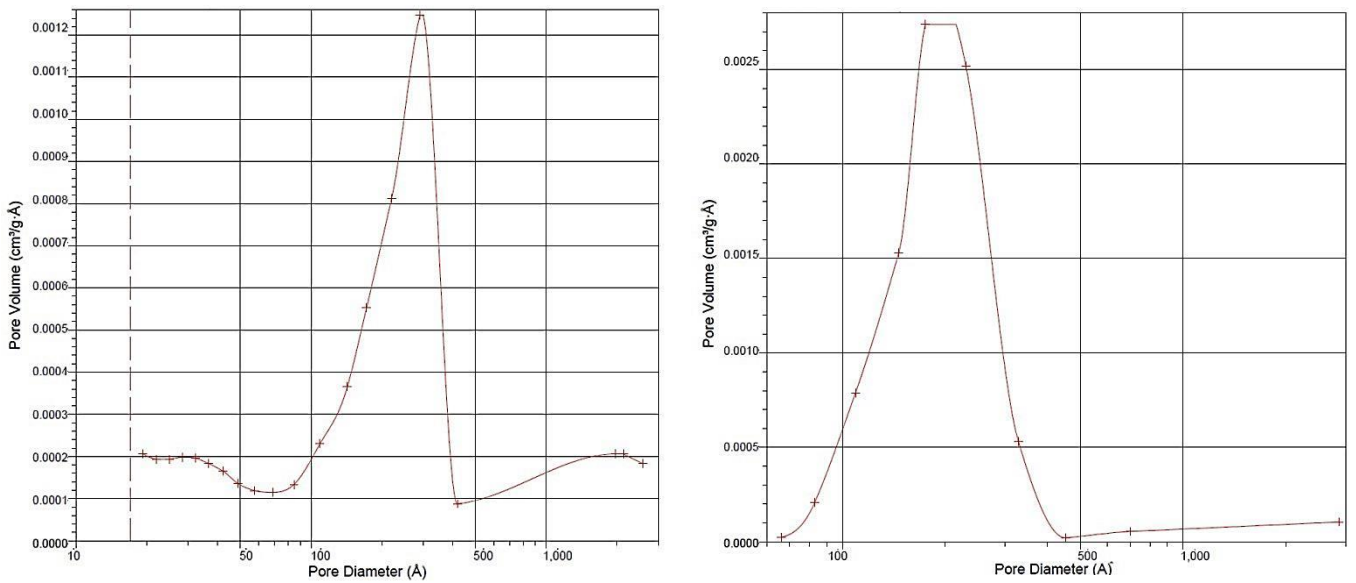


Figure A.4. BJH (a) Adsorption and (b) Desorption dV/dD Pore Volume of the PP-20B.

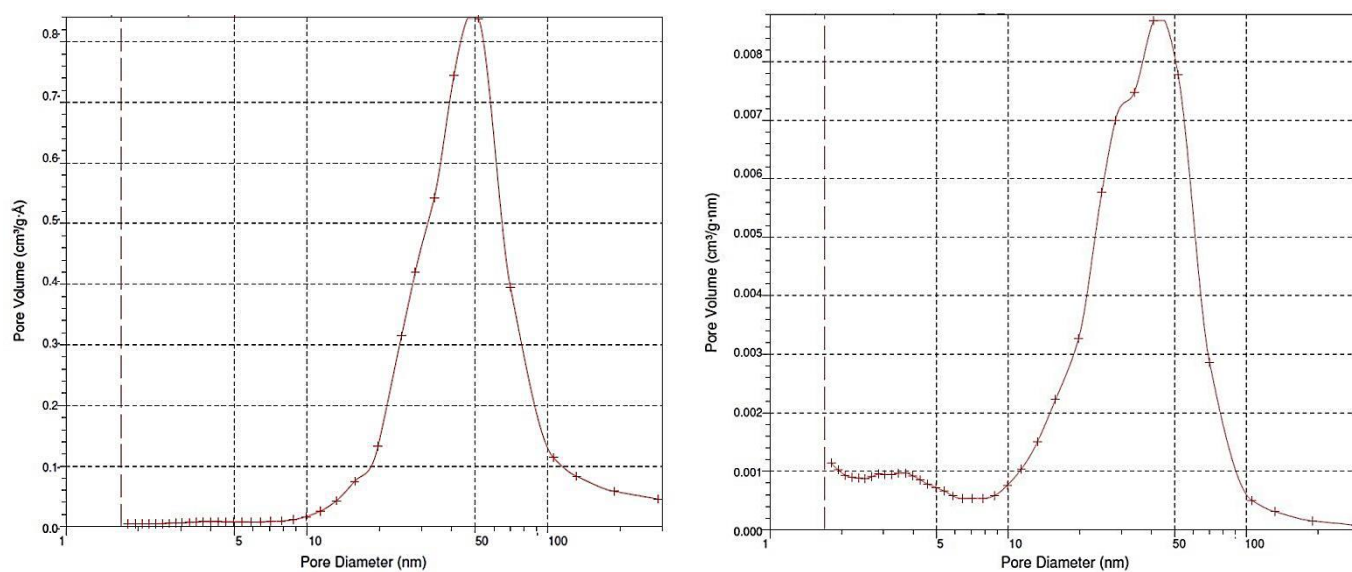


Figure A.5. BJH (a) Adsorption and (b) Desorption  $dV/dD$  Pore Volume of the PP/HDPE.

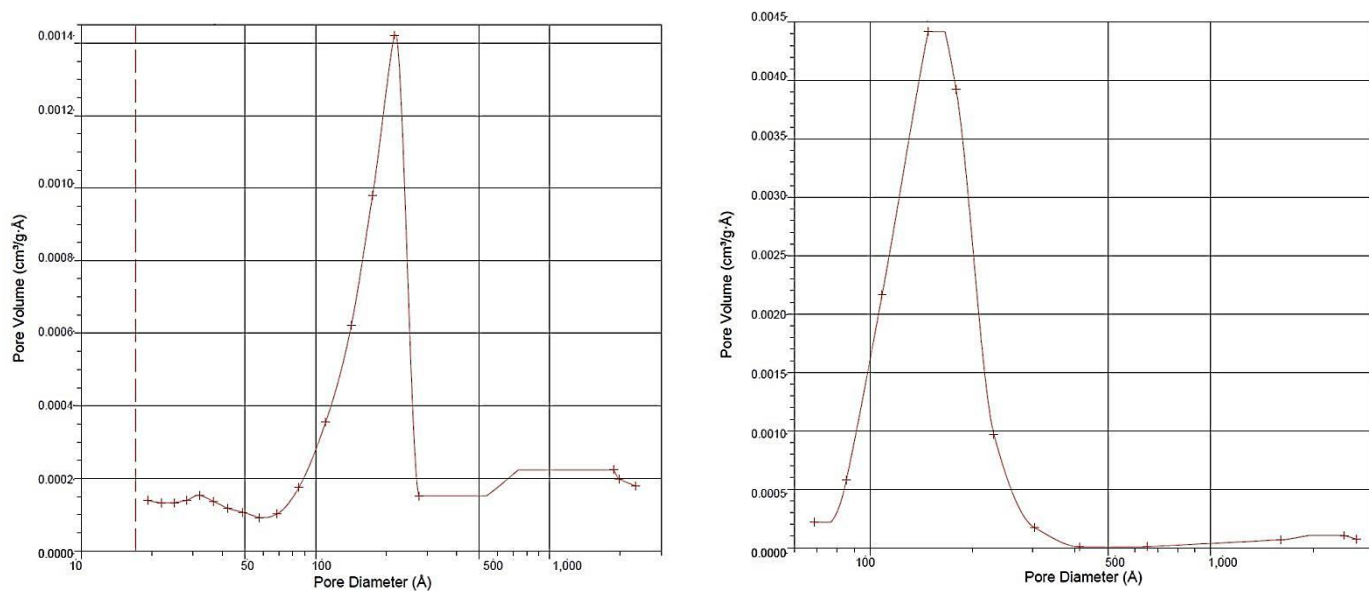


Figure A.6. BJH (a) Adsorption and (b) Desorption  $dV/dD$  Pore Volume of the PP-5T/HDPE.

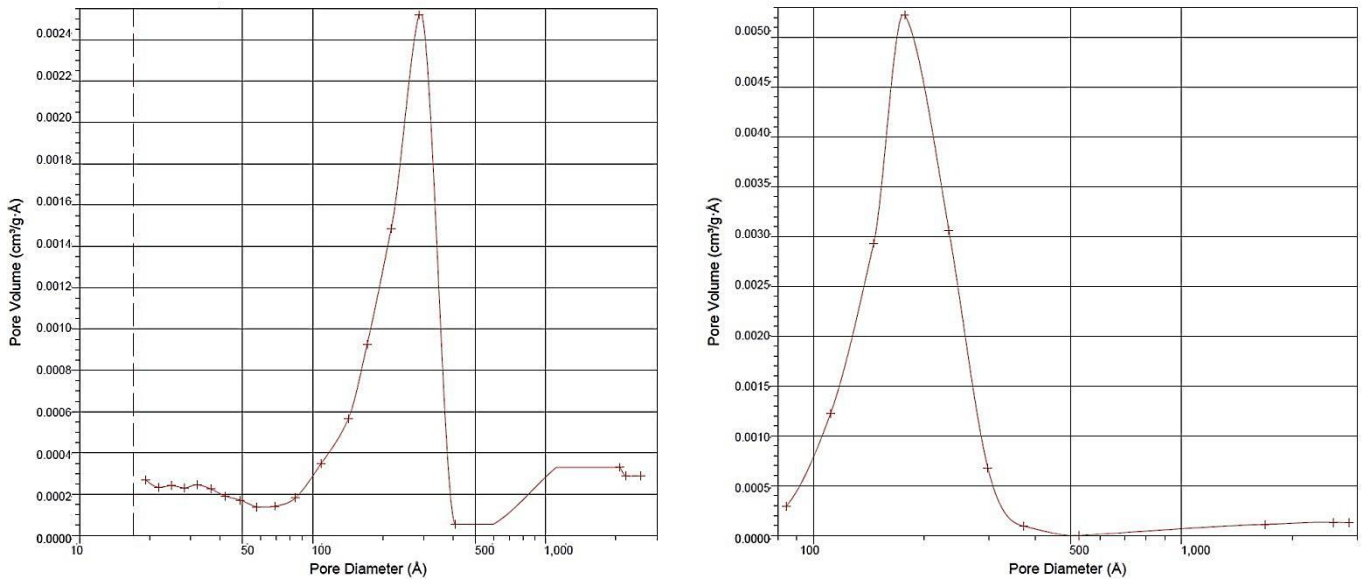


Figure A.7. BJH (a) Adsorption and (b) Desorption  $dV/dD$  Pore Volume of the PP-10T/HDPE.

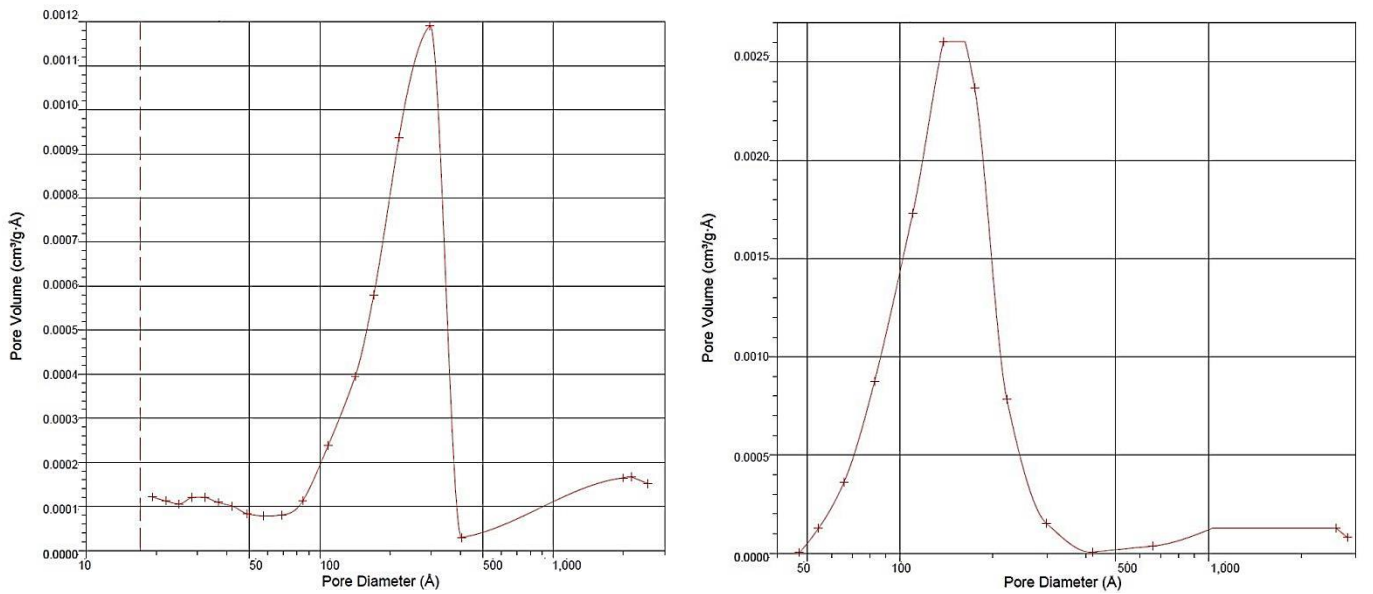


Figure A.8. BJH (a) Adsorption and (b) Desorption  $dV/dD$  Pore Volume of the PP-5C/HDPE.

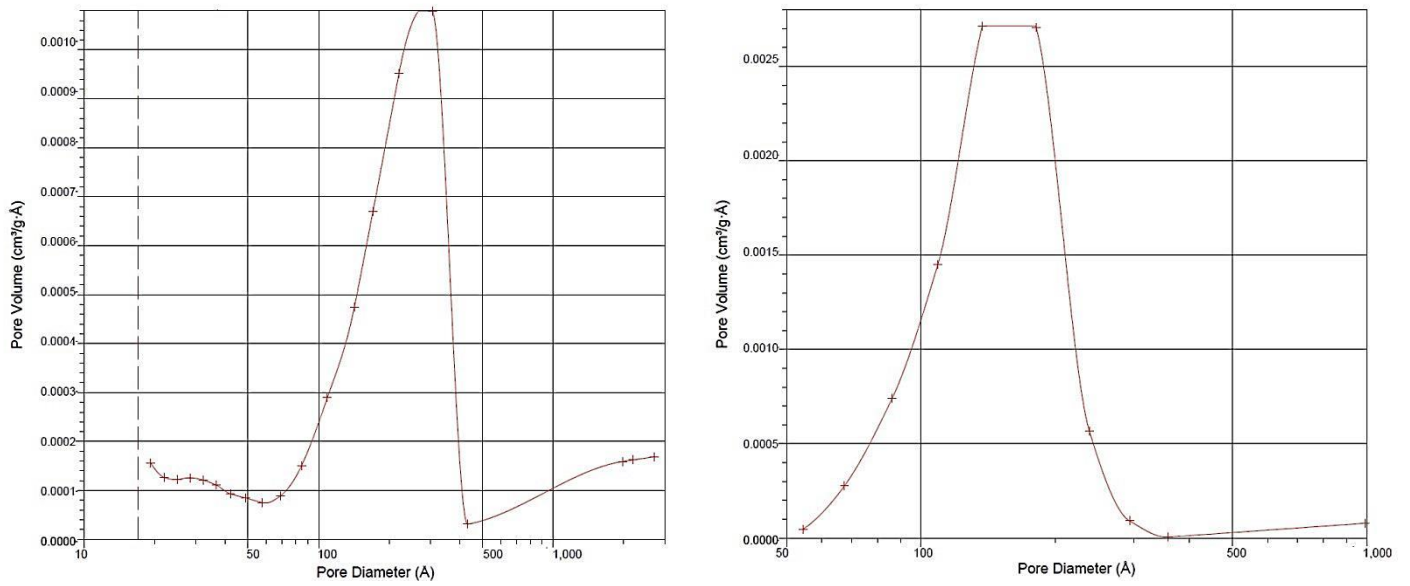


Figure A.9. BJH (a) Adsorption and (b) Desorption  $dV/dD$  Pore Volume of the PP-10C/HDPE.